EXPERIMENTAL AND THEORETICAL STUDIES OF HYDROGEN BONDING

by

Bradley Colin Bricknell

Submitted in partial fulfilment of the

requirements for the degree of

Doctor of Philosophy

in the

Department of Chemistry and Applied Chemistry,

University of Natal, Durban

Durban, Dec 1995

PREFACE

This thesis presents work performed by the author in the Department of Chemistry and Applied Chemistry, University of Natal, King George V Avenue, Durban, 4001, under the supervision of Professor T. A. Ford and Professor T. M. Letcher.

This thesis is the original work of the author and has not been submitted in part, or in whole, to any other university. Where use has been made of the work of others, it has been duly acknowledged in the text.

Dedicated to Bonita, without whose help this project would never have been started, let alone finished.

ACKNOWLEDGEMENTS

I would like to thank my supervisors, Professor T. M. Letcher and Professor T. A. Ford for their guidance, support, interest and assistance. Thanks also to Maganthran Govender and Tankiso Tshehla for all their practical assistance and their friendship.

The interesting times on the sports field, conversations and friendships of colleagues and technical staff too numerous to mention is gratefully acknowledged.

My greatest thanks go to my wife, Bonita, for her love and sustaining influence. My daughters, Janelle and Kiara, have also been wonderful influences in my life.

I would like to thank my parents for their love and support through the years, and finally, I would like to thank the Foundation for Research and Development and my supervisors for financial support for the duration of this project.

ABSTRACT

The theoretical and experimental work in this thesis is primarily aimed at i) the quantification of the strengths of a number of hydrogen bonded systems, and ii) exploring the relationships that exist between the various physico-chemical properties determined in this study, which are related to the hydrogen bonding phenomenon.

To this end a three part study of some hydrogen bonded systems has been undertaken. The study involves using a number of theoretical and experimental procedures, including a theoretical *ab initio* molecular orbital study, infrared spectroscopic determinations and a thermodynamic investigation involving measuring enthalpies and volumes of mixing and applying a theoretical model of interacting liquid mixtures.

Conclusions based on *ab initio* molecular orbital theory, thermodynamic and infrared spectroscopic results conducted in this work include:

i) the proton donating ability of the three hydrogen donor moieties studied in this work decreases in the order O-H > N-H ≈ S-H,

ii) the proton accepting competence of the three electron donor atoms considered in this work decreases in the order N > O > S in all cases except in the liquid phase systems involving dipropylamine and propane-1-thiol as proton donors, where the proton accepting ability of the atoms is in the opposite order i.e. S > O > N, and

iii) a direct correlation exists between the shift in the A-H stretching wavenumber and the hydrogen bond interaction energy.

Although a number of factors influence the stability of the hydrogen bond, it was also tentatively concluded that in liquid phase systems involving weakly self-associated hydrogen bond donor molecules, the available surface area of the proton accepting atom becomes the dominant strength determining factor, otherwise factors such as basicity and electronegativity dominate.

TABLE OF CONTENTS

CHAPTER 4. PART C - EXPERIMENTAL INFRARED SPECTROSCOPIC STUDY OF MOLECULAR INTERACTIONS

LIST OF SYMBOLS

AH...B	A hydrogen bond with A and B atoms having electronegativities greater than that of H
H_m^E	Excess enthalpy of mixing
V_m^E	Excess volume of mixing
$H_{i,m}^E(x_i=0)$	Partial molar enthalpy at infinite dilution
$\Delta H_{H\text{-bond}}$	Hydrogen bond interaction energy derived from $H_{i,m}^E(x_i=0)$ values
$\Delta h_{H\text{-bond}}$	Semi-quantitative interaction energy derived from $H_m^E(x=0.5)$ values
ΔH_{AB}	Hydrogen bond energy obtained from ERAS
K_A	Self-association constants of component A
p_i^*	Reduction parameter of component i for pressure
V_{mol}	Molar volume
V_i^*	Molar hard core volume for component i
α_i	Thermal expansion coefficient
κ_i	Compressibility coefficient
s_i	Surface to volume ratio of component i
Δh_A^*	Hydrogen bond self-association energy of component A
Δv_A^*	Self-association volume of component A
Δh_{AB}^*	Hydrogen bond cross-association energy of component A with component B
Δv_{AB}^*	Cross-association volume of A with B
X_{AB}	van der Waals interaction parameter
K_{AB}	Association constant of A with B
Q_{AB}	Entropy parameter
$\hat{H}$	Hamiltonian, a differential operator

$E^{eff}(R)$	Effective electronic energy
ΔE_{es}	The Morokuma electrostatic interaction
ΔE_{ct}	The Morokuma charge transfer or electron delocalization interaction
ΔE_{pl}	The Morokuma polarization interaction
ΔE_{ex}	The Morokuma exchange repulsion
ΔE_{mix}	The Morokuma coupling term which accounts for higher order interaction between the various components
Ψ	A wavefunction
δ	Bending or bond angle deformation.
γ	Bending, in cases when the deformation of the bond angle involves motion of the atoms out of the symmetry plane of the molecule or complex.
T_x	The in-plane shear (intermolecular mode)
T_z	The hydrogen bond stretch (intermolecular mode)
R_y	The in-plane bend (intermolecular mode)
T_y	The out-of-plane shear (intermolecular mode)
R_x	The out-of-plane bend (intermolecular mode)
R_z	A torsion mode (intermolecular mode)
$\Delta E'$	The BSSE corrected intermolecular energy
$\Delta\nu$(AH)	Shift in the A-H stretching peak
Δr(AH)	Change in the length of the A-H bond
R(A...B)	Heavy atom bond distance
$A\hat{H}...B$	Hydrogen bond angle
ΔE_e^0	Difference between the ground state electronic energies of reactants and products at 0 K
$\Delta(\Delta E_e)$	Change in electronic energy difference between 0 K and 298K
ΔE_v^0	Difference between the zero point vibrational energies of reactants and products at 0 K,
$\Delta(\Delta E_v)$	Change in the vibrational energy difference between reactants and products

ΔE_r	Difference in rotational energies between reactants and products at 298 K
ΔE_t	Difference in translational energies between reactants and products at 298K.
X^E	The excess quantity, an extensive property of a phase
X^{id}	Property of the hypothetical ideal solution.
X^*	Property of the pure unmixed components at the same T and P as the solution.
G	Gibbs free energy
S	Entropy
X_m	A molar quantity, an intensive quantity
τ	Period of oscillation = $1/\nu$
H_i	Partial molar enthalpy
H_m^E/x_1x_2	At $x=0$ equals the partial molar enthalpy at infinite dilution
H_c^E	Chemical contribution to H_m^E
H_{ph}^E	Physical contribution to H_m^E
H_{max}^E	Maximum value on an excess enthalpy of mixing curve
$H_m^E(x=0.5)$	Excess enthalpy value at a mole fraction of 0.5

CHAPTER 1.
INTRODUCTION

Hydrogen bonding, an interaction that can be characterized as the sharing of a proton by two electron pairs, is of great consequence to life on this planet. Man himself is fabricated of hydrogen bonding substances. In addition, man feeds, clothes and houses himself in hydrogen bonded materials. In 1939 Linus Pauling declared,[1]

> "Although the hydrogen bond is not a strong bond (its bond energy, that is the energy of the reaction XH + Y = XHY, being only about 5 kcal mol^{-1})*, it has great significance in determining the properties of substances. Because of its small bond energy and the small activation energy involved in its formation and rupture, the hydrogen bond is especially suited to play a part in reactions occurring at normal temperatures. It has been recognised that hydrogen bonds restrain protein molecules to their native configurations, and I believe that as the methods of structural chemistry are further applied to physiological problems it will be found that the significance of the hydrogen bond for physiology is greater than that of any other single structural feature."

Hydrogen bonds are of paramount importance in the behaviour of many compounds of interest in biochemistry and molecular biology, such as

* 21 kJ mol^{-1}

enzymes and nucleic acids. These bonds are responsible for the conformations of polypeptide chains in proteins and for the double-stranded helical conformation of the deoxyribonucleic acid (DNA) molecule, which is intimately related to its role as the carrier of genetic information. Hydrogen bonds are also the means through which hemoglobin and myoglobin distribute oxygen throughout the animal body[2] and, amongst other things, provide water with its unique properties. It was Pimentel and McClellan[3] who boldly proclaimed that " it is hardly an exaggeration to say that in the chemistry of living systems the hydrogen bond is as important as the carbon-carbon bond."

This thesis is primarily concerned with the properties of certain hydrogen bonds and the quantification of the strengths of those hydrogen bonds. The work involves a three part study of a number of hydrogen bonded molecular complexes. The techniques employed in this work include theoretical *ab initio* molecular orbital (MO) studies, liquid infrared spectroscopic determinations and a thermodynamic investigation involving enthalpies and volumes of mixing and a theoretical model of interacting liquid mixtures.

In this work the analysis was performed on mixtures involving the OH...O, OH...N, OH...S, NH...O, NH...N, NH...S, SH...O, SH...N and SH...S hydrogen bonds. The interacting components were chosen so that for any pair of interacting species, only one hydrogen bond was possible. Because of the constraint that the molecules to be studied experimentally had to be liquid at room temperature and atmospheric pressure and also to ensure sufficiently low volatility, the particular members of the homologous series to be studied were limited to those which contain alkyl groups consisting of

at least three carbon atoms. However, because of the magnitude of the computational effort involved, the work was restricted to studying only the lightest members of each particular series as models. Thus (and in an attempt to reduce the effect of different alkyl side chains), all monomer species were fully methylated in the *ab initio* MO analysis and fully propylated in both the liquid infrared and thermodynamic investigations. By standardizing the alkyl moiety of each donor and acceptor, it was ensured that any differences in the properties of the various complexes were localized in the specific AH...B interaction involved, where A and B are the proton donor and the proton acceptor respectively.

The first part of the investigation involved a theoretical study of the hydrogen bonded complexes formed from the following molecules: methanol, dimethylamine, methane thiol, dimethyl ether, trimethylamine and dimethyl sulphide. The structures, interaction energies and infrared spectra were predicted by means of *ab initio* MO theory at the Hartree-Fock (HF) level of theory, using the 6-31G** basis set. Previous theoretical work, at various levels of sophistication, on the molecules involved in these interactions include the geometries, wavenumbers and vibrational assignments of methanol[4-9], methane thiol[6,10,11], dimethyl ether [5,8,12-14], dimethyl sulphide[12,15-17], dimethylamine[4,5,18-21] and trimethylamine.[22,23]

The second part of the project involved a thermodynamic analysis of molecules analogous to those studied in the first part of the project. A number of different procedures were applied to the experimentally determined excess enthalpy, H_m^E, and excess volume, V_m^E, results in order to

characterize and quantify the propensities and relative strengths of the hydrogen bonded interactions under consideration. The enthalpy of mixing is a reflection of the overall interactions and dissociations that occur in a mixture. Methods of measurement, correlation and calculation of these properties occupy much of the attention of the world's thermodynamicists because of their importance in the development of effective models and theories of liquids. A sound and competent theoretical understanding of mixtures would enable more accurate predictions of the properties of liquid mixtures, which, in turn, would be of great use in the chemical processing industry.

The techniques used here in the thermodynamic study include: (a) measuring partial molar enthalpies at infinite dilution to determine hydrogen bond strengths, (b) comparing H_m^E data at $x = 0.5$ and (c) applying one of the most recent models that accounts for association in liquid mixtures, the Extended Real Associated Solution (ERAS) model,[24,25] to the mixture data.

Many workers[26-30] have established that in alkanol-hydrocarbon systems, which have only one self-associating component, the partial molar enthalpies of mixing of alkanols at infinite dilution, $H_{i,m}^E(x_i = 0)$, are approximately equal to the energies of hydrogen bonds between the alkanols. We have extended this treatment to describe the hydrogen bond strengths in mixtures containing two associated components, where one of the components shows relatively weak self-association. The ERAS model has also been utilized in this study. Originally developed to describe excess properties of binary (alkanol + alkane) mixtures,[24] the ERAS model has been extended to describe mixtures in which one of the components shows only a weak

self-association but a relatively strong mutual association with the other component.[25]

In this work H_m^E and V_m^E values have been determined over the whole concentration range for mixtures of propan-1-ol + dipropyl ether (OH...O), + tripropylamine (OH...N), + dipropyl sulphide (OH...S), + heptan-4-one (OH...O); for dipropylamine + dipropyl ether (NH...O), + tripropylamine (NH...N), + dipropyl sulphide (NH...S), + heptan-4-one (NH...O) and also for propane-1-thiol + dipropyl ether (SH...O), + tripropylamine (SH...N), + dipropyl sulphide (SH...S), + heptan-4-one (SH...O). H_m^E values have also been determined for the following mixtures: heptane + propan-1-ol, + dipropyl ether, + dipropylamine, + tripropylamine, and + propane-1-thiol.

Finally, infrared spectroscopic determinations were conducted in the liquid state on the same series of molecules used in the thermodynamic investigation. Of particular interest was the intramolecular A-H stretching vibration which shifts as a result of hydrogen bonded complexation and has been used previously as a measure of the strength of the hydrogen bonded interaction.[3] These results have been compared with, and used to legitimate, the trends that have been established in the thermodynamic analysis of the hydrogen bonded molecular complexes.

The study of the above mixtures has not only yielded valuable experimental data but has also highlighted the often enigmatic and unpredictable behaviour of liquid mixtures. The *ab initio* theoretical results on molecules that are gases at room temperature reveal a consistent order of hydrogen bond strength. Thus, irrespective of the proton donor used, the proton

accepting ability of those atoms under consideration is always in the same order, i.e. N > O > S. However, when certain related mixtures in the liquid phase are considered, the proton accepting capabilities of those atoms are reversed, i.e. S > O > N. An explanation of this anomaly is attempted.

Ultimately, the aim of this work is to explore the relationships between the measured spectroscopic and calorimetric properties, and to investigate the dependence of these measured quantities on the structural features of the interacting species.

1.1 Molecular Interactions

Covalent and ionic bonds result from strong attractive forces between atoms that are responsible for the stability of molecules. However, these are not the only attractive forces that can act between atoms. Atoms of a noble gas like He or Ar cannot form chemical bonds with each other, yet they form liquid and solid phases with the evolution of heat,[31] showing that an attractive force must exist. This type of attractive force also exists between molecules and is then termed an intermolecular interaction.

In the early twentieth century, much speculation existed concerning the origin and nature of intermolecular interactions, but it was not until the establishment of the principle of quantum mechanics in the late 1920's that the correct theory of intermolecular forces, which describes molecular behaviour both at long and short distances, was constructed.[32,33] The origin of the forces between molecules is electromagnetic in nature, arising from the charges on the electrons and nuclei of the atoms and molecules.[32] These electromagnetic interactions may be categorised as short range repulsive, and long range attractive forces. Five types of intermolecular forces are generally recognised: repulsion due to the exclusion principle, electrostatic forces, polarization forces, dispersion interactions and charge transfer interactions.

1.1.1 Repulsion forces

From the low compressibilities of solids and liquids, we can conclude that repulsions between molecules very close together are very large. From the large latent heats of vaporization, it is evident that the attractions to be overcome in separating molecules are also relatively large.[32] The

interactions between molecules can be represented in terms of the potential energy, relative to zero at infinite separation, as a function of their separation, and is given in Fig. 1.1:[34]

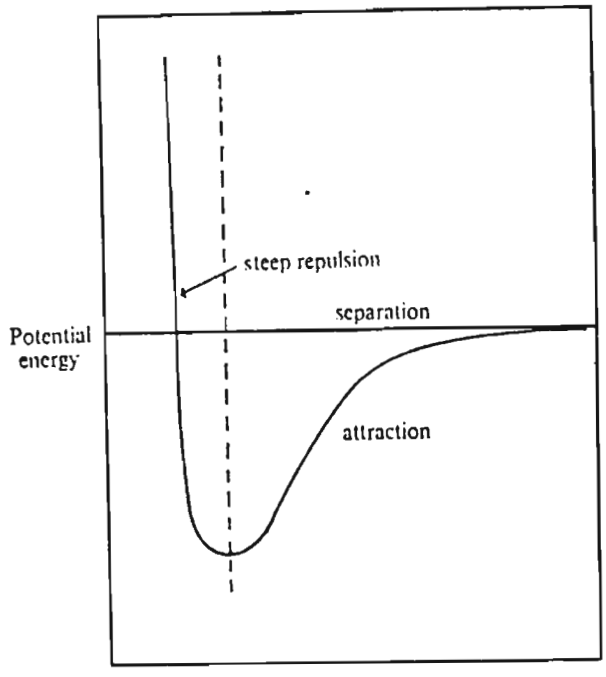

Fig. 1.1 Expected form of potential energy against separation for a pair of molecules.

When atoms or molecules with closed shells of electrons approach each other to such a degree that overlap of the electron clouds begins, the energy increases and mutual repulsion occurs. This repulsion is essentially a manifestation of the Pauli exclusion principle.[35] Quantum mechanical calculations indicate that the repulsive potential energy has the form[36]

$$V(r)=f(r)\exp(-Br) \tag{1.1}$$

where $f(r)$ is a polynomial in r (the distance of separation of the nuclei) and B is a constant for a given type of molecule. These short range repulsive forces are often termed exchange or overlap forces.

1.1.2 Electrostatic forces

At larger separations, where there is little overlap, attractive interactions may occur. A net electrical charge will clearly result in a long range coulombic interaction. However, even between molecules with no net charge, charge distribution may facilitate a direct electrostatic energy. Direct electrostatic contributions to the interaction energy of two uncharged molecules can occur when they have spherically unsymmetrical charge distributions, which are often described in terms of multiple moments of the molecule. The strongest of these contributions is the dipole-dipole interaction, where molecules with permanent dipole moments attract each other. The potential energy of a pair of dipoles depends not only on their distance apart, but on their relative orientation. The minimum potential energy V_{AB} for a given separation r is obtained when the dipoles are aligned in the most favourable orientation.[36]

$$V_{AB}=-\frac{\mu_A\mu_B}{\varepsilon r^3} \tag{1.2}$$

where μ_A, μ_B are the dipole moments and ϵ is the permittivity of the medium. In the liquid state, where the molecules are in constant motion, the net attraction is a weighted average over all possible orientations.[36]

$$V_{AB} = -\frac{2\mu_A^2\mu_B^2}{3r^6\varepsilon^2 kT} \qquad (1.3)$$

gives the average potential energy of a pair of dipoles at temperature T.

1.1.3 Polarization or induction energy

The electric field resulting from the charge distribution of one molecule may induce modifications in the electronic distribution of a neighbouring molecule. This gives rise to another interaction energy - induction energy. This polarization effect on a nearby molecule, by one that has a permanent dipole moment, is often referred to as a dipole-induced dipole interaction. This energy is attractive for all orientations and falls off as r^{-6}. For a pair of molecules A and B with polarizabilities α_A and α_B, the energy is given by the relation

$$V_{AB} = -\frac{(\alpha_A\mu_B^2 + \alpha_B\mu_A^2)}{r^6} \qquad (1.4)$$

1.1.4 Dispersion Forces

Together with electrostatic and induction energy, a third attractive force exists. These interactions are called dispersion or London forces.[35] The first detailed treatments of the weak forces between atoms and molecules were based on the idea that these forces result from the polarization of one molecule in the field of a permanent dipole moment or quadrupole moment of another molecule , or from the interaction of the permanent dipole or quadrupole moments themselves. With the development of quantum mechanics it has been recognised, especially by London[35] that for most molecules these interactions are small compared with another interaction, namely that corresponding to the polarization of one molecule in the rapidly changing field due to the instantaneous configuration of electrons and nuclei of another molecule. It is a most important source of attractive intermolecular energy, and acts on all atoms and molecules, polar or non-polar. Even though the average dipole moment of a spherically symmetrical atom or molecule may be zero, the electrons of that atom or molecule are in continuous motion, and therefore at any instant, a temporary dipole moment can occur. This instantaneous dipole can induce a dipole moment in a nearby atom or molecule, which results in an attractive force. Except for highly polar molecules like water, the dispersion energy is a major contribution to the long range intermolecular energy.[32]

In 1930, London[36] showed that the potential energy of a pair of noble gas atoms is given by the expression

$$V(r)=\frac{A}{r^6}+\frac{B}{r^8}+\frac{C}{r^{10}}+.... \qquad (1.5)$$

Precise calculations of even the first term in (1.5) have been made only for the hydrogen atom, noble gas atoms and the hydrogen molecule. London's calculations led to the approximate formula for the interaction between two molecules A and B

$$V_{AB}(r)=-\frac{3h\nu_A h\nu_B}{2(h\nu_A+h\nu_B)}\frac{\alpha_A\alpha_B}{r^6} \qquad (1.6)$$

where ν_A, ν_B are frequencies characteristic of the molecules, α_A and α_B are their polarizabilities, and h is Planck's constant.

These four interactive forces, viz. electrostatic, dispersion, induction and overlap energy, are collectively called van der Waals forces. They are responsible for the formation of molecular aggregates called van der Waals complexes. Molecular interactions between sub-systems A and B, leading to the formation of a super-system AB, are termed van der Waals interactions when they satisfy the following accepted requirements:[37]

i) No covalent bond is broken or formed.

ii) The geometric and electronic structures of the sub-systems change very little.

iii) The stabilization energy associated with the process is usually smaller than 40 kJ mol^{-1}.

iv) The distance between the closest atoms of sub-systems A and B is

usually larger than 200 pm.

v) The super-system AB is formed spontaneously.

1.1.5 Charge transfer interactions

Another important type of interaction is the charge transfer interaction. When molecules with unoccupied low energy states ('acceptors') are allowed to associate with molecules with lone pairs of electrons ('donors') there is a possibility of a contribution to the wave function of the pair of unlike molecules from states which involve the unoccupied energy levels of the acceptor, and the lone pair electrons of the donor. Thus in a mixture of, say, propan-1-ol with an ether, there is a strong interaction involving a lone pair of electrons on the ether oxygen and the low-lying electronic levels of the O-H group on the alcohol. The transfer of charge from one molecule to another is often accompanied by the appearance of a characteristic absorption band in the visible or ultraviolet (UV) region of the spectrum.[38]

A specific type of interaction, which involves all of the interactions listed above, is that known as a hydrogen bond. This type of interaction is the subject of this investigation, and will be discussed in more detail below.

1.2 The Hydrogen Bond

Between the two extremes of chemical bonds and pure van der Waals interactions is an interaction of intermediate energy which produces molecular aggregates. These aggregates are termed complexes, and the process of forming them is called "association".[3] The hydrogen bond is such an associative interaction. It occurs between a proton donor group, A-H, and a proton acceptor group, B, where A is an electronegative atom with an electronegativity greater than that of hydrogen (C,N,P,O,S,Se,F,Cl,Br,I)[35] and the acceptor group is a lone electron pair of an electronegative atom, or a π orbital of a multiple bond in an unsaturated system. Hydrogen bonding is a distinctly directional, localised interaction[35] with the equilibria among the molecular complexes being rapid and reversible. The bonds are more or less linear, but substantial variations in the A-$\hat{H}$...B angle can occur.

This type of bond is limited to the hydrogen atom because this atom is the only one that does not have a filled shell of electrons surrounding, and thus shielding, its nucleus. When a hydrogen atom is covalently bonded to an electronegative atom, such as oxygen, there is a relatively high probability that the bonding electrons are near the oxygen atom thus leaving the proton almost 'bare' and therefore partially positively charged.[39] This proton can therefore exert an attractive force on the lone pair electrons of, for example, a nitrogen atom in a neighbouring molecule and in this way form a hydrogen bond. Hydrogen bonds may be either intermolecular or intramolecular. Intermolecular hydrogen bonds are formed between two separate molecules;

Intermolecular hydrogen bonds are formed between two separate molecules; intramolecular, between groups within a single molecule.

There are various theories of the nature of the hydrogen bond. The classical *electrostatic model* found prominence when Pauling[40] argued that the bonding properties of the hydrogen atom depend upon the single 1*s* orbital which cannot form more than one pure covalent bond. He therefore concluded that hydrogen bond formation must be due to ionic forces. The argument is supported by the fact that the strongest hydrogen bonds are formed when A and B are fluoride ions, followed by hydrogen bonds involving oxygen atoms, while the N-H proton donor molecules usually form relatively weak hydrogen bonds.[3] The electrostatic model does not, however, account for all of the phenomena associated with hydrogen bond formation. Coulson[41] listed the following types of evidence:

i) The increase in the infrared absorption intensity of the A-H stretching vibration, ν(AH), is far in excess of that explainable by the electrostatic model[42-44]

ii) The absence of correlation between the hydrogen bond strength and the dipole moment of the base. [45,46]

iii) The lowered intensity of the CAH bending mode, δ(CAH). It was argued that the intensity of this mode would be expected to increase, not decrease, if the enhancement of the intensity of the stretching mode is properly attributed to the increased ionic character of the A-H bond.

Also, the relatively similar hydrogen bond properties of acetone, diethyl ether and dioxane, with dipole moments of 2.85 D*, 1.15 D and 0.4 D respectively, is difficult to rationalize.

Alternative interpretations impart some covalent character to the hydrogen bond. Coulson and Danielson[47] concluded from early semiempirical studies of O-H...O hydrogen bonds (assuming a constant O-H bond length of 100 pm) that the O...O bond (280 pm) is essentially electrostatic, the covalent contribution amounting to only a few percent. However they continued by asserting that with short heavy atom bonds (250 pm) covalency begins to be appreciable.

Molecular orbital descriptions of the hydrogen bond are informative. Pimentel[48] considered HF_2^- qualitatively with molecular orbitals composed of linear combinations of atomic orbitals. Using only fluorine *2p* orbitals and the hydrogen *1s* orbital, four molecular orbitals result. Since the hydrogen bond involves four electrons, the ground state involves occupation of the bonding orbital and the nonbonding orbital. One pair of electrons formally takes part in bonding in an orbital extending over two bonds while the other electron pair occupies a nonbonding orbital which places the excess charge on the fluorine atoms, the location dictated by the relative electronegativities. He concluded by stating that the importance of the electronegativities of A and B arises in the nonbonding orbital where the second pair of electrons must be housed. Electronegativities thus play a rather passive role in the molecular orbital discussion.

* $1D = 3.336 \times 10^{-30}$ C m

Ab initio self consistent field (SCF) molecular orbital theory has been applied to the study of the hydrogen bond. The pioneering undertaking was conducted by Clementi in 1961.[49] Since then molecular orbital methods have been extensively used in the study of hydrogen bonded molecular complexes and they have played an important role in the progress of our understanding of the structures and properties of hydrogen bonded systems. An example is the interpretation of the hydrogen bond by Morokuma[50] in which he indicated that the hydrogen bond energy is partitioned into five contributions, viz. electrostatic, induction, dispersion, exchange repulsion and charge transfer (see section 2.4.7). The charge transfer component is simply the covalent contribution to the hydrogen bond energy. If the repulsive term is estimated to be as large as the electrostatic attractions, the electrostatic model does not account for much of the energy. Coulson[47] accounted for this additional energy in terms of dispersive forces while Pimentel[3] suggested that the dispersive energy term might be considered a legitimate refinement of the electrostatic model.

Formation of the hydrogen bond, A-H...B, is accompanied by the following measurable effects.

1. Changes in the vibrational spectra of A-H and B[3];

   i) The frequency of the A-H stretching band decreases.
   ii) The width of the A-H stretching band increases.
   iii) The intensity of the A-H stretching band increases.
   iv) The frequency of the CAH deformation mode increases.

v) There are new low frequency modes associated with stretching and bending of the hydrogen bond itself.

2. The A...B distance is found to be shorter than the sum of the van der Waals radii.

3. The A-H bond becomes slightly longer on formation of the hydrogen bond, H...B, which in turn is considerably longer than a typical H-B chemical bond.[32]

4. Measurable properties such as enthalpies of mixing are evident, which are a reflection of association.

The energy of a hydrogen bond is in the order of 3-40 kJ mol^{-1},[35] which is intermediate between those of chemical bonds and those of pure van der Waals interactions.

CHAPTER 2.

PART A - THEORETICAL STUDY OF MOLECULAR INTERACTIONS

2.1 Introduction

In 1900, Max Planck found an empirical equation which reproduced the shape of the black-body radiation curves within experimental error over the entire wavelength range. In developing a theoretical derivation for this equation he had to assume that in the absorption and emission of radiation by the walls of the cavity the energy exchange takes place *only* in discrete amounts he called *energy quanta*.[51] In 1905, Einstein applied the concept to explain the photoelectric effect.[52] He proposed that light be viewed as being comprised of discrete units of energy, each such unit being called a *photon.* Bohr[53] in 1913, also used the concept to explain the spectrum of the hydrogen atom. Energy is not absorbed continuously, but in quantized amounts such that the energy of the photon is exactly equal to the difference in the energies of the two stationary states between which the transition has occurred.

Evidently light has wave and particle nature which can be described in terms of photons, which are associated with waves of frequency

$$\nu = \frac{E}{h} \qquad (2.1)$$

where h is a constant of nature, now called Planck's constant. In 1923, on

the basis of analogy with electromagnetic radiation, de Broglie[54] predicted that a similar duality might exist in the case of the electron. He formulated a relationship between mass and wavelength which was used by Erwin Schrödinger to formulate an equation which formed the basis for a purely mathematical description of electrons in atoms. It is known as the Schrödinger equation.[55-57] In classical mechanics there are separate equations for wave motion and for particle motion, whereas in quantum mechanics, in which the distinction between particles and waves is not clear-cut, there is only the Schrödinger equation.

Quantum mechanics, the science relating atomic or molecular properties to the motion and interactions of electrons and nuclei, is the key to theoretical chemistry. The Schrödinger differential equation, theoretically, could lead to the prediction of most chemical phenomena, using only a few physical constants. However, it soon became clear that the equation was an almost impossible mathematical problem for all but the very simplest of systems. Solutions to the Schrödinger wave equation for molecules larger than H_2 could therefore only be obtained by using approximation techniques. Two approximation techniques, the molecular orbital method and the valence bond method, are in use today. The molecular orbital method has proved to be easier to apply to complicated molecules,[58] and is the theory employed by the Gaussian series of computational programs (see section 2.3). The molecular orbital programs compute values of geometrical parameters that produce the lowest energy structure. Iterative calculations are used in the procedure. Two computational molecular orbital methods, both of which succeed in producing a feasible model of reality, exist. Both methods, *ab*

initio and semiempirical, involve approximations.[59]

Ab initio ("from the beginning") theory, a rigorous, nonparameterized molecular orbital treatment derived from first principles,[60] calculates all integrals exactly. Often the basis set consists of a finite number of gaussian-type orbitals centred on each nucleus. Ab initio calculations are more complete than semiempirical ones, but more expensive and time consuming. In the simplest version of *ab initio* molecular orbital theory, a single assignment of electrons to orbitals is made. These orbitals are then brought together to form a suitable many-electron wavefunction, Ψ, which is the simplest molecular orbital approximation to the solution of the Schrödinger equation.[61]

To use *ab initio* molecular orbital theory, a number of molecular orbital models can be applied, the Hartree-Fock model being the simplest to use for chemical applications. The Hartree-Fock (HF) theory is based on the variational method in quantum mechanics.[61] Solutions to equations employed in the theory necessarily involve iterative procedures, which are continued until the results are self consistent, i.e. remain the same after successive iterations within the required degree of accuracy. Since the resulting molecular orbitals are derived from their own effective potential, the technique is called the self-consistent-field (SCF) theory.[61] Hartree-Fock theory uses a limited basis set in the orbital expansion, thus imparting limited flexibility to the molecular orbitals. It also makes use of a single assignment of electrons to orbitals, therefore giving an incomplete description of the correlation between the motions of electrons. The inadequate description of electron correlation (configuration interaction) in the Hartree-Fock theory often leads to calculated HF energies that are higher than expected.[60] The Hartree-Fock energy is the lowest energy that can be achieved for a single determinantal wavefunction. Sometimes "restricted" Hartree-Fock is used to emphasize that the wavefunction is restricted to a

single determinantal function for a configuration wherein electrons of (alpha) spin occupy the same space orbitals as do the electrons of (beta) spin.[58]

A number of methods have been formulated to deal with electron correlation, including full configuration interaction, limited configuration interaction and Møller-Plesset perturbation theory.[61]

2.2 Ab initio Molecular Orbital Calculations - Theoretical Considerations

2.2.1 Schrödinger Equation

The fundamental equation of quantum theory is the Schrödinger wave equation. It belongs to a special class of equations called eigenvalue equations. Such equations have the format[62]

$$Op(f)=cf \tag{2.2}$$

where Op is an operator, *f* is a function and *c* is a constant. The function *f* that satisfies the above equation is called an eigenfunction of the operator. The constant *c* is called the eigenvalue associated with the eigenfunction *f*. Many properties, including the energy, of a stationary state of a molecule can be obtained by solution of this equation. For phenomena that do not depend on time, the Schrodinger equation can be written simply as [63]

$$\hat{H}\Psi=E\Psi \tag{2.3}$$

Here $\hat{H}$ is the Hamiltonian, a differential operator which is a sum of terms each corresponding to a different component of the total energy. The Hamiltonian can easily be written down for an atom or molecule of arbitrary complexity, provided the effects of relativity are neglected. E is the numerical value of the energy of the state, and Ψ is the wave function or

eigenfunction. The square of the wave function, Ψ^2, is interpreted as the probability distribution of the particles within the molecule.[34,61,63]

The Schrödinger equation depends on the positions of all the particles in the system, and on the interactions between them, and so for atoms with more than a few electrons, it becomes very complicated. The situation is further complicated by the fact that certain symmetry properties have to be imposed on the solutions of the molecular Schrödinger equation, properties that arise from the intrinsic angular momentum, or "spin" of the electrons. As indicated above, the Schrödinger equation can only be solved exactly for the case of the hydrogen atom, and the hydrogen molecular ion, H_2^+. In order for any progress to be made, it is clear that approximations have to be made.

2.2.2 Born-Oppenheimer Approximation

The first important simplification in molecular quantum theory was due to Born and Oppenheimer,[61] who pointed out that the large disparity between the masses of the nuclei and the electrons allows the motion of the electrons and the nuclei to be treated separately. Because the electrons can follow any change in the positions of the nuclei very rapidly, it makes it a reasonable approximation to assume that the electron distribution depends only on the instantaneous positions of the nuclei and not on their velocities. The approximation of separating the electronic and nuclear motions is called the Born-Oppenheimer approximation, and is basic to quantum chemistry. By using this approximation, the electronic Schrödinger equation - the

equation governing the motions of the electrons in the electrostatic field generated by fixed nuclei - can be solved.

Solving the problem of electron motion in the field of fixed nuclei leads to an effective electronic energy $E^{eff}(R)$, which depends on the relative nuclear coordinates, denoted by R. The Schrödinger equation for electrons in the field of fixed nuclei can be written as [61]

$$\hat{H}^{elec}\Psi^{elec}(r,R)=E^{eff}(R)\Psi^{elec}(r,R) \qquad (2.4)$$

Here, ψ^{elec} is the electronic wave function which depends on the electronic coordinates, r, as well as the nuclear coordinates, R. The electronic Hamiltonian, $\hat{H}^{elec}$, corresponds to the motion of electrons only in the field of fixed nuclei, and is

$$\hat{H}^{elec}=\hat{T}^{elec}+\hat{V} \qquad (2.5)$$

where T^{elec} is the electronic kinetic energy,

$$\hat{T}^{elec}=-\left(\frac{h^2}{8\pi^2 m}\right)\sum_{i}^{electrons}\left(\frac{\partial^2}{\partial x_i^2}+\frac{\partial^2}{\partial y_i^2}+\frac{\partial^2}{\partial z_i^2}\right) \qquad (2.6)$$

and V is the coulomb potential energy,

$$V=\sum_{i}^{elec}\sum_{s}^{nuclei}\frac{z_s e^2}{r_{is}}+\sum_{i}^{elec}\sum_{j}^{elec}\frac{e^2}{r_{ij}}+\sum_{s}^{nuclei}\sum_{t}^{nuclei}\frac{z_s z_t e^2}{R_{st}} \qquad (2.7)$$

where $i<j$ and $s<t$. The first part of equation (2.5) corresponds to electron-nuclear attraction, the second to electron-electron repulsion and the third to nuclear-nuclear repulsion.

In order to eliminate fundamental physical constants from the electronic Schrodinger equation (2.2), new units are often adopted. Firstly, the bohr radius, a_0, is introduced which defines the atomic unit of length (the bohr).

$$a_o=\frac{h^2}{(4\pi^2 me^2)} \qquad (2.8)$$

New coordinates (x′, y′, z′) may then be defined as:

$$x'=\frac{x}{a_o} \qquad (2.9)$$

Secondly, a new atomic unit of energy, E_H, the hartree is introduced, which is the coulomb repulsion between two electrons separated by 1 bohr:

$$E_H=\frac{e^2}{a_o} \tag{2.10}$$

If new energies are defined as

$$E'=\frac{E}{E_H} \tag{2.11}$$

substitution of (2.7) and (2.9) into the electronic Schrödinger equation (2.2) gives

$$\hat{H}'\Psi'=E'\Psi' \tag{2.12}$$

where the Hamiltonian, $\hat{H}'$, in atomic units, is

$$\begin{aligned} H'=&-\frac{1}{2}\sum_{i}^{elec}\left(\frac{\partial^2}{\partial x_i^2}+\frac{\partial^2}{\partial y_i^2}+\frac{\partial^2}{\partial z_i^2}\right) \\ &-\sum_{i}^{elec}\sum_{s}^{nuclei}\left(\frac{Z_s}{r_{is}}\right)+\sum_{i}^{elec}\sum_{j}^{elec}\left(\frac{1}{r_{ij}}\right) \\ &+\sum_{s}^{nuclei}\sum_{t}^{nuclei}\left(\frac{Z_sZ_t}{R_{st}}\right) \end{aligned} \tag{2.13}$$

where $i<j$ and $s<t$. The electronic state of the molecule is now calculated by solving the Schrödinger equation (2.10) for any given molecular geometry. The lowest-energy solution of this equation is associated with the ground state of the molecule.

2.2.3 Molecular Orbital Theory

Schrödinger equations can be written down to describe the behaviour of electrons in molecules, but solutions to these equations can only be obtained by using approximation techniques. Two approaches have been widely used in arriving at approximate solutions of the Schrödinger equation for molecules in their lowest electronic energy states. These approaches differ in the choice of trial wave functions whose parameters are then optimized by the variation method.[64] One of these approaches, the *valence bond* method developed by Heitler and London, Slater and Pauling, is related to Lewis' concept of the electron pair bond. The other, the *molecular orbital* method developed by Hund, Mulliken, Lennard-Jones and Hückel, is related to the treatment of complex molecules.[58,61,63,64] In their elementary forms both of these methods gives results that are quantitatively crude. When both are refined by the use of more complicated trial functions, the difference between them disappears. Comparison of the two methods leads to the following synopsis:[58]

i) Both emphasize the importance of the displacement of charge into the internuclear region.

ii) The valence bond method overestimates electron correlation, while the molecular orbital method underestimates it.

iii) The valence bond theory emphasizes the structure of a bond as a distinct entity in the molecule, while the molecular orbital method views the molecule as a whole, which is an advantage when spectroscopic properties of the molecule are being considered.

iv) The molecular orbital method has proved to be easier to apply to complicated molecules, and will be the theory applied in this work.

The molecular orbital approach begins by considering a system in which the nuclei are in their equilibrium positions in the stable molecule, and discusses the way in which the electrons, associated with all the nuclei, can be described by wavefunctions. The theory uses one-electron functions to approximate the full wave function. It considers orbitals that spread over the entire molecule, i.e. molecular orbitals, and suggests that a particular set of electrons cannot be identified as belonging to a given bond, for if the orbitals spread throughout the nuclear framework, so too do the electrons. A molecular orbital, $\psi(x, y, z)$, is a function of the cartesian coordinates x, y, z of a single electron. Its square, ψ^2, is the probability distribution of the electrons in space.

The complete wavefunction for a single electron is the product of a molecular orbital and a spin function, $\psi(x, y, z)\alpha(\zeta)$ or $\psi(x, y, z)\beta(\zeta)$. It is termed a spin orbital, $\chi(x, y, z, \zeta)$. It was pointed out by Slater[59] that there is a simple way of writing wavefunctions, which guarantees that there will be antisymmetry for interchange of electronic space and spin coordinates; one writes the wavefunction as a determinant. This determinantal wavefunction does have the property of antisymmetry. In building up a determinantal wavefunction, one chooses a set of molecular orbitals, ψ_1, ψ_2, ψ_3,...., and assigns electrons of α or β spin to these orbitals. Most molecules have an even number of electrons in their ground states and may be represented by closed-shell wavefunctions with orbitals either doubly occupied or empty. The full many-electron molecular orbital wavefunction

for the closed-shell ground state of a molecule with n(even) electrons, doubly occupying n/2 orbitals, is often called a Slater determinant, and can be written[61]

$$\Psi=(n!)^{-1/2}\begin{vmatrix}\psi_1(1)\alpha(1) & \psi_1(1)\beta(1) & \psi_2(1)\alpha(1)\ldots\psi_{n/2}(1)\beta(1)\\ \psi_1(2)\alpha(2) & \psi_1(2)\beta(2) & \psi_2(2)\alpha(2)\ldots\psi_{n/2}(2)\beta(2)\\ \\ \psi_1(n)\alpha(n) & \psi_1(n)\beta(n) & \psi_2(n)\alpha(n)\ldots\psi_{n/2}(n)\beta(n)\end{vmatrix} \quad (2.14)$$

where α and β are spin functions.

In practical applications of the molecular orbital theory, individual molecular orbitals are expressed as linear combinations of a finite set of N prescribed one-electron functions known as basis functions,

$$\psi_i=\sum_{\mu=1}^{N} c_{\mu i}\phi_\mu \quad (2.15)$$

where ψ_i is an individual orbital, ϕ_μ are the basis functions and $c_{\mu i}$ are molecular orbital expansion coefficients (which provide the orbital description with flexibility). In the application of the theory, atomic orbitals of constituent atoms are often used as basis functions. In such cases, the molecular orbitals are obtained by the *linear combination of atomic orbitals* (LCAO) approximation. In the 1920's, Heitler and London showed that the chemical bond existing between the two equivalent hydrogen atoms in H_2 can be described mathematically by taking a linear combination of the 1*s* orbitals of the two H atoms that are partners in the molecule. When this is

done, the combination

$$\Psi = a_1\psi_{1s_1} + a_2\psi_{1s_2} \qquad (2.16)$$

is a new solution of the Schrödinger equation that has a unique low-energy internuclear distance that approximates the bond distance in H_2. The right side of the above equation is a LCAO. The Heitler-London method is called the valence bond approximation.[65] It arrives at a description of chemical bonding from a somewhat different logical premise than that of the molecular orbital method. Both methods arrive at equivalent mathematical descriptions as they are attempts to describe the same thing. The LCAO method is only one of many ways to approximate a molecular orbital. In this work a LCAO-MO description of the molecules will be considered.

2.2.4 *Ab initio* calculations

A rigorous variational calculation on a system involves the following steps:[63]

i) Write down the hamiltonian operator H for the system

ii) Select some mathematical functional form ψ as the trial wavefunction

iii) Minimize

$$\bar{E} = \int \psi^* \bar{H} \psi d\tau / \int \psi^* \psi d\tau \qquad (2.17)$$

with respect to variations in the parameters .

Semiempirical methods are not rigorous variational calculations. Although they make use of the secular determinant technique from variation theory, no hamiltonian operators are ever written out explicitly. In semiempirical molecular orbital theory, only the valence electrons are considered because the inner shell electrons are assumed effectively to screen the nuclei. Many integrals that are time consuming to compute are neglected, while the basis set (see section 2.2.5) is preset and usually has one Slater-type orbital for each valence orbital on an atom. These are called semiempirical methods because they combine the theoretical form with parameters fitted from experimental data.[63]

The term *ab initio* is used to describe calculations in which the three steps listed above are all explicitly performed.

2.2.5 Basis Sets

Most molecular quantum mechanical methods begin the calculation with the choice of a basis set. The use of an adequate basis set is an essential requirement for the success of the calculation. In section 2.2.3, it was discussed how atomic orbitals of constituent atoms are used as basis functions. Two types of atomic basis functions that have received widespread support are Slater-type atomic orbitals (STOs) and Gaussian-type atomic orbitals (GTOs).

STOs give a good description of the electron density around an atom, but

integrals involving them are hard to evaluate.[59] GTOs do not give as true a description of electron density, especially near the nuclei, so more GTOs are needed to compensate for this deficiency. They do, however, have an advantage in that they are easier to evaluate computationally.

The Gaussian series of ab initio programs (see section 2.3.1) deals primarily with GTOs[60] as do most other ab initio programs in use. Gaussian functions include an exponential term of the form exp $(-\alpha r^2)$. The radial dependence of such a function is compared with that for a hydrogen-like function (which is identical to a 1s STO).[63]

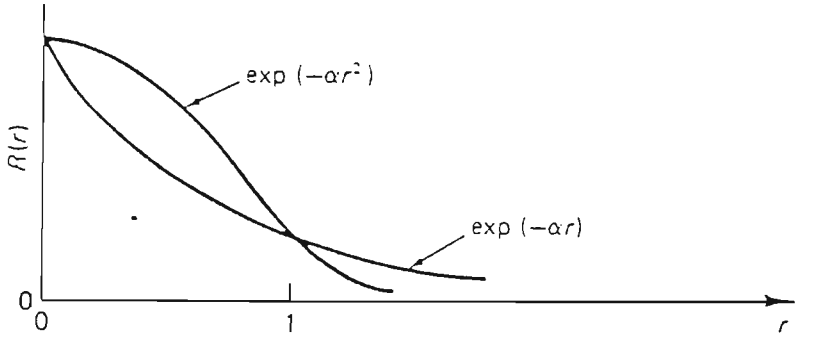

Fig.2.1 Radial dependence of hydrogen-like and gaussian functions.

In practice each STO in a basis set is replaced by a number of Gaussian functions. One first creates primitive Gaussian functions by choosing several values for α. Once this approximation is optimized, the linear combination of Gaussian functions is 'frozen', being treated thereafter as a single

function. This linear combination of primitive Gaussian functions is called a contracted Gaussian function.[62]

A minimal basis set is the smallest number of atomic orbitals necessary to accommodate all the electrons of the atoms in their ground states and maintain overall spherical symmetry of the atoms, e.g. 1s on hydrogen; 1s, 2s, $2p_x$, $2p_y$ and $2p_z$ on carbon.[54,62] The STO-nG basis set is a fixed set of n Gaussian functions, which gives an approximate representation of a minimal basis set of STOs.[60] In other words, the Gaussian functions simulate STOs. The smallest basis set is STO-3G.

Minimal basis sets are inadequate in describing systems with anisotropic distributions of the electrons.[61] Such difficulties can be overcome by including more than a single set of valence p- or d-type functions in the basis set. Two sets of isotropic p-functions, for example, are included in the representation, one held tightly to the nucleus and one relatively diffuse. This allows independent variation of the radial parts of the two sets of p-functions, thus forming more contracted (or more diffuse) functions that would be more appropriate in describing, for example, σ and π systems, respectively. A basis set formed by doubling all functions in a minimal representation is known as a *double-zeta* basis set, while one in which only the basis functions for the outer, valence shells are doubled, is known as a *split-valence* basis set.[61]

In polarization basis sets, which are the next level of improvement in the basis set, p- or d-functions are added to the relevant atoms, giving added

flexibility to the basis set. These functions allow electron density to polarize in energetically favourable directions. Basis sets incorporating diffuse functions are also available to the user, which provide a more accurate description of molecules in which a large portion of the valence-electron density is allocated to diffuse lone-pair or to antibonding orbitals.

In this work, all calculations were conducted using the 6-31G** basis set, which is analyzed as follows:[61]

The inner (1s) shell of first row elements (B to F) is represented by a single function which is expanded in terms of six primitive Gaussians. The valence shell (2s and 2p) is split into an inner, tightly held part, which is expanded in terms of three primitive Gaussians, and an outer, more diffuse part, which is written in terms of one primitive Gaussian. A * indicates that a single set of Gaussian d-type functions has been added to each non-hydrogen atom. Two asterisks, as in the basis set under consideration, indicates that in addition to the above, a set of Gaussian p-type functions has been included in representations of each H or He atom.

2.2.6 Computing Vibrational Properties

The vibrational motion of a molecule is observed experimentally via infrared and Raman spectroscopy. These techniques can be used to determine the structure of a molecule and its environment since these factors affect the vibrational frequencies. In order to gain useful information, it is necessary

to determine what vibrational motion corresponds to each peak in the spectra. This assignment can prove difficult, due to the large number of closely spaced peaks often observed even in fairly simple molecules. In order to aid in this assignment, computer simulations can be used to calculate the vibrational frequencies of the molecules. There are a number of computational methods available which have varying degrees of accuracy and difficulty.

The simplest description of a vibration is that of a harmonic oscillator, which describes the motion of springs exactly and of pendula with small amplitudes reasonably well.[52] A harmonic oscillator is defined by the potential energy, being proportional to the square of the distance displaced from an equilibrium position. In a classical treatment of a vibrating object, the motion is fastest at the equilibrium position and comes to a complete stop for an instant at the turning point, where all the energy is potential energy. The probability of finding the object is highest at the turning point. A quantum mechanical description of a harmonic oscillator uses the same potential energy function but gives radically different results. In a quantum description there are no turning points, with the probability of finding an object at large distances becoming increasingly small.

The vibration of a molecule is best described using a quantum mechanical approach. However, molecules do not behave according to a harmonic oscillator description. However such a description is used as an approximate treatment for low vibrational quantum numbers. Solving the quantum mechanical Schrödinger equation involves approximations and *ab initio*

methods employ mathematical approximations only. Owing to the difference between the harmonic and the true potentials, frequencies computed with *ab initio* methods (which use a quantum harmonic oscillator approximation) tend to be overestimated.[61] A good estimate of the experimental results is often achieved by multiplying the *ab initio* wavenumbers by a factor of 0.9.

Before frequencies can be calculated, the program must compute the geometry of the molecule since the normal vibrational modes are centred at the equilibrium geometry. When a negative frequency is computed for a particular stationary point, it indicates that the stationary point corresponds to a maximum of potential energy with respect to the positions of the nuclei. A negative frequency characterizes a transition state and signifies that the stationary point does not correspond with a genuine minimum on the potential energy curve.

Peak intensities can also be calculated computationally. Infrared and Raman peak intensities depend on the probability that a particular wavelength photon will be absorbed or scattered. These probabilities can be computed from the wave function by first computing the transition dipole moment.

2.2.7 Energy Decomposition Analysis

Ab intio SCF MO theories have been extensively employed for the interpretation of the nature of the hydrogen bond interaction. The hydrogen bond energy has often been conveniently decomposed into various

components in order to understand the mechanism and character of hydrogen bonding. Such an estimate was first conducted by Coulson[41] for the $H_2O...H_2O$ interaction. The total energy was decomposed into the electrostatic energy, the dispersion energy, the repulsion energy, the delocalization energy and the net hydrogen bond energy. Grahn[66] used a simple quantum mechanical model to evaluate the electrostatic energy and the polarization energy. The stabilization energy gained by the bond formation has been broken down by Morokuma[67,68] into electrostatic (E_{es}), electron-exchange repulsion (E_{ex}), polarization (E_{pl}), charge transfer (E_{ct}) and coupling, or mixing, energies. This charge distribution decomposition analysis has proven to be a powerful method for direct analysis of the origin of molecular interactions.[69-72]

The stabilization energy

$$\Delta E = E_{complex} - \sum E_{monomers} \qquad (2.18)$$

and the charge distribution rearrangement

$$\Delta \rho(r) = \rho(r)_{complex} - \sum \rho(r)_{monomers} \qquad (2.19)$$

may thus be separated as follows:

$$\Delta E = E_{es} + E_{pl} + E_{ex} + E_{ct} + E_{mix} \qquad (2.20)$$

$$\Delta \rho(r) = \rho_{pl}(r) + \rho_{ex}(r) + \rho_{ct}(r) + \rho_{mix}(r) \qquad (2.21)$$

These terms have the following physical meanings:[67]

es is the electrostatic interaction. It includes the interactions of all permanent charges and multipoles, such as dipole-dipole, dipole-quadrupole, etc. This interaction may be either attractive or repulsive.

pl is the polarization interaction, or the effect of the distortion of the electron distribution of molecule A by molecule B, the distortion of B by A, and the higher order coupling resulting from such distortions. It includes the interactions of all permanent charges or multipoles and induced multipoles, such as dipole-induced dipole, quadrupole-induced dipole, etc. This interaction is always attractive.

ex is the exchange repulsion. This is the short-range repulsion due to overlap of the electron distribution of A with that of B.

ct is the charge transfer or electron delocalization interaction. It is the interaction caused by the charge transfer from occupied molecular orbitals of A to vacant molecular orbitals of B, and from occupied molecular orbitals of B to vacant molecular orbitals of A, and the higher order coupled interactions.

mix is the coupling term. It is the difference between the total interaction energy, ΔE, and the sum of the above four components and accounts for higher order interaction between the various components.

Using model wave functions such as the partially antisymmetrized wave function or the wave functions from a model Hartree-Fock matrix, individual components of the total interaction energy may be specified within the Hartree-Fock method. We now further define contribution nomenclature and the appropriately associated wavefunctions.

The separated molecules, A and B, have wavefunctions $\mathbb{A}\psi_A^0$ and $\mathbb{A}\psi_B^0$, respectively, with the sum of the energy E_0, where $\mathbb{A}$ is an antisymmetrizer.[68] As the molecules approach, the following wavefunctions can be constructed:

i) *The Hartree (nonantisymmetrized) product of isolated molecular wavefunctions.* The wavefunction is $\mathbb{A}\psi_A^0.\mathbb{A}\psi_B^0$ and the energy is E_1. This describes the classical Coulombic interaction of the two rigid molecules.

ii) *The Hartree product of two molecular wavefunctions which are individually optimized in the presence of the other molecule.* The wavefunction is $\mathbb{A}\psi_A.\mathbb{A}\psi_B$ and the energy is E_2. Here, each molecule is polarized by the presence of the other.

iii) *The Hartree-Fock (antisymmetrized) product of two molecular wavefunctions.* The wavefunction is $\mathbb{A}(\Psi_A^0.\Psi_B^0)$ and the energy is E_3. Molecular orbitals in Ψ_A^0 are not, in general, orthogonal to molecular orbitals in Ψ_B^0. The same energy is calculated more simply by the wavefunction in which occupied molecular orbitals are orthogonalized to each other. The electron exchange between A and B is

incorporated in the calculation.

iv) *The SCF wavefunction for the whole system.* The wavefunction is $\mathbb{A}_{\psi AB}$ and the energy is E_4.

The difference between E_0 and E_1 is the electrostatic energy. That between E_1 and E_2 is the polarization and dispersion contribution E_{pd}. E_{es} and E_{pd} are van der Waals interactions. $E_1 - E_3$ is the exchange repulsion. From E_3 to E_4 the system gains E_{pd} as well as charge transfer, E_{ct}, between the molecules. Similarly, $E_2 - E_4$ includes both E_{ex} and E_{ct}. E_{ct} is thus obtained by $E_2 + E_3 - E_1 - E_4$.

2.3 *Ab initio* Molecular Orbital Calculations - Practical Considerations

2.3.1 *Ab initio* Programs

The optimized geometries, energies and vibrational wavenumbers reported in this work were performed using the Gaussian 92[73] program, running on a Hewlett-Packard HP720 computer. Owing to the relative complexity of the monomer and aggregate species, we were precluded from performing the calculations at the second order Møller-Plesset (MP2)[74] or higher level, and they were carried out at the restricted Hartree-Fock level instead[61]. The 6-31G** basis set was employed.[75] Molecular orbital calculations were effected using *ab initio* Hartree-Fock theory, based on the LCAO approach. Results of all calculations appear in subsequent chapters.

Gaussian 92 is a connected system of programs capable of performing semiempirical and *ab initio* molecular orbital calculations. It represents further development of the Gaussian 70, Gaussian 76, Gaussian 80, Gaussian 82, Gaussian 86, Gaussian 88 and Gaussian 90[76-82] systems already published. The Gaussian series of programs deals exclusively with Gaussian-type orbitals and includes several optional GTO basis sets of varying size. These include minimal basis sets, double zeta and split-valence basis sets, and basis sets which include both polarization and diffuse functions.

Gaussian 80 was the first of the series to contain procedures extending

beyond the Hartree-Fock single determinant model. Electron correlation calculations employing Møller-Plesset perturbation theory[74] were made possible. Since Gaussian 80, correlation calculations have been extended to fourth order Møller-Plesset perturbation theory (MP4). In Gaussian 80, three automatic geometry optimization procedures were incorporated - Berny,[83] Murtaugh-Sargent[84] and Fletcher-Powell.[85] Unless otherwise specified, the program defaults to the Berny optimization method. In the Berny method, four criteria are used to determine whether a minimum energy geometry has been obtained. These are the maximum force, the root mean square force, the maximum displacement between the most recent point and the next to be computed and the root mean square displacement. In addition, convergence criteria options have been introduced which limit the forces and step sizes that are used to determine optimum energies and vibrational frequencies. These convergence criteria are designated TIGHT and VERYTIGHT.

Gaussian 86 saw the introduction of several semiempirical models as well as the predictions of the infrared intensities along with the frequencies. In Gaussian 88, direct SCF methods were introduced which permit recomputation of the two-electron integrals on each SCF iteration, thereby avoiding the need for extensive external storage. Gaussian 90 saw the efficiency of direct SCF frequency calculations improved, and the incorporation of direct and semi-direct MP2 methods. New features and efficiency improvements in Gaussian 92 increased the performance of all direct (no integral storage required) and "in-core" (storing the atomic orbital integrals in memory) calculations, as well as all frequency calculations.

2.3.2 Calculation of Structure and Geometry

To initiate an *ab initio* molecular orbital calculation , an input file is required. The input for the Gaussian series of programs is divided into a number of sections. Firstly, the method and level of theory employed is specified. For example, the route card "# RHF/6-31G**" indicates that a restricted Hartree-Fock calculation with the split-valence 6-31G basis set with polarization functions placed on all atoms, should be carried out.
The "#" sign denotes initialization of the input.

On the same line, the task to be performed is specified, together with the convergence criterion, for an optimization, for example, optimization of geometry to an energy minimum, single point calculation, calculation of harmonic vibration frequency, etc. OPT=TIGHT indicates an optimization at the tight convergence level.

The second section of the input is a description of the computation while the third section specifies the charge and multiplicity, and the geometry of the molecule of interest. The number of electrons of α and β spin is specified (implicitly) by first giving the net charge, followed by the multiplicity. The Z-matrix gives the description of the molecular geometry, and is given in terms of bond lengths, bond angles and dihedral angles. The identities and starting values of the geometrical parameters to be varied are then given.

For complete optimization of a molecule consisting of N atoms without symmetry, a total of 3N-6 (3N-5 for a diatomic molecule) independent

parameters must be considered. This number represents the 3N degrees of freedom of the molecule minus the three translations and three rotations (two for diatomic molecules). The number of independent parameters is reduced by the use of symmetry. Once the molecular geometry is specified, the program initiates a complete theoretical treatment of the equilibrium structure, which involves minimization of the energy with respect to each independent geometrical parameter. The resulting structure is termed "optimized".

In this work the VERYTIGHT convergence criterion was used.

2.3.3 Representation of Structure and Normal Modes

Calculation of the normal modes of vibration is executed by the Gaussian series of programs by specifying the FREQ keyword. The input file specifies the computationally determined optimized geometry of the molecular complex under consideration. In order to facilitate the assignments of the calculated infrared wavenumbers and intensities to particular modes of vibration, the Cartesian coordinates of the displacement vectors of each atom, for each mode, are added to the principal cartesian coordinates, thereby defining the coordinates of the positions achieved by the atoms at the turning points of each normal mode of vibration. With the aid of the information obtained from the output file, pictorial representations of these vibrational modes can then be drafted by means of the program

SCHAKAL.[86] The Cartesian coordinates were also used by the SCHAKAL program for the visualization of the optimised structures of the molecular complexes.

a) Nomenclature

Due to the sizes of the molecular complexes involved in this project, only the intramolecular and intermolecular modes affected by and arising as a result of the formation of a hydrogen bond will be discussed. The nomenclature is as follows:[87,88]

Intramolecular modes

i) ν - bond stretch or compression. In the case of coupled stretching modes, the subscripts *s* (symmetric) and *a* (antisymmetric) will be used.

ii) δ - bending or bond angle deformation. Bending modes may likewise be designated symmetric or antisymmetric.

iii) γ - bending, in cases when the deformation of the bond angle involves motion of the atoms out of the symmetry plane of the molecule or complex.

Intermolecular modes[88,89]

When two non-linear monomeric species, X and Y, having n_X and n_Y atoms respectively, associate to form a hydrogen bonded complex, the number of normal modes of vibration of the complex, $3(n_X + n_Y)-6$, exceeds the sum of the normal modes of the monomers by six.[88] These six additional modes are intermolecular vibrations and are derived from the counter translational

and rotational motions of the two monomers against one another,[3] such that the angular momentum and the position of the centre of mass of the complex are conserved.[89]

The counter translational and rotational motions of the monomer units are designated T_α and R_α (α = x, y, z), specifying translation along, and rotation about, the α axis respectively.[88,89] The descriptions of these modes[89] used in this work are: T_x, the in-plane shear, T_z, the hydrogen bond stretch, R_y, the in-plane bend, T_y, the out-of-plane shear, R_x, the out-of-plane bend and R_z, a torsion mode.

2.3.4 Basis Set Superposition Error (BSSE)

A standard definition of the interaction energy, ΔE, for a complex X...Y is given by:

$$\Delta E = E_{XY} - (E_X - E_Y) \qquad (2.22)$$

where E_{XY} is the energy of the complex and E_X and E_Y are the energies of the monomers, X and Y, respectively. The energies of the monomers are determined separately using their own basis sets. However, in the energy calculation of the X...Y complex, all the orbitals of both X and Y are available to the dimer. As a consequence, the basis set of each monomer is extended by the presence of the other, which results in a mathematical lowering of the monomer energies. This is referred to as the basis set

superposition error (BSSE).[90]

Counterpoise calculations are sometimes used to estimate the magnitude of the BSSE.[91] This provides a crude estimate. In this method the energies of the monomers X and Y are calculated separately within the basis set of the whole dimer X...Y. This is achieved by specifying the dimer as usual (in the Z-matrix) and, together with the MASSAGE keyword, providing additional information which changes the nuclear and electronic charges in one monomer to zero. This monomer is known as the ghost molecule. Basis functions are assigned before the massage input is processed, so both monomers will have their normal basis functions, while the number of electrons is computed after the massage input is processed. Setting the nuclear charges to zero in one monomer will automatically remove both the nuclear charges and the electrons from those atoms. Both monomers, X and Y, will now have a corrected intermolecular interaction energy, E_X' and E_Y' respectively. Hence the BSSE corrected intermolecular energy $\Delta E'$ is:[92,93]

$$\Delta E'=E_{XY}-(E_X'+E_Y') \qquad (2.23)$$

where

$$BSSE=\Delta E'-\Delta E \qquad (2.24)$$

An attractive energy will result in ΔE or $\Delta E'$ being negative. As a result of the initial overestimation of the interaction energy, the BSSE will be a positive quantity. The full counterpoise procedure as originally promoted by Boys and Bernardi [91] was employed for computing the BSSE for all molecular complexes considered in this project.

2.4 Theoretical Results

2.4.1 Optimized Geometries of the Monomers

The optimized geometries of the CH_3OH, $(CH_3)_2NH$, CH_3SH, $(CH_3)_2O$, $(CH_3)_3N$ and $(CH_3)_2S$ monomers, together with those of the hydrogen bonded molecular complexes $CH_3OH.(CH_3)_2O$, $CH_3OH.(CH_3)_3N$, $CH_3OH.(CH_3)_2S$, $(CH_3)_2NH.(CH_3)_2O$, $(CH_3)_2NH.(CH_3)_3N$, $(CH_3)_2NH.(CH_3)_2S$, $CH_3SH.(CH_3)_2O$, $CH_3SH.(CH_3)_3N$ and $CH_3SH.(CH_3)_2S$, were carried out using the Gaussian-92 computer program at the restricted Hartree-Fock (RHF) level of theory using the BERNY optimization[83] method. The 6-31G** split valence basis set was employed and optimizations were effected with the VERYTIGHT convergence criterion.[73] Table 2.1 lists the computed properties of the six monomer species. In the cases of CH_3OH, $(CH_3)_2O$ and $(CH_3)_2NH$ two stationary points were investigated. For CH_3OH these were the structures in which the OH bond was staggered (I) and eclipsed (II) with respect to the CH_3 group; for the $(CH_3)_2O$ the two conformations were those in which the CH bonds lying in the plane of the heavy atoms were *anti* (I) and *syn* (II) to the opposite CO bonds; similarly for $(CH_3)_2NH$ they were the species in which the CH bonds lying in the heavy atom plane were *anti* (I) and *syn* (II) in relation to the opposite CN bonds. The trimethylamine monomer was optimized only in the conformation in which one of the CH bonds for each methyl group was constrained to be *anti* to the axial nitrogen lone pair. Methane thiol and dimethyl sulphide were optimized in a similar configuration to the lowest conformations of methanol (conformation I) and dimethyl ether (conformation I), respectively.

The optimized structures of all six monomers are reported in Tables 2.2 to 2.9, and the atom numbering conventions are illustrated in Figures 2.2 - 2.7, by means of plots executed using the SCHAKAL[86] plotting program. Tables 2.2 to 2.9 also show the experimental bond angles, the dihedral angles, some literature *ab initio* structures for comparison and the calculated - experimental differences determined in this work.

Table 2.1. Point group symmetries, absolute energies and dipole moments calculated for the methanol, dimethyl ether, dimethylamine, trimethylamine, methane thiol and dimethyl sulphide monomers.

Monomer	conformation	Point group	Absolute energy/a.u.	Dipole moment/D[a]
CH_3OH	I	C_s	-115.0467101	1.83
	II	C_s	-115.0446452	1.93
$(CH_3)_2O$	I	C_{2v}	-154.0741083	1.48
	II	C_{2v}	-154.0668203	1.61
$(CH_3)_2NH$	I	C_s	-134.2516371	1.09
	II	C_s	-134.2416687	1.22
$(CH_3)_3N$		C_{3v}	-173.2828593	0.75
CH_3SH		C_s	-437.7090273	1.78
$(CH_3)_2S$		C_{2v}	-476.7450049	1.80

[a] 1 D $\equiv$ 3.336×10^{-30} C m.

Table 2.2. Optimized structural parameters of the methanol monomer, in the staggered conformation (I), corresponding literature values, and calculated-experimental differences.

Parameter[a]	Calculated (this work)	(ref. 4)[c]	Experimental (ref. 7)[d]	Difference[b] (this work)
$r(OH_1)$ /pm	94.23	94.2	94.5	-0.3
r(CO) /pm	139.85	139.9	142.5	-2.6
$r(CH_2)$ /pm	108.20	108.2	109.4	-1.2
$r(CH_3)$, $r(CH_4)$ /pm	108.82	108.8	109.4	-0.6
$C\hat{O}H_1$ /deg	109.7	109.7	108.5	1.2
$H_2\hat{C}O$ /deg	107.3	107.3		
$H_3\hat{C}O$, $H_4\hat{C}O$ /deg	112.1	112.1		
$H_3\hat{C}H_4$ /deg	108.6	108.6	108.6	0.0
$H_2\hat{C}H_3$, $H_2\hat{C}H_4$ /deg	108.3	108.3	108.6	-0.3
$H_3\hat{C}OH_1$, $H_4\hat{C}OH_1$ [e]/deg	61.2			

[a] See Figure 2.2 for numbering of atoms

[b] Difference = calculated - experimental parameter

[c] RHF/6-31G**

[d] Effective geometry

[e] Dihedral angle

Table 2.3. Optimized structural parameters of the methanol monomer, in the eclipsed conformation (II), corresponding literature values, and calculated-experimental differences.

Parameter[a]	Calculated (this work)	Experimental (ref. 7)[c]	Difference[b] (this work)
$r(OH_1)$ /pm	94.03	94.5	-0.5
r(CO) /pm	140.22	142.5	-2.2
$r(CH_2)$ /pm	108.64	109.4	-0.8
$r(CH_3)$, $r(CH_4)$ /pm	108.52	109.4	-0.9
$C\hat{O}H_1$ /deg	110.36	108.5	1.8
$H_2\hat{C}O$ /deg	112.3		
$H_3\hat{C}O$, $H_4\hat{C}O$ /deg	109.9		
$H_3\hat{C}H_4$ /deg	108.4	108.6	-0.2
$H_2\hat{C}H_3$, $H_2\hat{C}H_4$ /deg	108.1	108.6	-0.5
$H_3\hat{C}OH_1$, $H_4\hat{C}OH_1$ [d]/deg	120.4		

[a] See figure 2.2 for numbering of atoms

[b] Difference = calculated - experimental parameter

[c] Effective geometry

[d] Dihedral angle

Table 2.4. Optimized structural parameters of the dimethyl ether monomer, in conformation I , corresponding literature values, and calculated-experimental differences.

Parameter[a]	Calculated (this work)	Calculated (ref. 14)[c]	Experimental (ref. 13)[d]	Difference[b] (this work)
$r(C_1O)$, $r(C_2O)$ /pm	139.15	139.15	141.0	-1.8
$r(C_1H_1)$, $r(C_2H_4)$ /pm	108.19	108.20	109.1	-0.9
$r(C_1H_2)$, $r(C_1H_3)$, $r(C_2H_5)$, $r(C_2H_6)$ /pm	108.97	108.97	110.0	-1.0
$C_1\hat{O}C_2$ /deg	113.9	113.89	111.7	2.2
$H_1\hat{C}_1O$, $H_4\hat{C}_2O$ /deg	107.7		107.2	0.5
$H_2\hat{C}_1O$, $H_3\hat{C}_1O$, $H_5\hat{C}_2O$, $H_6\hat{C}_2O$ /deg	111.6		110.8	0.8
$H_2\hat{C}_1H_3$, $H_5\hat{C}_2H_6$ /deg	108.3	108.29	108.7	-0.4
$H_1\hat{C}_1H_2$, $H_1\hat{C}_1H_3$, $H_4\hat{C}_2H_5$, $H_4\hat{C}_2H_6$ /deg	108.8	108.82	109.6	-0.8
$H_2\hat{C}_1OC_2$, $H_3\hat{C}_1OC_2$, $H_5\hat{C}_2OC_1$, $H_6\hat{C}_2OC_1$°/deg	60.7			

[a] See Figure 2.5 for numbering of atoms

[b] Difference = calculated - experimental parameter

[c] RHF/6-31G**

[d] Substitution structure [e] Dihedral angle

Table 2.5. Optimized structural parameters of the dimethyl ether monomer, in conformation II , experimental values, and calculated-experimental differences.

Parameter[a]	Calculated (this work)	Experimental (ref. 13)[c]	Difference[b] (this work)
$r(C_1O)$, $r(C_2O)$ /pm	139.56	141.0	-1.4
$r(C_1H_1)$, $r(C_2H_4)$ /pm	108.63	109.1	-0.4
$r(C_1H_2)$, $r(C_1H_3)$, $r(C_2H_5)$, $r(C_2H_6)$ /pm	108.59	110.0	-1.6
$C_1\hat{O}C_2$ /deg	113.9	111.7	2.2
$H_1\hat{C}_1O$, $H_4\hat{C}_2O$ /deg	112.2	107.2	5.0
$H_2\hat{C}_1O$, $H_3\hat{C}_1O$, $H_5\hat{C}_2O$, $H_6\hat{C}_2O$ /deg	109.8	110.8	-1.0
$H_2\hat{C}_1H_3$, $H_5\hat{C}_2H_6$ /deg	108.3	108.7	-0.4
$H_1\hat{C}_1H_2$, $H_1\hat{C}_1H_3$, $H_4\hat{C}_2H_5$, $H_4\hat{C}_2H_6$ /deg	56.9		
$H_2\hat{C}_1OC_2$, $H_3\hat{C}_1OC_2$, $H_5\hat{C}_2OC_1$, $H_6\hat{C}_2OC_1$[d]/deg	60.7		

[a] See Figure 2.5 for numbering of atoms

[b] Difference = calculated - experimental parameter

[c] Substitution structure

[d] Dihedral angle

Theoretical bond lengths and angles for the lowest energy structures are in good agreement with experimental values. The C-A bond lengths in the proton donors, in all cases, are shorter than the experimental values. The errors in the calculated RHF/6-31G** bond lengths vary from complex to complex. For example, the C-O bond length deviates by 1.9% from the experimental value in methanol, and by 1.3% in the case of dimethyl ether. The C-N bond length difference in dimethylamine is 1.1%, while for trimethylamine a difference of 0.4 % is observed. At this level of theory, the calculations are relatively successful in reproducing the C-S bond lengths in methane thiol and dimethyl sulphide, where percentage variances from experimental values were found to be 0.1 and 0.4 respectively. All the C-H bond lengths are slightly underestimated (except in the case of C_1H_2 in dimethylamine, which is correctly reproduced), with a mean absolute percentage difference of 0.7, representing a very good agreement with the experimental data. The computed bond angles around the O, N and S atoms are usually overestimated, as has been found before at this level.[94] It is a well known fact that the 6-31G** basis set tends to predict shorter bond lengths and to overestimate the bond angles.[61] In no instance does a calculated bond angle deviate by more than 2.2°, or 1.9 % from experiment. Our values are also generally in good agreement with the other calculated geometrical parameters, allowing for differences caused by the use of different basis sets in some cases. The asymmetry of the methyl group is reproduced faithfully in each case, with the longer bonds of the set invariably being found *anti* to the N lone pair in the case of trimethylamine, and *syn* to the O and S lone pairs in the case of dimethyl ether (conformation I) and dimethyl sulphide, respectively. In the cases of $(CH_3)_2O$

and $(CH_3)_3N$ this distinction has been observed experimentally,[13,18] while for $(CH_3)_2NH$ Wollrab and Laurie were able to distinguish between the bond lengths of the C_1H_2, C_2H_5 pair and the four remaining CH bonds, but failed to separate the two different pairs from among C_1H_3, C_1H_4, C_2H_6 and C_2H_7 [21]. The asymmetry of the methyl groups bonded to atoms bearing lone pairs of electrons has been interpreted in terms of the different interactions existing between orbitals containing bonding pairs and lone pairs of electrons.[5,95]

The staggered conformation of methanol is energetically more stable than the eclipsed form. Methanol contains diastereotopic methyl hydrogens. The in-plane CH_2 bond, antiperiplanar to the O-H bond, in the staggered conformation is the shorter of those in the methyl set, while the in-plane CH_2 bond in the methyl group in the eclipsed form is the longest of the set. Conformation I of dimethyl ether is more stable than conformation II. As in the case of dimethyl sulphide, the molecule has C_{2v} symmetry, with each methyl group being staggered against the opposite C-O or C-S bond. Again, the in-plane C_1H_1/C_2H_4 bond in conformation I is the shorter of those in the methyl sets, while the in-plane C_1H_1/C_2H_4 bond of the methyl group in conformation II is the longer of the sets. In the case of methane thiol, the in-plane CH_2 bond, antiperiplanar to the S-H bond, in the staggered conformation is the longer of those in the methyl group.

Table 2.6. Optimized structural parameters of the dimethylamine monomer, in conformation I , corresponding literature values, and calculated-experimental differences.

Parameter[a]	Calculated (this work)	Calculated (ref. 4)[c]	Experimental (ref. 96)[d]	Difference[b] (this work)
$r(NH_1)$ /pm	99.94	99.9	101.9	-2.0
(C_1N), $r(C_2N)$ /pm	144.57	146.1	146.2	-1.6
$r(C_1H_2)$, $r(C_2H_5)$ /pm	108.45	108.0	108.4	0.0
$r(C_1H_3)$, $r(C_2H_6)$ /pm	109.40	109.0	109.8	-0.4
$r(C_1H_4)$, $r(C_2H_7)$ /pm	108.54	108.1	109.8	-1.3
C_1NC_2 /deg	113.8	115.1	112.2	1.6
H_1NC_1, $H_1N\hat{C}_2$ /deg	110.2	112.3	108.9	1.3
$H_2\hat{C}_1N$, $H_5\hat{C}_2N$ /deg	109.7	109.4	109.7	0.0
$H_3\hat{C}_1N$, $H_6\hat{C}_2N$ /deg	114.0	114.0	113.8	0.2
$H_4\hat{C}_1N$, $H_7\hat{C}_2N$ /deg	109.4	109.2	108.2	1.2
$H_3\hat{C}_1H_4$, $H_6\hat{C}_2H_7$ /deg	107.6	107.6	107.2	0.4
$H_2\hat{C}_1H_3$, $H_5\hat{C}_2H_6$ /deg	108.1	108.5	109.0	-0.9
$H_2\hat{C}_2H_4$, $H_5\hat{C}_2H_7$ /deg	107.8	108.0	109.0	-1.2
$H_2\hat{C}_1NC_2$, $H_5\hat{C}_2NC_1$ °/deg	178.3		f	
$H_2\hat{C}_1NH_1$, $H_5\hat{C}_2NH_1$ °/deg	60.3		g	
$H_3\hat{C}_1NH_1$, $H_6\hat{C}_2NH_1$ °/deg	119.7		g	
$H_4\hat{C}_1NH_1$, $H_7\hat{C}_2NH_1$ °/deg	180.0		g	

[a] See Figure 2.3 for numbering of atoms

[b] Difference = calculated - experimental parameter

[c] RHF/ (73/53) Gaussian lobe basis set

[d] Substitution structure

[e] Dihedral angle

[f] H_2 and H_5 atoms lie in the CNC plane, within experimental error

[g] CH_3 groups tilted towards the N lone pair by 3.4°

Table 2.7. Optimized structural parameters of the trimethylamine monomer, corresponding literature values, and calculated-experimental differences.

Parameter[a]	Calculated (this work)	Calculated (ref. 23)[c]	Experimental (ref. 22)[d]	Difference[b] (this work)
(C_1N), $r(C_2N)$, $r(C_3N)$ /pm	144.49	145.32	145.1	-0.6
$r(C_1H_1)$, $r(C_2H_4)$, $r(C_3H_7)$ /pm	109.63	110.58	110.9	-1.3
$r(C_1H_2)$, $r(C_1H_3)$ $r(C_2H_5)$, $r(C_2H_6)$ $r(C_3H_8)$, $r(C_3H_9)$ /pm	108.43	109.32	108.8	-0.4
C_1NC_2, C_2NC_3, C_3NC_1/deg	112.0	110.44	110.9	1.1
$H_1\hat{C}_1N$, $H_4\hat{C}_2N$ $H_7\hat{C}_3N$ /deg	112.7	112.81	111.7	1.0
$H_2\hat{C}_1N$, $H_3\hat{C}_1N$, $H_5\hat{C}_2N$ $H_6\hat{C}_2N$, $H_8\hat{C}_3N$, $H_9\hat{C}_3N$/deg	110.1	109.50	110.1	0.0
$H_2\hat{C}_1H_3$, $H_5\hat{C}_2H_6$ $H_8\hat{C}_3H_9$/deg	108.9	108.30	108.6	0.3
$H_1\hat{C}_1H_2$, $H_1\hat{C}_1H_3$, $H_4\hat{C}_2H_5$, $H_4\hat{C}_2H_6$, $H_7\hat{C}_3H_8$, $H_7\hat{C}_3H_9$ /deg	107.5	108.31	108.1	-0.6
$H_1\hat{C}_1NX$, $H_4\hat{C}_2NX$, $H_7\hat{C}_3NX$ [e,f]/deg	180.0		g	

Table 2.7 cont.

$H_2\hat{C}_1NX$, $H_3\hat{C}_1NX$, $H_5\hat{C}_2NX$, $H_6\hat{C}_2NX$, $H_8\hat{C}_3NX$, $H_9\hat{C}_3NX$ [e,f]/deg	60.0	g

[a] See Figure 2.6 for numbering of atoms

[b] Difference = calculated - experimental parameter

[c] MP2/6-31G*

[d] Substitution structure

[e] Dihedral angle

[f] X is located on the symmetry axis in the *anti* position to the C_1H_1, C_2H_4 and C_3H_7 bonds.

[g] CH_3 groups tilted towards the N lone pair by 1.3°

Table 2.8. Optimized structural parameters of the methane thiol monomer, experimental values, and calculated-experimental differences.

Parameter[a]	Calculated (this work)	Experimental (ref. 97)[c]	Difference[b] (this work)
$r(SH_1)$ /pm	132.72	133.5	-0.8
r(CS) /pm	181.74	181.9	-0.2
$r(CH_2)$ /pm	108.17	109.2	-1.0
$r(CH_3)$, $r(CH_4)$ /pm	108.11	109.2	-1.1
$C\hat{S}H_1$ /deg	98.02	96.5	1.5
$H_2\hat{C}S$ /deg	106.59		
$H_3\hat{C}S$, $H_4\hat{C}S$ /deg	111.24		
$H_3\hat{C}H_4$ /deg	110.10	109.75	0.3
$H_2\hat{C}H_3$, $H_2\hat{C}H_4$ /deg	108.78	109.75	-1.0
$H_3\hat{C}SH_1$, $H_4\hat{C}SH_1$ [d]/deg	61.56	e	

[a] See Figure 2.4 for numbering of atoms

[b] Difference = calculated - experimental parameter

[c] Effective geometry

[d] Dihedral angle

[e] Methyl tilt is 2.17°

Table 2.9. Optimized structural parameters of the dimethyl sulphide monomer, corresponding literature values, and calculated-experimental differences.

Parameter[a]	Calculated (this work)	Calculated (ref. 12)[c]	Experimental (ref. 98)[d]	Difference[b] (this work)
$r(C_1S)$, $r(C_2S)$ /pm	180.80	181.7	180.2	0.6
$r(C_1H_1)$, $r(C_2H_4)$ /pm	108.23	109.2	109.1	-0.9
$r(C_1H_2)$, $r(C_1H_3)$ $r(C_2H_5)$, $r(C_2H_6)$ /pm	108.32	109.3	109.1	-0.8
$C_1\hat{S}C_2$ /deg	100.18	99.5	98.9	1.3
$H_1\hat{C}_1S$, $H_4\hat{C}_2S$ /deg	107.37	107.3	106.6	0.8
$H_2\hat{C}_1S$, $H_3\hat{C}_1S$ $H_5\hat{C}_2S$, $H_6\hat{C}_2S$ /deg	111.14	110.9	110.8	0.3
$H_2\hat{C}_1H_3$, $H_5\hat{C}_2H_6$ /deg	108.76	108.9	109.5	-0.7
$H_1\hat{C}_1H_2$, $H_1\hat{C}_1H_3$ $H_4\hat{C}_2H_5$, $H_4\hat{C}_2H_6$ /deg	109.59	109.8	109.6	0.0
$H_2\hat{C}_1SC_2$, $H_3\hat{C}_1SC_2$ $H_5\hat{C}_2SC_1$, $H_6\hat{C}_2SC_1$ [e]/deg	61.2			

[a] See Figure 2.7 for numbering of atoms

[b] Difference = calculated - experimental parameter

[c] MIDI-4 basis set with polarization functions

[d] Substitution structure

[e] Dihedral angle

In all cases except methane thiol, the CH bond of the methyl groups nearest the heavy atom lone pair is the shorter and stronger of the set. It seems natural to seek an interpretation of this phenomenon in terms of "lone pair" effects. Such an interpretation has been undertaken by Wolfe *et al.*[6] In the case of methanol (staggered form), there are two energetically nonequivalent lone pairs. One, n_p, is derived mainly from the *2p* atomic orbital of oxygen that is perpendicular to the H-O-C plane; the other, n_s, is a hybrid orbital containing contributions from the *2p* atomic orbital of oxygen that lies in the H-O-C plane, and from the *1s* atomic orbital of hydrogen and the *2s* or *2p* atomic orbitals of carbon.[99,100] The experimental energy difference between n_p and n_s is 148.7 kJ mol^{-1}. [101]

Symmetry allowed charge transfer is possible[6]

a) between n_p and π^*,

b) between n_s and π^* and

c) between π and σ^*_{OH}.

Interaction a) leads to a weakening of the out-of-plane CH_3/CH_4 bonds, because CH_2 lies in the *xz* nodal plane and its atomic orbital coefficient is zero in both π and π^* orbitals. Interactions b) and c) both lead to a preferential weakening of CH_2, because the H_2 atomic orbital coefficient is larger than those of H_3 and H_4. Wolfe *et al.* [6] explain that since the magnitude of a stabilizing orbital interaction is inversely proportional to the energy difference between the donor and acceptor orbitals, interaction a) is expected to dominate, causing CH_3 and CH_4 of methanol to be weaker than CH_2.

The n_p, π^* interaction that accounts for the relative strengths and lengths of the C-H bonds of methanol, must, in methane thiol, be overcome by an interaction that leads to a preferential weakening of the C-H bond antiperiplanar to S-H. This can be caused by the combined effects of the (n_s and $\pi^{*\prime}$) and ($\pi^{\prime}$ and $\sigma^*_{A\text{-}H}$) interactions outweighing that of (n_p and π^*). It is also noted that the non-bonding n_p and n_s orbitals of sulphur lie higher, and the antibonding σ^*_{SH} orbital lies lower, than the corresponding orbitals of oxygen. Thus the difference in the C-H bond length trends in methanol and methane thiol can, to a large extent, be attributed to the effect of the lower lying σ^*_{SH} acceptor orbital.

Many published reports[102-108] refer to this phenomenon as hyperconjugation, a case of adjacent orbital control. Hamlow *et al.*[107] explain that in amines, a nitrogen lone pair interacts with the antibonding axial CH molecular orbital in such molecules.

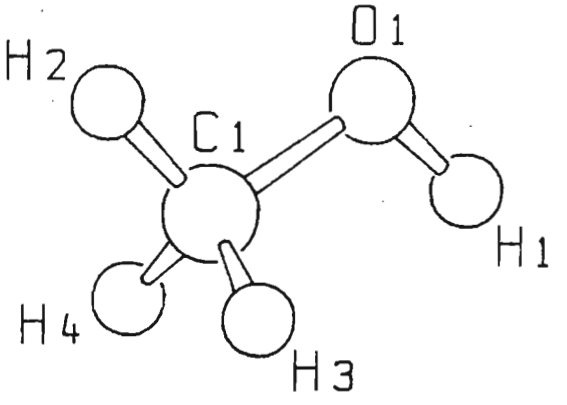

Fig. 2.2 Schakal plot of methanol in conformation I.

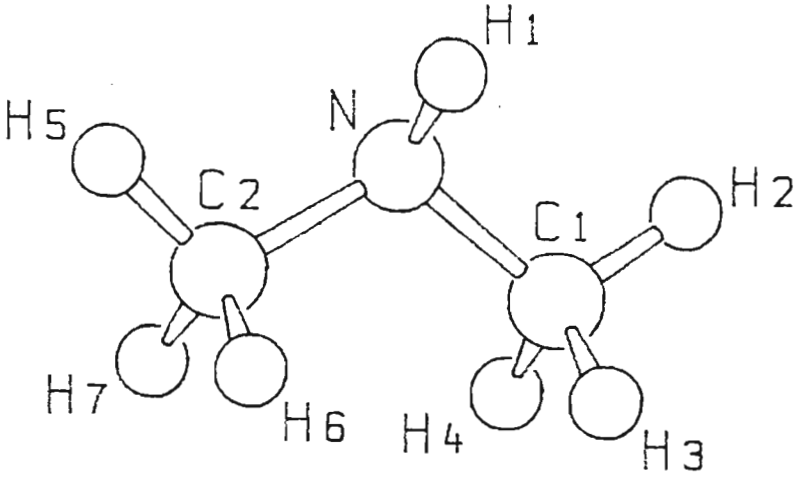

Fig. 2.3 Schakal plot of dimethylamine.

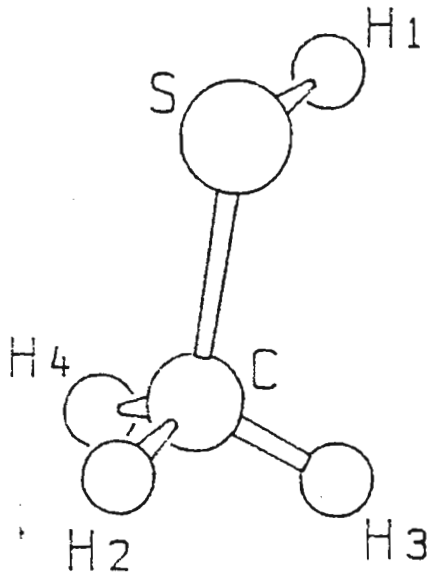

Fig. 2.4 Schakal plot of methane thiol.

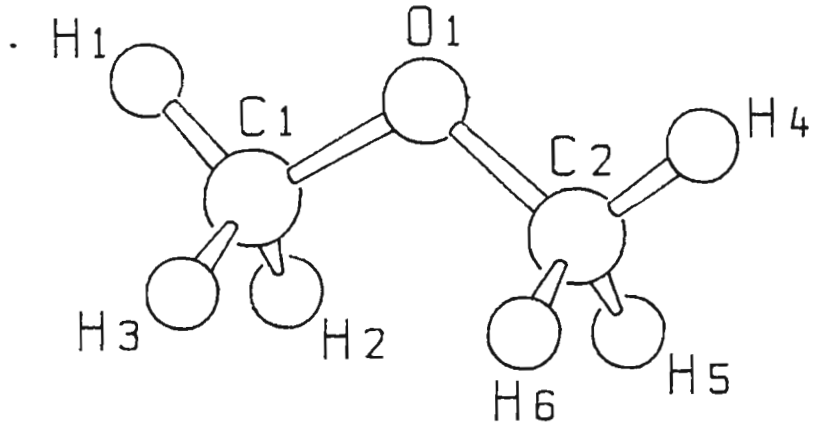

Fig. 2.5 Schakal plot of dimethyl ether in conformation I.

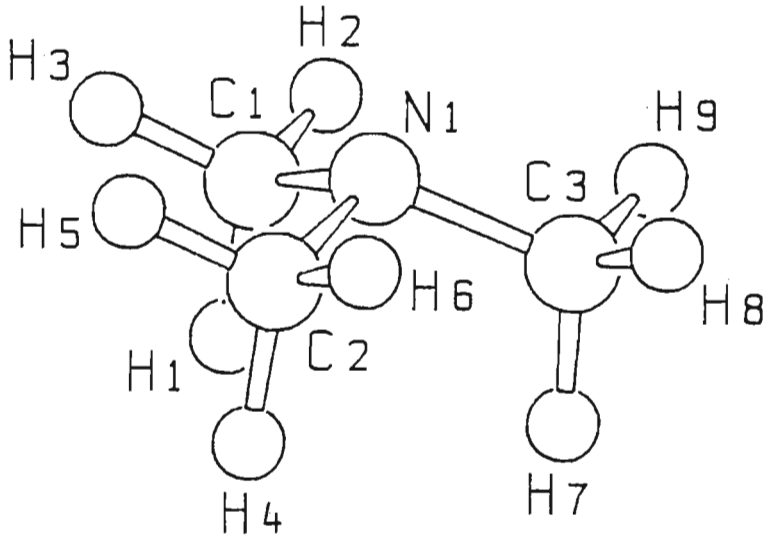

Fig. 2.6 Schakal plot of trimethylamine.

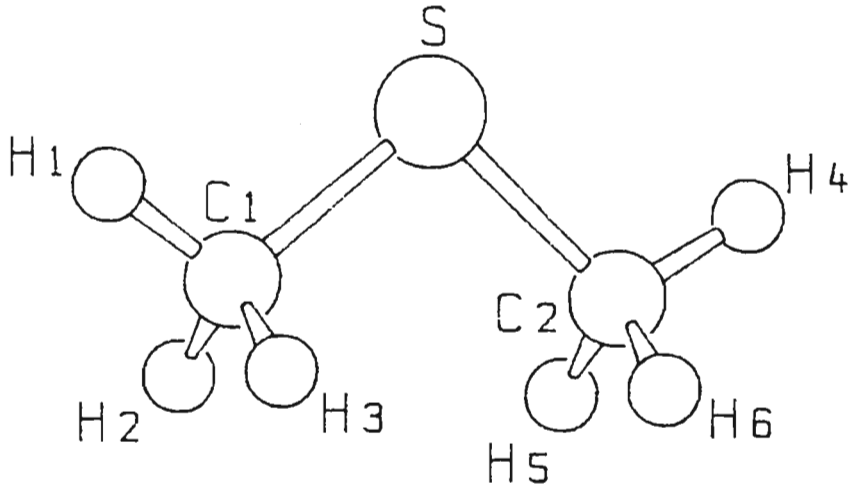

Fig. 2.7 Schakal plot of dimethyl sulphide.

2.4.2 Vibrational Spectra of Monomers CH_3OH, $(CH_3)_2NH$, CH_3SH, $(CH_3)_2O$, $(CH_3)_3N$ and $(CH_3)_2S$

A comparison of calculated and experimental gas phase vibrational wavenumbers for the monomers is provided in Tables 2.10 - 2.15. Descriptions of the normal modes of vibration, derived from the calculated eigenvectors, and plotted using the SCHAKAL[86] plotting program (see Figs. 2.2 - 2.9) are included.

In this work it is noted that the RHF/6-31G** combination of level of theory and basis set is capable of reproducing the intramolecular wavenumbers of the monomers with a mean degree of overestimation of about 11%, which is consistent with other findings.[109-113] The overestimation results from electron correlation effects, which reduce the overestimation to about 5%-10%[114] and the remaining variance is due to anharmonicity effects.[115]

Table 2.10. Computed wavenumbers of the methanol monomer, and comparison with experimental values.

Symmetry species	Mode	Approximate description	Wavenumber/cm^{-1} Calculated	Experimental[a]	ν_{calc}/ν_{expt}
a′	ν_1	ν(OH)	4193	3681	1.14
	ν_2	ν_a(CH_3)	3278	3000	1.09
	ν_3	ν_s(CH_3)	3157	2844	1.11
	ν_4	δ_a(CH_3)	1646	1477	1.11
	ν_5	δ_s(CH_3)	1624	1455	1.12
	ν_6	δ(COH)	1491	1345	1.11
	ν_7	ρ(CH_3)	1189	1060	1.12
	ν_8	ν(CO)	1157	1033	1.12
a″	ν_9	ν_a(CH_3)	3206	2960	1.08
	ν_{10}	δ_a(CH_3)	1634	1477	1.11
	ν_{11}	ρ(CH_3)	1284	1165	1.10
	ν_{12}	τ(OH)	341	295	1.16
				Mean wavenumber ratio	1.11

[a] Refs. 116-118.

Table 2.11. Computed wavenumbers of the dimethylamine monomer, and comparison with experimental values.

Symmetry species	Mode	Approximate description	Wavenumber/cm^{-1} Calculated	Experimental[a]	ν_{calc}/ν_{expt}
a'	ν_1	ν(NH)	3783	3374	1.12
	ν_2	ν_a(CH_3)	3258	2982	1.09
	ν_3	ν_a(CH_3)	3217	2962	1.09
	ν_4	ν_s(CH_3)	3115	2791	1.11
	ν_5	δ_a(CH_3)	1648	1483	1.11
	ν_6	δ_a(CH_3)	1634	1467	1.11
	ν_7	δ_s(CH_3)	1608	1445	1.11
	ν_8	ρ(CH_3)	1382	1240	1.11
	ν_9	ρ(CH_3)	1300	1145	1.13
	ν_{10}	ν_s(CNC)	1011	930	1.09
	ν_{11}	δ_s(CNH)	831	735	1.13
	ν_{12}	δ(CNC)	416	384	1.08
	ν_{13}	τ(CH_3)	279	230	1.21
a"	ν_{14}	ν_a(CH_3)	3255	2982	1.09
	ν_{15}	ν_a(CH_3)	3213	2955	1.09
	ν_{16}	ν_s(CH_3)	3107	2791	1.11
	ν_{17}	δ_a(CH_3)	1652	1485	1.11
	ν_{18}	δ_a(CH_3)	1620	1463	1.11
	ν_{19}	δ_s(CH_3)	1615	1441	1.12
	ν_{20}	ρ(CH_3)	1575	1412	1.12
	ν_{21}	ν_a(CNC)	1277	1158	1.10
	ν_{22}	ρ(CH_3)	1194	1079	1.10
	ν_{23}	δ_a(CNH)	1123	1022	1.10
	ν_{24}	τ(CH_3)	238	257	0.93

Table 2.11 cont.

Mean wavenumber ratio	1.10

[a] Ref. 20,21

Although the experimental values that appear in the table of the vibrational modes of the dimethylamine monomer (Table 2.11) are as they appeared in the work of Buttler and McKean[21] and in Gamer and Wolff,[20] the vibrational mode assignments are different. The assignment variations arise in the a" symmetry species from ν_{17} through to ν_{23}, where ν_{17} (1485 cm^{-1}) had been previously assigned to the NH out-of-plane bending vibration; ν_{18} through to ν_{20} (1473, 1441 and 1412 cm^{-1}) to the CH_3 deformation vibrations; ν_{21} and ν_{22} (1158 and 1079 cm^{-1}) to CH_3 rocking vibrations and ν_{23} (1022 cm^{-1}) to the CN stretching vibration. Normal coordinate analysis of the *ab initio* vibrational spectrum convinced us that these assignments were incorrect. It revealed the likelihood that the mode at 1123 cm^{-1} in the predicted spectrum belonged to the out-of-plane bending vibration, due to the high out-of-plane displacement of the NH hydrogen. None of the other seven vibrations under scrutiny displayed this particular characteristic to the same degree. Satisfaction that the 1123 cm^{-1} band be assigned to the δ_a(CNH) vibration demanded closer examination of the experimentally assigned modes, since 1123 cm^{-1} could not possibly correlate with an experimental wavenumber at 1485 cm^{-1}.

The three CH_3 deformation modes in the a' symmetry species should correspond closely in wavenumber with those in the a" species. Gamer and Wolff had the a' modes 1483, 1467 and 1445 cm^{-1} corresponding with the a" modes 1463, 1441 and 1412 cm^{-1}, respectively. A more consistent and plausible assignment would be to allocate the band at 1485 cm^{-1}, previously assigned to the NH out-of-plane bending vibration, to the antisymmetric CH

bending vibration. Thus, the three a" CH bending vibrations corresponding to 1483, 1467 and 1445 cm^{-1} in the a' set would be 1485, 1463 and 1441 cm^{-1}, respectively.

The remaining four modes of uncertain origin have to consist of two CH_3 rocking vibrations, one antisymmetric CN stretching vibration and the out-of-plane CNH bending vibration. *Ab initio* wavenumbers for these particular modes were found to be 1575, 1277, 1194 and 1123 cm^{-1}. For the reasons already expounded, the band at 1123 cm^{-1} was assigned to the δ_a(CNH) vibration. The antisymmetric CN stretching vibration is easily detectable through normal coordinate analysis as, by definition, it requires a large out-of-plane motion of the nitrogen atom. Only the vibration at 1277 cm^{-1} satisfied this prerequisite. This requires that the two remaining wavenumbers, at 1575 and 1194 cm^{-1}, be assigned to CH_3 rocking motions. The corresponding experimental wavenumbers have 1158 cm^{-1} assigned to the antisymmetric CN stretching vibration; 1412 and 1079 cm^{-1} to the CH_3 rocking motions and 1022 cm^{-1} to the NH antisymmetric bending motion.

Testing the internal consistency of the wavenumbers for this new experimental assignment, it is observed that the symmetrical CN stretching mode (930 cm^{-1}) is lower than the antisymmetric CN stretch (1158 cm^{-1}) and that the symmetric NH deformation (735 cm^{-1}) is lower than the antisymmetric NH bending motion (1022 cm^{-1}). The ν_{calc}/ν_{expt} ratio for each of these seven reassigned modes was 1.10.

Table 2.12. Computed wavenumbers of the methane thiol monomer, and comparison with experimental values.

Symmetry species	Mode	Approximate description	Wavenumber/cm^{-1} Calculated	Experimental[a]	ν_{calc}/ν_{expt}
a′	ν_1	$\nu_a(CH_3)$	3313	3015	1.10
	ν_3	$\nu_s(CH_3)$	3216	2948	1.09
	ν_4	ν(SH)	2892	2605	1.11
	ν_2	$\delta_a(CH_3)$	1617	1453	1.11
	ν_5	$\delta_s(CH_3)$	1502	1332	1.13
	ν_6	$\rho(CH_3)$	1207	1072	1.12
	ν_8	δ(CSH)	868	802	1.08
	ν_7	ν(CS)	770	710	1.08
a″	ν_9	$\nu_a(CH_3)$	3305	3012	1.10
	ν_{10}	$\delta_a(CH_3)$	1605	1444	1.11
	ν_{11}	$\rho(CH_3)$	1077	956	1.12
	ν_{12}	τ(SH)	241		
				Mean wavenumber ratio	1.10

[a] Ref. 119

Table 2.13. Computed wavenumbers of the dimethyl ether monomer, and comparison with experimental values.

Symmetry species	Mode	Approximate description	Wavenumber/cm^{-1} Calculated	Experimental[a]	ν_{calc}/ν_{expt}
a_1	ν_1	$\nu_a(CH_3)$	3281	2996	1.10
	ν_2	$\nu_s(CH_3)$	3153	2817	1.12
	ν_3	$\delta_a(CH_3)$	1654	1464	1.13
	ν_4	$\delta_s(CH_3)$	1634	1452	1.13
	ν_5	$\rho(CH_3)$	1395	1244	1.12
	ν_6	$\nu_s(COC)$	1042	928	1.12
	ν_7	$\delta(COC)$	443	418	1.06
a_2	ν_8	$\nu_a(CH_3)$	3192	2952	1.08
	ν_9	$\delta_a(CH_3)$	1621	1464	1.11
	ν_{10}	$\rho(CH_3)$	1272	1150	1.11
	ν_{11}	$\tau(CH_3)$	211	203	1.04
b_1	ν_{12}	$\nu_a(CH_3)$	3278	2996	1.09
	ν_{13}	$\nu_s(CH_3)$	3137	2817	1.11
	ν_{14}	$\delta_a(CH_3)$	1634	1464	1.12
	ν_{15}	$\delta_s(CH_3)$	1597	1452	1.10
	ν_{16}	$\rho(CH_3)$	1345	1227	1.10
	ν_{17}	$\nu_a(COC)$	1228	1102	1.11
b_2	ν_{18}	$\nu_a(CH_3)$	3194	2925	1.09
	ν_{19}	$\delta_a(CH_3)$	1633	1464	1.12
	ν_{20}	$\rho(CH_3)$	1308	1179	1.11
	ν_{21}	$\tau(CH_3)$	263	242	1.09
				Mean wavenumber ratio	1.10

[a] Ref. 120-121

Table 2.14. Computed wavenumbers of the trimethylamine monomer, and comparison with experimental values.

Symmetry species	Mode	Approximate description	Wavenumber/cm^{-1} Calculated	Experimental[a]	ν_{calc}/ν_{expt}
a_1	ν_1	$\nu_s(CH_3)$	3225	2953	1.09
	ν_2	$\nu_s(CH_3)$	3101	2776	1.12
	ν_3	$\delta_a(CH_3)$	1638	1459	1.12
	ν_4	$\delta_s(CH_3)$	1625	1444	1.13
	ν_5	$\rho(CH_3)$	1326	1186	1.12
	ν_6	$\nu_s(NC_3)$	900	828	1.09
	ν_7	$\delta_s(NC_3)$	381	368	1.04
a_2	ν_8	$\nu_a(CH_3)$	3261	2977[b]	1.10
	ν_9	$\delta_a(CH_3)$	1628	1453[b]	1.12
	ν_{10}	$\rho(CH_3)$	1167	1046[b]	1.12
	ν_{11}	$\tau(CH_3)$	256	252[c]	1.02
e	ν_{12}	$\nu_a(CH_3)$	3269	2981	1.10
	ν_{13}	$\nu_s(CH_3)$	3215	2953	1.09
	ν_{14}	$\nu_s(CH_3)$	3085	2776	1.11
	ν_{15}	$\delta_a(CH_3)$	1649	1471	1.12
	ν_{16}	$\delta_a(CH_3)$	1613	1444	1.12
	ν_{17}	$\delta_s(CH_3)$	1580	1409	1.12
	ν_{18}	$\rho(CH_3)$	1441	1275	1.13
	ν_{19}	$\rho(CH_3)$	1218	1103	1.10
	ν_{20}	$\nu_a(NC_3)$	1152	1043	1.10
	ν_{21}	$\delta_a(NC_3)$	459	424	1.08
	ν_{22}	$\tau(CH_3)$	283	269[d]	1.05
				Mean wavenumber ratio	1.10

[a] Ref. 23

[b] Calculated from ref. 23.

[c] Estimated from microwave intensity measurements (ref. 122).

[d] Ref. 121.

Table 2.15. Computed wavenumbers of the dimethyl sulphide monomer, and comparison with experimental values.

Symmetry species	Mode	Approximate description	Wavenumber/cm^{-1} Calculated	Experimental[a]	ν_{calc}/ν_{expt}
a_1	ν_1	$\nu_a(CH_3)$	3295	3000	1.10
	ν_2	$\nu_s(CH_3)$	3197	2930	1.09
	ν_3	$\delta_a(CH_3)$	1618	1447	1.12
	ν_4	$\delta_s(CH_3)$	1514	1330	1.14
	ν_5	$\rho(CH_3)$	1159	1036	1.12
	ν_6	$\nu_s(CSC)$	752	695	1.08
	ν_7	$\delta(CSC)$	286		
a_2	ν_8	$\nu_a(CH_3)$	3282	2970[b]	1.10
	ν_9	$\delta_a(CH_3)$	1594	1427[b]	1.12
	ν_{10}	$\rho(CH_3)$	1051	946[b]	1.11
	ν_{11}	$\tau(CH_3)$	193	175[b]	1.10
b_1	ν_{12}	$\nu_a(CH_3)$	3278	2975	1.10
	ν_{13}	$\delta_a(CH_3)$	1605	1436	1.12
	ν_{14}	$\rho(CH_3)$	1087	978	1.11
	ν_{15}	$\tau(CH_3)$	202		
b_2	ν_{16}	$\nu_a(CH_3)$	3295	2994	1.10
	ν_{17}	$\nu_s(CH_3)$	3198	2926	1.09
	ν_{18}	$\delta_a(CH_3)$	1609	1440	1.12
	ν_{19}	$\delta_s(CH_3)$	1488	1314	1.13
	ν_{20}	$\rho(CH_3)$	1005	904	1.11
	ν_{21}	$\nu_a(CSC)$	816	742	1.10
				Mean wavenumber ratio	1.11

[a] Ref. 14 [b] Ref. 13

Methanol and methane thiol both have twelve normal modes, eight a' and four a" modes, all of which are both Raman and infrared active. Dimethylamine has 24 normal modes which have the representation $\Gamma = 7a_1 + 4a_2 + 6b_1 + 7b_2$, while trimethylamine, which has C_{3v} symmetry, has 33 modes which transform as $\Gamma = 7a_1 + 4a_2 + 11e$. Dimethyl ether and dimethyl sulphide both have 21 normal modes with representations $\Gamma = 7a_1 + 4a_2 + 6b_1 + 4b_2$ and $\Gamma = 7a_1 + 4a_2 + 4b_1 + 6b_2$ respectively. It is noted that the representations for these two monomers should be the same. The Gaussian program used to calculate these symmetry species has probably defined the planes of the molecules differently due to the differing moments of inertia involved.

The O-H stretching vibration, ν(OH), (Table 2.10) is observed at 4193 cm^{-1} for the staggered, lowest energy conformation of methanol, which is an overestimation of about 14% of the experimentally determined value. ν(NH) in dimethylamine (Table 2.11) is calculated at 3783 cm^{-1} while the S-H stretching vibration in methanethiol (Table 2.12) is predicted to be 2892 cm^{-1}, with a mean degree of overestimation of 12% and 11% respectively.

For the antisymmetric methyl deformations, the two normal modes, $\delta_a(CH_3)$(a') and $\delta_a(CH_3)$(a"), neighbour one another and often threaten to overlap. For methanol, these modes, ν_4 and ν_{10}, are observed at 1646 cm^{-1} and 1634 cm^{-1}. Similarly, methane thiol has the ν_4 and ν_{10} modes at 1617 cm^{-1} and 1605 cm^{-1} respectively, while the analogous modes in dimethylamine, ν_5 and ν_{17}, are observed at 1648 cm^{-1} and 1652 cm^{-1} respectively.

The a_1 symmetry species C-A stretching mode in the proton accepting monomers, ν_s(CAC), is observed at 1042 cm^{-1} in dimethyl ether (Table 2.13), 900 cm^{-1} in trimethylamine (Table 2.14) and at 752 cm^{-1} for dimethyl

sulphide (Table 2.15). The corresponding mode in the proton donating monomers, of symmetry species a', exists at 1158 cm^{-1} in the case of methanol, at 1011 cm^{-1} in the dimethylamine theoretical spectrum and at 770 cm^{-1} for that of methane thiol. The CAH symmetrical bending mode in the proton donating molecules is located at 868 cm^{-1} in methane thiol, at 831 cm^{-1} in dimethylamine and at a much higher wavenumber of 1491 cm^{-1} in methanol. The CAC bending mode in the proton accepting monomers exists at the lower end of the infrared spectrum with the δ(COC) mode in dimethyl ether found at 443 cm^{-1}, the δ_s(CNC) mode in trimethylamine at 381 cm^{-1} and the δ(CSC) vibrational mode of dimethyl sulphide at 286 cm^{-1}.

The vibrational bands for the a' and a" methyl wagging (rocking) modes for methane thiol (Table 2.12) are observed at 1207 and 1077 cm^{-1}. The unusually large splitting seems to be the result of strong coupling between the a' symmetric wagging mode and the CSH bending mode at 868 cm^{-1}. May and Pace[119] show that this claim is supported by results observed for CH_3SD. In the experimental spectrum of CH_3SD, the two wagging vibrations have wavenumbers of 1007 and 963 cm^{-1} and the CSD bending mode, 623 cm^{-1} (The CH_3SH wagging vibrations in the experimental spectrum are found at 1072 and 956 cm^{-1} with that of the CSH bend at 802 cm^{-1}). The corresponding vibrations in methanol (Table 2.10) are observed at 1189 and 1284 cm^{-1} and in dimethylamine (Table 2.11) at 1382, 1300, 1575 and 1277 cm^{-1}.

The torsional vibration in the proton donating species belongs to the a" symmetry representation and is found at relatively low frequencies. The wavenumbers for methanol, dimethylamine and methane thiol are 341, 238 and 241 cm^{-1} respectively. The torsional vibrational modes in the proton accepting molecules belong to the a_2 and b_2 symmetry species. These modes are recorded at 211 and 263 cm^{-1} in dimethyl ether and at 193 and

202 cm^{-1} in the case of dimethyl sulphide. The trimethylamine torsional modes belong to the a_2 and e symmetry representations and are found at 256 and 283 cm^{-1}.

Vibrational intensities (Table 2.16) compare reasonably well with available experimental data. In the case of methanol, the ν_1 mode, with a *medium* experimental intensity, has a calculated intensity of 42 km mol^{-1}. Other *medium* intensity designations include ν_2, ν_3, ν_6, ν_9 and ν_{12} where the computed intensities are 50 km mol^{-1}, 64 km mol^{-1}, 44 km mol^{-1}, 99 km mol^{-1} and 145 km mol^{-1} respectively. The weak bands at ν_4, ν_5, ν_7 and ν_{10} in the experimental spectrum are correctly reproduced at the currently employed level of theory.

The absolute gas-phase infrared intensities for the well separated bands of dimethyl ether are used for comparative analysis.[17] ν_6, ν_{14}, ν_{16} and ν_{18} were found experimentally to possess intensities of about 34 km mol^{-1}, 26 km mol^{-1}, 155 km mol^{-1} and 294 km mol^{-1} respectively. Comparative intensities calculated in this work had intensity values at about 41 km mol^{-1}, 10 km mol^{-1}, 163 km mol^{-1} and 178 km mol^{-1} respectively.

The infrared spectrum of gaseous methane thiol records the most intense peaks for the ν_2, ν_3, ν_5 and ν_6 vibrational modes, which is in agreement with the values found in this work, using HF theory.

Table 2.16 Computed intensities of the infrared active bands of methanol, dimethylamine, methane thiol, dimethyl ether, trimethylamine and dimethyl sulphide.

Monomer	Mode (symmetry species)	Intensity /km mol^{-1}	Mode (symmetry species)	Intensity /km mol^{-1}
CH_3OH	$\nu_1(a')$	42.5	$\nu_7(a')$	79.6
	$\nu_2(a')$	49.7	$\nu_8(a')$	69.7
	$\nu_3(a')$	64.0	$\nu_9(a")$	99.1
	$\nu_4(a')$	3.6	$\nu_{10}(a")$	1.2
	$\nu_5(a')$	9.8	$\nu_{11}(a")$	3.2
	$\nu_6(a')$	43.8	$\nu_{12}(a")$	145.5
$(CH_3)_2NH$	$\nu_1(a')$	0.7	$\nu_{13}(a')$	3.0
	$\nu_2(a')$	64.3	$\nu_{14}(a")$	37.5
	$\nu_3(a')$	72.0	$\nu_{15}(a")$	35.6
	$\nu_4(a')$	153.5	$\nu_{16}(a")$	47.1
	$\nu_5(a')$	1.5	$\nu_{17}(a")$	15.7
	$\nu_6(a')$	6.9	$\nu_{18}(a")$	0.1
	$\nu_7(a')$	1.6	$\nu_{19}(a")$	14.4
	$\nu_8(a')$	0.6	$\nu_{20}(a")$	3.3
	$\nu_9(a')$	16.1	$\nu_{21}(a")$	38.9
	$\nu_{10}(a')$	5.6	$\nu_{22}(a")$	0.1
	$\nu_{11}(a')$	131.4	$\nu_{23}(a")$	10.2
	$\nu_{12}(a')$	7.9	$\nu_{24}(a")$	0.1
CH_3SH	$\nu_1(a')$	11.3	$\nu_7(a')$	2.0
	$\nu_2(a')$	34.9	$\nu_8(a')$	4.3
	$\nu_3(a')$	15.0	$\nu_9(a")$	15.1

Table 2.16. cont.

	$\nu_4(a')$	6.6	$\nu_{10}(a'')$	5.3
	$\nu_5(a')$	12.9	$\nu_{11}(a'')$	4.1
	$\nu_6(a')$	20.9	$\nu_{12}(a'')$	18.2
$(CH_3)_2O$	$\nu_1(a_1)$	45.2	$\nu_{14}(b_1)$	10.1
	$\nu_2(a_1)$	63.3	$\nu_{15}(b_1)$	16.1
	$\nu_3(a_1)$	0.1	$\nu_{16}(b_1)$	163.8
	$\nu_4(a_1)$	0.4	$\nu_{17}(b_1)$	34.3
	$\nu_5(a_1)$	12.1	$\nu_{18}(b_2)$	178.8
	$\nu_6(a_1)$	41.0	$\nu_{19}(b_2)$	7.7
	$\nu_7(a_1)$	3.3	$\nu_{20}(b_2)$	12.6
	$\nu_{12}(b_1)$	52.8	$\nu_{21}(b_2)$	8.6
	$\nu_{13}(b_1)$	54.9		
$(CH_3)_3N$	$\nu_1(a_1)$	61.6	$\nu_{14}(e)$	37.4
	$\nu_2(a_1)$	204.5	$\nu_{15}(e)$	5.9
	$\nu_3(a_1)$	15.6	$\nu_{16}(e)$	7.9
	$\nu_4(a_1)$	1.9	$\nu_{17}(e)$	4.7
	$\nu_5(a_1)$	23.5	$\nu_{18}(e)$	20.2
	$\nu_6(a_1)$	20.1	$\nu_{19}(e)$	10.5
	$\nu_7(a_1)$	11.8	$\nu_{20}(e)$	23.7
	$\nu_{12}(e)$	71.4	$\nu_{21}(e)$	0.0
	$\nu_{13}(e)$	43.0	$\nu_{22}(e)$	0.1
$(CH_3)_2S$	$\nu_1(a_1)$	17.7	$\nu_{14}(b_1)$	4.1
	$\nu_2(a_1)$	36.9	$\nu_{15}(b_1)$	1.1
	$\nu_3(a_1)$	0.2	$\nu_{16}(b_2)$	8.4
	$\nu_4(a_1)$	3.4	$\nu_{17}(b_2)$	38.6
	$\nu_5(a_1)$	17.2	$\nu_{18}(b_2)$	16.1

Table 2.16. cont.

$\nu_6(a_1)$	4.3	$\nu_{19}(b_2)$	9.2
$\nu_7(a_1)$	0.0	$\nu_{20}(b_2)$	0.0
$\nu_{12}(b_1)$	43.3	$\nu_{21}(b_2)$	0.8
$\nu_{13}(b_1)$	15.1		

2.4.3 Optimized Geometries of Molecular Complexes

Table 2.17 lists the minimum energies and the dipole moments calculated for the nine binary complexes $CH_3OH...O(CH_3)_2$, $CH_3OH...N(CH_3)_3$, $CH_3OH...S(CH_3)_2$, $(CH_3)_2NH...O(CH_3)_2$, $(CH_3)_2NH...N(CH_3)_3$, $(CH_3)_2NH...S(CH_3)_2$, $CH_3SH...O(CH_3)_2$, $CH_3SH...N(CH_3)_3$ and $CH_3SH...S(CH_3)_2$. Each complex optimized in the C_s point group. The optimized geometrical parameters of the adducts, obtained using the BERNY optimization procedure at the RHF/6-31G** level of theory, are collected in Tables 2.18 to 2.26, along with the changes in their values, relative to those in the monomers, resulting from hydrogen bonding. The atom numbering conventions are depicted in Figures 2.8 - 2.16, by means of SCHAKAL[86] plots. No previous optimized geometrical parameters, at any level of theory, have been found for the particular binary complexes studied in this work.

Table 2.17. Absolute energies and dipole moments calculated for the lowest energy binary complexes formed from methanol, dimethylamine, methane thiol, dimethyl ether, trimethylamine and dimethyl sulphide.

Complex	Absolute energy /a.u.	Dipole moment /D[a]
$CH_3OH...O(CH_3)_2$	-269.1289769	3.65
$CH_3OH...N(CH_3)_3$	-288.3390168	2.93
$CH_3OH...S(CH_3)_2$	-591.7944597	3.80
$(CH_3)_2NH...O(CH_3)_2$	-288.3285721	2.83
$(CH_3)_2NH...N(CH_3)_3$	-307.5310973	2.12
$(CH_3)_2NH...S(CH_3)_2$	-610.9970145	3.10
$CH_3SH...O(CH_3)_2$	-591.7864706	3.27
$CH_3SH...N(CH_3)_3$	-610.9957133	2.64
$CH_3SH...S(CH_3)_2$	-914.4553003	3.62

[a] $1D = 3.336 \times 10^{-30} C\ m$

Table 2.18. Optimized structural parameters of the methanol-dimethyl ether complex, and complex-monomer differences.

Parameter[a]	Complex	Monomer	Difference[b]
$r(H_1...O_2)$ /pm	200.85		
$r(O_1H_1)$ /pm	94.65	94.23	0.42
$r(C_1O_1)$ /pm	139.29	139.85	-0.56
$r(C_1H_2)$ /pm	108.33	108.20	0.13
$r(C_1H_3)$, $r(C_1H_4)$ /pm	108.96	108.82	0.14
$r(C_2O_2)$, $r(C_3O_2)$ /pm	139.66	139.15	0.51
$r(C_2H_5)$, $r(C_3H_8)$ /pm	108.13	108.19	-0.06
$r(C_2H_6)$, $r(C_3H_9)$ /pm	108.81	108.97	-0.16
$r(C_2H_7)$, $r(C_3H_{10})$ /pm	108.81	108.97	-0.16
$O_1\hat{H}_1...O_2$ /deg	171.5		
$H_1\hat{O}_2...C_2$, $H_1\hat{O}_2...C_3$ /deg	122.8		
$C_1\hat{O}_1H_1$ /deg	109.1	109.7	-0.6
$H_2\hat{C}_1O_1$ /deg	107.9	107.3	0.6
$H_3\hat{C}_1O_1$, $H_4\hat{C}_1O_1$ /deg	112.4	112.1	0.3
$H_2\hat{C}_1H_3$, $H_2\hat{C}_1H_4$ /deg	108.0	108.3	-0.3
$H_3\hat{C}_1H_4$ /deg	108.0	108.6	-0.6
$C_2\hat{O}_2C_3$ /deg	114.4	113.9	0.5
$H_5\hat{C}_2O_2$, $H_8\hat{C}_3O_2$ /deg	107.6	107.7	-0.1
$H_6\hat{C}_2O_2$, $H_9\hat{C}_3O_2$ /deg	111.2	111.6	-0.4
$H_7\hat{C}_2O_2$, $H_{10}\hat{C}_3O_2$ /deg	111.2	111.6	-0.4

Table 2.18 cont.

$H_5\hat{C}_2H_6$, $H_8\hat{C}_3H_9$ /deg	109.0	108.8	0.2
$H_5\hat{C}_2H_7$, $H_8\hat{C}_3H_{10}$ /deg	109.0	108.8	0.2
$H_6\hat{C}_2H_7$, $H_9\hat{C}_3H_{10}$ /deg	108.7	108.3	0.4
$\hat{C}_1O_1H_1X$ [c]/deg	0.0		
$\hat{C}_2O_2H_1O_1$, $\hat{C}_3O_2H_1O_1$ [c]/deg	89.6		
$H_3\hat{C}_1O_1H_1$, $H_4\hat{C}_1O_1H_1$ [c]/deg	61.0	61.2	-0.2
$H_5\hat{C}_2O_2H_1$, $H_8\hat{C}_3O_2H_1$ [c]/deg	0.0		
$H_6\hat{C}_2O_2H_1$, $H_9\hat{C}_3O_2H_1$ [c]/deg	119.3		
$H_7\hat{C}_2O_2H_1$, $H_{10}\hat{C}_3O_2H_1$ [c]/deg	119.3		

[a] See Figure 2.8 for numbering of atoms

[b] Difference = complex - monomer parameter

[c] Dihedral angle

X is a dummy atom situated on H_1 such that O_1H_1X is 90°.

Table 2.19. Optimized structural parameters of the methanol-trimethylamine complex, and complex-monomer differences.

Parameter[a]	Complex	Monomer	Difference[b]
$r(H_1...N)$ /pm	206.93		
$r(OH_1)$ /pm	95.06	94.23	0.83
$r(CO_1)$ /pm	139.14	139.85	-0.71
$r(C_1H_2)$ /pm	108.35	108.20	0.15
$r(C_1H_3)$, $r(C_1H_4)$ /pm	109.03	108.82	0.21
$r(C_2N)$ /pm	145.03	144.49	0.54
$r(C_3N)$, $r(C_4N)$ /pm	145.06	144.49	0.57
$r(C_2H_5)$ /pm	109.34	109.63	-0.29
$r(C_2H_6)$, $r(C_2H_7)$ /pm	108.42	108.43	-0.01
$r(C_3H_8)$, $r(C_4H_{11})$ /pm	109.34	109.63	-0.29
$r(C_3H_9)$, $r(C_4H_{13})$ /pm	108.37	108.43	-0.06
$r(C_3H_{10})$, $r(C_4H_{12})$ /pm	108.37	108.43	-0.06
$O\hat{H}_1...N$ /deg	177.1		
$H_1...NC_2$	109.6		
$H_1...NC_3$, $H_1...NC_4$ /deg	105.9		
$C_1\hat{O}H_1$ /deg	109.7	109.7	0.0
$H_2\hat{C}_1O$ /deg	109.0	107.3	1.7
$H_3\hat{C}_1O$, $H_4\hat{C}_1O$ /deg	112.5	112.1	0.4
$H_2\hat{C}_1H_3$, $H_2\hat{C}_1H_4$ /deg	107.9	108.3	-0.4
$H_3\hat{C}_1H_4$/deg	108.0	108.6	-0.6

Table 2.19 cont.

C_2NC_3, C_2NC_4 /deg	111.6	112.0	-0.4
C_3NC_4 /deg	111.9	112.0	-0.1
$H_5\hat{C}_2N$ /deg	112.5	112.7	-0.2
$H_6\hat{C}_2N$, $H_7\hat{C}_2N$ /deg	109.9	110.1	-0.2
$H_8\hat{C}_3N$, $H_{11}\hat{C}_4N$ /deg	112.6	112.7	-0.1
$H_9\hat{C}_3N$, $H_{13}\hat{C}_4N$ /deg	109.8	110.1	-0.3
$H_{10}\hat{C}_3N$, $H_{12}\hat{C}_4N$ /deg	109.8	110.1	-0.3
$H_5\hat{C}_2H_6$, $H_5\hat{C}_2H_7$ /deg	108.2	107.5	0.7
$H_6\hat{C}_2H_7$/deg	108.1	108.9	-0.8
$H_8\hat{C}_3H_9$, $H_{11}\hat{C}_4H_{13}$ /deg	108.3	107.5	0.8
$H_8\hat{C}_3H_{10}$, $H_{11}\hat{C}_4H_{12}$ /deg	108.3	107.5	0.8
$H_9\hat{C}_3H_{10}$, $H_{12}\hat{C}_4H_{13}$ /deg	108.0	108.9	-0.9
$C_1\hat{O}H_1N$ [c]/deg	180.0		
$H_3\hat{C}_1\hat{O}H_1$, $H_4\hat{C}_1\hat{O}H_1$ [c]/deg	61.1	61.2	-0.1
C_3NH_1O, C_4NH_1O [c]/deg	120.5		
$H_6\hat{C}_2NH_1$, $H_7\hat{C}_2NH_1$ [c]/deg	59.4		
$H_8\hat{C}_3NH_1$, $H_{11}\hat{C}_4NH_1$ [c]/deg	180.0		
$H_9\hat{C}_3NH_1$, $H_{13}\hat{C}_4NH_1$ [c]/deg	59.3		
$H_{10}\hat{C}_3NH_1$, $H_{12}\hat{C}_4NH_1$ [c]/deg	59.3		

[a] See Figure 2.9 for numbering of atoms

[b] Difference = complex - monomer parameter

[c] Dihedral angle

Table 2.20. Optimized structural parameters of the methanol-dimethyl sulphide complex, and complex-monomer differences.

Parameter[a]	Complex	Monomer	Difference[b]
$r(H_1...S)$ /pm	286.78		
$r(O_1H_1)$ /pm	94.32	94.23	0.09
$r(C_1O_1)$ /pm	139.67	139.85	-0.18
$r(C_1H_2)$ /pm	108.27	108.20	0.07
$r(C_1H_3)$, $r(C_1H_4)$ /pm	108.83	108.82	0.01
$r(C_2S)$, $r(C_3S)$ /pm	180.74	180.80	-0.06
$r(C_2H_5)$, $r(C_3H_8)$ /pm	108.21	108.23	-0.02
$r(C_2H_6)$, $r(C_3H_9)$ /pm	108.28	108.32	-0.04
$r(C_2H_7)$, $r(C_3H_{10})$ /pm	108.28	108.32	-0.04
$O_1\hat{H}_1...S$ /deg	166.2		
$H_1S...C_2$, $H_1S...C_3$ /deg	129.6		
$C_1\hat{O}H_1$ /deg	109.5		
$H_2\hat{C}_1O$ /deg	107.5	107.3	0.2
$H_3\hat{C}_1O$, $H_4\hat{C}_1O$ /deg	112.2	112.1	0.1
$H_2\hat{C}_1H_3$, $H_2\hat{C}_1H_4$ /deg	108.3	108.3	0.0
$H_3\hat{C}_1H_4$ /deg	108.3	108.6	-0.3
C_2SC_3 /deg	100.8	100.2	0.6
$H_5\hat{C}_2S$, $H_8\hat{C}_3S$ /deg	107.4	107.4	0.0
$H_6\hat{C}_2S$, $H_9\hat{C}_3S$ /deg	111.0	111.1	-0.1
$H_7\hat{C}_2S$, $H_{10}\hat{C}_3S$ /deg	111.0	111.1	-0.1

Table 2.20 cont.

$H_5\hat{C}_2H_6$, $H_8\hat{C}_3H_9$ /deg	108.9	108.8	0.1
$H_5\hat{C}_2H_7$, $H_8\hat{C}_3H_{10}$ /deg	108.9	108.8	0.1
$H_6\hat{C}_2H_7$, $H_9\hat{C}_3H_{10}$ /deg	109.7	109.6	0.1
$\hat{C}_1OH_1X$ [c]/deg	0.0		
$\hat{C}_2SH_1O_1$, $\hat{C}_3SH_1O_1$ [c]/deg	179.8		
$H_3\hat{C}_1O_1H_1$, $H_4\hat{C}_1O_1H_1$ [c]/deg	61.1	61.2	-0.1
$H_5\hat{C}_2SH_1$, $H_8\hat{C}_3SH_1$ [c]/deg	0.0		
$H_6\hat{C}_2SH_1$, $H_9\hat{C}_3SH_1$ [c]/deg	118.8		
$H_7\hat{C}_2SH_1$, $H_{10}\hat{C}_3SH_1$ [c]/deg	118.8		

[a] See Figure 2.10 for numbering of atoms

[b] Difference = complex - monomer parameter

[c] Dihedral angle

X is a dummy atom situated on H_1 such that O_1H_1X is 90°.

Table 2.21. Optimized structural parameters of the dimethylamine-dimethyl ether complex, and complex-monomer differences.

Parameter[a]	Complex	Monomer	Difference[b]
$r(H_1...O)$ /pm	235.42		
$r(NH_1)$ /pm	100.08	99.94	0.14
(C_1N), $r(C_2N)$ /pm	144.65	144.57	0.08
$r(C_1H_2)$, $r(C_2H_5)$ /pm	108.60	108.45	0.15
$r(C_1H_3)$, $r(C_2H_7)$ /pm	108.96	109.40	-0.44
$r(C_1H_4)$, $r(C_2H_6)$ /pm	108.96	108.54	0.42
$r(C_3O)$, $r(C_4O)$ /pm	139.40	139.15	0.25
$r(C_3H_8)$, $r(C_4H_{11})$ /pm	108.16	108.19	-0.03
$r(C_3H_9)$, $r(C_4H_{13})$ /pm	108.88	108.97	-0.09
$r(C_3H_{10})$, $r(C_4H_{12})$ /pm	108.00	108.97	-0.09
$N\hat{H}_1...O$ /deg	167.9		
$H_1...\hat{O}C_3$, $H_1...\hat{O}C_4$ /deg	123.0		
H_1NC_1, $H_1N\hat{C}_2$ /deg	108.9	110.2	-1.3
C_1NC_2 /deg	112.2	113.8	-1.6
$H_2\hat{C}_1N$, $H_5\hat{C}_2N$ /deg	109.7	109.4	0.3
$H_3\hat{C}_1N$, $H_7\hat{C}_2N$ /deg	111.9	114.0	-2.1
$H_4\hat{C}_1N$, $H_6\hat{C}_2N$ /deg	111.9	109.7	2.2
$H_2\hat{C}_1H_3$, $H_5\hat{C}_2H_7$ /deg	107.5	107.6	-0.1
$H_2\hat{C}_1H_4$, $H_5\hat{C}_2H_6$ /deg	107.5	107.8	-0.3
$H_3\hat{C}_1H_4$, $H_6\hat{C}_2H_7$ /deg	108.1	107.6	0.5

Table 2.21 cont.

$C_3\hat{O}_2C_4$ /deg	114.0	113.9	0.1
$H_8\hat{C}_3O$, $H_{11}\hat{C}_4O$ /deg	107.7	107.7	0.0
$H_9\hat{C}_3O$, $H_{13}\hat{C}_4O$ /deg	111.4	111.6	-0.2
$H_{10}\hat{C}_3O$, $H_{12}\hat{C}_4O$ /deg	111.4	111.6	-0.2
$H_8\hat{C}_3H_9$, $H_{11}\hat{C}_4H_{13}$ /deg	108.9	108.8	0.1
$H_8\hat{C}_3H_{10}$, $H_{11}\hat{C}_4H_{12}$ /deg	108.9	108.8	0.1
$H_9\hat{C}_3H_{10}$, $H_{12}\hat{C}_4H_{13}$ /deg	108.5	108.3	0.2
$\hat{C}_1NH_1O$, $\hat{C}_2NH_1O$ [c]/deg	61.3		
$H_2\hat{C}_1NH_1$, $H_5\hat{C}_2NH_1$ [c]/deg	180.0	180.0	0.0
$H_3\hat{C}_1NH_1$, $H_7\hat{C}_2NH_1$ [c]/deg	60.7	60.3	0.4
$H_4\hat{C}_1NH_1$, $H_6\hat{C}_2NH_1$ [c]/deg	60.7	60.3	0.4
$\hat{C}_3OH_1N$, $\hat{C}_4OH_1N$ [c]/deg	179.9		
$H_8\hat{C}_3OH_1$, $H_{11}\hat{C}_4OH_1$ [c]/deg	0.0		
$H_9\hat{C}_3OH_1$, $H_{13}\hat{C}_4OH_1$ [c]/deg	119.3		
$H_{10}\hat{C}_3OH_1$, $H_{12}\hat{C}_4OH_1$ [c]/deg	119.3		

[a] See Figure 2.11 for numbering of atoms

[b] Difference = complex - monomer parameter

[c] Dihedral angle

Table 2.22. Optimized structural parameters of the dimethylamine-trimethylamine complex, and complex-monomer differences.

Parameter[a]	Complex	Monomer	Difference[b]
$r(H_1...N_2)$ /pm	244.27		
$r(N_1H_1)$ /pm	100.20	99.94	0.26
(C_1N_1), $r(C_2N_1)$ /pm	144.63	144.57	-0.06
$r(C_1H_2)$, $r(C_2H_5)$ /pm	108.60	108.45	0.15
$r(C_1H_3)$, $r(C_2H_6)$ /pm	108.98	109.40	-0.42
$r(C_1H_4)$, $r(C_2H_7)$ /pm	108.98	108.54	0.44
$r(C_3N_2)$ /pm	144.77	144.49	0.28
$r(C_4N_2)$, $r(C_5N_2)$ /pm	144.79	144.49	0.30
$r(C_3H_8)$ /pm	109.45	109.63	-0.18
$r(C_3H_9)$, $r(C_3H_{10})$ /pm	108.44	108.43	0.01
$r(C_4H_{11})$, $r(C_5H_{14})$ /pm	109.45	108.63	-0.18
$r(C_4H_{12})$, $r(C_5H_{15})$ /pm	108.42	108.43	-0.01
$r(C_4H_{13})$, $r(C_5H_{16})$ /pm	108.42	108.43	-0.01
$N_1\hat{H}_1...N_2$ /deg	176.5		
$H_1...N_2C_3$ /deg	107.9		
$H_1...N_2C_4$, $H_1...N_2C_5$ /deg	106.6		
$H_1N_1C_1$, $H_1N_1\hat{C}_2$ /deg	109.1	110.2	-1.1
$C_1N_1C_2$ /deg	112.2	113.8	-1.6
$H_2\hat{C}_1N_1$, $H_5\hat{C}_2N_1$ /deg	109.8	109.7	0.1
$H_3\hat{C}_1N_1$, $H_6\hat{C}_2N_1$ /deg	111.9	114.0	-2.1

Table 2.22 cont.

$H_4\hat{C}_1N_1$, $H_7\hat{C}_2N_1$ /deg	111.9	109.4	2.5
$H_2\hat{C}_1H_3$, $H_5\hat{C}_2H_6$ /deg	107.5	108.1	-0.6
$H_2\hat{C}_1H_4$, $H_5\hat{C}_2H_7$ /deg	107.5	107.8	-0.3
$H_3\hat{C}_1H_4$, $H_6\hat{C}_2H_7$ /deg	108.0	107.6	0.4
$C_3N_2C_4$, $C_3N_2C_5$ /deg	111.8	112.0	-0.2
$C_4N_2C_5$ /deg	111.9	112.0	-0.1
$H_8\hat{C}_3N_2$ /deg	112.8	112.7	0.1
$H_9\hat{C}_3N_2$, $H_{10}\hat{C}_3N_2$ /deg	109.8	110.1	-0.3
$H_{11}\hat{C}_4N_2$, $H_{14}\hat{C}_5N_2$ /deg	112.8	112.7	0.1
$H_{12}\hat{C}_4N_2$, $H_{15}\hat{C}_5N_2$ /deg	109.8	110.1	-0.3
$H_{13}\hat{C}_4N_2$, $H_{16}\hat{C}_5N_2$ /deg	109.8	110.1	-0.3
$H_8\hat{C}_3H_9$, $H_8\hat{C}_3H_{10}$ /deg	108.1	107.5	0.6
$H_9\hat{C}_3H_{10}$ /deg	108.0	108.9	-0.9
$H_{11}\hat{C}_4H_{12}$, $H_{14}\hat{C}_5H_{15}$ /deg	108.1	107.5	0.6
$H_{11}\hat{C}_4H_{13}$, $H_{14}\hat{C}_5H_{16}$ /deg	108.1	107.5	0.6
$H_{12}\hat{C}_4H_{13}$, $H_{15}\hat{C}_5H_{16}$ /deg	108.0	108.9	-0.9
$N_1\hat{H}_1N_2C_3$ [c]/deg	0.0		
$\hat{C}_1N_1H_1N_2$, $\hat{C}_2N_1H_1N_2$ [c]/deg	90.1		
$H_2\hat{C}_1N_1H_1$, $H_5\hat{C}_2N_1H_1$ [c]/deg	180.0	178.3	1.7
$H_3\hat{C}_1N_1H_1$, $H_6\hat{C}_2N_1H_1$ [c]/deg	60.7	60.3	0.4
$H_4\hat{C}_1N_1H_1$, $H_7\hat{C}_2N_1H_1$ [c]/deg	60.7	60.3	0.4
$\hat{C}_3N_2H_1N_1$ [c]/deg	0.0		
$\hat{C}_4N_2H_1N_1$, $\hat{C}_5N_2H_1N_1$ [c]/deg	120.2		
$H_8\hat{C}_3N_2H_1$ [c]/deg	180.0		

Table 2.22 cont.

$H_9\hat{C}_3N_2H_1$, $H_{10}\hat{C}_3N_2H_1$ °/deg	59.3
$H_{11}\hat{C}_4N_2H_1$, $H_{14}\hat{C}_5N_2H_1$ °/deg	180.0
$H_{12}\hat{C}_4N_2H_1$, $H_{15}\hat{C}_5N_2H_1$ °/deg	59.3
$H_{13}\hat{C}_4N_2H_1$, $H_{16}\hat{C}_5N_2H_1$ °/deg	59.3

[a] See Figure 2.12 for numbering of atoms

[b] Difference = complex - monomer parameter

[c] Dihedral angle

Table 2.23. Optimized structural parameters of the dimethylamine-dimethyl sulphide complex, and complex-monomer differences.

Parameter[a]	Complex	Monomer	Difference[b]
$r(H_1...S)$ /pm	325.54		
$r(NH_1)$ /pm	100.04	99.94	0.10
(C_1N), $r(C_2N)$ /pm	144.78	144.57	0.21
$r(C_1H_2)$, $r(C_2H_5)$ /pm	108.57	108.45	0.12
$r(C_1H_3)$, $r(C_2H_7)$ /pm	108.90	109.40	-0.50
$r(C_1H_4)$, $r(C_2H_6)$ /pm	108.90	108.54	0.36
$r(C_3S)$, $r(C_4S)$ /pm	180.78	180.80	-0.02
$r(C_3H_8)$, $r(C_4H_{11})$ /pm	108.22	108.23	-0.01
$r(C_3H_9)$, $r(C_4H_{13})$ /pm	108.30	108.32	-0.02
$r(C_3H_{10})$, $r(C_4H_{12})$ /pm	108.30	108.32	-0.02
$N_1\hat{H}_1...S$ /deg	152.6		
$H_1...SC_3$, $H_1...SC_4$ /deg	129.8		
H_1NC_1, $H_1N\hat{C}_2$ /deg	108.9	110.2	-1.3
C_1NC_2 /deg	112.4	113.8	-1.4
$H_2\hat{C}_1N$, $H_5\hat{C}_2N$ /deg	109.5	109.4	0.1
$H_3\hat{C}_1N$, $H_7\hat{C}_2N$ /deg	111.8	114.0	-2.2
$H_4\hat{C}_1N$, $H_6\hat{C}_2N$ /deg	111.8	109.7	2.1
$H_2\hat{C}_1H_3$, $H_5\hat{C}_2H_7$ /deg	107.6	107.6	0.0
$H_2\hat{C}_1H_4$, $H_5\hat{C}_2H_6$ /deg	107.6	107.8	-0.2
$H_3\hat{C}_1H_4$, $H_6\hat{C}_2H_7$ /deg	108.2	107.8	0.4

Table 2.23 cont.

C_3SC_4 /deg	100.4	100.2	0.2
$H_8\hat{C}_3S$, $H_{11}\hat{C}_4S$ /deg	107.4	107.4	0.0
$H_9\hat{C}_3S$, $H_{12}\hat{C}_4S$ /deg	111.1	111.1	0.0
$H_{10}\hat{C}_2S$, $H_{13}\hat{C}_3S$ /deg	111.1	111.1	0.0
$H_8\hat{C}_3H_9$, $H_{11}\hat{C}_4H_{13}$ /deg	108.8	108.8	0.0
$H_8\hat{C}_3H_{10}$, $H_{11}\hat{C}_4H_{12}$ /deg	108.8	108.8	0.0
$H_9\hat{C}_3H_{10}$, $H_{12}\hat{C}_4H_{13}$ /deg	109.7	109.6	0.1
$\hat{C}_1NH_1S$, $\hat{C}_2NH_1S$ [c]/deg	61.4		
$H_2\hat{C}_1NH_1$, $H_5\hat{C}_2NH_1$ [c]/deg	180.0	180.0	0.0
$H_3\hat{C}_1NH_1$, $H_6\hat{C}_2NH_1$ [c]/deg	60.8	60.3	0.5
$H_4\hat{C}_1NH_1$, $H_7\hat{C}_2NH_1$ [c]/deg	60.8	60.3	0.5
$\hat{C}_3SH_1N$, $\hat{C}_4SH_1N$ [c]/deg	179.9		
$H_8\hat{C}_3SH_1$, $H_{11}\hat{C}_4SH_1$ [c]/deg	0.0		
$H_9\hat{C}_3SH_1$, $H_{12}\hat{C}_4SH_1$ [c]/deg	118.8		
$H_{10}\hat{C}_3SH_1$, $H_{13}\hat{C}_4SH_1$ [c]/deg	118.8		

[a] See Figure 2.13 for numbering of atoms

[b] Difference = complex - monomer parameter

[c] Dihedral angle

Table 2.24. Optimized structural parameters of the methane thiol-dimethyl ether complex, and complex-monomer differences.

Parameter[a]	Complex	Monomer	Difference[b]
$r(H_1...O)$ /pm	232.17		
$r(SH_1)$ /pm	132.76	132.72	0.04
$r(C_1S)$ /pm	181.72	181.74	-0.02
$r(C_1H_2)$ /pm	108.18	108.17	0.01
$r(C_1H_3)$, $r(C_1H_4)$ /pm	108.13	108.11	0.02
$r(C_2O)$, $r(C_3O)$ /pm	139.42	139.15	0.27
$r(C_2H_5)$, $r(C_3H_8)$ /pm	108.17	108.19	-0.02
$r(C_2H_6)$, $r(C_3H_9)$ /pm	108.89	108.97	-0.08
$r(C_2H_7)$, $r(C_3H_{10})$ /pm	108.89	108.97	-0.08
$S\hat{H}_1...O$ /deg	175.0		
$H_1\hat{O}...C_2$, $H_1\hat{O}...C_3$ /deg	123.0		
C_1SH_1 /deg	98.0		
$H_2\hat{C}_1S$ /deg	106.9	106.6	0.3
$H_3\hat{C}_1S$, $H_4\hat{C}_1S$ /deg	111.2	111.2	0.0
$H_2\hat{C}_1H_3$, $H_2\hat{C}_1H_4$ /deg	108.8	108.8	0.0
$H_3\hat{C}_1H_4$ /deg	109.8	110.1	-0.3
$C_2\hat{O}C_3$ /deg	114.1	113.9	0.2
$H_5\hat{C}_2O$, $H_8\hat{C}_3O$ /deg	107.7	107.7	0.0
$H_6\hat{C}_2O$, $H_9\hat{C}_3O$ /deg	111.4	111.6	-0.2
$H_7\hat{C}_2O$, $H_{10}\hat{C}_3O$ /deg	111.4	111.6	-0.2

Table 2.24 cont.

$H_5\hat{C}_2H_6$, $H_8\hat{C}_3H_9$ /deg	108.9	108.8	0.1
$H_5\hat{C}_2H_7$, $H_8\hat{C}_3H_{10}$ /deg	108.9	108.8	0.1
$H_6\hat{C}_2H_7$, $H_9\hat{C}_3H_{10}$ /deg	108.5	108.3	0.2
$\hat{C}_1SH_1X$ [c]/deg	0.0		
$\hat{C}_2OH_1S$, $\hat{C}_3OH_1S$ [c]/deg	179.7		
$H_3\hat{C}_1SH_1$, $H_4\hat{C}_1SH_1$ [c]/deg	61.4	61.6	-0.2
$H_5\hat{C}_2OH_1$, $H_8\hat{C}_3OH_1$ [c]/deg	0.0		
$H_6\hat{C}_2OH_1$, $H_9\hat{C}_3OH_1$ [c]/deg	119.3		
$H_7\hat{C}_2OH_1$, $H_{10}\hat{C}_3OH_1$ [c]/deg	119.3		

[a] See Figure 2.14 for numbering of atoms

[b] Difference = complex - monomer parameter

[c] Dihedral angle

X is a dummy atom situated on H_1 such that SH_1X is 90°.

Table 2.25. Optimized structural parameters of the methane thiol-trimethylamine complex, and complex-monomer differences.

Parameter[a]	Complex	Monomer	Difference[b]
$r(H_1...N)$ /pm	240.73		
$r(SH_1)$ /pm	133.10	132.72	0.38
$r(C_1S)$ /pm	181.73	181.74	-0.01
$r(C_1H_2)$ /pm	108.18	108.17	0.01
$r(C_1H_3)$, $r(C_1H_4)$ /pm	108.15	108.11	0.04
$r(C_2N)$ /pm	144.74	144.49	0.25
$r(C_3N)$, $r(C_4N)$ /pm	144.79	144.49	0.30
$r(C_2H_5)$ /pm	109.44	109.63	-0.19
$r(C_2H_6)$, $r(C_2H_7)$ /pm	108.45	108.43	0.02
$r(C_3H_8)$, $r(C_4H_{11})$ /pm	109.44	109.63	-0.19
$r(C_3H_9)$, $r(C_4H_{13})$ /pm	108.42	108.43	-0.01
$r(C_3H_{10})$, $r(C_4H_{12})$ /pm	108.42	108.43	-0.01
$S\hat{H}_1...N$ /deg	177.4		
$H_1...NC_2$	107.8		
$H_1...NC_3$, $H_1...NC_4$ /deg	109.9		
C_1SH_1 /deg	98.3		
$H_2\hat{C}_1S$ /deg	107.0	106.6	0.4
$H_3\hat{C}_1S$, $H_4\hat{C}_1S$ /deg	111.3	111.2	0.1
$H_2\hat{C}_1H_3$, $H_2\hat{C}_1H_4$ /deg	108.7	108.8	-0.1
$H_3\hat{C}_1H_4$/deg	109.9	110.1	-0.2

Table 2.25 cont.

C_2NC_3, C_2NC_4 /deg	111.8	112.0	-0.2
C_3NC_4 /deg	111.9	112.0	-0.1
$H_5\hat{C}_2N$ /deg	112.8	112.7	-0.1
$H_6\hat{C}_2N$, $H_7\hat{C}_2N$ /deg	109.9	110.1	-0.2
$H_8\hat{C}_3N$, $H_{11}\hat{C}_4N$ /deg	112.8	112.7	0.1
$H_9\hat{C}_3N$, $H_{13}\hat{C}_4N$ /deg	109.9	110.1	-0.2
$H_{10}\hat{C}_3N$, $H_{12}\hat{C}_4N$ /deg	109.8	110.1	-0.3
$H_5\hat{C}_2H_6$, $H_5\hat{C}_2H_7$ /deg	108.0	107.5	0.5
$H_6\hat{C}_2H_7$/deg	108.0	108.9	-0.9
$H_8\hat{C}_3H_9$, $H_{11}\hat{C}_4H_{13}$ /deg	108.1	107.5	0.6
$H_8\hat{C}_3H_{10}$, $H_{11}\hat{C}_4H_{12}$ /deg	108.1	107.5	0.6
$H_9\hat{C}_3H_{10}$, $H_{12}\hat{C}_4H_{13}$ /deg	107.9	108.9	-1.0
C_1SH_1N [c]/deg	180.0		
$H_3\hat{C}_1SH_1$, $H_4\hat{C}_1SH_1$ [c]/deg	61.4	61.6	-0.2
C_3NH_1S, C_4NH_1S [c]/deg	210.2		
$H_6\hat{C}_2NH_1$, $H_7\hat{C}_2NH_1$ [c]/deg	59.4		
$H_8\hat{C}_3NH_1$, $H_{11}\hat{C}_4NH_1$ [c]/deg	180.0		
$H_9\hat{C}_3NH_1$, $H_{13}\hat{C}_4NH_1$ [c]/deg	59.3		
$H_{10}\hat{C}_3NH_1$, $H_{12}\hat{C}_4NH_1$ [c]/deg	59.3		

[a] See Figure 2.15 for numbering of atoms

[b] Difference = complex - monomer parameter

[c] Dihedral angle

Table 2.26. Optimized structural parameters of the methane thiol-dimethyl sulphide complex, and complex-monomer differences.

Parameter[a]	Complex	Monomer	Difference[b]
$r(H_1...S)$ /pm	325.38		
$r(S_1H_1)$ /pm	132.67	132.72	-0.05
$r(C_1S_1)$ /pm	181.73	181.74	-0.01
$r(C_1H_2)$ /pm	108.19	108.17	0.02
$r(C_1H_3)$, $r(C_1H_4)$ /pm	108.08	108.11	-0.03
$r(C_2S_2)$, $r(C_3S_2)$ /pm	180.80	180.80	0.00
$r(C_2H_5)$, $r(C_3H_8)$ /pm	108.22	108.23	-0.01
$r(C_2H_6)$, $r(C_3H_9)$ /pm	108.30	108.32	-0.02
$r(C_2H_7)$, $r(C_3H_{10})$ /pm	108.30	108.32	-0.02
$S_1\hat{H}_1...S_2$ /deg	153.8		
$H_1S_2...C_2$, $H_1S_2...C_3$ /deg	129.79		
$C_1S_1H_1$ /deg	97.9		
$H_2\hat{C}_1S_1$ /deg	106.7	106.6	0.1
$H_3\hat{C}_1S_1$, $H_4\hat{C}_1S_1$ /deg	111.2	111.2	0.0
$H_2\hat{C}_1H_3$, $H_2\hat{C}_1H_4$ /deg	108.9	108.8	0.1
$H_3\hat{C}_1H_4$ /deg	109.9	110.1	-0.2
$C_2S_2C_3$ /deg	100.4	100.2	0.2
$H_5\hat{C}_2S_2$, $H_8\hat{C}_3S_2$ /deg	107.4	107.4	0.0
$H_6\hat{C}_2S_2$, $H_9\hat{C}_3S_2$ /deg	111.1	111.1	0.0
$H_7\hat{C}_2S_2$, $H_{10}\hat{C}_3S_2$ /deg	111.1	111.1	0.0

Table 2.26 cont.

$H_5\hat{C}_2H_6$, $H_8\hat{C}_3H_9$ /deg	108.8	108.8	0.0
$H_5\hat{C}_2H_7$, $H_8\hat{C}_3H_{10}$ /deg	108.8	108.8	0.0
$H_6\hat{C}_2H_7$, $H_9\hat{C}_3H_{10}$ /deg	109.7	109.6	0.1
$\hat{C}_1S_1H_1X$ [c]/deg	0.0		
$\hat{C}_2S_2H_1S_1$, $\hat{C}_3S_2H_1S_1$ [c]/deg	179.9		
$H_3\hat{C}_1S_1H_1$, $H_4\hat{C}_1S_1H_1$ [c]/deg	61.4	61.6	-0.2
$H_5\hat{C}_2S_2H_1$, $H_8\hat{C}_3S_2H_1$ [c]/deg	0.0		
$H_6\hat{C}_2S_2H_1$, $H_9\hat{C}_3S_2H_1$ [c]/deg	118.8		
$H_7\hat{C}_2S_2H_1$, $H_{10}\hat{C}_3S_2H_1$ [c]/deg	118.8		

[a] See Figure 2.16 for numbering of atoms

[b] Difference = complex - monomer parameter

[c] Dihedral angle

X is a dummy atom situated on H_1 such that SH_1X is 90°.

All the complexes possess C_s symmetry. In very weak hydrogen bonded interactions, the constituent subunits will be almost unperturbed, and the intramolecular geometrical parameters obtained will be almost identical with those of the isolated molecules.[3] An analysis of the above tables indicates that changes in the geometrical parameters of the interacting moieties upon complexation are minor. In fact, the only intramolecular bond length change above 0.6 % for any of the complexes is in the OH...N hydrogen bonded complex (Table 2.19), where the OH bond length increases by 0.83 pm. The

only significant intramolecular bond angle change occurs in the dimethylamine complexes (Tables 2.21 - 2.23), where the HCN bond angles that involve the two out-of-plane hydrogen atoms on each of the methyl subunits of dimethylamine increase by approximately 2 % in all three complexes. The SH...S hydrogen bonded complex registers no intramolecular bond length or bond angle changes that exceed 0.19 %. The most extreme change in the geometrical parameters of the OH...S complex (Table 2.20) is 0.6 % (for $C\hat{S}C$) while that for SH...O complex (Table 2.24) is 0.3 % (for $C_2\hat{S}_2C_3$). The largest overall changes in the parameters occur in the cases where the proton acceptor atom is nitrogen.

The covalent A-H bond increases in length upon complexation in all cases except in the SH...S hydrogen bonded interaction (Table 2.26), where the SH bond length decreases. In all three sets of complexes with common proton donors, the A-H bond length order increases as the proton acceptor atom changes from sulphur to oxygen to nitrogen. As it is generally assumed that the A-H bond is lengthened in strong hydrogen bonds[123] it appears that, based on this parameter, the proton accepting strength of the atoms under consideration is in the order N > O > S. The fact that the SH...S hydrogen bond causes the S-H bond length to decrease seems to imply that the interaction between the two monomer subunits is negligible. A more in-depth analysis of the changes in some of the geometrical parameters upon complexation will be undertaken in section 2.4.5.

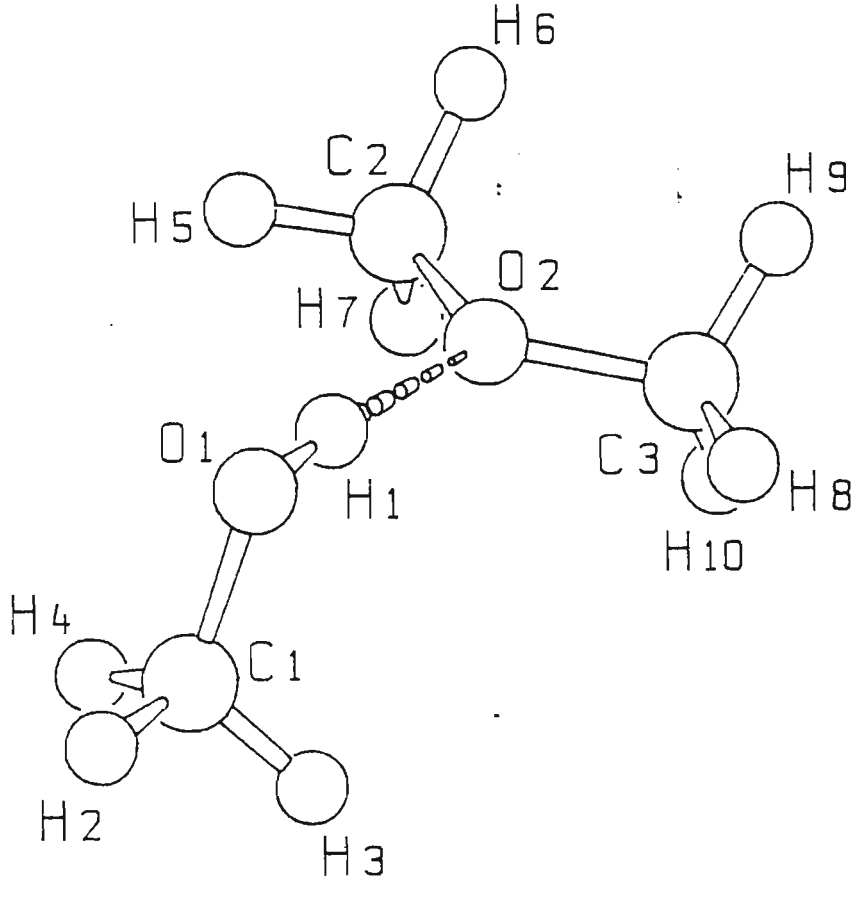

Fig. 2.8. Schakal plot of the OH...O hydrogen bonded complex.

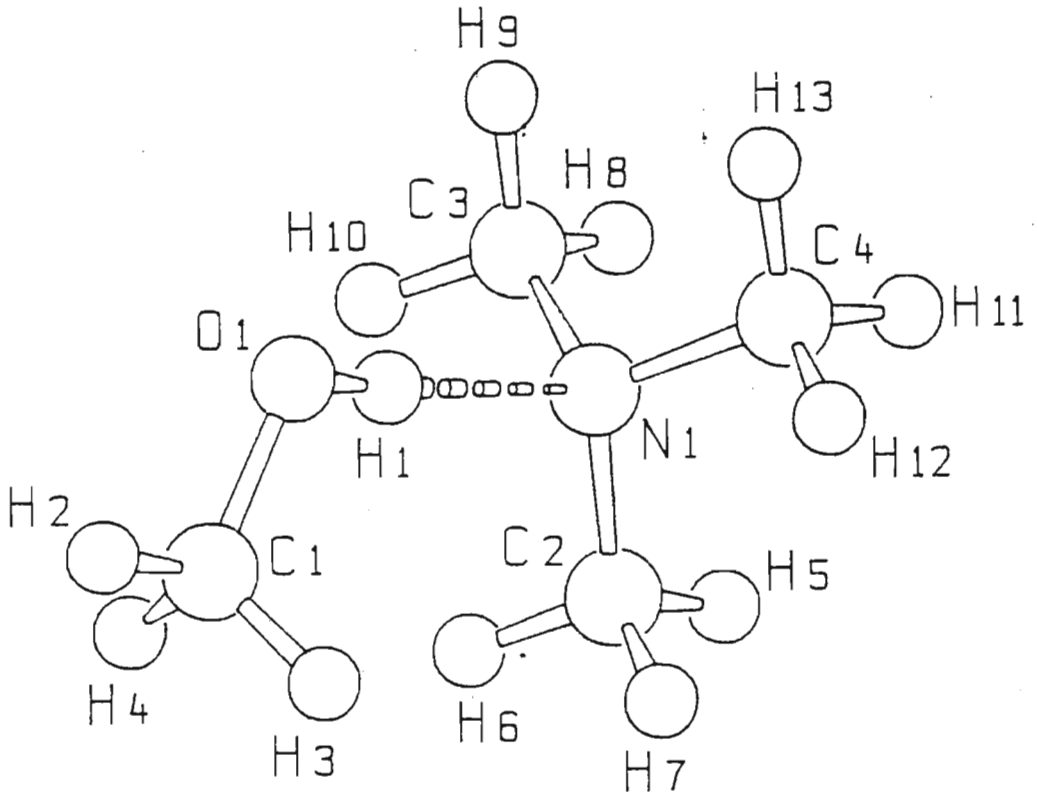

Fig. 2.9. Schakal plot of the OH...N hydrogen bonded complex.

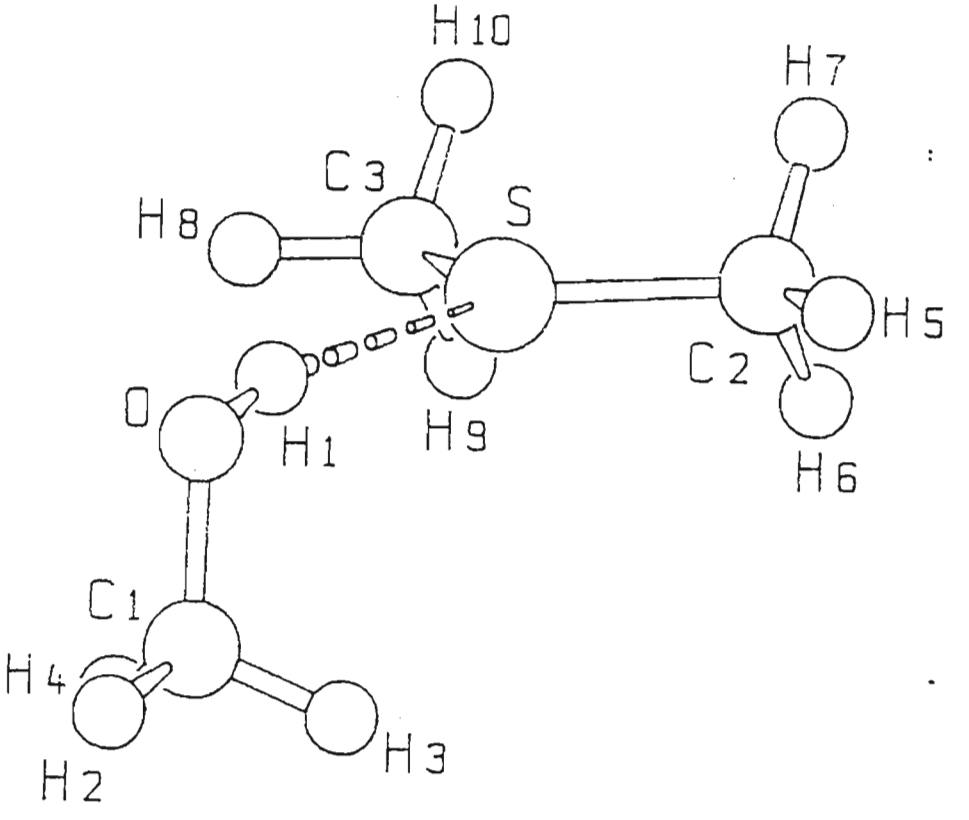

Fig. 2.10. Schakal plot of the OH...S hydrogen bonded complex.

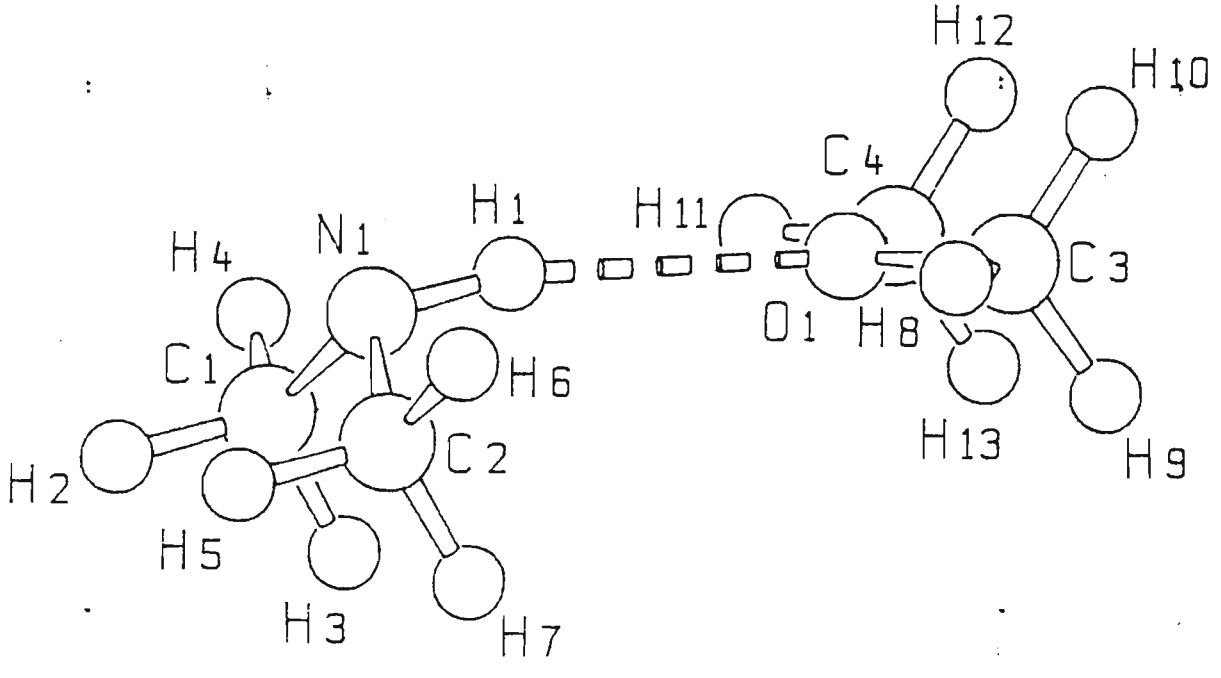

Fig. 2.11. Schakal plot of the NH..:O hydrogen bonded complex.

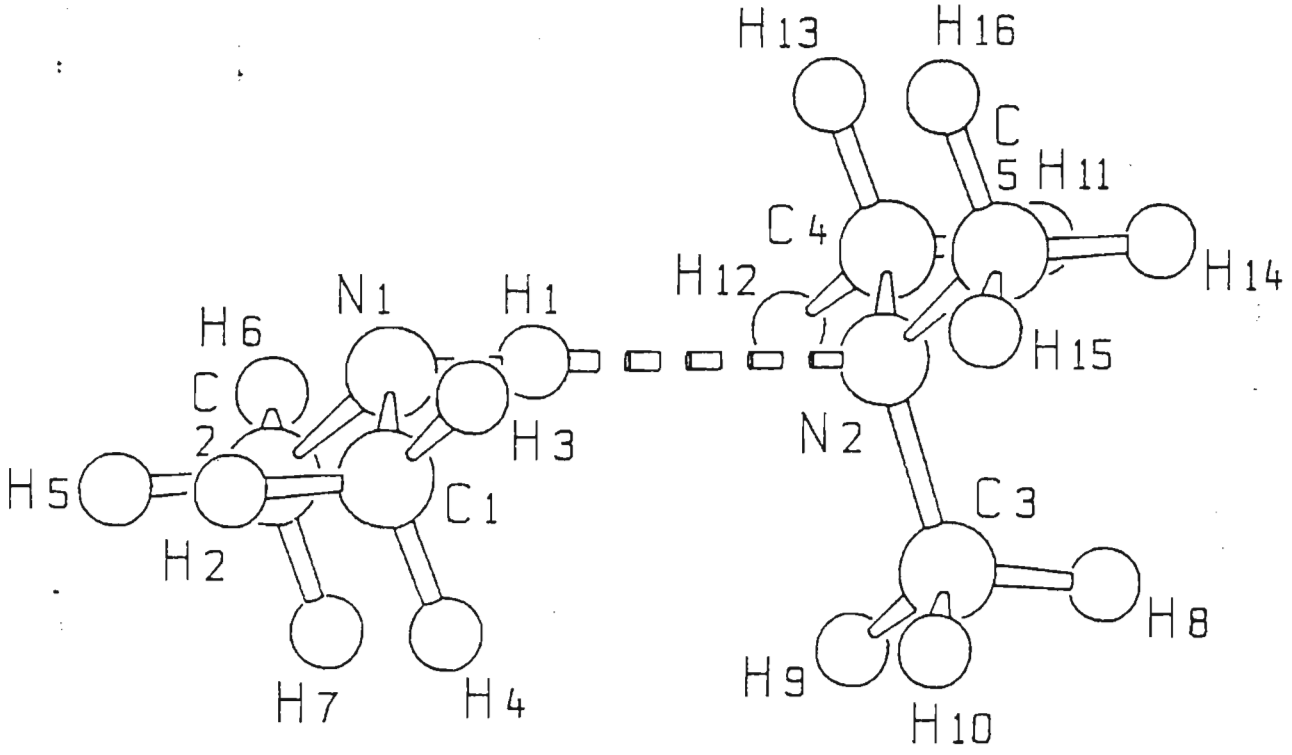

Fig. 2.12. Schakal plot of the NH...N hydrogen bonded complex.

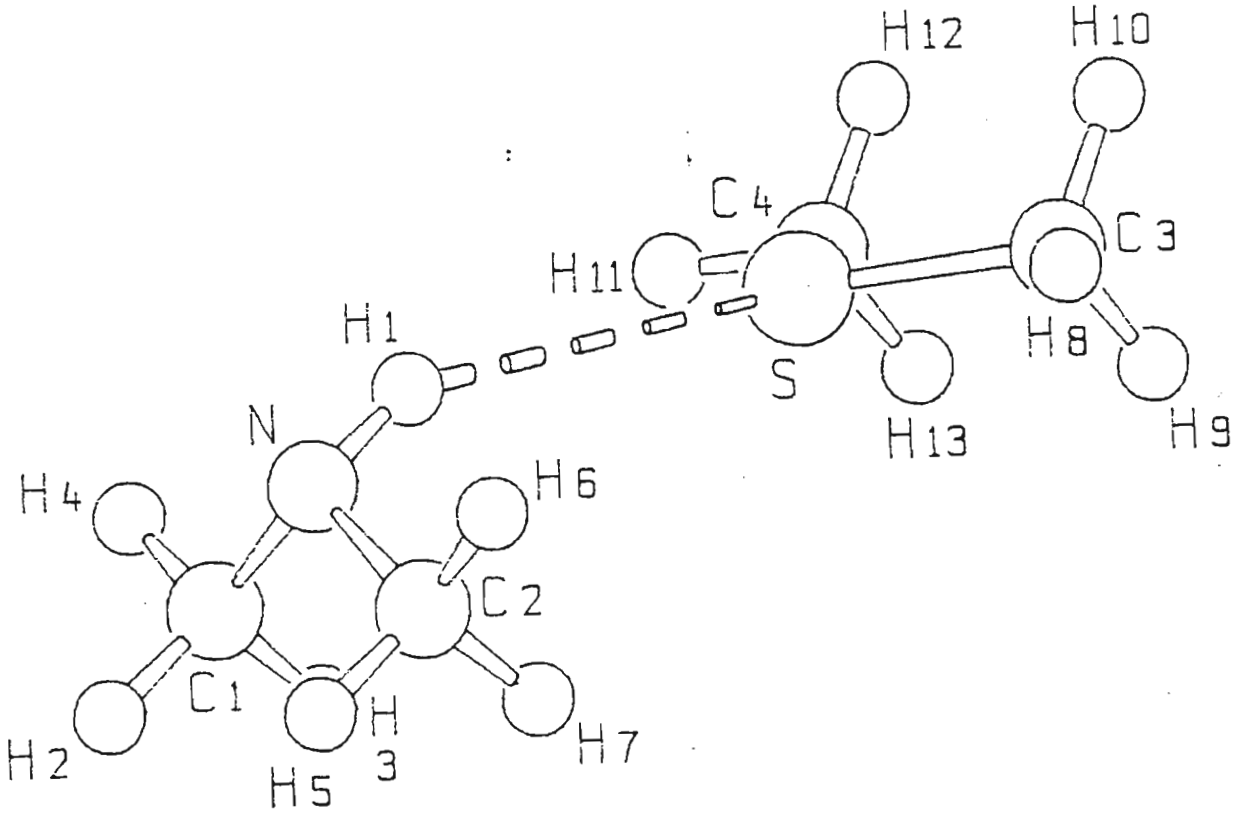

Fig. 2.13. Schakal plot of the NH...S hydrogen bonded complex.

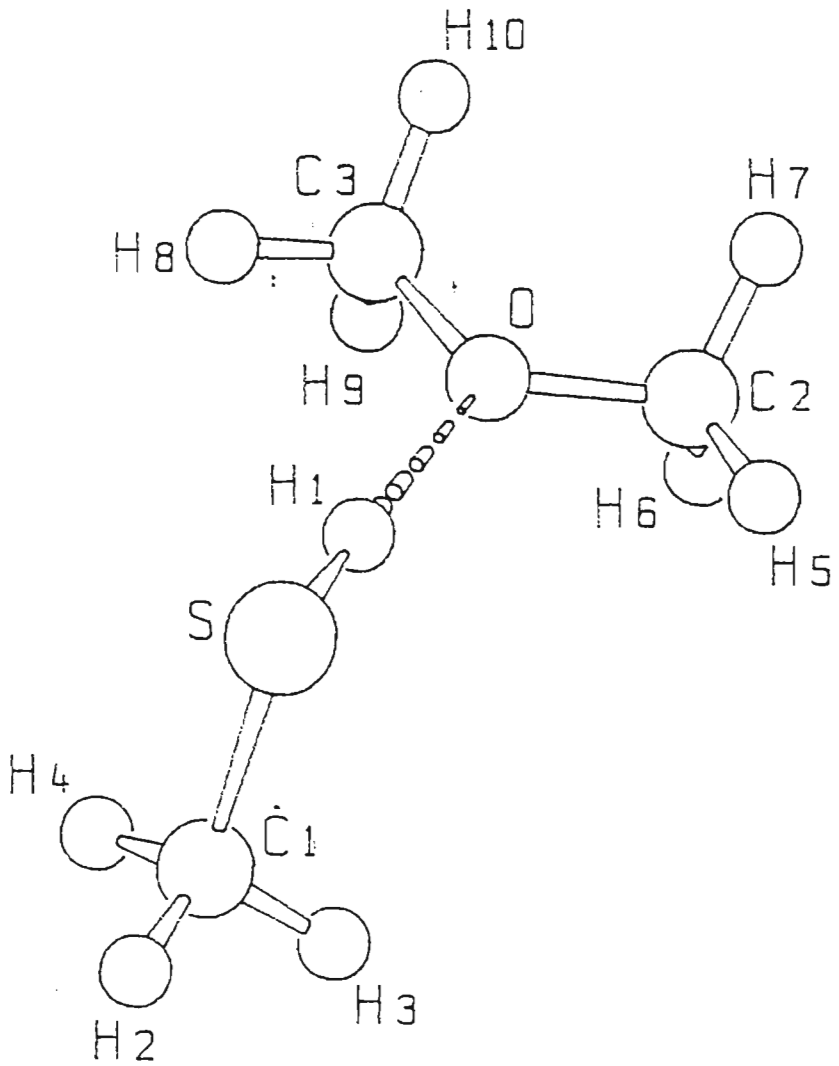

Fig. 2.14. Schakal plot of the SH...O hydrogen bonded complex.

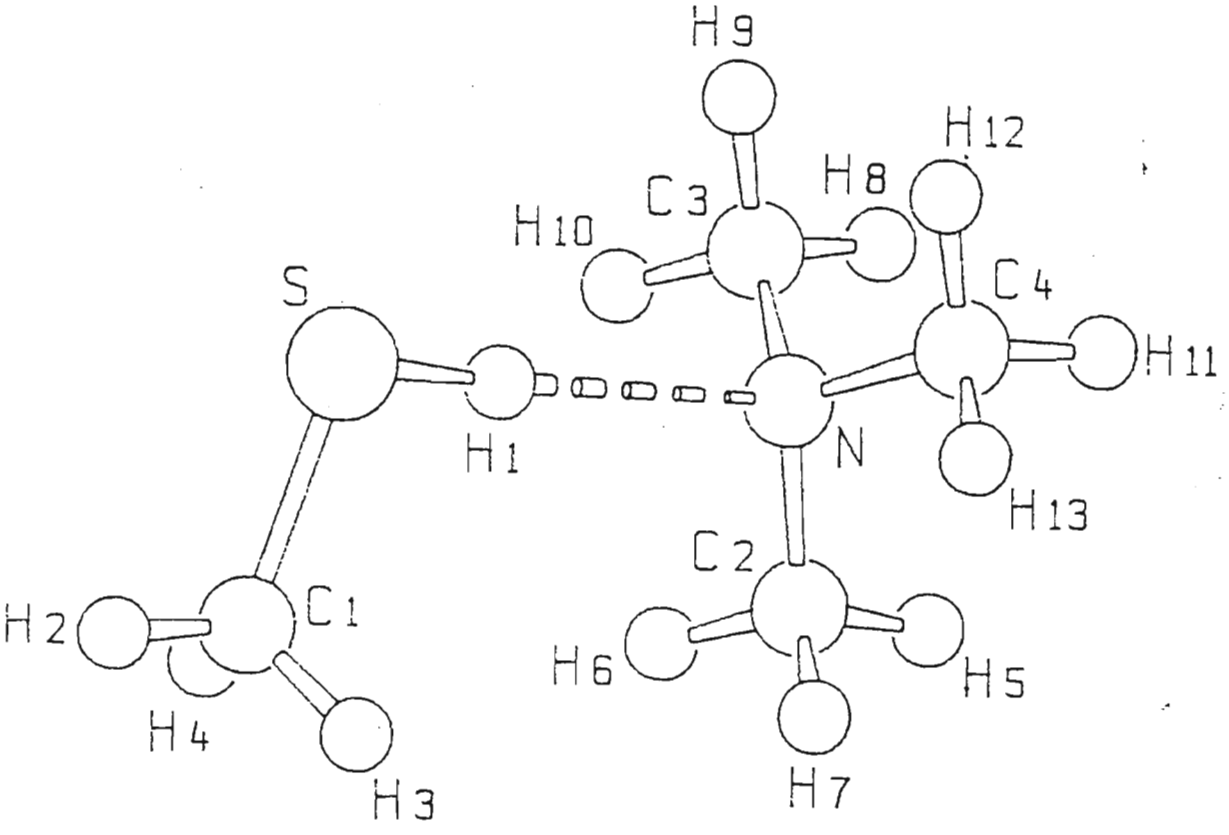

Fig. 2.15. Schakal plot of the SH...N hydrogen bonded complex.

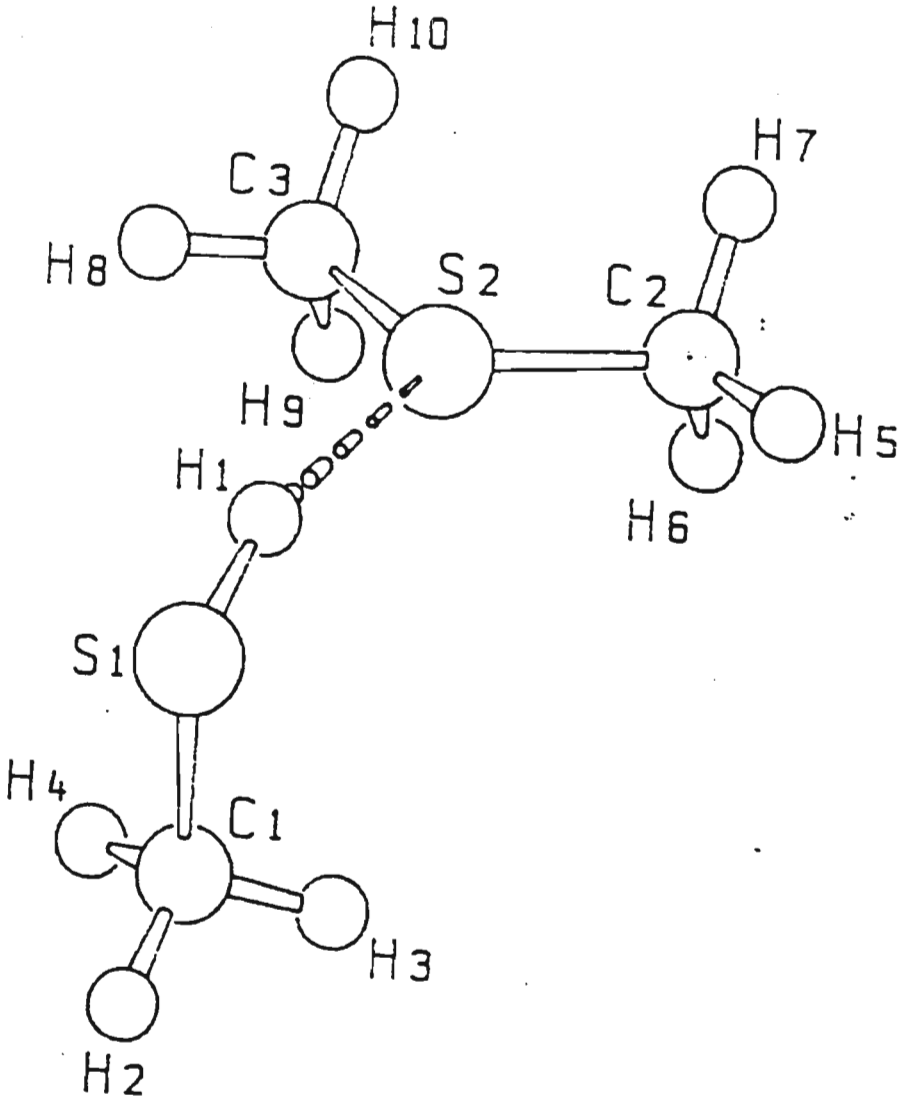

Fig. 2.16. Schakal plot of the SH...S hydrogen bonded complex.

2.4.4 Vibrational Spectra of the Molecular Complexes

Through *ab initio* molecular orbital calculations, a theoretical capability has become available for predicting vibrational spectra. They have become valuable in assisting with the assignments of the vibrational bands of molecular complexes. For example, large perturbations as a result of complexation can make the vibrational assignments of these complexes very difficult. Also, when degeneracies are lifted, or when inactive modes become activated as a result of the lowering of symmetry which often accompanies complex formation, a knowledge of the wavenumbers and intensities of a particular molecular group can be invaluable in determining the correct assignment for a given observed vibrational band.[39]

The vibrations of molecules associated through hydrogen bonds have been described in detail in a number of standard texts.[3,31-35,124] Most of the descriptions of the vibrational spectra of hydrogen bonded species have concentrated on the AH stretching, ν(AH), in-plane bending, δ(AH...B), and out-of-plane bending , γ(AH...B), modes of the AH group involved in the AH...B hydrogen bond. When two non-linear monomeric species interact to form a hydrogen bonded complex, the number of normal modes of vibration of the complex, $3(n_x+n_y)$-6, exceeds the sum of the numbers of normal modes of the individual monomers by six. Three translational and three rotational degrees of freedom become vibrational degrees of freedom of the complex[3](see section 2.3.3). Of these, one involves stretching of the A...B bond while the other five are called deformations because each involves some sort of orientational change with respect to the hydrogen bond. The counter translational and rotational motions of the monomer units may be designated T_α and R_α (α=x,y,z), which symbols describe translation along, and rotation about, the α axis respectively.[89]

As a result of the relative weakness of a typical hydrogen bond compared

with an orthodox covalent chemical bond, and its consequently lower stretching and bending force constants, and because of the larger reduced mass of a hydrogen bonded complex compared with those of the separate associating monomers, the intermolecular modes are usually observed at very low wavenumbers, usually below 700 cm^{-1}. As a result, the number of hydrogen bonded molecular complexes for which the full set of intermolecular modes has been observed experimentally is very small.[92] The *ab initio* calculations of the infrared spectra of the hydrogen bonded molecular complexes include both the intramolecular and intermolecular sets of vibrations.

Table 2.27. Computed wavenumbers of the methanol-dimethyl ether complex, and comparison with those of the monomers.

Symmetry species	Mode	Approximate description[a]	Wavenumber/cm^{-1} Complex	Monomer	Difference[b]
a′	ν_1	ν(OH)(M)	4124	4193	-69
	ν_2	ν(CH_3)(E)	3291	3281	10
	ν_3	ν(CH_3)(M)	3258	3278	-20
	ν_4	ν(CH_3)(E)	3217	3194	23
	ν_5	ν(CH_3)(E)	3167	3153	14
	ν_6	ν(CH_3)(M)	3143	3157	-14
	ν_7	δ(CH_3)(E)	1652	1654	-2
	ν_8	δ(CH_3)(M)	1647	1646	1
	ν_9	δ(CH_3)(E)	1634	1634	0
	ν_{10}	δ(CH_3)(E)	1633	1633	0
	ν_{11}	δ(CH_3)(M)	1625	1624	1
	ν_{12}	δ(COH)(M)	1537	1491	46
	ν_{13}	ρ(CH_3)(E)	1399	1395	4
	ν_{14}	ρ(CH_3)(E)	1308	1308	0
	ν_{15}	ρ(CH_3)(M)	1203	1189	14
	ν_{16}	ν(CO)(M)	1195	1157	38
	ν_{17}	ν_s(COC)(E)	1032	1042	-10
	ν_{18}	δ(COC)(E)	445	443	2
	ν_{19}	τ(CH_3)(E)	259	263	-4
	ν_{20}	δ(OH...O)	146	c	
	ν_{21}	ν(OH...O)	78	c	
	ν_{22}	Ry(con)[d]	18	c	
a"	ν_{23}	ν(CH_3)(E)	3289	3278	11
	ν_{24}	ν(CH_3)(E)	3215	3192	23

Table 2.27 cont.

ν_{25}	$\nu(CH_3)(M)$	3185	3206	-21
ν_{26}	$\nu(CH_3)(E)$	3153	3137	16
ν_{27}	$\delta(CH_3)(M)$	1634	1634	0
ν_{28}	$\delta(CH_3)(E)$	1633	1634	-1
ν_{29}	$\delta(CH_3)(E)$	1621	1621	0
ν_{30}	$\delta(CH_3)(E)$	1598	1597	1
ν_{31}	$\rho(CH_3)(E)$	1338	1345	-7
ν_{32}	$\rho(CH_3)(M)$	1287	1284	3
ν_{33}	$\rho(CH_3)(E)$	1272	1272	0
ν_{34}	$\rho_a(COC)(E)$	1225	1228	-3
ν_{35}	$\gamma(OH...O)$	646	c	
ν_{36}	$\tau(CH_3)(E)$	207	211	-4
ν_{37}	$\tau(CH_3)(M)$	127	341	-214
ν_{38}	$R_x(con)$[d]	29	c	
ν_{39}	$R_x(anti)$[d]	-25	c	

[a] M and E refer to the methanol and dimethyl ether monomers in which each normal mode is primarily localized.

[b] Difference = complex - monomer wavenumber.

[c] Intermolecular mode

[d] See ref. 89 for explanation of notation.

Table 2.28. Computed wavenumbers of the methanol-trimethylamine complex, and comparison with those of the monomers.

Symmetry species	Mode	Approximate description[a]	Wavenumber/cm^{-1} Complex	Monomer	Difference[b]
a′	ν_1	ν(OH)(M)	4019	4193	-174
	ν_2	$\nu(CH_3)$(T)	3276	3269	7
	ν_3	$\nu(CH_3)$(M)	3255	3278	-23
	ν_4	$\nu(CH_3)$(T)	3237	3225	12
	ν_5	$\nu(CH_3)$(T)	3226	3215	11
	ν_6	$\nu(CH_3)$(M)	3136	3157	-21
	ν_7	$\nu(CH_3)$(T)	3131	3101	30
	ν_8	$\nu(CH_3)$(T)	3117	3085	32
	ν_9	$\delta(CH_3)$(M)	1648	1646	2
	ν_{10}	$\delta(CH_3)$(T)	1645	1649	-4
	ν_{11}	$\delta(CH_3)$(T)	1641	1638	3
	ν_{12}	$\delta(CH_3)$(T)	1628	1625	3
	ν_{13}	$\delta(CH_3)$(M)	1624	1624	0
	ν_{14}	$\delta(CH_3)$(T)	1617	1613	4
	ν_{15}	$\delta(CH_3)$(T)	1582	1580	2
	ν_{16}	δ(COH)(M)	1567	1491	76
	ν_{17}	$\rho(CH_3)$(T)	1431	1441	-10
	ν_{18}	$\rho(CH_3)$(T)	1338	1326	12
	ν_{19}	$\rho(CH_3)$(T)	1224	1218	6
	ν_{20}	$\rho(CH_3)$(M)	1214	1189	25
	ν_{21}	ν(CO)(M)	1205	1157	48
	ν_{22}	$\nu(NC_3)$(T)	1144	1152	-8
	ν_{23}	$\nu(NC_3)$(T)	897	900	-3
	ν_{24}	$\delta(NC_3)$(T)	458	459	-1

Table 2.28 cont.

	ν_{25}	$\delta(NC_3)(T)$	416	381	35
	ν_{26}	$\tau(CH_3)(T)$	279	283	
	ν_{27}	δ(OH...N)	160	c	
	ν_{28}	ν(OH...N)	100	c	
	ν_{29}	R_y(anti)[d]	44	c	
a"	ν_{30}	$\nu(CH_3)(T)$	3273	3269	4
	ν_{31}	$\nu(CH_3)(T)$	3265	3261	4
	ν_{32}	$\nu(CH_3)(T)$	3231	3215	16
	ν_{33}	$\nu(CH_3)(M)$	3175	3206	-31
	ν_{34}	$\nu(CH_3)(T)$	3117	3085	32
	ν_{35}	$\delta(CH_3)(T)$	1646	1649	-3
	ν_{36}	$\delta(CH_3)(M)$	1634	1634	0
	ν_{37}	$\delta(CH_3)(T)$	1623	1628	-5
	ν_{38}	$\delta(CH_3)(T)$	1618	1613	5
	ν_{39}	$\delta(CH_3)(T)$	1580	1580	0
	ν_{40}	$\rho(CH_3)(T)$	1435	1441	-6
	ν_{41}	$\rho(CH_3)(M)$	1286	1284	2
	ν_{42}	$\rho(CH_3)(T)$	1221	1218	3
	ν_{43}	$\rho(CH_3)(T)$	1165	1167	-2
	ν_{44}	$\rho(NC_3)(T)$	1142	1152	-10
	ν_{45}	γ(OH...N)	722	c	
	ν_{46}	$\delta(NC_3)(T)$	451	459	-8
	ν_{47}	$\tau(CH_3)(T)$	289	283	6
	ν_{48}	$\tau(CH_3)(T)$	252	256	-4
	ν_{49}	$\tau(CH_3)(M)$	135	341	-206
	ν_{50}	R_x(anti)[d]	29	c	
	ν_{51}	R_z(anti)[d]	-14	c	

[a] M and T refer to the methanol and trimethylamine monomers in which

each normal mode is primarily localized.

[b] Difference = complex - monomer wavenumber.

[c] Intermolecular mode

[d] See ref. 89 for explanation of notation.

Table 2.29. Computed wavenumbers of the methanol-dimethyl sulphide complex, and comparison with those of the monomers.

Symmetry species	Mode	Approximate description[a]	Wavenumber/cm^{-1} Complex	Monomer	Difference[b]
a'	ν_1	ν(OH)(M)	4183	4193	-10
	ν_2	ν(CH_3)(S)	3299	3295	4
	ν_3	ν(CH_3)(S)	3285	3279	6
	ν_4	ν(CH_3)(M)	3268	3278	-10
	ν_5	ν(CH_3)(S)	3201	3197	4
	ν_6	ν(CH_3)(M)	3156	3157	-3
	ν_7	δ(CH_3)(M)	1646	1646	0
	ν_8	δ(CH_3)(M)	1624	1624	0
	ν_9	δ(CH_3)(S)	1617	1618	-1
	ν_{10}	δ(CH_3)(S)	1604	1605	-1
	ν_{11}	δ(CH_3)(S)	1515	1514	1
	ν_{12}	δ(COH)(M)	1498	1491	7
	ν_{13}	ρ(CH_3)(M)	1193	1189	4
	ν_{14}	ρ(CH_3)(S)	1166	1159	7
	ν_{15}	ν(CO)(M)	1160	1157	3
	ν_{16}	ρ(CH_3)(S)	1086	1087	-1
	ν_{17}	ν_s(CSC)(S)	751	752	-1
	ν_{18}	δ(CSC)(S)	285	286	-1
	ν_{19}	τ(CH_3)(S)	198	202	-4
	ν_{20}	δ(OH...S)	71	c	
	ν_{21}	ν(OH...S)	39	c	
	ν_{22}	R_y(con)[d]	-46	c	
a"	ν_{23}	ν(CH_3)(S)	3300	3295	5
	ν_{24}	ν(CH_3)(S)	3288	3282	6

Table 2.29 cont.

ν_{25}	$\nu(CH_3)(M)$	3203	3206	-3
ν_{26}	$\nu(CH_3)(S)$	3202	3198	4
ν_{27}	$\delta(CH_3)(M)$	1633	1634	-1
ν_{28}	$\delta(CH_3)(S)$	1609	1609	0
ν_{29}	$\delta(CH_3)(S)$	1594	1595	-1
ν_{30}	$\delta(CH_3)(S)$	1489	1488	1
ν_{31}	$\rho(CH_3)(M)$	1286	1284	2
ν_{32}	$\rho(CH_3)(S)$	1054	1052	2
ν_{33}	$\rho(CH_3)(S)$	1008	1005	3
ν_{34}	$\nu_a(CSC)(S)$	818	816	2
ν_{35}	$\gamma(OH...S)$	413	c	
ν_{36}	$\tau(CH_3)(S)$	190	193	-3
ν_{37}	$\tau(CH_3)(M)$	93	341	-248
ν_{38}	$R_x(con)$[d]	17	c	
ν_{39}	$R_x(anti)$[d]	-15	c	

[a] M and S refer to the methanol and dimethyl sulphide monomers in which each normal mode is primarily localized.

[b] Difference = complex - monomer wavenumber.

[c] Intermolecular mode

[d] See ref. 89 for explanation of notation.

Table 2.30. Computed wavenumbers of the dimethylamine -dimethyl ether complex, and comparison with those of the monomers.

Symmetry species	Mode	Approximate description[a]	Wavenumber/cm^{-1} Complex	Monomer	Difference[b]
a′	ν_1	ν(NH)(D)	3776	3783	-7
	ν_2	ν(CH_3)(E)	3285	3281	4
	ν_3	ν(CH_3)(D)	3234	3258	-24
	ν_4	ν(CH_3)(E)	3206	3194	12
	ν_5	ν(CH_3)(D)	3194	3217	-23
	ν_6	ν(CH_3)(E)	3161	3153	8
	ν_7	ν(CH_3)(D)	3143	3115	28
	ν_8	δ(CH_3)(E)	1653	1654	-1
	ν_9	δ(CH_3)(D)	1645	1648	-3
	ν_{10}	δ(CH_3)(D)	1637	1634	3
	ν_{11}	δ(CH_3)(E)	1634	1634	0
	ν_{12}	δ(CH_3)(E)	1632	1633	-1
	ν_{13}	δ(CH_3)(D)	1611	1608	3
	ν_{14}	ρ(CH_3)(E)	1397	1395	2
	ν_{15}	ρ(CH_3)(D)	1386	1382	4
	ν_{16}	ρ(CH_3)(D)	1317	1300	17
	ν_{17}	ρ(CH_3)(E)	1308	1308	0
	ν_{18}	ν_s(COC)(E)	1037	1042	-5
	ν_{19}	ν_s(CNC)(D)	1020	1011	9
	ν_{20}	δ_s(CNH)(D)	920	831	89
	ν_{21}	δ(COC)(E)	444	443	1
	ν_{22}	δ(CNC)(D)	438	416	22
	ν_{23}	τ(CH_3)(D)	302	279	23
	ν_{24}	τ(CH_3)(E)	261	263	-2

Table 2.30 cont.

	ν_{25}	ν(NH...O)	70	c	
	ν_{26}	R_y(con)[d]	21		
	ν_{27}	δ(NH...O)	-89	c	
a"	ν_{28}	$\nu(CH_3)$(E)	3283	3278	5
	ν_{29}	$\nu(CH_3)$(D)	3228	3255	-27
	ν_{30}	$\nu(CH_3)$(E)	3204	3192	12
	ν_{31}	$\nu(CH_3)$(D)	3192	3213	-21
	ν_{32}	$\nu(CH_3)$(E)	3146	3137	9
	ν_{33}	$\nu(CH_3)$(D)	3133	3107	26
	ν_{34}	$\delta(CH_3)$(D)	1673	1652	21
	ν_{35}	$\delta(CH_3)$(E)	1633	1634	-1
	ν_{36}	$\delta(CH_3)$(D)	1628	1620	8
	ν_{37}	$\delta(CH_3)$(E)	1620	1621	-1
	ν_{38}	$\delta(CH_3)$(D)	1619	1615	4
	ν_{39}	$\delta(CH_3)$(E)	1598	1597	1
	ν_{40}	$\rho(CH_3)$(D)	1574	1575	-1
	ν_{41}	$\rho(CH_3)$(E)	1340	1345	-5
	ν_{42}	$\rho(CH_3)$(E)	1272	1272	0
	ν_{43}	$\rho(CH_3)$(D)	1263	1277	-14
	ν_{44}	ν_a(COC)(E)	1227	1228	-1
	ν_{45}	ν_a(CNC)(D)	1204	1194	10
	ν_{46}	δ_a(CNH)(D)	1127	1123	4
	ν_{47}	$\tau(CH_3)$(D)	229	238	-9
	ν_{48}	$\tau(CH_3)$(E)	207	211	-4
	ν_{49}	γ(NH...O)	63	c	
	ν_{50}	R_x(anti)[d]	35	c	
	ν_{51}	R_z(anti)[d]	-14	c	

[a] D and E refer to the dimethylamine and dimethyl ether monomers in which

each normal mode is primarily localized.

[b] Difference = complex - monomer wavenumber.

[c] Intermolecular mode

[d] See ref. 89 for explanation of notation.

Table 2.31. Computed wavenumbers of the dimethylamine -trimethylamine complex, and comparison with those of the monomers.

Symmetry species	Mode	Approximate description[a]	Wavenumber/cm^{-1} Complex	Monomer	Difference[b]
a'	ν_1	ν(NH)(D)	3750	3783	-33
	ν_2	ν(CH_3)(T)	3269	3269	0
	ν_3	ν(CH_3)(D)	3233	3258	-25
	ν_4	ν(CH_3)(T)	3230	3225	5
	ν_5	ν(CH_3)(T)	3221	3215	6
	ν_6	ν(CH_3)(D)	3192	3217	-25
	ν_7	ν(CH_3)(D)	3141	3115	26
	ν_8	ν(CH_3)(T)	3119	3101	18
	ν_9	ν(CH_3)(T)	3105	3085	20
	ν_{10}	δ(CH_3)(T)	1646	1649	-3
	ν_{11}	δ(CH_3)(D)	1644	1648	-4
	ν_{12}	δ(CH_3)(T)	1641	1638	3
	ν_{13}	δ(CH_3)(D)	1637	1634	3
	ν_{14}	δ(CH_3)(T)	1626	1625	1
	ν_{15}	δ(CH_3)(T)	1617	1613	4
	ν_{16}	δ(CH_3)(D)	1611	1608	3
	ν_{17}	δ(CH_3)(T)	1580	1580	0
	ν_{18}	ρ(CH_3)(T)	1435	1441	-6
	ν_{19}	ρ(CH_3)(D)	1386	1382	4
	ν_{20}	ρ(CH_3)(T)	1332	1326	6
	ν_{21}	ρ(CH_3)(D)	1317	1300	17
	ν_{22}	ρ(CH_3)(T)	1220	1218	2
	ν_{23}	ν_a(NC_3)(T)	1147	1152	-5
	ν_{24}	ν_s(CNC)(D)	1027	1011	16

Table 2.31 cont.

	ν_{25}	δ_s(CNH)(D)	940	831	109
	ν_{26}	ν_s(NC_3)(T)	898	900	-2
	ν_{27}	δ_a(NC_3)(T)	457	459	-2
	ν_{28}	δ(CNC)(D)	440	416	24
	ν_{29}	δ_s(NC_3)(T)	398	381	17
	ν_{30}	τ(CH_3)(D)	302	279	23
	ν_{31}	τ(CH_3)(T)	284	283	1
	ν_{32}	ν(NH...N)	70	c	
	ν_{33}	R_y(anti)[d]	55	c	
	ν_{34}	δ(NH...N)	-73	c	
a"	ν_{35}	νCH_3)(T)	3267	3269	-2
	ν_{36}	ν(CH_3)(T)	3260	3261	-1
	ν_{37}	ν(CH_3)(D)	3228	3255	-27
	ν_{38}	ν(CH_3)(T)	3223	3215	8
	ν_{39}	ν(CH_3)(D)	3190	3213	-23
	ν_{40}	ν(CH_3)(D)	3130	3107	23
	ν_{41}	ν(CH_3)(T)	3105	3085	20
	ν_{42}	δ(CH_3)(D)	1679	1652	27
	ν_{43}	δ(CH_3)(T)	1645	1649	-4
	ν_{44}	δ(CH_3)(D)	1629	1620	9
	ν_{45}	δ(CH_3)(T)	1624	1628	-4
	ν_{46}	δ(CH_3)(D)	1620	1615	5
	ν_{47}	δ(CH_3)(T)	1617	1613	4
	ν_{48}	δ(CH_3)(T)	1580	1580	0
	ν_{49}	ρ(CH_3)(D)	1574	1575	-1
	ν_{50}	ρ(CH_3)(T)	1437	1441	-4
	ν_{51}	ρ(CH_3)(D)	1264	1277	-13
	ν_{52}	ρ(CH_3)(T)	1221	1218	3
	ν_{53}	ν_a(CNC)(D)	1204	1194	10

Table 2.31 cont.

ν_{54}	$\rho(CH_3)(T)$	1164	1167	-3
ν_{55}	$\nu(NC_3)(T)$	1146	1152	-6
ν_{56}	$\delta_a(CNH)(D)$	1128	1123	5
ν_{57}	$\delta_a(NC_3)(T)$	455	459	-4
ν_{58}	$\tau(CH_3)(T)$	286	283	3
ν_{59}	$\tau(CH_3)(T)$	257	256	1
ν_{60}	$\tau(CH_3)(D)$	228	238	-10
ν_{61}	γ(NH...N)	68	c	
ν_{62}	R_x(anti)[d]	35	c	
ν_{63}	R_z(anti)[d]	-10	c	

[a] D and T refer to the dimethylamine and trimethylamine monomers in which each normal mode is primarily localized.

[b] Difference = complex - monomer wavenumber.

[c] Intermolecular mode

[d] See ref. 89 for explanation of notation.

Table 2.32. Computed wavenumbers of the dimethylamine-dimethyl sulphide complex, and comparison with those of the monomers.

Symmetry species	Mode	Approximate description[a]	Wavenumber/cm^{-1} Complex	Monomer	Difference[b]
a′	ν_1	ν(NH)(D)	3775	3783	-8
	ν_2	ν(CH$_3$)(S)	3297	3295	2
	ν_3	ν(CH$_3$)(S)	3282	3279	-3
	ν_4	ν(CH$_3$)(D)	3239	3258	-19
	ν_5	ν(CH$_3$)(D)	3202	3217	-15
	ν_6	ν(CH$_3$)(S)	3199	3197	2
	ν_7	ν(CH$_3$)(D)	3149	3115	34
	ν_8	δ(CH$_3$)(D)	1646	1648	-2
	ν_9	δ(CH$_3$)(D)	1636	1634	2
	ν_{10}	δ(CH$_3$)(S)	1618	1618	0
	ν_{11}	δ(CH$_3$)(D)	1611	1608	3
	ν_{12}	δ(CH$_3$)(S)	1605	1605	0
	ν_{13}	δ(CH$_3$)(S)	1515	1514	1
	ν_{14}	ρ(CH$_3$)(D)	1383	1382	1
	ν_{15}	ρ(CH$_3$)(D)	1317	1300	17
	ν_{16}	ρ(CH$_3$)(S)	1160	1159	1
	ν_{17}	ρ(CH$_3$)(S)	1087	1087	0
	ν_{18}	ν_s(CNC)(D)	1012	1011	1
	ν_{19}	δ_s(CNH)(N)	883	831	52
	ν_{21}	ν_s(CSC)(S)	752	752	0
	ν_{20}	δ(CNC)(D)	437	416	21
	ν_{22}	τ(CH$_3$)(D)	299	279	20
	ν_{23}	δ(CSC)(S)	286	286	0
	ν_{24}	τ(CH$_3$)(S)	200	202	-2

Table 2.32 cont.

	ν_{25}	ν(NH...S)	32	c	
	ν_{26}	Ry(con)[d]	-25	c	
	ν_{27}	δ(NH...S)	-106	c	
a"	ν_{28}	$\nu(CH_3)$(S)	3298	3295	3
	ν_{29}	$\nu(CH_3)$(S)	3285	3282	3
	ν_{30}	$\nu(CH_3)$(D)	3234	3255	-21
	ν_{31}	$\nu(CH_3)$(D)	3200	3213	-13
	ν_{32}	$\nu(CH_3)$(S)	3200	3198	2
	ν_{33}	$\nu(CH_3)$(D)	3140	3107	33
	ν_{34}	$\delta(CH_3)$(D)	1651	1652	-1
	ν_{35}	$\delta(CH_3)$(D)	1623	1620	3
	ν_{36}	$\delta(CH_3)$(D)	1617	1615	2
	ν_{37}	$\delta(CH_3)$(S)	1609	1609	0
	ν_{38}	$\delta(CH_3)$(S)	1594	1594	0
	ν_{39}	$\rho(CH_3)$(D)	1573	1575	-2
	ν_{40}	$\delta(CH_3)$(S)	1489	1488	1
	ν_{41}	ν_a(CNC)(D)	1260	1277	-17
	ν_{42}	$\rho(CH_3)$(D)	1203	1194	9
	ν_{43}	δ_a(CNH)(D)	1122	1123	-1
	ν_{44}	$\rho(CH_3)$(S)	1052	1051	1
	ν_{46}	$\rho(CH_3)$(S)	1006	1005	1
	ν_{47}	ν_a(CSC)(S)	817	816	1
	ν_{45}	$\tau(CH_3)$(D)	228	238	-10
	ν_{48}	$\tau(CH_3)$(S)	192	193	-1
	ν_{49}	γ(NH...S)	45	c	
	ν_{50}	R_x(anti)[d]	19	c	
	ν_{51}	R_z(anti)[d]	-13	c	

[a] D and S refer to the dimethylamine and dimethylsulphide monomers in

which each normal mode is primarily localized.

[b] Difference = complex - monomer wavenumber.

[c] Intermolecular mode

[d] See ref. 89 for explanation of notation.

Table 2.33. Computed wavenumbers of the methane thiol-dimethyl ether complex, and comparison with those of the monomers.

Symmetry species	Mode	Approximate description[a]	Wavenumber/cm^{-1} Complex	Monomer	Difference[b]
a'	ν_1	$\nu(CH_3)(S)$	3303	3313	-10
	ν_2	$\nu(CH_3)(E)$	3285	3281	4
	ν_3	$\nu(CH_3)(S)$	3213	3216	-3
	ν_4	$\nu(CH_3)(E)$	3206	3194	12
	ν_5	$\nu(CH_3)(E)$	3160	3153	7
	ν_6	$\nu(SH)(M)$	2889	2892	-3
	ν_7	$\delta(CH_3)(E)$	1653	1654	-1
	ν_8	$\delta(CH_3)(E)$	1634	1634	0
	ν_9	$\delta(CH_3)(E)$	1633	1633	0
	ν_{10}	$\delta(CH_3)(S)$	1619	1617	2
	ν_{11}	$\delta(CH_3)(S)$	1502	1502	0
	ν_{12}	$\rho(CH_3)(E)$	1397	1395	2
	ν_{13}	$\rho(CH_3)(E)$	1308	1308	0
	ν_{14}	$\rho(CH_3)(S)$	1219	1207	12
	ν_{15}	$\nu_s(COC)(E)$	1036	1042	6
	ν_{16}	$\delta(CSH)(S)$	886	868	18
	ν_{17}	$\nu(CS)(S)$	777	770	7
	ν_{18}	$\delta(COC)(E)$	444	443	1
	ν_{19}	$\tau(CH_3)(E)$	261	263	-2
	ν_{20}	$\delta(SH...O)$	75	c	
	ν_{21}	$\nu(SH...O)$	29	c	
	ν_{22}	Ry(con)[d]	17	c	
a"	ν_{23}	$\nu(CH_3)(S)$	3302	3305	-3
	ν_{24}	$\nu(CH_3)(E)$	3283	3278	5

Table 2.33 cont.

ν_{25}	$\nu(CH_3)(E)$	3203	3194	9
ν_{26}	$\nu(CH_3)(E)$	3145	3137	8
ν_{27}	$\delta(CH_3)(E)$	1634	1634	0
ν_{28}	$\delta(CH_3)(E)$	1621	1621	0
ν_{29}	$\delta(CH_3)(S)$	1605	1605	0
ν_{30}	$\delta(CH_3)(E)$	1598	1597	1
ν_{31}	$\rho(CH_3)(E)$	1340	1345	-5
ν_{32}	$\rho(CH_3)(E)$	1272	1272	0
ν_{33}	$\nu_a(COC)(E)$	1227	1228	-1
ν_{34}	$\rho(CH_3)(S)$	1068	1077	-9
ν_{35}	$\gamma(SH...O)$	386	c	
ν_{36}	$\tau(CH_3)(E)$	210	211	-1
ν_{37}	$\tau(CH_3)(S)$	115	241	-126
ν_{38}	$R_x(con)$[d]	23	c	
ν_{39}	$R_x(anti)$[d]	9	c	

[a] S and E refer to the methane thiol and dimethyl ether monomers in which each normal mode is primarily localized.

[b] Difference = complex - monomer wavenumber.

[c] Intermolecular mode

[d] See ref. 89 for explanation of notation.

Table 2.34. Computed wavenumbers of the methane thiol-trimethylamine complex, and comparison with those of the monomers.

Symmetry species	Mode	Approximate description[a]	Wavenumber/cm^{-1} Complex	Monomer	Difference[b]
a′	ν_1	$\nu(CH_3)(S)$	3302	3313	-11
	ν_2	$\nu(CH_3)(T)$	3269	3269	0
	ν_3	$\nu(CH_3)(T)$	3230	3225	5
	ν_4	$\nu(CH_3)(T)$	3219	3215	4
	ν_5	$\nu(CH_3)(S)$	3211	3216	-5
	ν_6	$\nu(CH_3)(T)$	3121	3101	20
	ν_7	$\nu(CH_3)(T)$	3106	3085	21
	ν_8	$\nu(SH)(S)$	2838	2892	-54
	ν_9	$\delta(CH_3)(T)$	1645	1649	-4
	ν_{10}	$\delta(CH_3)(T)$	1640	1638	2
	ν_{11}	$\delta(CH_3)(T)$	1626	1625	1
	ν_{12}	$\delta(CH_3)(S)$	1620	1617	3
	ν_{13}	$\delta(CH_3)(T)$	1616	1613	3
	ν_{14}	$\delta(CH_3)(T)$	1580	1580	0
	ν_{15}	$\delta(CH_3)(S)$	1502	1502	0
	ν_{16}	$\rho(CH_3)(T)$	1436	1441	-5
	ν_{17}	$\rho(CH_3)(T)$	1332	1326	6
	ν_{18}	$\rho(CH_3)(S)$	1230	1207	23
	ν_{19}	$\rho(CH_3)(T)$	1219	1218	1
	ν_{20}	$\nu_a(NC_3)(T)$	1147	1152	-5
	ν_{21}	$\delta(CSH)(S)$	903	868	35
	ν_{22}	$\nu_s(NC_3)(T)$	897	900	-3
	ν_{23}	$\nu(CS)(S)$	777	770	7
	ν_{24}	$\delta_a(NC_3)(T)$	457	459	-2

Table 2.34 cont.

	ν_{25}	$\delta_s(NC_3)(T)$	398	381	17
	ν_{26}	$\tau(CH_3)(T)$	282	283	-1
	ν_{27}	δ(SH...N)	78	c	
	ν_{28}	ν(SH...N)	55	c	
	ν_{29}	Ry(anti)[d]	29	c	
a"	ν_{30}	$\nu(CH_3)(S)$	3299	3305	-6
	ν_{31}	$\nu(CH_3)(T)$	3267	3269	-2
	ν_{32}	$\nu(CH_3)(T)$	3258	3261	-3
	ν_{33}	$\nu(CH_3)(T)$	3223	3215	8
	ν_{34}	$\nu(CH_3)(T)$	3105	3085	20
	ν_{35}	$\delta(CH_3)(T)$	1646	1649	-3
	ν_{36}	$\delta(CH_3)(T)$	1624	1628	-4
	ν_{37}	$\delta(CH_3)(T)$	1617	1613	4
	ν_{38}	$\delta(CH_3)(S)$	1607	1605	2
	ν_{39}	$\delta(CH_3)(T)$	1580	1580	0
	ν_{40}	$\rho(CH_3)(T)$	1437	1441	-4
	ν_{41}	$\rho(CH_3)(T)$	1220	1218	2
	ν_{42}	$\rho(CH_3)(T)$	1164	1167	-3
	ν_{43}	$\nu_a(NC_3)(T)$	1146	1152	-6
	ν_{44}	$\rho(CH_3)(S)$	1068	1077	-9
	ν_{45}	$\rho_a(NC_3)(T)$	457	459	-2
	ν_{46}	γ(SH...N)	425	c	
	ν_{47}	$\tau(CH_3)(T)$	285	289	-4
	ν_{48}	$\tau(CH_3)(T)$	254	252	2
	ν_{49}	$\tau(CH_3)(S)$	125	241	-116
	ν_{50}	R_x(anti)[d]	30	c	
	ν_{51}	R_z(anti)[d]	-9	c	

[a] S and T refer to the methane thiol and trimethylamine monomers in which

each normal mode is primarily localized.

[b] Difference = complex - monomer wavenumber.

[c] Intermolecular mode

[d] See ref. 89 for explanation of notation.

Table 2.35. Computed wavenumbers of the methane thiol-dimethyl sulphide complex, and comparison with those of the monomers.

Symmetry species	Mode	Approximate description[a]	Wavenumber/cm^{-1} Complex	Monomer	Difference[b]
a'	ν_1	$\nu(CH_3)(M)$	3306	3313	-7
	ν_2	$\nu(CH_3)(S)$	3297	3295	2
	ν_3	$\nu(CH_3)(S)$	3281	3279	3
	ν_4	$\nu(CH_3)(M)$	3216	3216	0
	ν_5	$\nu(CH_3)(S)$	3199	3197	2
	ν_6	$\nu(SH)(M)$	2898	2892	6
	ν_7	$\delta(CH_3)(S)$	1618	1618	0
	ν_8	$\delta(CH_3)(M)$	1617	1617	0
	ν_9	$\delta(CH_3)(S)$	1605	1605	0
	ν_{10}	$\delta(CH_3)(S)$	1515	1514	1
	ν_{11}	$\delta(CH_3)(M)$	1503	1502	1
	ν_{12}	$\rho(CH_3)(M)$	1210	1207	3
	ν_{13}	$\rho(CH_3)(S)$	1160	1159	1
	ν_{14}	$\rho(CH_3)(S)$	1087	1087	7
	ν_{15}	$\delta(CSH)(M)$	870	868	2
	ν_{16}	$\nu(CS)(M)$	774	770	4
	ν_{17}	$\nu_s(CSC)(S)$	752	752	0
	ν_{18}	$\delta(CSC)(S)$	286	286	0
	ν_{19}	$\tau(CH_3)(S)$	201	202	-1
	ν_{20}	$\delta(SH...S)$	34	c	
	ν_{21}	$\nu(SH...S)$	24	c	
	ν_{22}	Ry(con)[d]	-16	c	
a"	ν_{23}	$\nu(CH_3)(M)$	3309	3305	4
	ν_{24}	$\nu(CH_3)(S)$	3297	3295	2

Table 2.35 cont.

ν_{25}	$\nu(CH_3)(S)$	3285	3282	3
ν_{26}	$\nu(CH_3)(S)$	3200	3198	2
ν_{27}	$\delta(CH_3)(S)$	1610	1609	1
ν_{28}	$\delta(CH_3)(M)$	1603	1605	-2
ν_{29}	$\delta(CH_3)(S)$	1595	1595	0
ν_{30}	$\delta(CH_3)(S)$	1489	1488	1
ν_{31}	$\rho(CH_3)(M)$	1071	1077	-6
ν_{32}	$\rho(CH_3)(S)$	1053	1051	2
ν_{33}	$\rho(CH_3)(S)$	1006	1005	1
ν_{34}	$\nu_a(CSC)(S)$	816	816	0
ν_{35}	$\gamma(SH...S)$	283	c	
ν_{36}	$\tau(CH_3)(S)$	192	193	-1
ν_{37}	$\tau(CH_3)(M)$	63	241	-178
ν_{38}	$R_x(con)$[d]	17	c	
ν_{39}	$R_x(anti)$[d]	-13	c	

[a] M and S refer to the methane thiol and dimethyl sulphide monomers in which each normal mode is primarily localized.

[b] Difference = complex - monomer wavenumber.

[c] Intermolecular mode

[d] See ref. 89 for explanation of notation.

Table 2.36. Computed intensities of the infrared active bands of the nine hydrogen bonded molecular complexes.

Monomer	Mode (symmetry species)	Intensity /km mol^{-1}	Mode (symmetry species)	Intensity /km mol^{-1}
$CH_3OH.O(CH_3)_2$	$\nu_1(a')$	344.8	$\nu_{21}(a')$	4.4
	$\nu_2(a')$	34.7	$\nu_{22}(a')$	3.9
	$\nu_3(a')$	74.6	$\nu_{23}(a")$	37.0
	$\nu_4(a')$	145.0	$\nu_{24}(a")$	0.007
	$\nu_5(a')$	67.3	$\nu_{25}(a")$	109.8
	$\nu_6(a')$	66.4	$\nu_{26}(a")$	47.1
	$\nu_7(a')$	0.1	$\nu_{27}(a')$	2.7
	$\nu_8(a')$	3.6	$\nu_{28}(a")$	8.8
	$\nu_9(a')$	2.0	$\nu_{29}(a")$	0.02
	$\nu_{10}(a')$	13.0	$\nu_{30}(a")$	10.6
	$\nu_{11}(a')$	9.1	$\nu_{31}(a")$	160.8
	$\nu_{12}(a')$	43.0	$\nu_{32}(a")$	3.0
	$\nu_{13}(a')$	13.8	$\nu_{33}(a")$	0.02
	$\nu_{14}(a')$	12.3	$\nu_{34}(a")$	44.7
	$\nu_{15}(a')$	58.4	$\nu_{35}(a")$	110.3
	$\nu_{16}(a')$	65.2	$\nu_{36}(a")$	0.0
	$\nu_{17}(a')$	65.4	$\nu_{37}(a")$	0.3
	$\nu_{18}(a')$	5.9	$\nu_{38}(a")$	2.6
	$\nu_{19}(a')$	8.0	$\nu_{39}(a")$	3.3
	$\nu_{20}(a')$	0.4		
$CH_3OH.N(CH_3)_3$	$\nu_1(a')$	562.6	$\nu_{27}(a')$	0.91
	$\nu_2(a')$	54.3	$\nu_{28}(a")$	1.3
	$\nu_3(a')$	75.8	$\nu_{29}(a")$	1.0

Table 2.36 cont.

	ν_4(a′)	55.0	ν_{30}(a")	49.8
	ν_5(a′)	33.6	ν_{31}(a")	10.9
	ν_6(a′)	68.4	ν_{32}(a")	29.4
	ν_7(a′)	180.5	ν_{33}(a′)	105.8
	ν_8(a′)	33.9	ν_{34}(a")	37.9
	ν_9(a′)	1.5	ν_{35}(a")	10.2
	ν_{10}(a′)	7.2	ν_{36}(a")	0.2
	ν_{11}(a′)	20.3	ν_{37}(a")	0.01
	ν_{12}(a′)	4.6	ν_{38}(a")	6.4
	ν_{13}(a′)	12.1	ν_{39}(a")	2.6
	ν_{14}(a′)	5.0	ν_{40}(a")	18.3
	ν_{15}(a′)	14.3	ν_{41}(a")	3.3
	ν_{16}(a′)	31.7	ν_{42}(a")	10.6
	ν_{17}(a′)	15.5	ν_{43}(a")	0.002
	ν_{18}(a′)	24.9	ν_{44}(a")	26.2
	ν_{19}(a′)	24.0	ν_{45}(a")	99.3
	ν_{20}(a′)	1.7	ν_{46}(a")	0.2
	ν_{21}(a′)	95.9	ν_{47}(a")	0.5
	ν_{22}(a′)	19.7	ν_{48}(a")	0.0
	ν_{23}(a′)	34.5	ν_{49}(a")	0.6
	ν_{24}(a′)	0.04	ν_{50}(a")	0.2
	ν_{25}(a′)	22.3	ν_{51}(a")	7.3
	ν_{26}(a′)	0.43		
$CH_3OH.S(CH_3)_2$	ν_1(a′)	132.8	ν_{21}(a′)	1.6
	ν_2(a′)	15.0	ν_{22}(a′)	5.6
	ν_3(a′)	36.1	ν_{23}(a")	5.9
	ν_4(a′)	67.3	ν_{24}(a")	0.001

Table 2.36 cont.

	ν_5(a′)	37.3	ν_{25}(a")	114.9
	ν_6(a′)	59.8	ν_{26}(a")	13.1
	ν_7(a′)	5.2	ν_{27}(a′)	1.2
	ν_8(a′)	9.7	ν_{28}(a")	16.8
	ν_9(a′)	0.2	ν_{29}(a")	0.01
	ν_{10}(a′)	15.5	ν_{30}(a")	8.5
	ν_{11}(a′)	4.7	ν_{31}(a")	2.9
	ν_{12}(a′)	39.2	ν_{32}(a")	0.002
	ν_{13}(a′)	76.6	ν_{33}(a")	0.006
	ν_{14}(a′)	55.6	ν_{34}(a")	1.5
	ν_{15}(a′)	23.7	ν_{35}(a")	118.2
	ν_{16}(a′)	1.7	ν_{36}(a")	0.0
	ν_{17}(a′)	6.0	ν_{37}(a")	2.9
	ν_{18}(a′)	0.02	ν_{38}(a")	2.5
	ν_{19}(a′)	1.1	ν_{39}(a")	3.7
	ν_{20}(a′)	1.8		
$(CH_3)_2NH.O(CH_3)_2$	ν_1(a′)	48.5	ν_{27}(a′)	0.9
	ν_2(a′)	41.6	ν_{28}(a")	43.0
	ν_3(a′)	115.0	ν_{29}(a")	6.2
	ν_4(a′)	168.4	ν_{30}(a")	0.006
	ν_5(a′)	89.9	ν_{31}(a")	42.9
	ν_6(a′)	74.0	ν_{32}(a")	53.2
	ν_7(a′)	90.9	ν_{33}(a′)	67.8
	ν_8(a′)	0.12	ν_{34}(a")	11.4
	ν_9(a′)	3.5	ν_{35}(a")	12.5
	ν_{10}(a′)	8.1	ν_{36}(a")	0.3
	ν_{11}(a′)	0.2	ν_{37}(a")	0.5
	ν_{12}(a′)	8.2	ν_{38}(a")	7.5

Table 2.36 cont.

	$\nu_{13}(a')$	0.4	$\nu_{39}(a")$	9.9
	$\nu_{14}(a')$	12.8	$\nu_{40}(a")$	6.1
	$\nu_{15}(a')$	0.8	$\nu_{41}(a")$	148.4
	$\nu_{16}(a')$	18.9	$\nu_{42}(a")$	0.003
	$\nu_{17}(a')$	12.7	$\nu_{43}(a")$	37.5
	$\nu_{18}(a')$	55.8	$\nu_{44}(a")$	37.6
	$\nu_{19}(a')$	4.4	$\nu_{45}(a")$	0.05
	$\nu_{20}(a')$	115.8	$\nu_{46}(a")$	8.1
	$\nu_{21}(a')$	4.6	$\nu_{47}(a")$	0.03
	$\nu_{22}(a')$	4.8	$\nu_{48}(a")$	0.0
	$\nu_{23}(a')$	2.3	$\nu_{49}(a")$	0.5
	$\nu_{24}(a')$	7.1	$\nu_{50}(a")$	0.2
	$\nu_{25}(a')$	0.2	$\nu_{51}(a")$	0.4
	$\nu_{26}(a')$	6.1		
$(CH_3)_2NH.N(CH_3)_3$	$\nu_1(a')$	83.5	$\nu_{33}(a')$	0.4
	$\nu_2(a')$	61.9	$\nu_{34}(a')$	1.1
	$\nu_3(a')$	93.6	$\nu_{35}(a")$	61.2
	$\nu_4(a')$	86.0	$\nu_{36}(a")$	2.2
	$\nu_5(a')$	35.3	$\nu_{37}(a")$	9.2
	$\nu_6(a')$	93.0	$\nu_{38}(a")$	29.2
	$\nu_7(a')$	97.7	$\nu_{39}(a")$	42.6
	$\nu_8(a')$	200.2	$\nu_{40}(a")$	65.0
	$\nu_9(a')$	37.4	$\nu_{41}(a")$	39.0
	$\nu_{10}(a')$	5.0	$\nu_{42}(a")$	8.4
	$\nu_{11}(a')$	4.7	$\nu_{43}(a")$	9.8
	$\nu_{12}(a')$	18.3	$\nu_{44}(a")$	0.02
	$\nu_{13}(a')$	7.0	$\nu_{45}(a")$	0.2

Table 2.36 cont.

	$\nu_{14}(a')$	1.3	$\nu_{46}(a'')$	7.4
	$\nu_{15}(a')$	5.5	$\nu_{47}(a'')$	5.6
	$\nu_{16}(a')$	0.4	$\nu_{48}(a'')$	3.4
	$\nu_{17}(a')$	3.2	$\nu_{49}(a'')$	5.2
	$\nu_{18}(a')$	18.5	$\nu_{50}(a'')$	16.9
	$\nu_{19}(a')$	0.4	$\nu_{51}(a'')$	35.8
	$\nu_{20}(a')$	23.6	$\nu_{52}(a'')$	10.2
	$\nu_{21}(a')$	18.9	$\nu_{53}(a'')$	0.1
	$\nu_{22}(a')$	9.7	$\nu_{54}(a'')$	0.01
	$\nu_{23}(a')$	22.6	$\nu_{55}(a'')$	23.8
	$\nu_{24}(a')$	0.6	$\nu_{56}(a'')$	6.9
	$\nu_{25}(a')$	95.8	$\nu_{57}(a'')$	0.02
	$\nu_{26}(a')$	32.5	$\nu_{58}(a'')$	0.6
	$\nu_{27}(a')$	0.03	$\nu_{59}(a'')$	0.0
	$\nu_{28}(a')$	3.4	$\nu_{60}(a'')$	0.03
	$\nu_{29}(a')$	18.9	$\nu_{61}(a'')$	0.2
	$\nu_{30}(a')$	3.1	$\nu_{62}(a'')$	0.0
	$\nu_{31}(a')$	0.6	$\nu_{63}(a'')$	0.5
	$\nu_{32}(a')$	0.0		
$(CH_3)_2NH.S(CH_3)_2$	$\nu_1(a')$	5.6	$\nu_{27}(a')$	2.3
	$\nu_2(a')$	16.8	$\nu_{28}(a'')$	7.0
	$\nu_3(a')$	39.0	$\nu_{29}(a'')$	0.0
	$\nu_4(a')$	103.7	$\nu_{30}(a'')$	7.6
	$\nu_5(a')$	96.7	$\nu_{31}(a'')$	39.8
	$\nu_6(a')$	47.6	$\nu_{32}(a'')$	34.2
	$\nu_7(a')$	80.9	$\nu_{33}(a')$	66.2
	$\nu_8(a')$	4.9	$\nu_{34}(a'')$	8.2
	$\nu_9(a')$	6.8	$\nu_{35}(a'')$	0.01

Table 2.36 cont.

	$\nu_{10}(a')$	0.1	$\nu_{36}(a'')$	12.3
	$\nu_{11}(a')$	0.5	$\nu_{37}(a'')$	16.3
	$\nu_{12}(a')$	14.9	$\nu_{38}(a'')$	0.003
	$\nu_{13}(a')$	4.8	$\nu_{39}(a'')$	4.6
	$\nu_{14}(a')$	0.7	$\nu_{40}(a'')$	7.1
	$\nu_{15}(a')$	18.0	$\nu_{41}(a'')$	35.9
	$\nu_{16}(a')$	20.8	$\nu_{42}(a'')$	0.003
	$\nu_{17}(a')$	3.9	$\nu_{43}(a'')$	9.0
	$\nu_{18}(a')$	3.4	$\nu_{44}(a'')$	0.0
	$\nu_{19}(a')$	121.0	$\nu_{45}(a'')$	0.005
	$\nu_{20}(a')$	5.2	$\nu_{46}(a'')$	1.1
	$\nu_{21}(a')$	5.8	$\nu_{47}(a'')$	0.02
	$\nu_{22}(a')$	2.4	$\nu_{48}(a'')$	0.0
	$\nu_{23}(a')$	0.01	$\nu_{49}(a'')$	0.6
	$\nu_{24}(a')$	1.0	$\nu_{50}(a'')$	0.5
	$\nu_{25}(a')$	0.1	$\nu_{51}(a'')$	0.4
	$\nu_{26}(a')$	2.4		
$CH_3SH.O(CH_3)_2$	$\nu_1(a')$	14.9	$\nu_{21}(a')$	5.7
	$\nu_2(a')$	41.0	$\nu_{22}(a')$	2.7
	$\nu_3(a')$	44.8	$\nu_{23}(a'')$	18.2
	$\nu_4(a')$	146.6	$\nu_{24}(a'')$	40.4
	$\nu_5(a')$	71.6	$\nu_{25}(a'')$	0.01
	$\nu_6(a')$	29.4	$\nu_{26}(a'')$	56.9
	$\nu_7(a')$	0.2	$\nu_{27}(a')$	11.2
	$\nu_8(a')$	1.1	$\nu_{28}(a'')$	0.1
	$\nu_9(a')$	7.7	$\nu_{29}(a'')$	3.1

Table 2.36 cont.

	ν_{10}(a′)	7.4	ν_{30}(a")	12.5
	ν_{11}(a′)	11.1	ν_{31}(a")	155.3
	ν_{12}(a′)	13.0	ν_{32}(a")	0.01
	ν_{13}(a′)	12.4	ν_{33}(a")	37.9
	ν_{14}(a′)	21.1	ν_{34}(a")	3.5
	ν_{15}(a′)	65.6	ν_{35}(a")	21.9
	ν_{16}(a′)	1.4	ν_{36}(a")	0.0
	ν_{17}(a′)	3.6	ν_{37}(a")	0.5
	ν_{18}(a′)	5.8	ν_{38}(a")	1.2
	ν_{19}(a′)	7.6	ν_{39}(a")	0.8
	ν_{20}(a′)	0.2		
$CH_3SH.N(CH_3)_3$	ν_1(a′)	14.7	ν_{27}(a′)	0.2
	ν_2(a′)	59.9	ν_{28}(a′)	1.6
	ν_3(a′)	61.0	ν_{29}(a′)	0.9
	ν_4(a′)	38.0	ν_{30}(a")	18.7
	ν_5(a′)	32.6	ν_{31}(a")	56.4
	ν_6(a′)	195.1	ν_{32}(a")	6.7
	ν_7(a′)	37.9	ν_{33}(a′)	30.6
	ν_8(a′)	79.7	ν_{34}(a")	38.4
	ν_9(a′)	8.4	ν_{35}(a")	9.2
	ν_{10}(a′)	15.6	ν_{36}(a")	0.003
	ν_{11}(a′)	1.8	ν_{37}(a")	5.4
	ν_{12}(a′)	5.4	ν_{38}(a")	5.2
	ν_{13}(a′)	8.0	ν_{39}(a")	3.0
	ν_{14}(a′)	3.0	ν_{40}(a")	17.8
	ν_{15}(a′)	9.9	ν_{41}(a")	9.7
	ν_{16}(a′)	17.1	ν_{42}(a")	0.0

Table 2.36 cont.

	ν_{17}(a′)	25.3	ν_{43}(a")	23.7
	ν_{18}(a′)	23.4	ν_{44}(a")	3.4
	ν_{19}(a′)	14.2	ν_{45}(a")	1.4
	ν_{20}(a′)	22.1	ν_{46}(a")	18.4
	ν_{21}(a′)	1.7	ν_{47}(a")	0.7
	ν_{22}(a′)	36.3	ν_{48}(a")	0.0
	ν_{23}(a′)	3.3	ν_{49}(a")	0.2
	ν_{24}(a′)	0.03	ν_{50}(a")	0.002
	ν_{25}(a′)	23.2	ν_{51}(a")	2.7
	ν_{26}(a′)	0.5		
$CH_3SH.S(CH_3)_2$	ν_1(a′)	15.8	ν_{21}(a′)	1.9
	ν_2(a′)	16.9	ν_{22}(a′)	4.4
	ν_3(a′)	38.6	ν_{23}(a′)	5.9
	ν_4(a′)	33.4	ν_{24}(a")	14.0
	ν_5(a′)	39.1	ν_{25}(a")	6.6
	ν_6(a′)	2.6	ν_{26}(a")	0.003
	ν_7(a′)	0.2	ν_{27}(a′)	0.2
	ν_8(a′)	9.8	ν_{28}(a")	5.4
	ν_9(a′)	15.0	ν_{29}(a")	0.004
	ν_{10}(a′)	5.1	ν_{30}(a")	7.9
	ν_{11}(a′)	11.7	ν_{31}(a")	3.7
	ν_{12}(a′)	19.5	ν_{32}(a")	0.002
	ν_{13}(a′)	21.6	ν_{33}(a")	0.004
	ν_{14}(a′)	3.3	ν_{34}(a")	1.1
	ν_{15}(a′)	0.8	ν_{35}(a")	18.5
	ν_{16}(a′)	4.0	ν_{36}(a")	0.0
	ν_{17}(a′)	5.3	ν_{37}(a")	3.3
	ν_{18}(a′)	0.01	ν_{38}(a")	1.4

Table 2.36 cont.

$\nu_{19}(a')$	1.1	$\nu_{39}(a'')$	0.7
$\nu_{20}(a')$	0.8		

When hydrogen bonding occurs between a proton donor group A-H and an acceptor group B, and a hydrogen bonded complex is formed, the following effects are observed in the infrared region:[35]

a) The absorption bands due to the A-H stretching vibrations are shifted to lower wavenumbers. These shifts range from a few cm^{-1} to several hundred cm^{-1} or more. This is due to the weakening of the force constant for the A-H stretching mode caused by the formation of the hydrogen bond.

b) The shifted absorption bands due to the hydrogen bonded A-H stretching vibrations are much broader than the corresponding bands of the non-hydrogen bonded A-H group.

c) In addition to the broadening, the integrated intensity of fundamental A-H stretching bands increases, sometimes by factors of up to ten or more. The reasons for the intensity effects are probably related to the fact that hydrogen bonds have substantial electrostatic character and the intensity of absorption due to infrared active vibrations is directly proportional to the rate of change of the electrostatic dipole moment with internuclear distance.

d) the A-H deformation modes are shifted to higher frequencies. These shifts are smaller than those found for the A-H stretching vibrations. Formation of hydrogen bonds constrains the deformation vibrations and therefore increases the force constants for these modes. These modes do not show any appreciable band broadening or intensity change when hydrogen bonding occurs.

e) New vibrational modes, corresponding to H...B stretching and deformation, are found at low frequencies in the far infrared region.

f) The vibrational modes of the hydrogen bond acceptor, B, are shifted by hydrogen bonding to either higher or lower wavenumbers, and the shifts are generally smaller than those found for the donor A-H vibrations.

A brief synopsis of the vibrational band changes due to hydrogen bonding is chronicled in Table 2.37.

Table 2.37. Computed changes in the A-H stretching vibrations, the intensities of the A-H stretching vibrations and the A-H deformation modes between complex and monomer, for the nine hydrogen bonded molecular complexes.

Complex	$\Delta\nu$(AH) /cm^{-1}	ν(AH) Intensity /km mol^{-1}	$\Delta\delta$(CAH) /cm^{-1}
OH...O	-69	302.3	46
OH...N	-174	520.1	76
OH...S	-10	90.3	7
NH...O	-7	47.8	89(symm)
NH...N	-33	82.8	109(symm)
NH...S	-8	4.9	52(symm)
SH...O	-3	14.4	18
SH...N	-54	64.9	35
SH...S	+6	-12.4	2

The predicted *ab initio* results in Table 2.37 are informative. The AH stretching mode, ν(AH), is red shifted in all cases, except in the case of the SH...S hydrogen bonded interaction. The degree of change, which has previously been used as a measure of the strength of the hydrogen bonded interaction, is greatest in the alcohol complexes, illustrating the energetic superiority of the OH group as a proton donor over those of the NH and SH moieties. Within the isolated groups of given proton donors, the shift in

ν(AH) is always greatest for complexes involving nitrogen as the proton acceptor, followed by that for oxygen and finally by that for sulphur.

Not only does the AH stretching mode shift to lower frequencies as a result of hydrogen bonding, but in addition its intensity increases. Table 2.37 clearly demonstrates that the change in the intensity of the AH stretching vibrational mode mirrors that of the shift in the mode itself. For example, the change in the intensity of the AH stretching vibrational mode is largest for the complex involving the OH...N hydrogen bond, while in all cases, the N electron donor is always involved in the largest intensity changes.

Another observable feature of hydrogen bonding is the blue shift of the A-H deformation modes. This is a characteristic of all the A-H bending modes studied in this work. The blue shift of the A-H deformation mode, δ(CAH), is usually smaller than the red shift of ν(AH). This result is certainly an attribute of the alcohol complexes, but not a feature of the others, where $\Delta\delta$(CAH) is larger than $\Delta\nu$(AH).

New vibrational modes, resulting from the formation of a hydrogen bond, are found at low frequencies in the far infrared region. Each complex registers six new intermolecular modes, corresponding to H...B stretching and deformations. The highest intermolecular wavenumber of any of the complexes is found at 722 cm^{-1} in the case of the OH...N stretching mode (see Table 2.28). Negative intermolecular frequencies have been predicted for all the complexes; the SH...O complex (Table 2.33) being the exception. Three is the highest number of negative frequencies, which was calculated

for the complex involving the NH...S hydrogen bond (see Table 2.32). This is usually an indication that, although a local minimum on the potential energy curve may have been achieved, the global or genuine minimum has not. Causative factors for this effect include, amongst other things, the attainment of a transition-state conformation or an inadequate level of theory. Re-orientation of the molecules in the hydrogen bonded complexes could not improve the situation and we are left to assume that if optimization of our complexes at the level of second order Moller-Plessett perturbation theory were possible, a genuine minimum on the potential energy curve would have been achieved with the subsequent elimination of any negative frequencies.

2.4.5 Calculation of Interaction Energies and other Structural and Electronic Properties

Table 2.38 lists the computed interaction energies and their basis set superposition errors for the nine binary complexes $CH_3OH...O(CH_3)_2$, $CH_3OH...N(CH_3)_3$, $CH_3OH...S(CH_3)_2$, $(CH_3)_2NH...O(CH_3)_2$, $(CH_3)_2NH...N(CH_3)_3$, $(CH_3)_2NH...S(CH_3)_2$, $CH_3SH...O(CH_3)_2$, $CH_3SH...N(CH_3)_3$ and $CH_3SH...S(CH_3)_2$.

In order to obtain the energy of the hydrogen bond, the sum of the energies of the two monomers was subtracted from the energy of the molecular complex. The energy difference gives the energy contribution due to the specific hydrogen bond. However, in the energy determination of the X...Y heterodimer, all the orbitals of both X and Y are available to the dimer. As a consequence the basis set of each monomer is extended by the presence of the other, which results in a mathematical lowering of the monomer energies. This is referred to as the basis set superposition error (BSSE).[90] Counterpoise calculations[91] are used in the Gaussian program (MASSAGE keyword) to estimate the magnitude of the BSSE and correct the energy accordingly (see section 2.3.5).

Table 2.38. Computed interaction energies and their basis set superposition errors for the binary complexes formed from methanol, dimethylamine, methane thiol, dimethyl ether, trimethylamine and dimethyl sulphide.

Complex	Energy /kJ mol^{-1}		
	Uncorrected	BSSE	Corrected
$CH_3OH...O(CH_3)_2$	-21.42	3.70	-17.72
$CH_3OH...N(CH_3)_3$	-24.80	4.31	-20.49
$CH_3OH...S(CH_3)_2$	-7.21	0.96	-6.25
$(CH_3)_2NH...O(CH_3)_2$	-7.42	0.68	-6.74
$(CH_3)_2NH...N(CH_3)_3$	-9.24	1.46	-7.78
$(CH_3)_2NH...S(CH_3)_2$	-0.98	-1.36	-2.48
$CH_3SH...O(CH_3)_2$	-8.76	2.94	-5.82
$CH_3SH...N(CH_3)_3$	-10.05	3.91	-6.14
$CH_3SH...S(CH_3)_2$	-3.33	0.62	-2.71

Table 2.39. Major structural features of the hydrogen bonded fragments AH...B of the nine molecular complexes investigated.

Complex	Δr(AH)[a] /pm	R(A...B) /pm
$CH_3OH...O(CH_3)_2$	0.42	295.50
$CH_3OH...N(CH_3)_3$	0.83	301.99
$CH_3OH...S(CH_3)_2$	0.09	381.10
$(CH_3)_2NH...O(CH_3)_2$	0.14	335.50
$(CH_3)_2NH...N(CH_3)_3$	0.26	344.47
$(CH_3)_2NH...S(CH_3)_2$	0.10	425.58
$CH_3SH...O(CH_3)_2$	0.04	364.93
$CH_3SH...N(CH_3)_3$	0.38	373.83
$CH_3SH...S(CH_3)_2$	-0.05	458.05

[a] Δr(AH) = r(AH)(complex) - r(AH)(monomer)

Table 2.40. Net Mulliken charges of the monomer fragments involved in the hydrogen bonded complexes formed from methanol, dimethylamine, methane thiol, dimethyl ether, trimethylamine and dimethyl sulphide.

Complex	Monomer fragment	Mulliken charge/*me*
$CH_3OH...O(CH_3)_2$	CH_3OH	-21.1
	$O(CH_3)_2$	21.1
$CH_3OH...N(CH_3)_3$	CH_3OH	-25.6
	$N(CH_3)_3$	25.6
$CH_3OH...S(CH_3)_2$	CH_3OH	-3.6
	$S(CH_3)_2$	3.6
$(CH_3)_2NH...O(CH_3)_2$	$(CH_3)_2NH$	-13.7
	$O(CH_3)_2$	13.7
$(CH_3)_2NH...N(CH_3)_3$	$(CH_3)_2NH$	-17.9
	$N(CH_3)_3$	17.9
$(CH_3)_2NH...S(CH_3)_2$	$(CH_3)_2NH$	-1.3
	$S(CH_3)_2$	1.3
$CH_3SH...O(CH_3)_2$	CH_3SH	-15.1
	$O(CH_3)_2$	15.1
$CH_3SH...N(CH_3)_3$	CH_3SH	-21.4
	$N(CH_3)_3$	21.4
$CH_3SH...S(CH_3)_2$	CH_3SH	-4.0
	$S(CH_3)_2$	4.0

Table 2.41. Mulliken charges, and their changes, of the atoms involved in the hydrogen bonded complexes formed from methanol, dimethylamine, methane thiol, dimethyl ether, trimethylamine and dimethyl sulphide.

Complex	Atom	Mulliken charge /*e*		
		Complex	Monomer	Difference
$CH_3OH...O(CH_3)_2$	O_1	-0.6703	-0.6338	-0.0365
	H_1	0.3770	0.3355	0.0415
	O_2	-0.6392	-0.6085	-0.0307
$CH_3OH...N(CH_3)_3$	O	-0.6760	-0.6338	-0.0422
	H_1	0.3847	0.3355	0.0492
	N	-0.6176	-0.5598	-0.0578
$CH_3OH...S(CH_3)_2$	O	-0.6499	-0.6338	-0.0161
	H_1	0.3558	0.3355	0.0203
	S	0.0867	0.1103	-0.0236
$(CH_3)_2NH...O(CH_3)_2$	N	-0.6369	-0.6215	-0.0154
	H_1	0.3004	0.2661	0.0343
	O	-0.6191	-0.6085	-0.0106
$(CH_3)_2NH...N(CH_3)_3$	N_1	-0.6395	-0.6215	-0.0180
	H_1	0.3031	0.2661	0.0370
	N_2	-0.5810	-0.5598	-0.0212
$(CH_3)_2NH...S(CH_3)_2$	N	-0.6246	-0.6215	-0.0031
	H_1	0.2808	0.2661	0.0147

Table 2.41 cont.

	S	0.1013	0.1103	-0.0090
$CH_3SH...O(CH_3)_2$	S	-0.0589	-0.0177	-0.0412
	H_1	0.0855	0.0477	0.0378
	O	-0.6189	-0.6085	-0.0104
$CH_3SH...N(CH_3)_3$	S	-0.0613	-0.0177	-0.0436
	H_1	0.0850	0.0477	0.0373
	N	-0.5805	-0.5598	-0.0207
$CH_3SH...S(CH_3)_2$	S_1	-0.0337	-0.0177	-0.0160
	H_1	0.0607	0.0477	0.0130
	S_2	0.1014	0.1103	-0.0089

Table 2.42. Hydrogen bond angles, AĤ...B, and their deviations from linearity for the hydrogen bonded complexes formed from methanol, dimethylamine, methane thiol, dimethyl ether, trimethylamine and dimethyl sulphide.

Complex	AĤ...B /deg	Deviation from linearity/deg
$CH_3OH...O(CH_3)_2$	171.5	8.5
$CH_3OH...N(CH_3)_3$	177.1	2.9
$CH_3OH...S(CH_3)_2$	166.2	13.8
$(CH_3)_2NH...O(CH_3)_2$	167.9	12.1
$(CH_3)_2NH...N(CH_3)_3$	176.5	3.5
$(CH_3)_2NH...S(CH_3)_2$	152.6	27.4
$CH_3SH...O(CH_3)_2$	175.0	5.0
$CH_3SH...N(CH_3)_3$	177.4	2.6
$CH_3SH...S(CH_3)_2$	153.8	26.2

Table 2.43. Heavy atom bond distances, R(A...B), sum of van der Waals radii for the two heavy atoms involved in the hydrogen bond, Σr_{VDW}, their difference, and the hydrogen bond lengths, r(H...B), for the hydrogen bonded complexes formed from methanol, dimethylamine, methane thiol, dimethyl ether, trimethylamine and dimethyl sulphide.

Complex	r(H...B) /pm	R(A...B) /pm[a]	Σr_{VDW} /pm[b]	R(A...B) - Σr_{VDW}/pm
$CH_3OH...O(CH_3)_2$	200.8	295.5	280.0	15.5
$CH_3OH...N(CH_3)_3$	206.9	302.0	290.0	12.0
$CH_3OH...S(CH_3)_2$	286.8	381.1	325.0	56.1
$(CH_3)_2NH...O(CH_3)_2$	235.4	335.5	290.0	45.5
$(CH_3)_2NH...N(CH_3)_3$	244.2	344.5	300.0	44.5
$(CH_3)_2NH...S(CH_3)_2$	325.5	425.6	335.0	90.6
$CH_3SH...O(CH_3)_2$	232.2	364.9	325.0	39.9
$CH_3SH...N(CH_3)_3$	240.7	373.8	335.0	38.8
$CH_3SH...S(CH_3)_2$	325.4	458.1	370.0	88.1

[a] R(A...B) = r(AH) + r(H...B)

[b] ref. 125

Table 2.38 lists the interaction energies for the nine binary hydrogen bonded complexes, with the OH...N bond being the strongest hydrogen bond and the SH...S bond being the weakest. BSSE accounts for between 9 and 39% of the total uncorrected energies, except in the case of the NH...S hydrogen

bond, where a negative BSSE is calculated. Although the BSSE can be negative in cases where the monomers are highly distorted on complexation, this is not, however, the case in this instance and therefore the negative BSSE must be an artefact. In respect of the electronic energies of the nine complexes under consideration, all other things being equal, the proton accepting ability of the atoms is always in the order N > O > S.

Pimentel and McClellan[3] have identified the lengthening of the covalent AH bond, the distance of separation of the A and B atoms, relative to the sum of their van der Waals radii[125] and the approach of the AH...B angle to linearity, as the most characteristic structural manifestations of hydrogen bonding. These major features associated with the hydrogen bond are listed in Tables 2.39, 2.42 and 2.43. The order of the extent of lengthening of the AH bonds among the complexes is OH...N > OH...O > SH...N > NH...N > NH...O > NH...S > OH...S > SH...O > SH...S. After subtracting the sum of the van der Waals radii of the O, N and S atoms, as appropriate, from the A...B distances, the approximate differences are 12 (OH...N), 15.5 (OH...O), 56 (OH...S), 44.5 (NH...N), 45.5 (NH...O), 90.6 (NH...S), 39 (SH...S), 40 (SH...O) and 88 pm (SH...S). The deviations from linearity are similarly dependent on the proton accepting atom in the hydrogen bond and clearly illustrate (Table 2.42) the order of proton accepting strength to be in the order N > O > S.

The sums of the Mulliken atomic charges[126,127] of the monomer fragments are presented in table 2.40. The figures confirm that the direction of charge transfer is from $(CH_3)_2O$, $(CH_3)_3N$ and $(CH_3)_2S$ to CH_3OH, $(CH_3)_2NH$ and

CH_3SH, as appropriate, as indicated by positive values for the electron donors and negative values for the electron acceptors. In Table 2.41, these Mulliken charge shifts are partitioned among the A, H and B atoms that participate in each of the hydrogen bond interactions. The results demonstrate that the bridging hydrogen atom consistently donates a sizeable fraction of electron density, the relative amount being dependent on the particular interaction, while the A and B atoms receive an amount of charge of similar magnitude. When the proton acceptor atom, B, is nitrogen, the amount of charge redistributed by B is larger than when B is oxygen, which in turn, is larger than when B is sulphur. Likewise, the proton donor atom, A, transfers a greater fraction of charge when the acceptor is nitrogen rather than oxygen, which similarly transfers a greater fraction of charge than when the acceptor is sulphur. These observations provide further evidence for our contention, above, that the OH group is a more potent proton donor than NH, which in turn is superior to SH, while the proton accepting proficiency of the atoms is in the order N > O > S.

The SH...S hydrogen bonded complex is of interest, in that both $\Delta r(AH)$ and $\Delta \nu(AH)$ for this complex have opposite signs from the others. Except for the SH..S complex, all the others experience an increase in the length of the A-H bond and a red shift of $\nu(AH)$. As it is generally accepted that the A-H bond length increases, and that $\Delta \nu(AH)$ is negative, on hydrogen bond formation, it is evident that the strength of the $CH_3SH...S(CH_3)_2$ interaction is very weak, if not zero.

2.4.6 Theoretical Predictions of ΔH

Based on the (BSSE corrected) electronic interaction energies, the enthalpy change for a general chemical reaction at 298 K is given by

$$\Delta H=\Delta E+\Delta(pV) \tag{2.25}$$

In order to estimate ΔH for the reaction by *ab initio* quantum mechanical methods, the electronic energies of both reactants and products, calculated at their optimized geometries, together with the differences in zero point vibrational, rotational and translational energies at 298 K, are required. The total energy change, ΔE, is given by [128]

$$\Delta E=\Delta E_e^0+\Delta(\Delta E_e)+\Delta E_v^0+\Delta(\Delta E_v)+\Delta E_r+\Delta E_t \tag{2.26}$$

where

ΔE_e^0 = difference between the ground state electronic energies of reactants and products at 0 K,

$\Delta(\Delta E_e)$ = change in electronic energy difference between 0 K and 298 K (reactants are normally in their ground electronic states at 298 K, hence this term is negligible),

ΔE_v^0 = difference between the zero point vibrational energies of reactants and products at 0 K,

$\Delta(\Delta E_v)$ = change in the vibrational energy difference between reactants and products,

ΔE_r = difference in rotational energies between reactants and products at 298 K,

ΔE_t = difference in translational energies between reactants and products at 298K.

E_v^0 for any substance is

$$E_v^0 = \frac{1}{2} Nhc \sum_i \nu_i \qquad (2.27)$$

where ν_i is the infrared vibrational wavenumber, the sum being taken over all 3n-6 vibrational modes of the molecule.

This energy is calculated in the Gaussian program by the FREQ[73] option. The contribution to the internal energy of a substance due to thermally populated vibrational modes at 298 K is

$$\Delta E_v = 298\, R\, (\sum \mu_i/(\exp\mu_i) - 1) \qquad (2.28)$$

where $\mu_i = 4.826 \times 10^{-3}\, \nu$ and R is the gas constant.
E_r can be calculated for each degree of rotational freedom by

$$E_r = \frac{1}{2} RT \qquad (2.29)$$

In the interactions considered here, there is a loss of 3 rotational degrees of freedom and hence the contribution to the total energy is -3/2 RT or -3.72 kJ mol^{-1} at 298 K. Similarly, for each mole lost or gained in the interaction,

there is a change in translational energy given by

$$\Delta E_t = -\frac{3}{2}RT \qquad (2.30)$$

In these reactions 1 mole is lost in going from reactants to products .

$\Delta(pV) = \Delta nRT = -1\ RT = -2.48\ kJ\ mol^{-1}$

The BSSE corrected energies in Table 2.38 of section 2.4.5 were used to compute the hydrogen bond enthalpies, in order to provide a set of thermodynamic parameters for more realistic comparison with the experimentally determined enthalpies of interaction. The calculated enthalpies along with the zero-point energy differences and their changes from 0 to 298 K, the changes in rotational and translational contributions and the pressure-volume components, are shown in Table 2.44.

Table 2.44.Energy contributions to the hydrogen bond enthalpies of the binary complexes formed from methanol, dimethylamine, methane thiol, dimethyl ether, trimethylamine and dimethyl sulphide

Type of Hydrogen Bond	Energy Component / kJ mol^{-1}						
	ΔE_e^0 [a]	ΔE_v^0	$\Delta(\Delta E_v)$	ΔE_r	ΔE_t	$\Delta(pV)$	ΔH
OH...O	-17.72	4.50	9.53	-3.72	-3.72	-2.48	-13.61
OH...N	-20.49	5.41	8.97	-3.72	-3.72	-2.48	-16.03
OH...S	-6.25	1.90	8.71	-3.72	-3.72	-2.48	-5.56
NH...O	-6.74	2.33	8.52	-3.72	-3.72	-2.48	-5.81
NH...N	-7.78	2.80	8.16	-3.72	-3.72	-2.48	-6.74
NH...S	-2.34	1.34	9.47	-3.72	-3.72	-2.48	-1.34
SH...O	-5.82	2.72	8.49	-3.72	-3.72	-2.48	-4.53
SH...N	-6.14	3.28	7.77	-3.72	-3.72	-2.48	-5.01
SH...S	-2.71	1.18	9.23	-3.72	-3.72	-2.48	-2.22

[a] See Table 2.38

The enthalpy sequence shows no deviation from that for the electronic energies of the complexes. Thus, from an enthalpy change perspective, the results are consistent with those established from electronic energy data in that the proton accepting capability of the atoms in question decreases in the order N > O > S.

2.4.7 Morokuma Decomposition Analysis

The total hydrogen bond energy of a system AH...B may be conveniently partitioned into components representing the electrostatic, charge transfer, polarization, exchange repulsion and other, higher order, contributions (see section 2.2.7). This decomposition scheme, formulated by Morokuma *et al.*[67,129,130] has been programmed by Peterson and Poirier in the MONSTERGAUSS code.[131] The results of applying the Morokuma decomposition procedure to the counterpoise-corrected interaction energies of the hydrogen bonded molecular complexes are collected in Table 2.45.

Table 2.45. Morokuma decompositions of the hydrogen bond energies of the binary complexes formed from methanol, dimethylamine, methane thiol, dimethyl ether, trimethylamine and dimethyl sulphide

Type of Hydrogen Bond	Energy Component / kJ mol^{-1}					
	ΔE_{es}	ΔE_{ct}	ΔE_{pl}	ΔE_{ex}	ΔE_{mix}	ΔE_{total}
OH...O	-32.84	-6.83	-3.72	24.20	2.36	-16.83
OH...N	-38.27	-7.91	-4.35	28.17	1.86	-20.50
OH...S	-8.82	-1.41	-1.03	4.23	0.71	-6.25
NH...O	-10.57	-2.84	-1.15	6.65	1.16	-6.75
NH...N	-13.54	-3.94	-1.49	9.61	1.60	-7.76
NH...S	-3.41	-0.57	-0.33	1.56	0.41	-2.34
SH...O	-12.43	-4.96	-1.32	11.06	1.84	-5.81
SH...N	-14.77	-6.90	-1.75	14.78	2.50	-6.15
SH...S	-4.17	-0.78	-0.36	2.19	0.40	-2.71

The slight differences between the totals recorded here and the BSSE corrected energies reported in section 2.4.5 are attributed to our use of two different programs for computing the counterpoise corrections to the interaction energies. Table 2.45 demonstrates that the predominant attractive component of the interaction energy in each case is the electrostatic term, which accounts for between 36 and 55% of the absolute sum of the individual components. It is interesting to note that electrostatic

contribution percentage increases significantly in each of the three cases where the sulphur atom functions as the proton acceptor (54%), as opposed to nitrogen and oxygen. This seems to imply a slightly greater ionic character in these cases. The electrostatic term contributions for the OH...N, OH...O and NH...O hydrogen bonded systems are all approximately 47% while those for the NH...N, SH...N and SH...O complexes amount to 45, 36 and 39% of the total energy, respectively.

The exchange repulsion is the chief contributor to the repulsive portion of the energy; this component represents about 30% of the total. Again, in the systems for which sulphur acts as the proton acceptor, the exchange repulsion contribution is different from the others, representing between 6 and 9 % less than those for the systems for which nitrogen and oxygen function as proton acceptors. These XH...S systems also display another unique feature in that $\Delta E_{es} \approx \Delta E$. This particular finding was also noted by Morokuma[66] in his study of complexes formed from H_2O and H_2CO molecules. This characteristic existed in the systems where the hydrogen bond length exceeded 250 pm. Our results are consistent with this in that only in the three cases where the sulphur atom functions as the proton acceptor does the hydrogen bond length exceed 250 pm (see chapter 2.4.5).

The polarization term is relatively unimportant in determining the origins of the interaction energies in the hydrogen bonded systems in this study although the charge transfer does tend to play a significant yet small role. The charge transfer accounts for roughly 10% of the total. Morokuma[68]

found that as the hydrogen bond length approached 210 pm ($H_2O...H_2O$), ΔE_{es}, ΔE_{ex} and ΔE_{ct} became almost identical in magnitude. Although our results do not reflect this discovery, they do reflect a marginal increase in the percentage charge transfer contribution for the systems involving O and N proton acceptors over the S proton acceptor, all other things being equal.

Umeyama and Morokuma[67] later concluded that at small separations ΔE_{es}, ΔE_{ct} and ΔE_{pl} can all be important attractive components, while at longer distances for the same complex, the short-range attractions, ΔE_{ct} and ΔE_{pl}, are usually unimportant. The fact that none of the complexes in this work has a calculated hydrogen bond distance shorter than 200 pm might account for the relatively small contributions from these two forces.

Umeyama and Morokuma[67] also maintained that a hydrogen bonded complex tended to maintain a linear A-H...B hydrogen bond principally to achieve the maximum ΔE_{es} stabilization which they found to be the most important component of the hydrogen bond energy. Fig.2.17 is a plot of the deviation from linearity of each of the nine hydrogen bonded complexes as a function of ΔE_{es}. The results shown in this graph are in general agreement with the aforementioned deductions. A separate relationship again seems to exist for each type of hydrogen bond, although it could be argued that a single correlation is present.

The sequence of magnitudes of the two major components is identical with that for the total hydrogen bond energy for each of the nine hydrogen bonded systems.

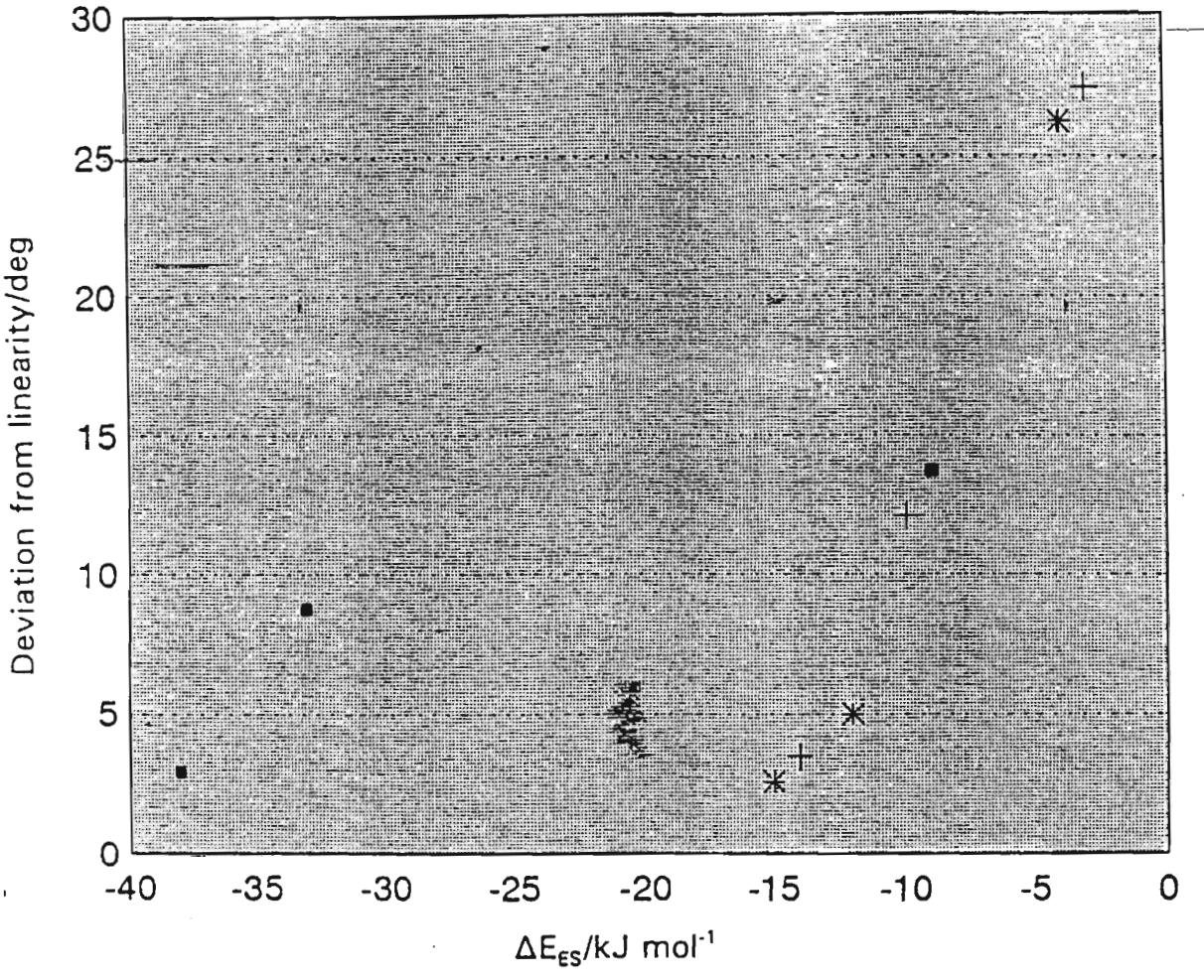

Fig. 2.17. The deviation from linearity of each of the nine hydrogen bonded complexes versus the (Morokuma) electrostatic energy change; ▪ OH proton donor, + NH proton donor, * SH proton donor.

2.4.8 Correlations

The vibrational spectra of molecules, fixed by the masses of the vibrating atoms, the molecular geometry and the force constants (restraining forces holding the atoms in their equilibrium positions), are significantly perturbed on hydrogen bond formation. The infrared spectroscopic technique has been identified as the most sensitive, characteristic and informative manifestation of the hydrogen bond.[132] The most conspicuous effect on the vibrational spectrum , as a result of hydrogen bonding, is the shift of the absorption of the A-H stretching mode, ν(AH), to lower frequencies. In many systems these shifts, $\Delta\nu$, are of the order of 10 % of ν(AH). It has become one of the most important qualitative yardsticks for hydrogen bond formation and quantitative indices of the hydrogen bond energy.[3] Many important relationships have been found between the physical properties of hydrogen bonded systems and $\Delta\nu$(AH). Pimentel and McClellan[3] found that $\Delta\nu$(AH) is inversely related to the A...B distance, whereas it is directly related to the enthalpy of hydrogen bonding, the A-H distance and the two spectral properties, half-width and intensity. Badger[133] submitted that there is a relation between the energy of a hydrogen bond and the shift in the frequency of the O-H stretching band. He proposed that a linear relationship exists between $\Delta\nu$ and ΔH, the enthalpy of hydrogen bond formation.[134] Later findings support the proposal that $\Delta\nu/\nu$ provides an index of ΔH of hydrogen bonding, but do not substantiate the proposed linear relationship of Badger and Bauer.[135-137]

Fig. 2.18 shows the calculated hydrogen bond enthalpy (see section 2.4.6)

as a function of $\Delta\nu$(AH) (see section 2.4.4). Although a general trend is observed when the ΔH:$\Delta\nu$(AH) relationship for all nine molecular complexes is plotted on the same graph, it is apparent that a separate relationship should be required for each type of hydrogen bond. Pimentel and Sederholm[138] came to a similar conclusion when examining the data of $\Delta\nu$ and the heavy atom bond distance R(A...B), for NH...O and NH...N systems. Nakamoto *et al.*[139] also concluded that each type of hydrogen bond has a distinct $\Delta\nu$-R relationship. Tamres and co-workers[140-142] found, using three different base types (aromatics, ethers and nitrogen bases), that each base type displays different intercepts but slopes that are surprisingly similar. Figs. 2.18, in which $\Delta\nu$ is plotted against ΔH and grouped according to the acid type (each point on a particular curve refers to the same proton donor), displays a similar phenomenon in that all three curves seem to display similar slopes. A monotonic relationship exists for the curves of the alcohol and the thiol complexes, but not for that of the secondary amine complexes. As ΔH seems to be a reliable indicator of the hydrogen bond strength, based on its direct relationship with the electronic interaction energy, ΔE (Fig. 2.30), it is evident that $\Delta\nu$(AH) is only effective as a measure of the hydrogen bond strength in the cases when OH and SH groups function as the proton donors.

On this basis, and having the luxury of only three acids and three bases, we have attempted to construct correlation graphs for each type of hydrogen bond in an attempt to investigate the dependence of the calculated enthalpy of hydrogen bonding on the structural and electronic properties of the interacting molecules. It is assumed in our discussion that ΔH is a reliable

indicator of the hydrogen bonded interaction energy.

Hydrogen bonds are assumed to be linear, but substantial variation in the A-$\hat{H}$...B angle can occur. Figs. 2.19 - 2.21 are plots of the A$\hat{H}$...B hydrogen bond angle as a function of ΔH for each of the hydrogen bonded molecular complexes grouped according to the proton donor involved. Each of the three graphs, where the proton donor molecule is methanol, dimethylamine and methane thiol respectively, clearly indicates that the weaker the AH...B hydrogen bond, the greater the deviation from linearity of that bond. The linearity of the hydrogen bond angle is less sensitive to the particular type of hydrogen bond when B is nitrogen than when it is oxygen or sulphur.

Hydrogen bond formation results in a distribution of charge around the individual atoms of the interacting molecular species. When a hydrogen atom is covalently bonded to an electronegative atom, a high probability exists that the bonding electrons are near this atom, thus leaving the proton almost 'bare'. This proton can therefore exert an attractive force on the lone pair electrons of another electronegative atom on a neighbouring molecule and in this way form a hydrogen bond. This interaction will result in further electron charge distribution away from the bridging hydrogen atom and this change in the charge of the hydrogen atom should be a good manifestation of the strength of the hydrogen bond. Figs. 2.22 - 2.24 effectively demonstrate this development, where linear relationships are evident in the cases where the proton donating atoms are oxygen and nitrogen. Electron density decreases around the hydrogen atom as the hydrogen bond strength increases.

The hydrogen bond interaction is mainly electrostatic in nature, but also involves some covalent character. This covalent contribution to the hydrogen bond energy is in the form of the charge transfer. The net Mulliken charges of the monomer fragments after hydrogen bond formation has occurred should be informative. Indeed, Figs. 2.25 - 2.27 reveal the direct relationship between this particular characteristic and ΔH, confirming that charge transfer between the two monomer fragments involved in the hydrogen bond increases with increasing strength of the interaction. There is again evidence of the existence of three separate relationships. The extent of intermolecular charge transfer would be expected to correlate with the Morokuma charge transfer component of the total hydrogen bond energy, $-\Delta E_{CT}$, listed in Table 2.44 of section 2.4.7. The plot of Δq vs $-\Delta E_{CT}$ is shown in Fig. 2.31. Again, the emergence of three separate, almost linear, relationships is evident, with two of the slopes being almost identical.

The direct relationship between $\Delta\nu$ and R(A...B), the heavy atom bond distance, is well documented.[138,139,143,144] Because a relationship exists between $\Delta\nu$ and ΔH, we predict that one will also exist between ΔH and R(A...B). However, when comparing hydrogen bonds that involve different types of atoms, it is necessary to compensate for the different sizes of these atoms. This is achieved by subtracting the sum of the van der Waals radii for the two electronegative atoms (A and B) involved in each hydrogen bond from the heavy atom bond distance. The van der Waals radii estimated by Pauling were used in this comparison.[126] This difference will give the interposed "space" between the two heavy atoms that the bridging hydrogen atom occupies in the hydrogen bonded interaction and is

effectively a measure of the covalency of the hydrogen bond. Because of the finding above that charge transfer between the two monomer fragments involved in the hydrogen bond (also a contributing factor in the total covalent character of the bond) increases with increasing strength of the interaction, one could assume that this available "space" will decrease with increasing strength of the hydrogen bond. Fig. 2.28 exposes the monotonic relationship of the enthalpy of hydrogen bonding and the effective measure of the covalency of the hydrogen bond and confirms the correctness of our assumption.

It is generally assumed that the covalent A-H bond length is lengthened in strong hydrogen bonds. Our results (Fig. 2.29) confirm that a monotonic relationship exists for all three "types" of hydrogen bond.

The correlative plots serve to illustrate that, in most cases, there is no single relationship that connects all nine types of hydrogen bond, and that each of the proton donors has a different dependence on ΔH than do the others. The correlations also serve to confirm the interrelationship of the energetic and the structural properties of these nine hydrogen bonded systems.

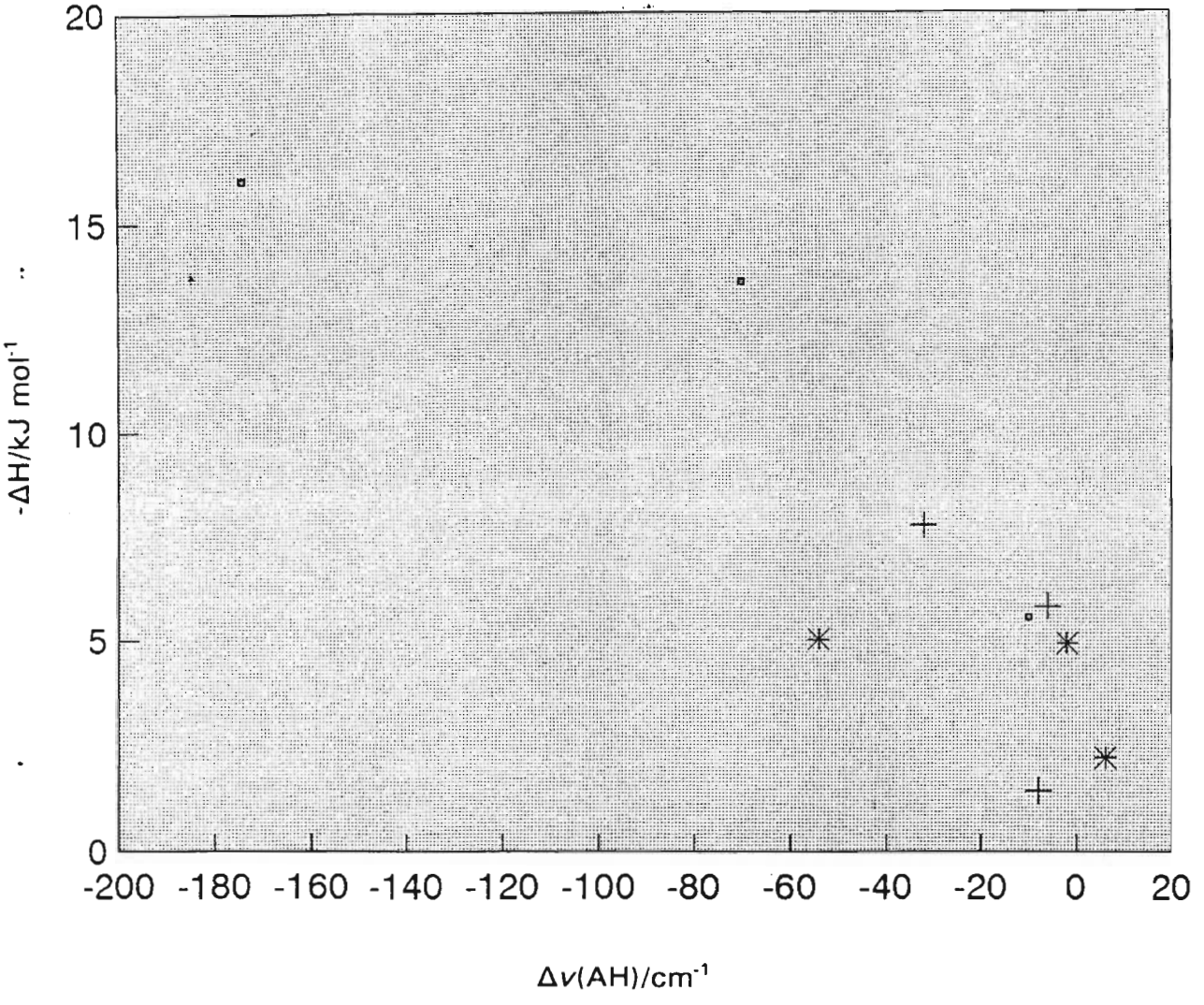

*Fig. 2.18. Plots of shift in the AH stretching band versus the computed hydrogen bond enthalpy; ▫ OH proton donor, + NH proton donor, * SH proton donor.*

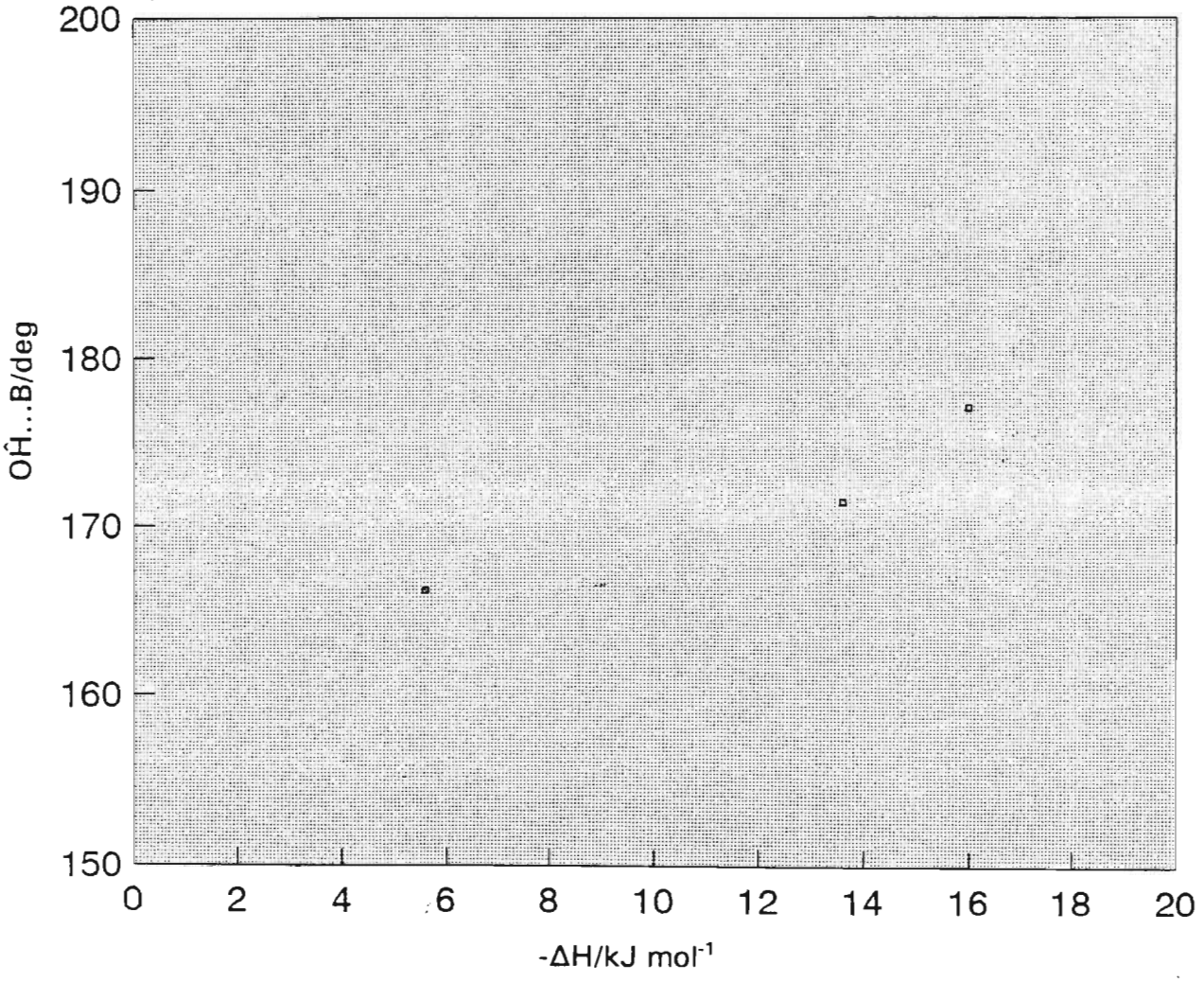

Fig. 2.19. Plot of the OĤ...B bond angle versus the computed hydrogen bond enthalpy.

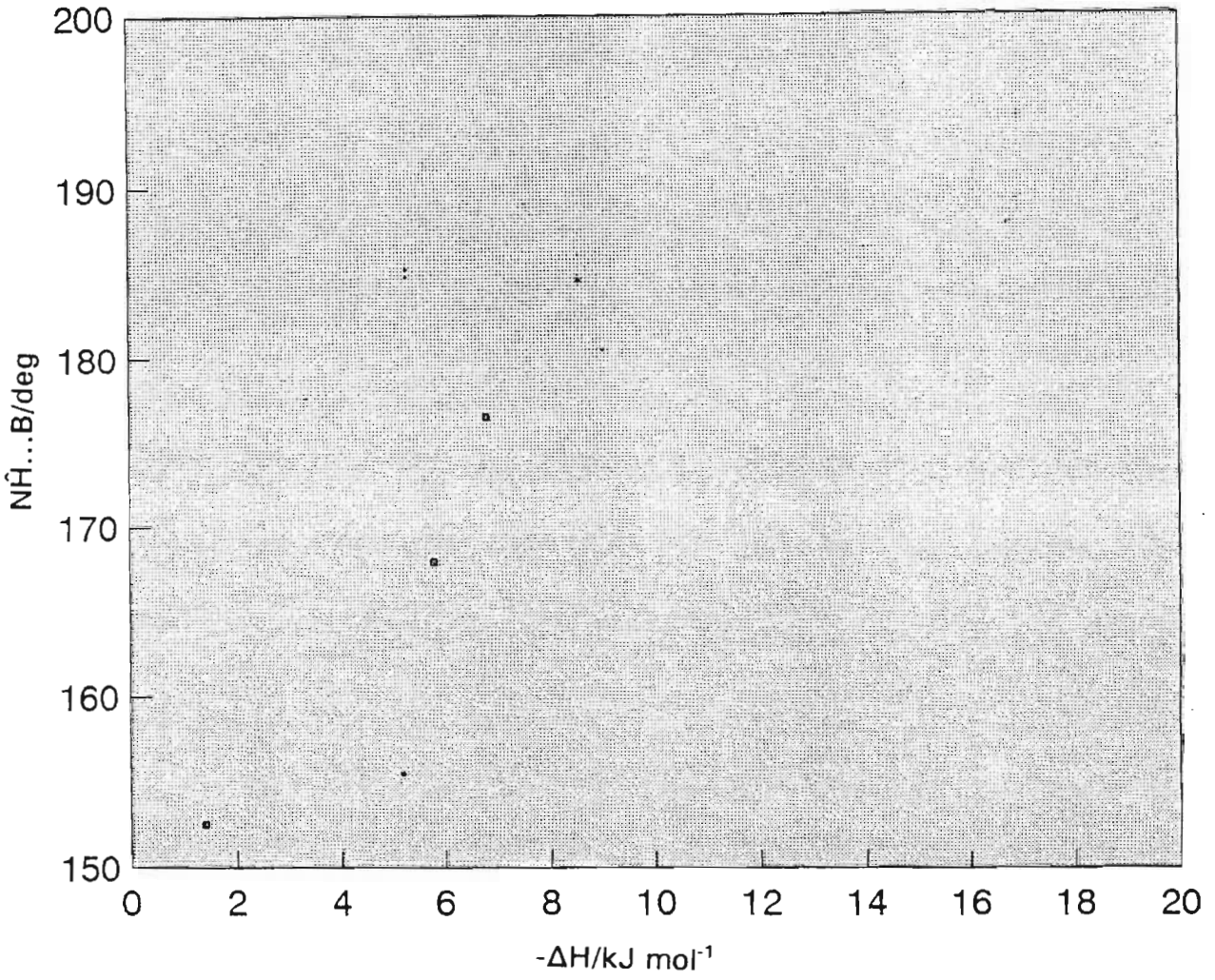

Fig. 2.20. Plot of the NĤ...B bond angle versus the computed hydrogen bond enthalpy.

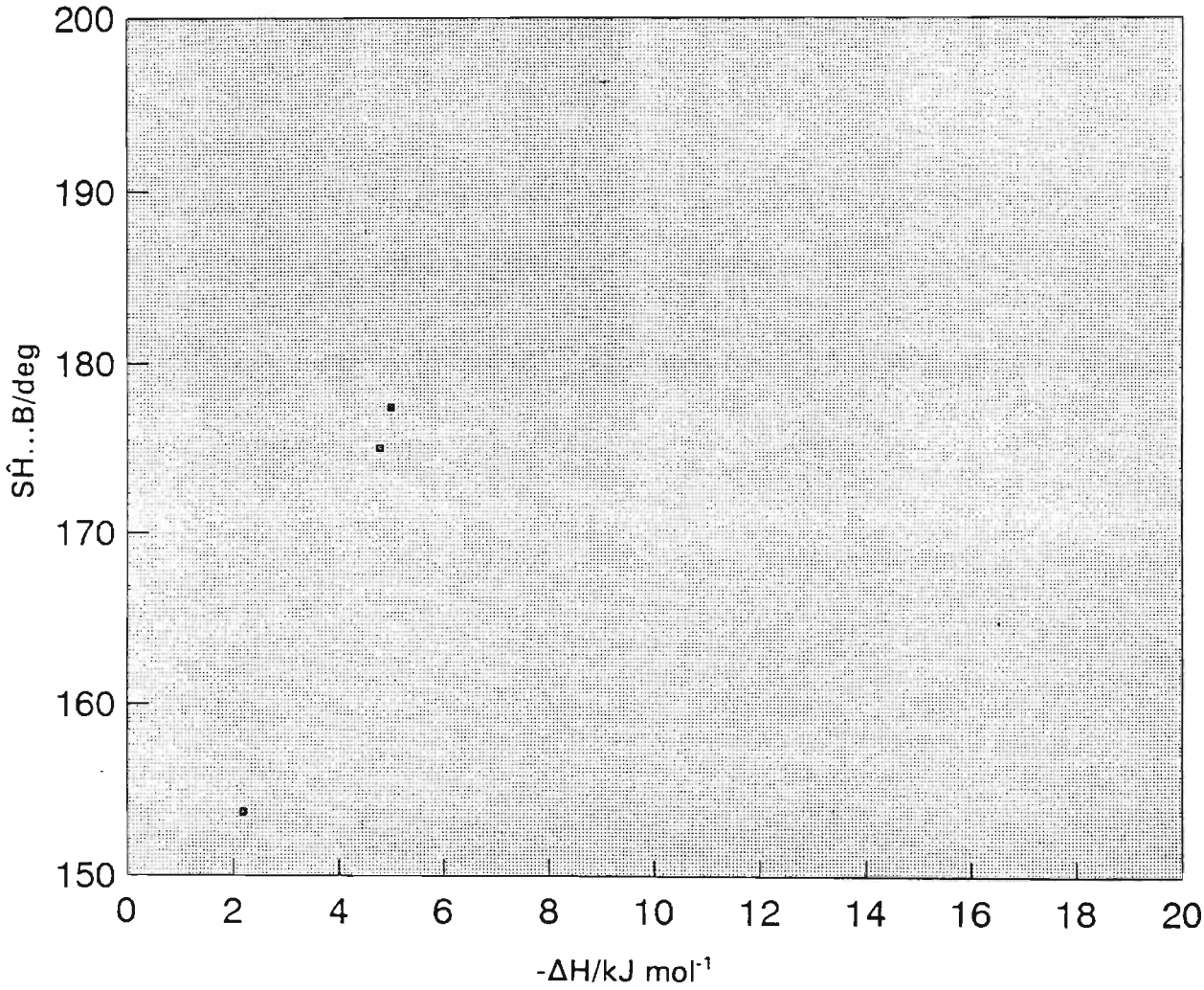

Fig. 2.21. Plot of the SĤ...B bond angle versus the computed hydrogen bond enthalpy.

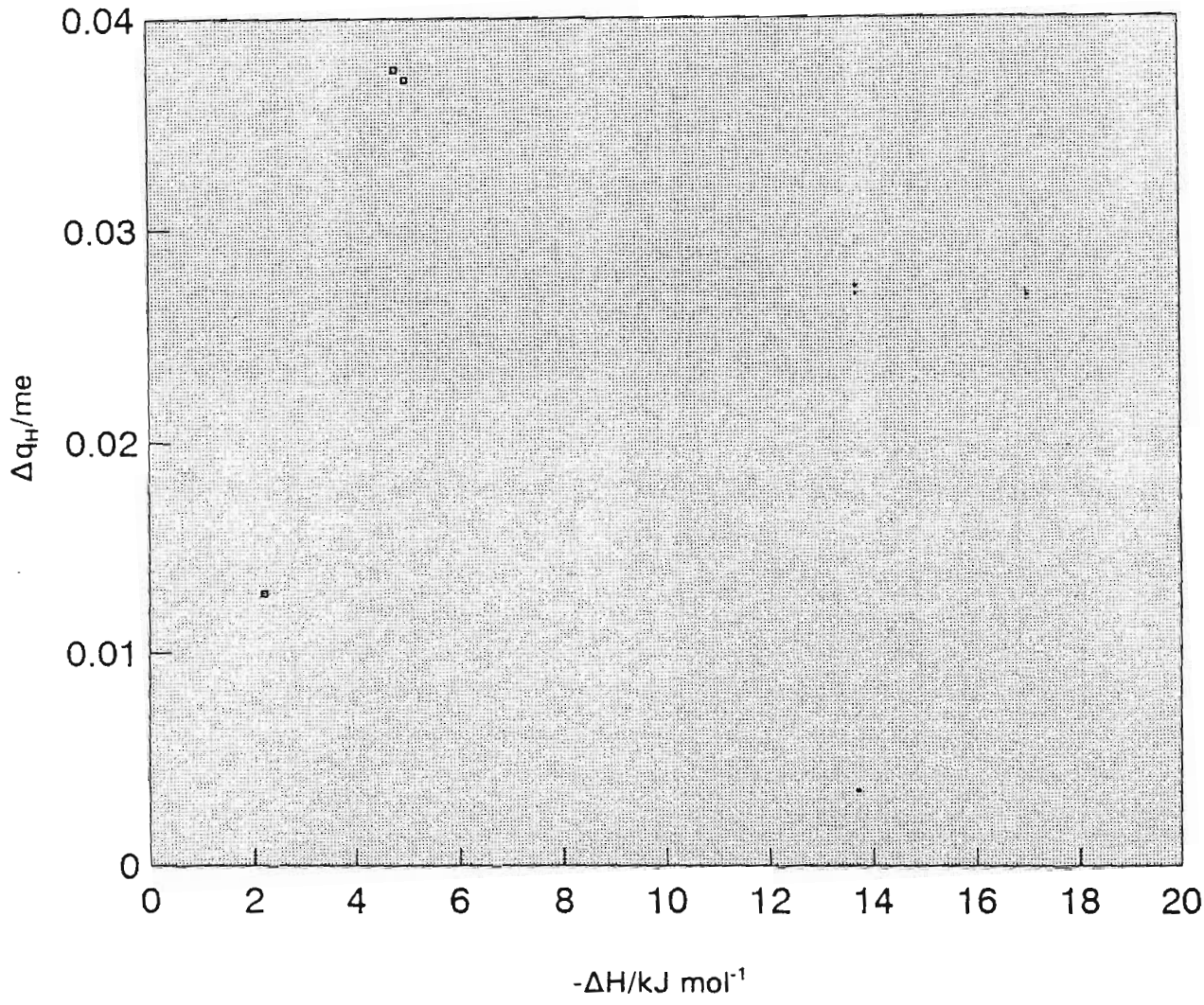

Fig. 2.22. Plot of the Mulliken atomic charge transfer of the bridging hydrogen atom versus the computed hydrogen bond enthalpy; OH proton donor.

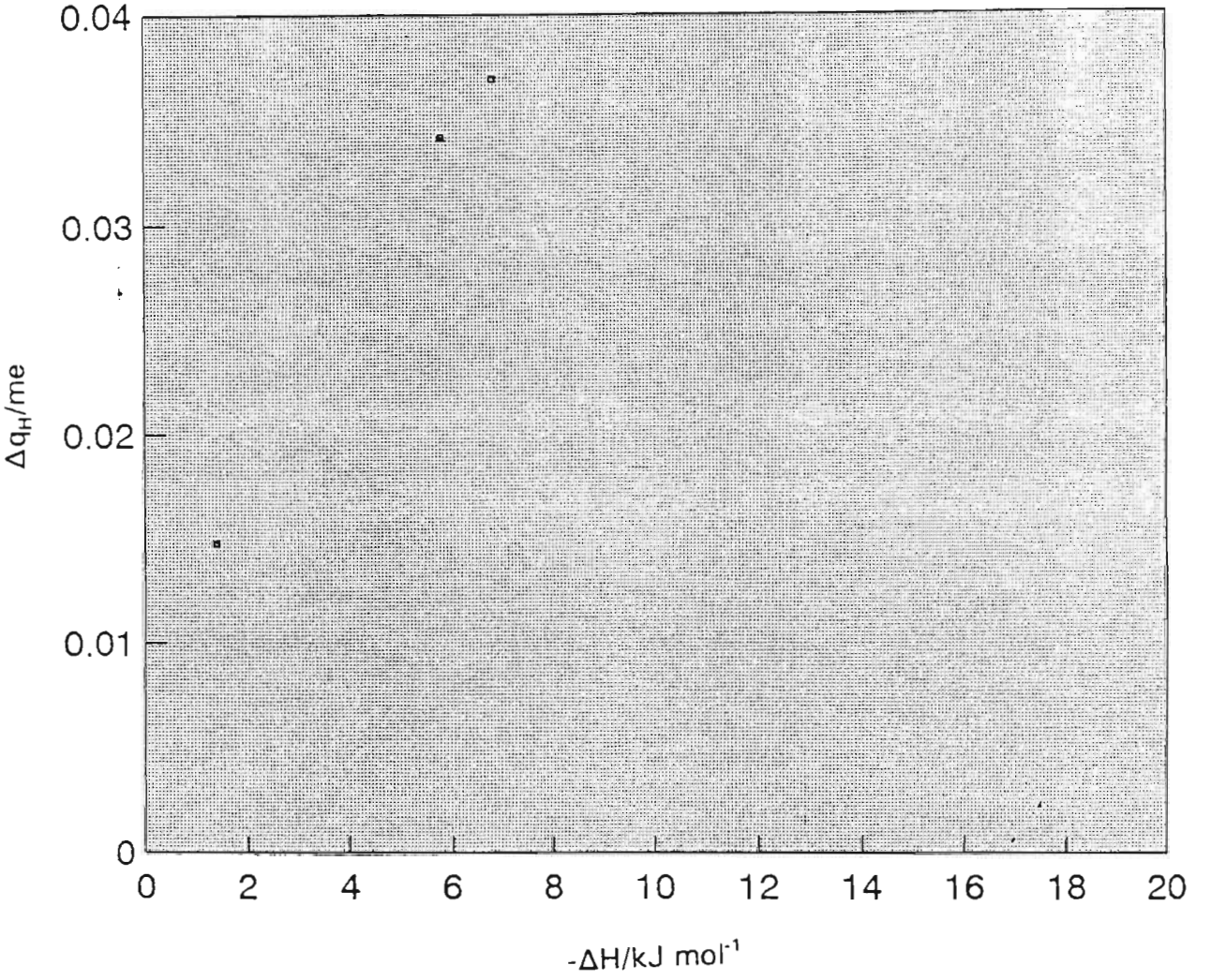

Fig. 2.23. Plot of the Mulliken atomic charge transfer of the bridging hydrogen atom versus the computed hydrogen bond enthalpy; NH proton donor.

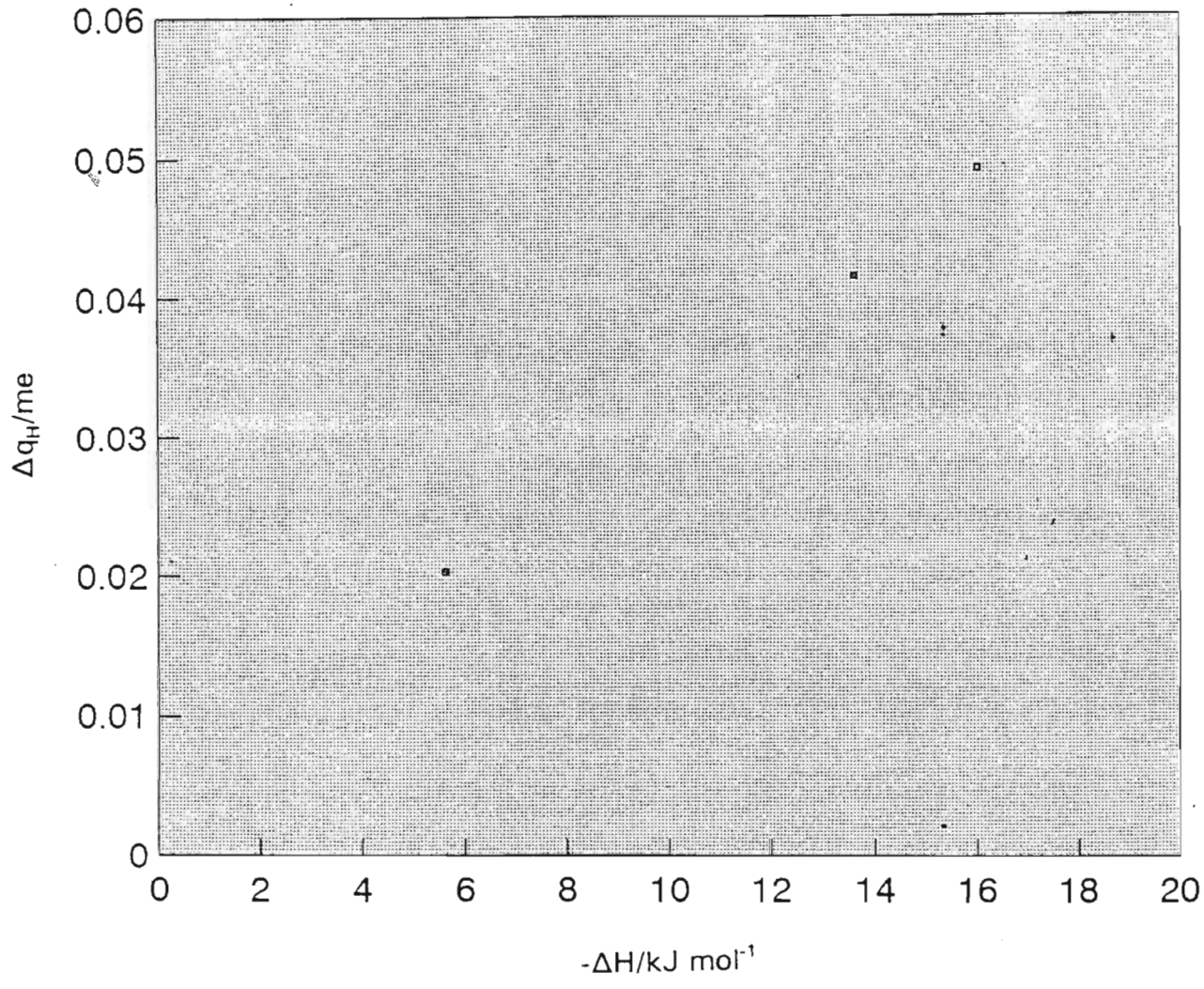

Fig. 2.24. Plot of the Mulliken atomic charge transfer of the bridging hydrogen atom versus the computed hydrogen bond enthalpy; SH proton donor.

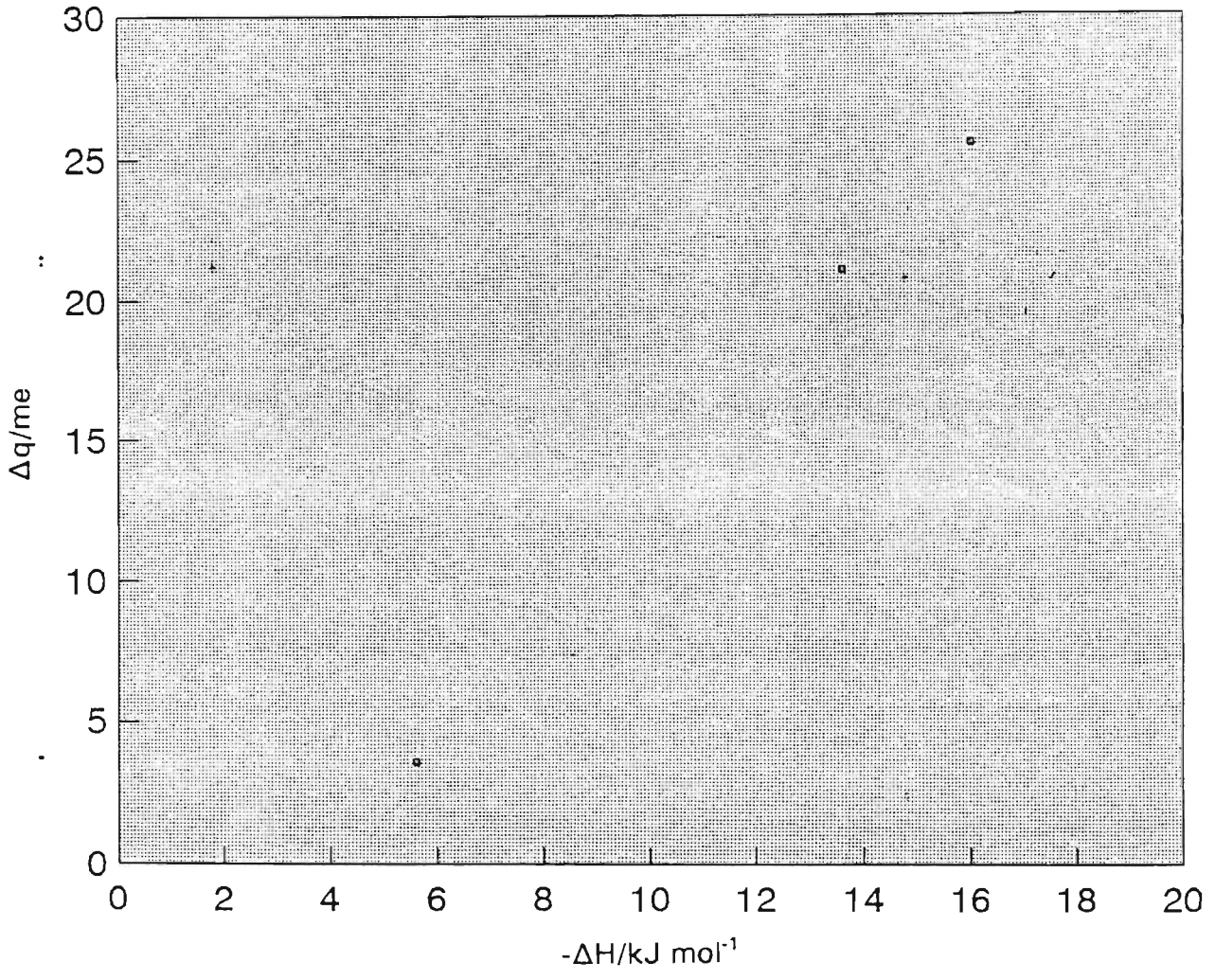

Fig. 2.25. Plot of the intermolecular Mulliken charge transfer versus the computed hydrogen bond enthalpy; OH proton donor.

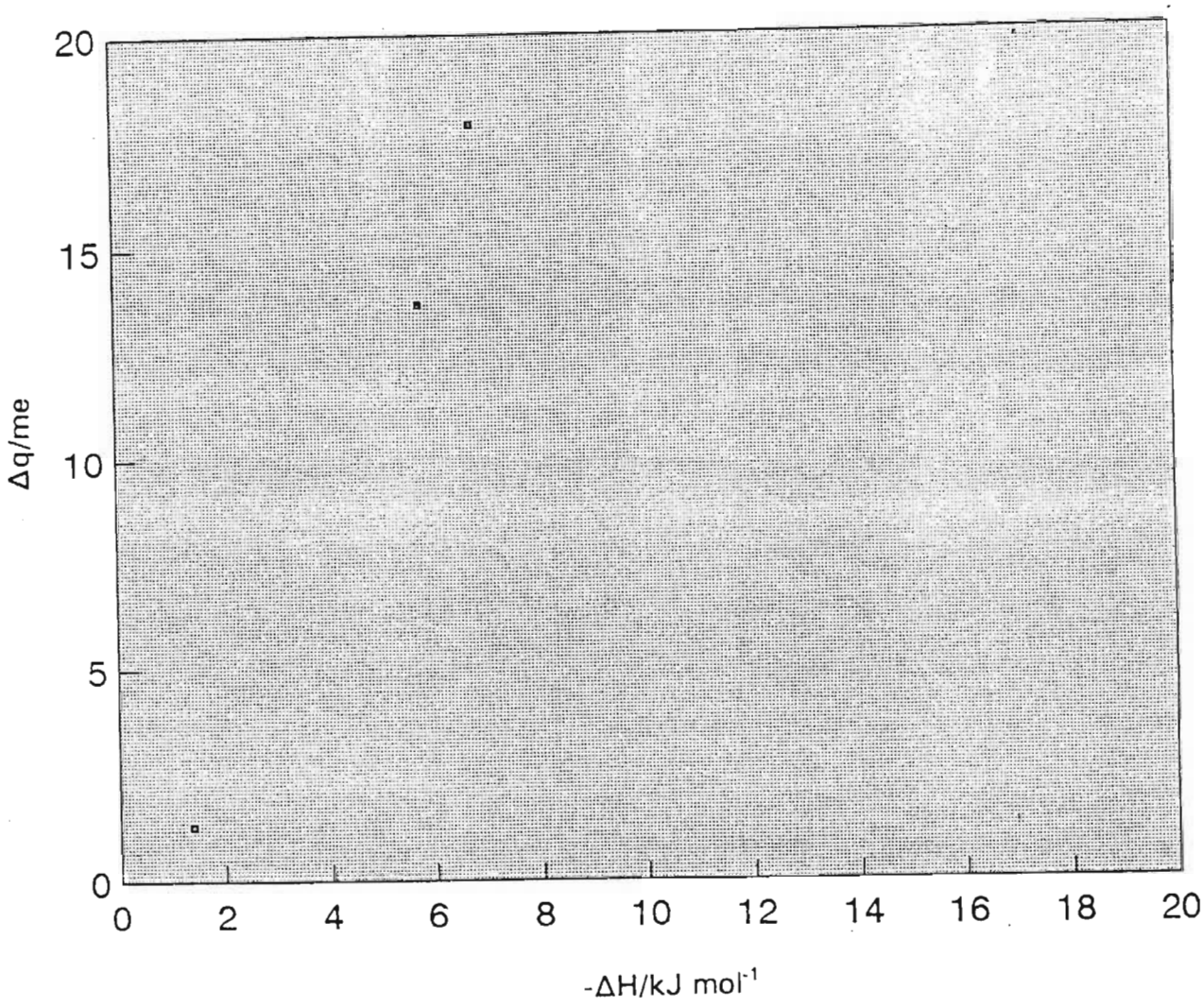

Fig. 2.26. Plot of the intermolecular Mulliken charge transfer versus the computed hydrogen bond enthalpy; NH proton donor.

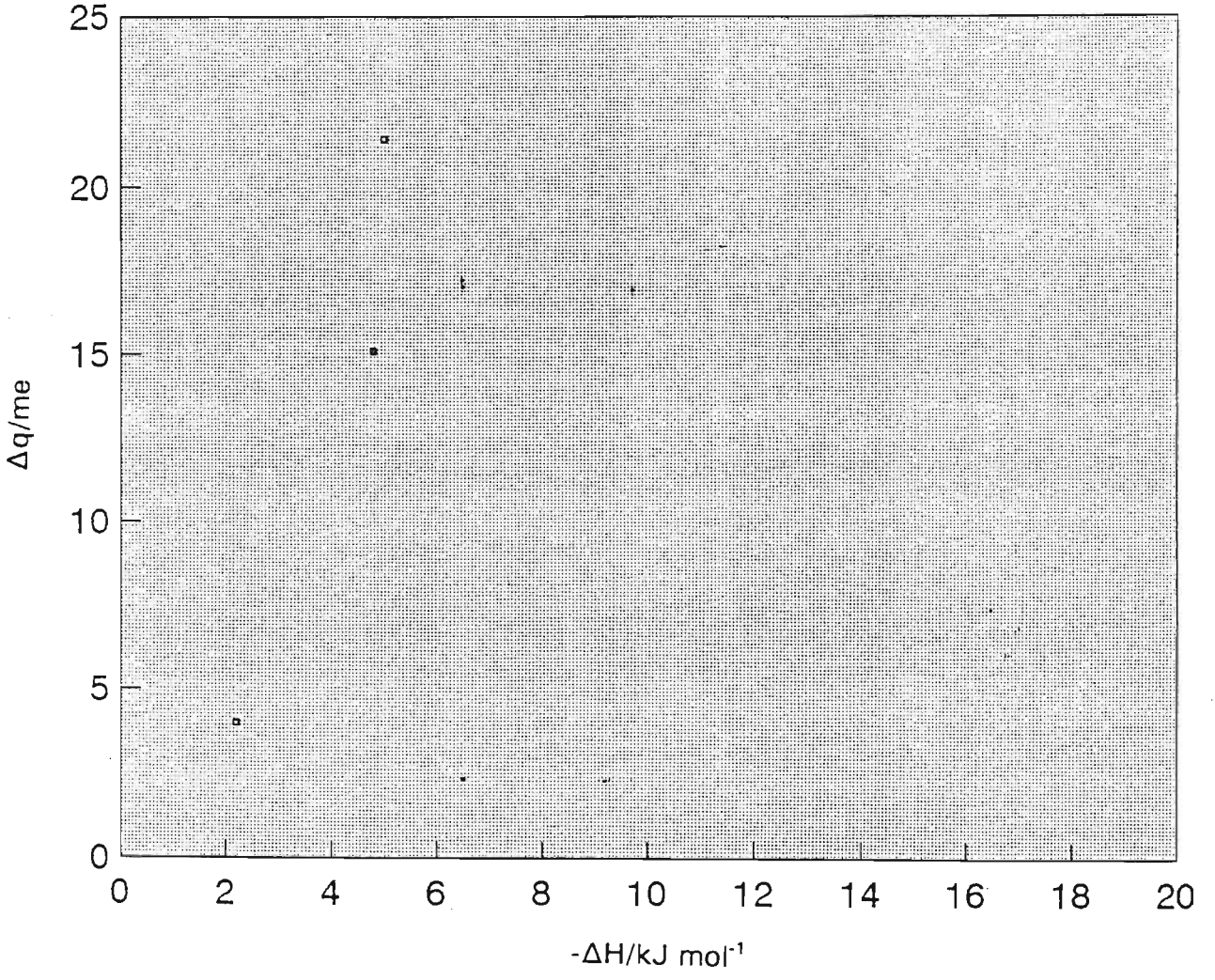

Fig. 2.27. Plot of the intermolecular Mulliken charge transfer versus the computed hydrogen bond enthalpy; SH proton donor.

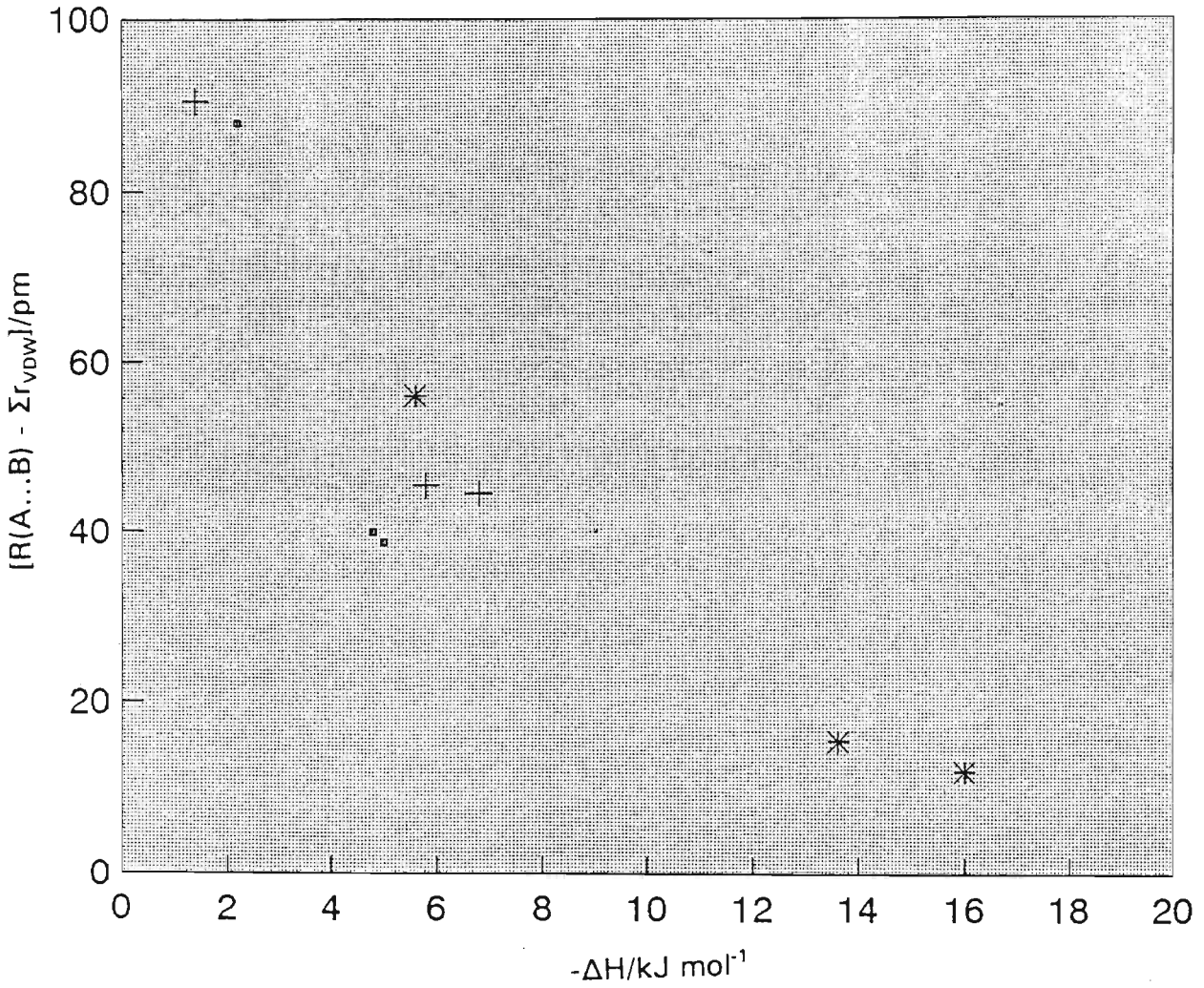

*Fig. 2.28. Plots of the A...B separation (minus the sum of the A and B van dèr Waals radii) versus the computed hydrogen bond enthalpy; * OH proton donor, + NH proton donor, ▫ SH proton donor.*

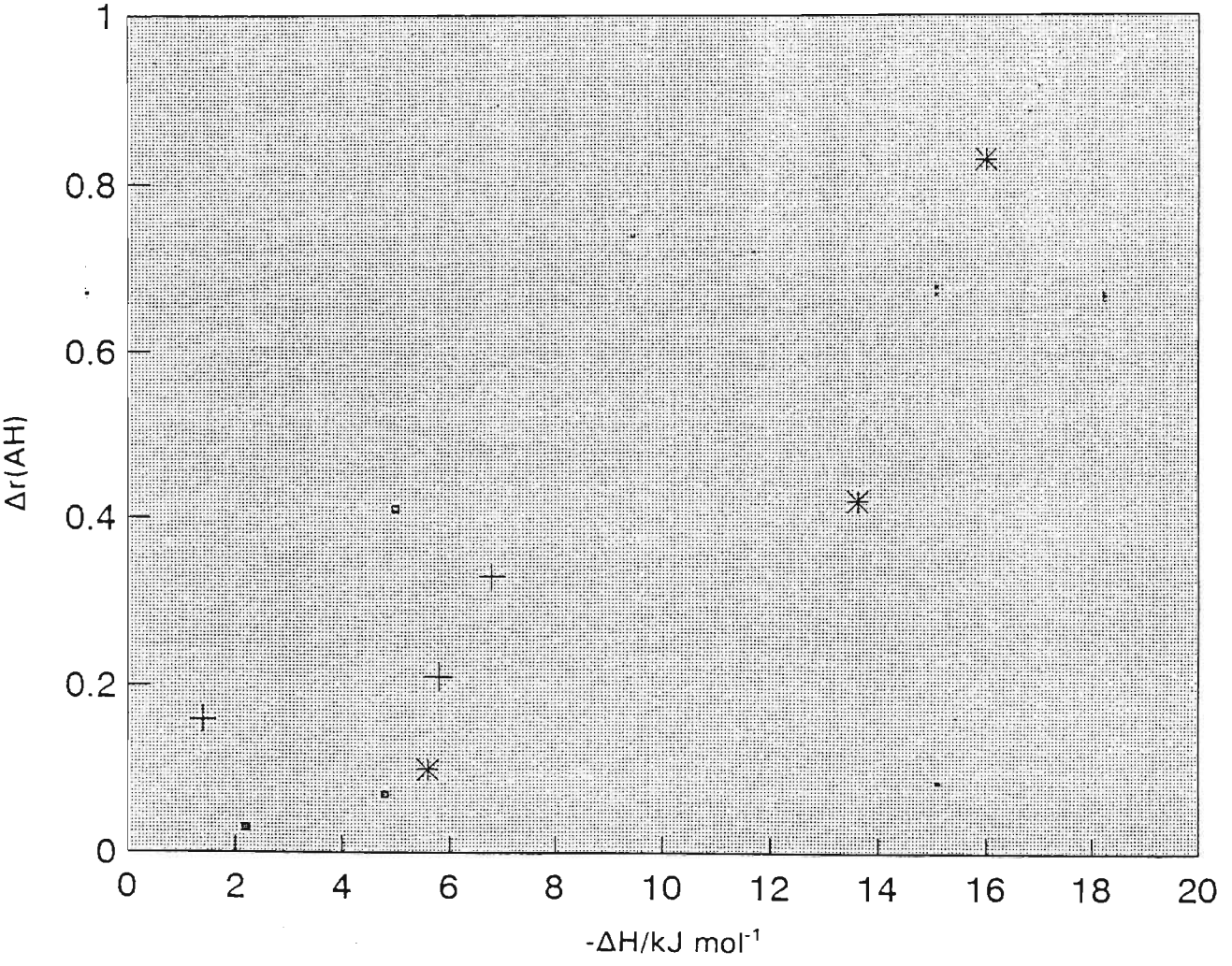

*Fig. 2.29. Plots of the lengthening of the AH bond versus the computed hydrogen bond enthalpy; * OH proton donor, + NH proton donor, ▫ SH proton donor.*

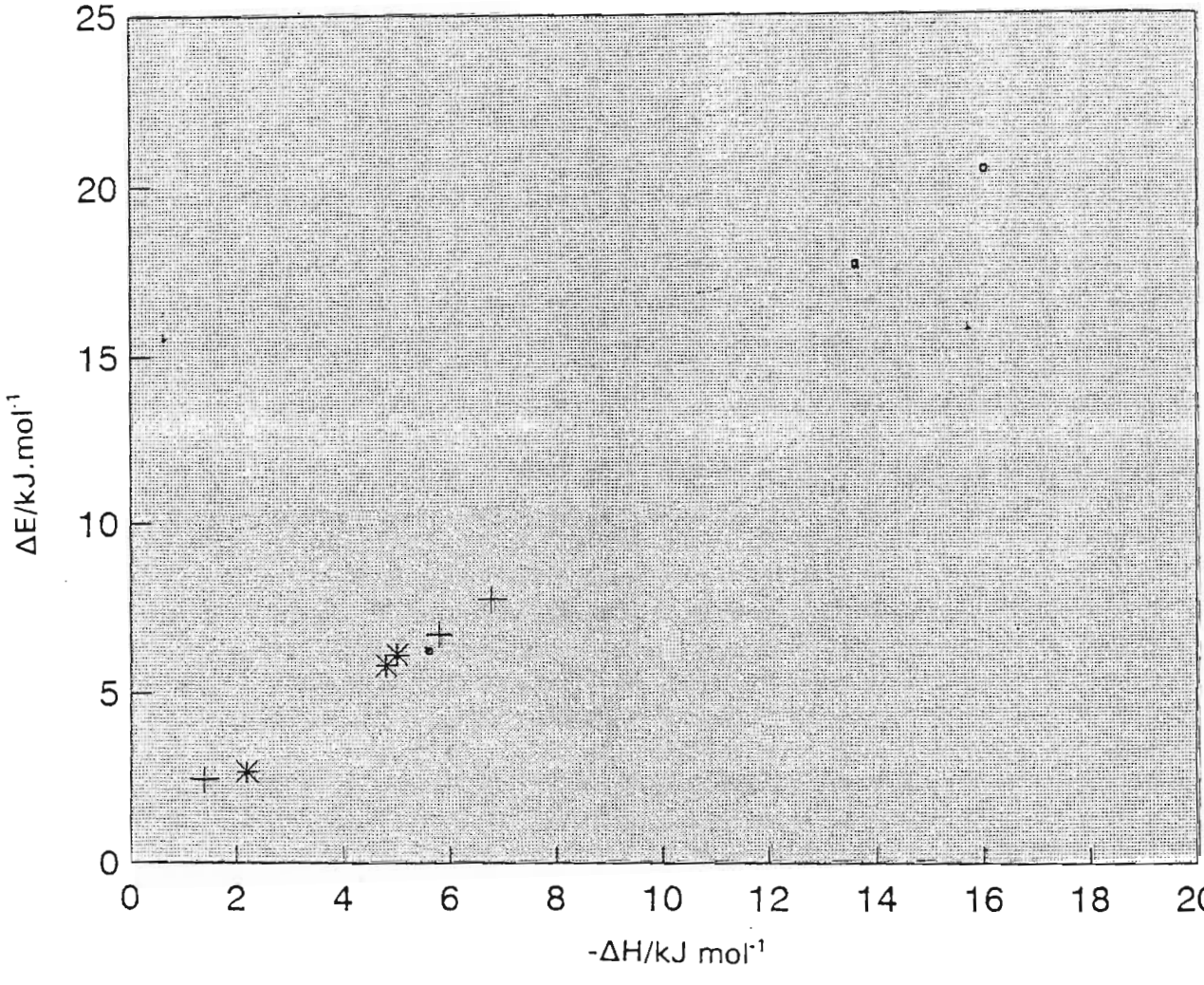

*Fig. 2.30. Plots of the calculated hydrogen bond electronic energy versus the computed hydrogen bond enthalpy; ▫ OH proton donor, + NH proton donor, * SH proton donor.*

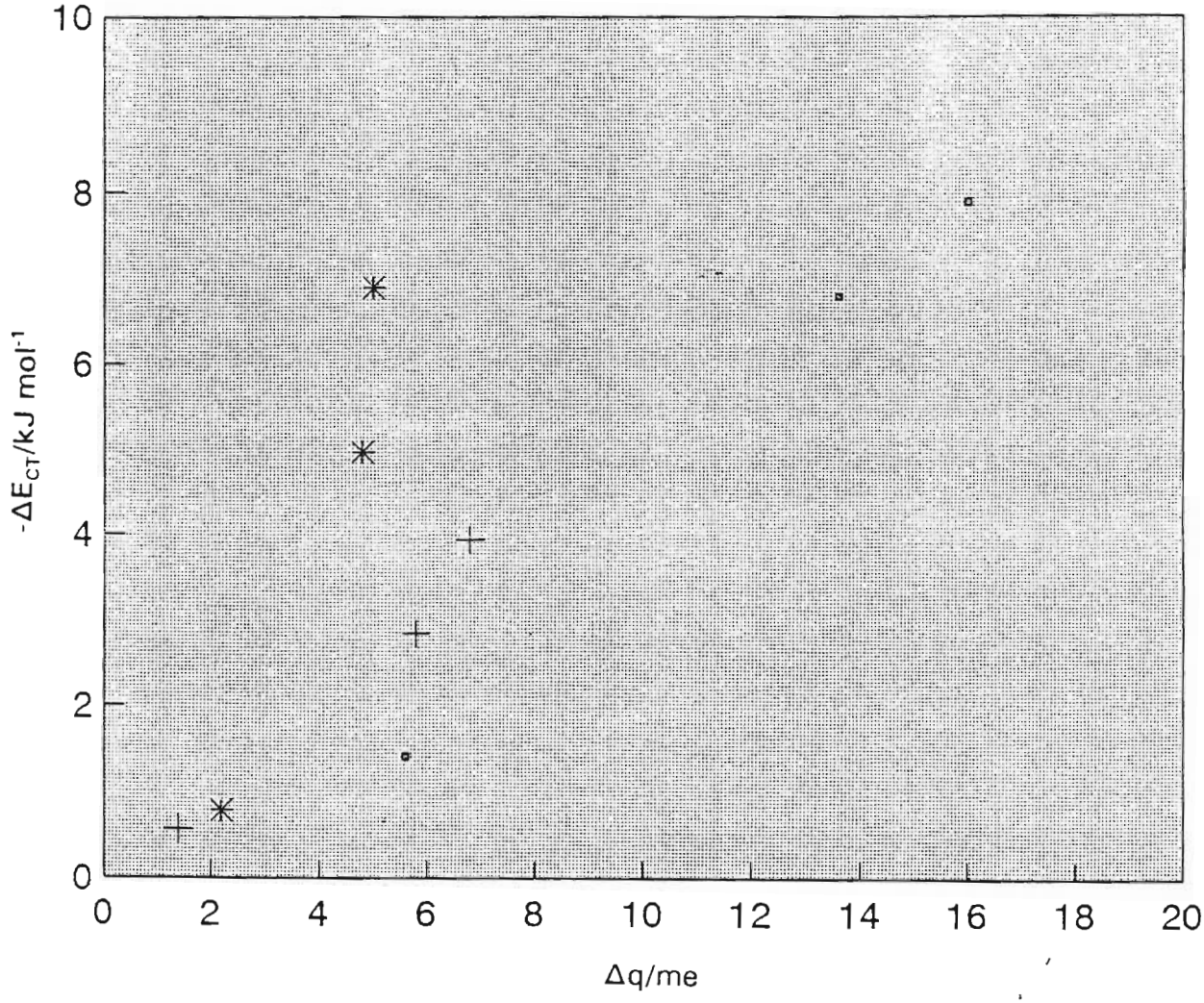

*Fig. 2.31. Plots of the intermolecular Mulliken charge transfer versus the Morokuma charge transfer energy component; ▫ OH proton donor, + NH proton donor, * SH proton donor.*

2.5 Discussion

The *ab initio* MO predictions of the properties of the hydrogen bonded complexes studied in this work highlight some engaging trends. The most salient tendencies involve the proton accepting and the proton donating abilities of the atoms comprising the hydrogen bond. The electronic energies, the deviations from linearity of the AH...B hydrogen bond, the lengthening of the covalent AH bond, the Mulliken charge shifts, the shifts in position and intensity of the A-H stretching band and the shifts in the A-H deformation modes clearly illustrate that the proton accepting competence of the three atoms considered in this work decreases in the order N > O > S. From the results of the interactions between molecules of HF, H_2O, NH_3 and CH_4, Umeyama and Morokuma concluded that the strength of the proton acceptors decreases in the order of N > O > F. Our results are also consistent with those determined by Yeo and Ford[145] in the $H_2O/NH_3/NH_2OH$ system, where the energetic superiority of the OH...N hydrogen bond over the OH...O hydrogen bond was demonstrated.

Umeyama and Morokuma[67] reported that the strength of the proton donors decreases in the order F-H > O-H > N-H > C-H. Based, once again, on the electronic energies, the deviations from linearity of the AH...B hydrogen bond, the lengthening of the covalent AH bond, the Mulliken charge shifts, the shifts in position and intensity of the A-H stretching band and the shifts in the A-H deformation modes of the various hydrogen bonded complexes studied here, we postulate that the proton donating ability decreases in the order O-H > N-H ≈ S-H, concurring with the assessment of Yeo and Ford

that the OH...O hydrogen bond is stronger than the NH...O hydrogen bond. An examination of various properties of the interacting monomers may hint at a plausible cause for the observable trends.

Table 2.46. Gas phase basicities for the proton accepting molecules studied in this work.

Molecules	Gas Phase Basicity /kJ mol^{-1}
$(CH_3)_3N$	909
$(CH_3)_2O$	771
$(CH_3)_2S$	807

Table 2.46 clearly illustrates that if the hydrogen bonded interaction were solely a function of the gas phase basicities of the proton acceptors, the proton accepting ability would decrease in the order N > S > O. The electronegativities of the relevant proton acceptor atoms decrease in the order O > N > S (3.5, 3.0 and 2.5, respectively). A combination of these two factors, basicity and electronegativity, might acknowledge a proton accepting ability in the order N > O > S, consistent with the experimentally observable trend. We therefore propose that the hydrogen bond strength is a function of a combination of the basicities and electronegativities of the proton acceptors. Reimann and Heintz[146] explained that this could be understood qualitatively by the fact that the free electron pair located at the

N atom has a higher polarizability, and therefore acts as a more efficient proton acceptor than either O or S.

The lengthening of the covalent AH bond, the distance of separation of the A and B atoms relative to the sum of their van der Waals radii,[126] the approach of the AH...B angle to linearity and the shift in the A-H stretching wavenumber, are the most characteristic structural manifestations of hydrogen bonding.[3] In this regard, the complex involving the SH...S hydrogen bond has delivered some anomalous results. The trends in both Δr(AH) and $\Delta \nu$(AH) for this complex are the reverse of all the others. Whereas the other complexes display an increase in the length of the A-H bond and a red shift of ν(AH), consistent with the formation of a hydrogen bond, the SH...S complex exhibits a decrease in the length of the A-H bond and a blue shift of ν(AH). Therefore, we are left to conclude that the $CH_3SH...S(CH_3)_2$ interaction is very weak, if not non-existent, an assertion that is further supported by the fact that the intensity of the A-H stretching band in the SH...S complex decreases on hydrogen bonding (see Table 2.37).

CHAPTER 3

PART B - EXPERIMENTAL THERMODYNAMIC STUDY OF MOLECULAR INTERACTIONS

3.1 Introduction

The aim of a theory in the field of material mixtures for a given type of behaviour is to create a model of the bulk state whose behaviour can be analysed mathematically in such a way that the bulk properties can be represented in terms of known molecular properties. If the model is a reasonable expression of the real behaviour then the "theory" could be used to explain a wide range of systems. One of the critical tests of a theory is that it predicts correctly a behaviour which was not specifically considered in creating the model.[36] Complications in the process are met by making physical approximations in the model since often only guesses can be made as to the kinds of molecular behaviour which might be consistent with the observed bulk behaviour.

Theories have been developed which account fairly well for the behaviour of both gases and solids. In the relatively simple theory of the gaseous state it is assumed that the molecules are widely separated in space and exert no influence on each other, which is consistent with the fact that at low densities all gases behave in exactly the same way.[36] In simple solids the highly ordered arrangement also leads to a simple model in which each particle is assumed to be confined to only a small region of space around a

particular point in the crystal and the only motion it has is a vibration around this point.

The properties of liquids can be considered as being intermediate between those of gases and solids.[147] However, a model that reproduces the behaviour of liquids must take into account that the molecules are sufficiently close together that their motions must be influenced by their interactions with one another but not sufficiently localised that this can be done by assuming a simple vibration about a fixed point.[148] Considering the complexity of liquids, it is not surprising then that very little progress has been made in theories of liquids than in theories applicable to gaseous and solid states.

When dealing with liquid mixtures there are the additional challenges of relating the behaviour of the mixture to two different types of molecules and of relating the intermolecular forces between unlike molecules to those between like molecules. Approaching this challenge effectively, lies essentially in limiting the aims. Instead of trying to construct a theory which will account for the bulk properties of a liquid mixture directly in terms of molecular properties of its components, one accounts for the bulk properties of the mixture in terms of bulk properties of the components and by making reasonable assumptions about the liquid state and about the relations between the various intermolecular interactions.

The approach taken by Williamson[36] is useful here:

$$\underset{n_A moles}{A(liquid)} + \underset{n_B moles}{B(liquid)} \rightarrow \underset{(n_A+n_B) moles}{(A+B)(mixture)} \qquad (3.1)$$

In attempting to calculate the change ΔX_m of property X for this process, the nature of the calculations might be represented by the equation

$$\begin{aligned}\Delta X_m = &(n_A+n_B)(calculated\ X\ for\ mixture)\\ &+(n_A+n_B)(ignorance\ of\ liquid\ state,\ mixture)\\ &-n_A(calculated\ X\ for\ pure\ A)\\ &-n_A(ignorance\ of\ liquid\ state\ A)\\ &-n_B(calculated\ X\ for\ pure\ B)\\ &-n_B(ignorance\ of\ liquid\ state\ B)\end{aligned} \qquad (3.2)$$

Particularly for mixtures in which A and B are similar, the terms "ignorance of liquid state" will at least partially cancel. Hence calculations based on even a relatively poor model of the liquid state might be expected to yield reasonable values for the changes in properties on mixing two liquids.

Experimentally determined H_m^E and V_m^E values have been used in this work to determine the propensities of the various liquid mixtures involving hydrogen bond formation. These results have also been used to evaluate the energy of hydrogen bonding. In all the mixtures discussed here, there are present intermolecular interactions other than hydrogen bonding which complicate the interpretation of the experimental results.

In this work three methods have been used in an attempt to quantify the hydrogen bonds under consideration. Firstly, partial molar enthalpies at infinite dilution, $H_{i,m}^E(x_i=0)$, have been determined from experimental H_m^E

values (see section 3.4.2). The results have been applied to an approximation procedure described by Woycicka *et al.*[28] and others [24-27] in order to determine the energies of hydrogen bonds in liquid mixtures. Secondly, a semi-quantitative method using H_m^E at x = 0.5 has been employed to corroborate the above findings (see chapter 3.6.3) and lastly a theory of mixing, the Extended Real Associated Solution (ERAS) model, has been applied (see section 3.5) to both the H_m^E and V_m^E data.

3.2 Excess Thermodynamic Properties

3.2.1 Introduction

The thermodynamic properties of a solution of two liquids are often expressed in terms of excess functions. For any extensive property X of a phase (ie G, H, V or S), the excess quantity X^E is defined by the relation:[149]

$$X^E \equiv X - X^{id} \tag{3.3}$$

where X^{id} is property of the hypothetical ideal solution. Thus, the excess enthalpy H^E of a mixture of liquids is defined as the difference between the actual enthalpy H of the solution and the enthalpy of a hypothetical ideal solution, H^{id}, with the same T, P, and composition.

Subtraction of

$$G^{id} = H^{id} - TS^{id} \tag{3.4}$$

from

$$G = H - TS \tag{3.5}$$

gives

$$G^E = H^E - TS^E \tag{3.6}$$

The change in property X on mixing the solution from its pure components at constant T and P is given by[149]

$$\Delta X_{mix} \equiv X - X^* \tag{3.7}$$

where mix refers to mixing, X is a property of the solution and X^* is a property of the pure unmixed components at the same T and P as the solution.

Excess functions are related to mixing quantities:

$$\begin{aligned} X^E &= X - X^{id} \\ &= X - X^{id} + X^* - X^* \\ &= X - X^* - (X^{id} - X^*) \\ &= \Delta X_{mix} - \Delta X_{mix}^{id} \end{aligned} \tag{3.8}$$

where X^E refers to H^E, V^E, G^E or S^E.

Since $\Delta H_{mix}^{id} = 0$ and $\Delta V_{mix}^{id} = 0$

$$H^E = \Delta H_{mix} \tag{3.9}$$

$$V^E = \Delta V_{mix} \tag{3.10}$$

$$S^E = \Delta S_{mix} - \Delta S_{mix}^{id} \tag{3.11}$$

and

$$G^E = \Delta G_{mix} - \Delta G_{mix}^{id} \tag{3.12}$$

Corresponding to any extensive quantity X of a phase, an intensive quantity called a molar quantity, X_m, is defined by the relation:[150]

$$X_m = \frac{X}{\sum_B n_B} \tag{3.13}$$

where *n* refers to number of moles. For example, H_m of a phase is the enthalpy of the phase divided by the total number of moles present in the phase. Similarly, X_m^E, as used in this work refers to the *molar excess quantity*.

3.2.2 Excess molar volumes of mixing

The volume changes resulting from the mixing of liquids are due to a number of factors. They include differences in the size and shape of the component molecules which may induce different "packing" orientations of the mixtures and different intermolecular interactions which may exist between like and unlike molecules. The first quantitative study on the volume changes of mixing was published by Scatchard[151] in 1937. Hildebrand and Scott[152] continued with this early work during a phase of development[153]in the early 1960's. The ease with which the excess

volumes of mixing can be measured has resulted in this value being used as a favourable method of testing the theories of liquid mixtures.[154]

Excess molar volumes, V_m^E, may be determined either (i) directly or (ii) indirectly. Direct measurements involve mixing the liquids and examining the volume change (dilatometric method) whereas the indirect method involves measuring the density of the liquid mixtures at different compositions using a pycnometer or densitometer.

3.2.2.1 Direct Determinations of Excess Volumes.

Direct dilatometric measurements have produced accurate volume change measurements. Handa and Benson[155] regard direct measuring methods as being more precise than indirect methods. A simple dilatometer is shown in Fig. 3.1. Mixing is accomplished by rocking the dilatometer to and fro. The excess molar volume of mixing is given by the relation

$$V_m^E = \frac{\Delta V}{(n_A + n_B)} = \frac{a\Delta h}{(n_A + n_B)} \qquad (3.14)$$

where *a* is the cross sectional area of the capillary and n_A and n_B are the moles of A and B.

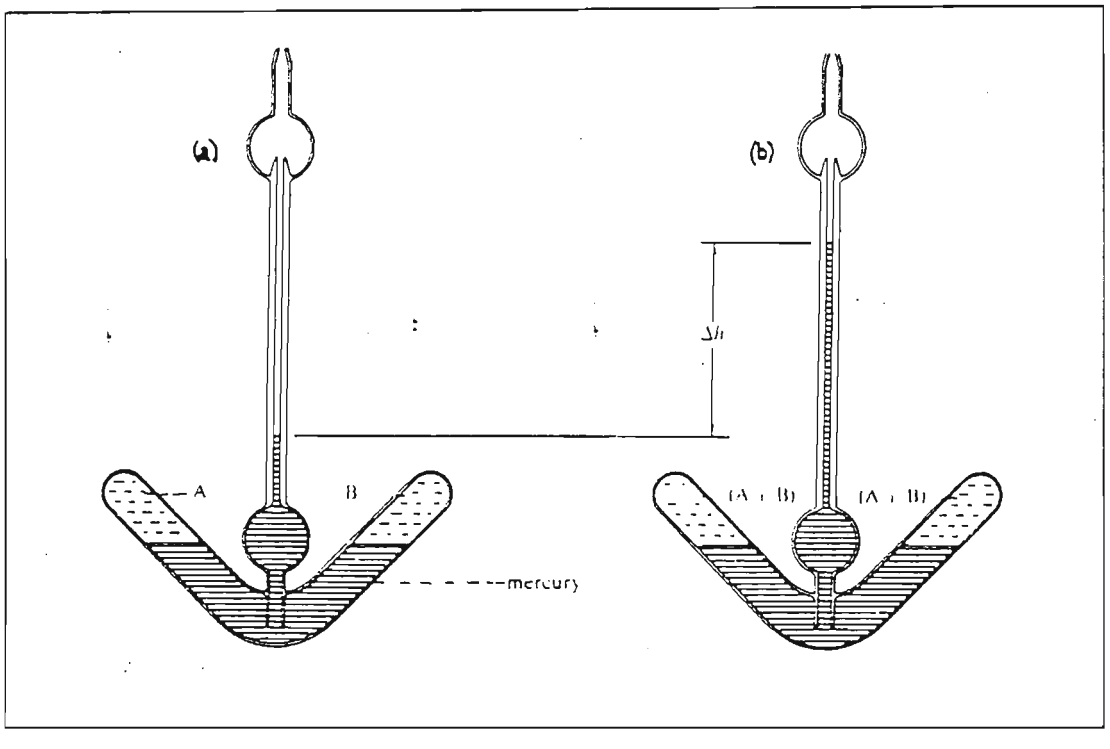

Fig. 3.1. A dilatometer for measuring volumes of mixing (a) before and (b) after mixing.

Two fundamental types of dilatometric apparatus have been designed for the direct measurement of volume changes; (a) batch or single composition dilatometry and (b) continuous dilution dilatometry.

(a) Batch dilatometry

One of the earliest designs for a single loading batch dilatometer was the device of Keyes and Hildebrand[156] and is illustrated in Fig 3.2.

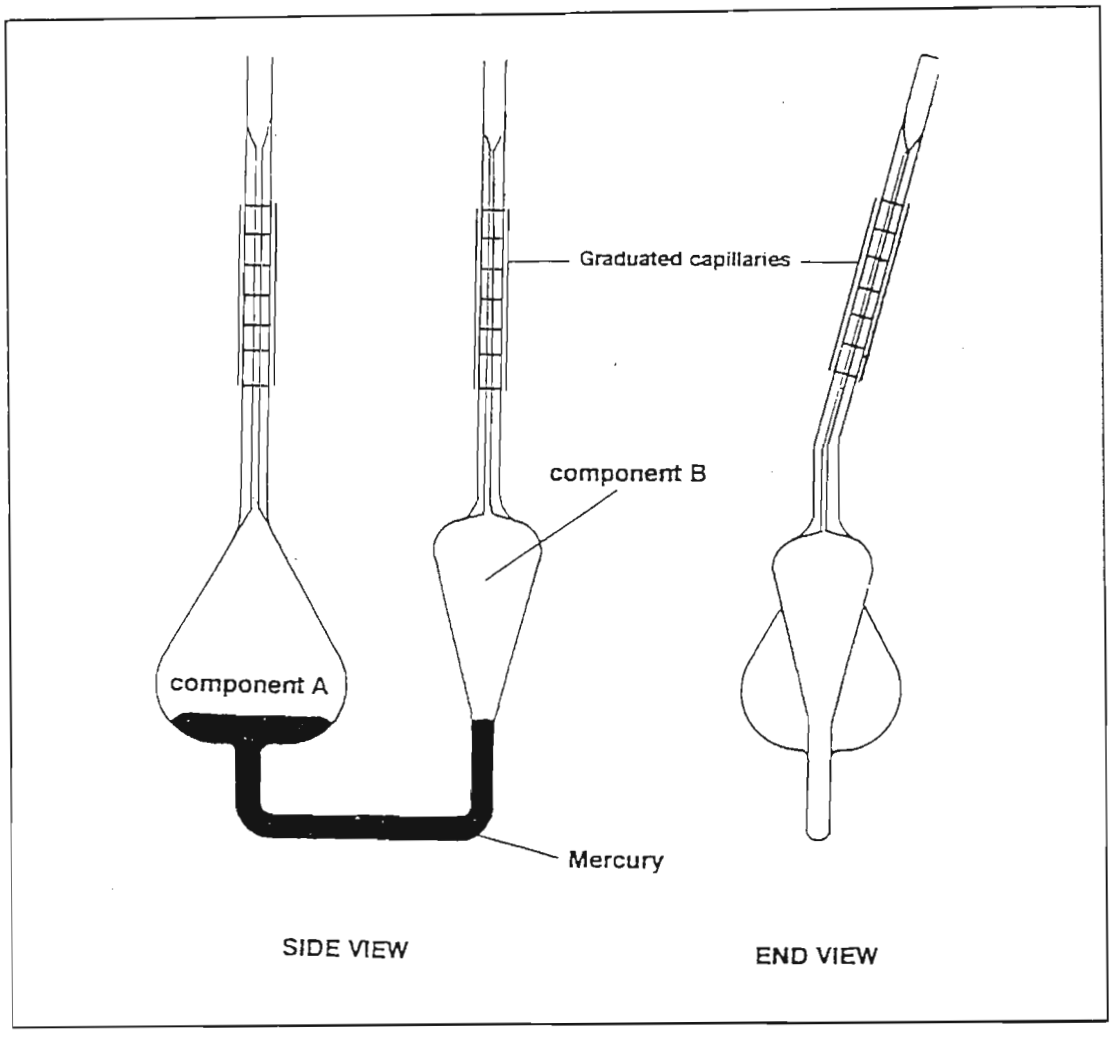

Fig. 3.2 The Keyes and Hildebrand dilatometer[156]

It consisted of a U-tube with mercury separating the two sample components at the bottom of the apparatus. Graduated capillaries on the two arms of the dilatometer provide the means of volume determination before and after mixing. The vessel is immersed entirely in a thermostatted bath and mixing is achieved by rocking the apparatus. The basic disadvantages of batch dilatometry was that each measurement involved a separate loading of the apparatus, and its time consuming nature. Most of the modifications of the existing design of Keyes and Hildebrand have been reviewed by Battino.[153]

(b) Continuous dilution dilatometers

Since the original design of a dilution dilatometer by Geffcken *et al.*[157] in 1937, dilution dilatometers have undergone several modifications. The disadvantage of batch dilatometry was that each measurement involved a separate loading of the apparatus. A recent design of dilatometer was developed by Kumaran and McGlashan.[158] It is a grease-free tilting dilution dilatometer which is easy to operate and calibrate, can be filled under atmospheric conditions and can be used for V_m^E determination of almost any magnitude. The Kumaran and McGlashan dilatometer works on the principle that when the instrument is tilted from the vertical mercury flows from B into the dilatometer tube thus displacing an equal volume of diluent liquid through C into the bulb. The apparatus is then brought back to the vertical and after thermal equilibrium the heights of the mercury at A,B,C and D are recorded. The volume is then calculated from:

$$V^E = \sum \Delta V/(n_1 + n_2) \qquad (3.15)$$

where n_1 and n_2 are the numbers of moles of the constituent liquids.

The disadvantage of most continuous dilution dilatometers is that they do not permit V_m^E measurements at a constant pressure. The dilatometer of Kumaran and McGlashan does take this pressure effect into account.[158] The height change of the mercury in the capillary causes a change in the mixing cell pressure, and this, together with the elasticity of glass and the compressibility of the liquid may, however, be sources of error.

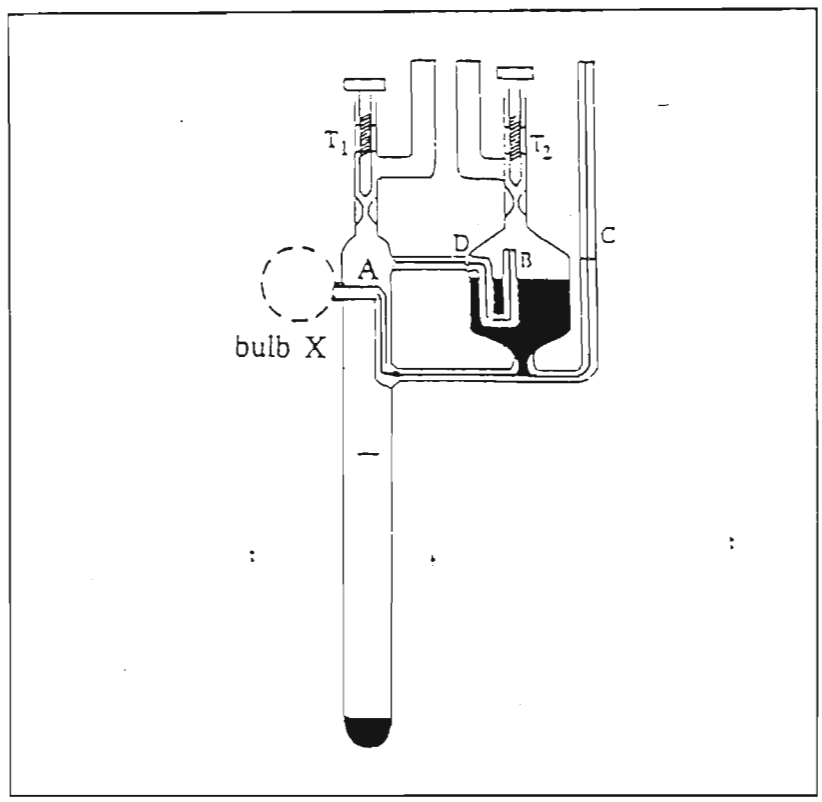

Fig. 3.3 Dilution dilatometer of Kumaran and McGlashan[158]

3.2.2.2 Indirect Determinations of Excess Volumes

Density is defined as mass divided by volume:

$$D = \frac{M}{V} \tag{3.16}$$

hence a simple and reliable method of determining density is to accurately find the mass and volume of a sample of the liquid or liquid mixture under examination. A rapid method of calculating density is, therefore, to fill a vessel with the sample liquid and to ascertain its mass. The volume of the

recipient vessel is then established by finding the mass of a pure liquid (normally water) which completely satiates the vessel. These vessels should be manufactured from a material such as a resistant glass that has a low coefficient of thermal expansion.[159] Bauer[159] describes the form and function of several such vessels or *pycnometers* or density bottles. Many are quick and easy to use but have low accuracies. Spiteri[160] describes the operation of the Sprengel-Ostwald pycnometer which is capable of an accuracy of up to $5x10^{-6}$ cm^3. In order to produce accurate measurements with these pycnometers compensations for buoyancy and vapour space have to be applied.[161] A difficulty that may be encountered with the pycnometric method of density evaluation is that there may be incomplete mixing of the components. A further problem also arises especially when using volatile liquids in that some of the liquid may be lost due to evaporation. Clearly both of these weaknesses in the experimental technique would generate spurious results. To this end a mixing bottle was developed by Wood and Brusie[162] that minimised these errors. Some 20 years later the design was improved upon by Battino.[153] Each chamber of Battino's bottle has a capacity of approximately 53 cm^3. These chambers are joined by a 10mm U-tube in such a way as to set them at an angle of 20° to the vertical. The angled chambers and the comparatively large bore of the connecting U-tube facilitates efficient mixing, which is a characteristic of Battino's design.

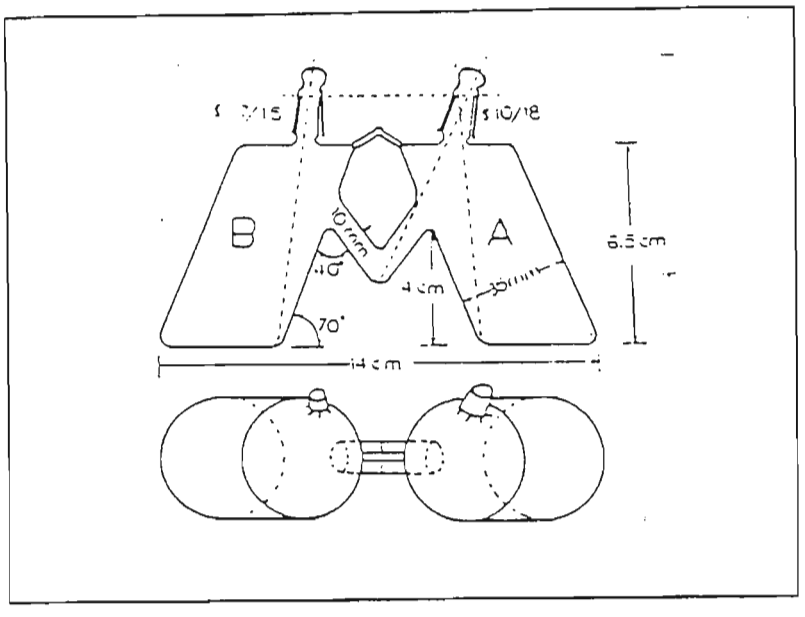

Fig. 3.4 Mixing bottle of Battino[153].

Magnetic float densitometry was developed to give greater accuracy in density measurements. Franks and Smith[163,164] describe a modified version of the magnetic float cell originally reported by Lamb and Lee.[165] The quartz float of the apparatus contained a small magnetic bar of 100cgs unit pole strength. The cell, made from pyrex with a capacity of 600 cm^3, was mounted in a thermostatted bath that was constructed entirely of non-magnetic materials. A precision of better than 1 part in 10^6 is reported for this apparatus. Masterton and Seiler[166] also describe a magnetic float densitometer and they claim a reproducibility precision of 3 ppm.

In this work a densitometer based on the initial design of Kratly, Leopold and Stabinger[167] and produced by Anton Paar was used to evaluate the densities of the liquid mixtures.

3.2.2.3 The Anton Paar DMA 601 Vibrating Tube Densitometer

The Anton Paar[167] densitometer has a glass U-tube measuring cell with a capacity of 0.7 cm^3 which is separated thermally from the electronics. The sample tube is constructed of borosilicate glass and is fused into a glass cylinder. The space between the U-shaped sample tube and the inner wall is filled with a gas of high thermal conductivity to promote a rapid temperature equilibrium of the sample inside the oscillator with a thermostat liquid which flows through the cylinder around the sample tube. The sample tube is electronically excited and density measurements are determined accurately by measurements of the period of oscillation of the sample tube.

An important requirement for measurement of densities to a high level of accuracy is a good temperature control of the sample tube. A shorter capillary tube inside the inner space of the wall cylinder is for the accurate temperature determination and monitoring of the measuring cell by the temperature sensor. The accuracy of the density measurements is very sensitive to the operating temperature. For this reason the temperature was controlled to within 0.001 K in this work. Uniform temperature control was achieved through the use of two variable speed mechanical stirrers. An auxiliary cooling system comprising of a 50 litre water bath cooled by a Grants refrigeration coil maintained the temperature control of the main water bath. Water from this auxiliary bath was pumped via a Haak immersion thermostat unit through a four meter coiled copper tube placed inside the primary cooling bath. Keeping the auxiliary bath at approximately 1 K below the operating temperature assisted in regulating the main bath

temperature. The thermostat liquid used in both the main and auxiliary water baths was distilled water treated with an algae inhibitor.

The thermostat system within the main water bath consisted of a permanent rheostatted immersion heater, and a 60 W light bulb connected to a Tronac temperature controller. Water from the primary bath was pumped through the water jacket by a submersible pump. All rubber tubing was insulated to reduce heat loss. A recently calibrated Hewlett Packard 2801A quartz thermometer monitored the temperature within the main water bath. A Paar digital thermometer, linked to a thermocouple, was used to monitor the temperature of the cell.

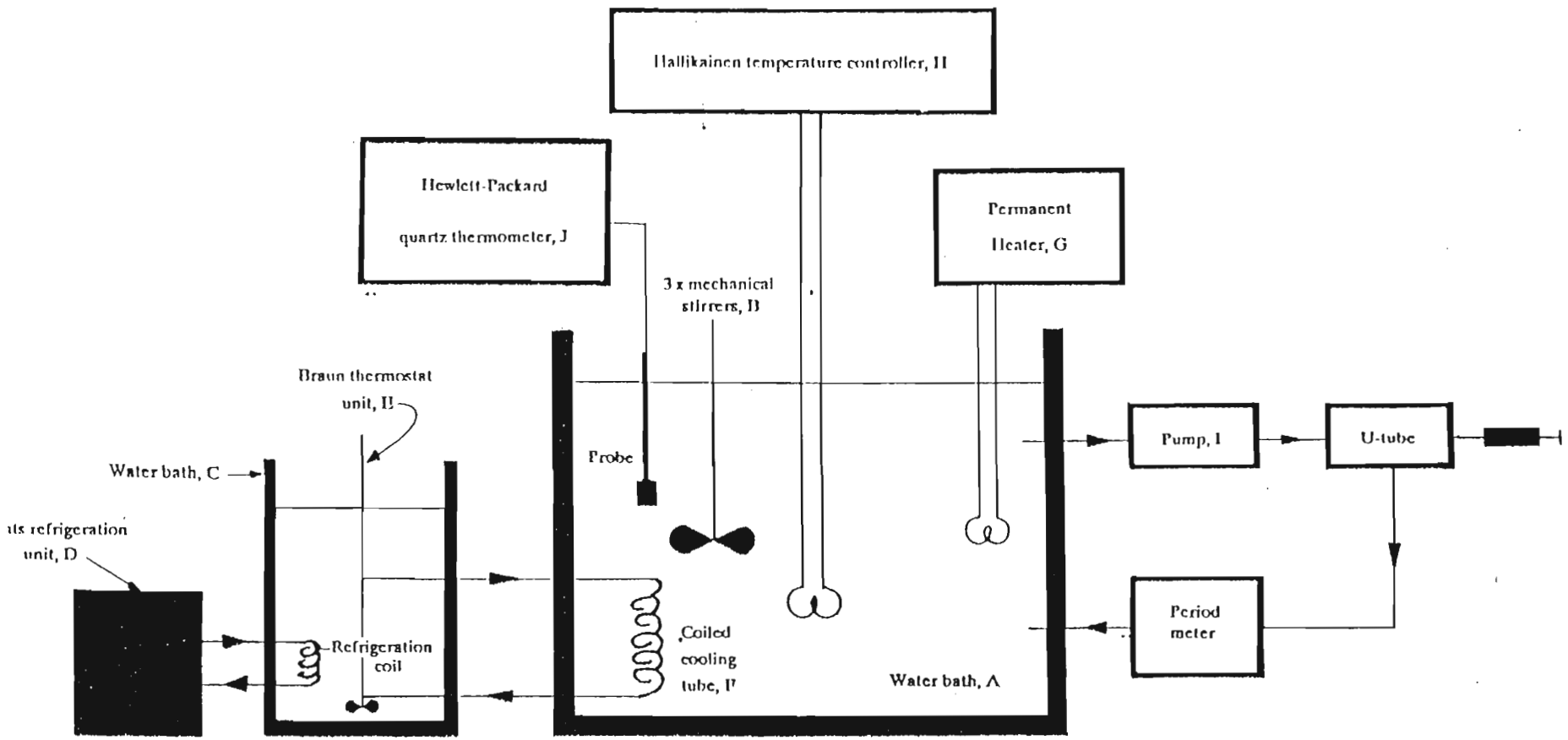

Fig. 3.5 Laboratory arrangement of the Anton Paar DMA 601 vibrating tude densitometer.

3.2.2.4 Operation Procedure

The densitometer was allowed to warm up for 30 minutes prior to any measurement taking in order to allow complete temperature equilibrium. The cell was also flushed thoroughly with ethanol and acetone, and compressed air blown through, prior to each experimental run. A constant period value, τ, for the air filled sample tube was obtained before the sample was introduced. Distilled, pre-boiled water (used as the calibrated standard sample) was then introduced into the cell by means of a glass syringe, equipped with a teflon nozzle, ensuring a leak proof fit at the syringe-sample cell junction. The injection process was effected slowly and carefully in order to reduce the risk of trapping air bubbles in the U-tube. The sample cell was always filled past its nodal points and the syringe was left in place at the inlet point during each measurement. The outlet of the cell was sealed with a teflon plug to reduce evaporation. The experimental sample solutions were introduced into the sample cell in exactly the same manner as the distilled water. Period values for air, distilled water, pure solvents and mixture samples were required for each determination of the excess volume.

With the cell illumination light off, the photoelectric portion of the excitation system was automatically activated. Each measuring cycle was allowed to continue until a constant period value was obtained. sample mixtures were made up in 5 cm^3 flasks with round glass stoppers. Care was taken to first add the least volatile component into the flask, and that the completed mixture left a very small vapour space in the stoppered flask. The mixtures were made up shortly before injection into the densitometer.

3.2.2.5 Theory of Density Measurement

The density determination for liquids is based on the electronic measurement of frequency. The device, into which the sample is placed, is capable of oscillating, and the natural frequency of the device is influenced by the mass (and hence the density) of the sample liquid. The direction of oscillation is perpendicular to a plane through the inlet and outlet opening of the sample tube. Since the natural frequency of the oscillating device is only influenced by that precisely defined volume proportion to the sample that fills the oscillator up to its inlet and outlet points, the relationship between sample mass and natural frequency of the oscillator can be transferred without error to the sample density.

Mechanical oscillating densitometers coupled to a digital readout display are widely used in industry and academia to measure the density of liquids and liquid mixtures. The functioning principle of this type of densitometer is that the resonant frequency of an electronically excited mechanical oscillator is appraised. The effective mass (M) of the oscillator may be defined as the mass of the oscillator (M_o) and the mass of the sample. The mass of the sample may be given as sample density (ρ) multiplied by the occupied volume (V).

Hence,

$$M = M_o - V\rho \qquad (3.17)$$

The vibrational mode of the oscillator is assumed to be approximated[155] by

that of a mass (M) attached to a spring with an elasticity constant (c). If it is assumed that the oscillations are unrestrained then the resultant frequency may be given by:

$$2\pi v = (c/M)^{\frac{1}{2}} = [\frac{c}{(M_o + V\rho)}]^{\frac{1}{2}} \qquad (3.18)$$

hence density

$$\rho = -\frac{M_o}{V + (c/4\pi^2 V)(1/v_2)} = A + B\tau^2 \qquad (3.19)$$

Where period of oscillation = $1/v = \tau$ and A and B are constants of the oscillator. Densities are measured relative to a standard material:

$$\rho_{mix} - \rho_o = B(\tau^2_{mix} - \tau^2_o) \qquad (3.20)$$

where ρ_0 is the density of the reference material, ρ_{mix} is the density of the mixture and τ_0 and τ_{mix} are the corresponding periods of oscillation. The instrument constants are usually determined at the beginning of an experimental run.

The excess molar volume at a composition x_i are given by the relation:

$$V_m^E=[(x_A m_A+x_B m_B)/\rho_{mix}]-[(x_A m_A/\rho_A]-[(x_B m_B)/\rho_B] \qquad (3.21)$$

where m_A and m_B are the molar masses of components A and B of the mixture. A computer program using the above equations was used to determine the excess volume quantities. Details of the program are given in Appendix A.

Appendix B gives a detailed error analysis for the V_m^E data obtained from density values used in this work. To obtain a maximum error of 0.002 cm^3 mol^{-1} in V_m^E, the masses must be known to a precision of 0.1 mg, and the τ values to 2 x 10^{-6} Hz^{-1} and the densities to 1 x 10^{-5} g cm^{-3}.The temperature was controlled to within 0.001 K in this work.

3.2.3 Excess Molar Enthalpies of Mixing

Chemical reactions have a nett heat evolution which gives basic information on the mechanism and extent of reactions, a process which often only calorimeters can measure. Direct measurements of heats of mixing involve an apparatus whose basic design consists of a cell in which the two liquids are initially separated. All that is required is an apparatus in which known quantities of two liquids can be brought to a constant temperature, a thermometer to measure the temperature change when the two liquids are mixed and an electric heater in which measured amounts of energy can be dissipated in order to calibrate the apparatus. Many types of calorimeters have been described,[168-170] the most common of which involve adiabatic

and isothermal methods.

When a mixture is formed in calorimeters with vapour spaces, important consideration should be given to the change in the composition of the vapour phase. For example, when the heat of mixing is small, evaporation or condensation of as little as 10^{-3} mole of liquid can produce a heat effect that is larger than the heat of mixing itself.[168] McGlashan has reported an error in H_m^E of up to 100 J mol^{-1} for calorimeters with vapour spaces of 0.25 cm^3. Much effort, therefore, has gone into designing calorimeters in which vapour spaces are eliminated completely. Modified designs appeared which attempted to reduce the effects of vapour spaces.[171,172] The mixing vessel of McGlashan and Larkin,[173] shown in Fig. 3.6, was one of the first calorimeters to eradicate the errors due to the presence of vapour space. The vessel consists of two compartments, A and B, in its upper half, and a capillary C with bulb D which can be attached to the vessel through the ground glass joint E and F. A heating element, H, and four thermistors (T_1 - T_4) distributed over the surface of the mixing vessel forms part of the Wheatstone bridge assembly. The vessel is filled with, and immersed in a bowl of mercury. The mercury is displaced from the upper compartments by introducing weighed quantities of the mixture through the opening on A by means of a hypodermic syringe.

The loaded vessel with the capillary tube, C, half filled with mercury and attached at the ground joint F, is placed in an evacuated enclosure within a thermostat until temperature equilibration is achieved. Thereafter, the liquids are mixed in the absence of a vapour space by rotation of the apparatus

through 180°. The temperature change on mixing is measured by the four thermistors.[173]

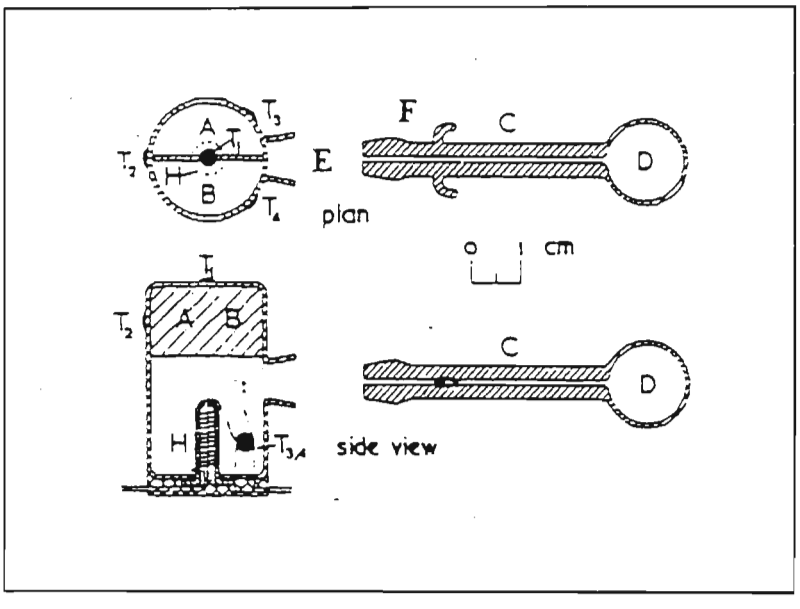

Fig. 3.6 Adiabatic calorimeter of McGlashan and Larkin[173]

The most precise measurements of enthalpies of mixing is achieved through flow microcalorimetry, where two liquids are injected at a known rate into a mixing vessel, where complete mixing is achieved in the absence of vapour space. Advantages of flow microcalorimetry include speed, sensitivity and the determination of both endothermic and exothermic results. One the earlier designs of McGlashan and Stoeckli,[174] although containing design inherent heat leaks, recorded an error in H_m^E of $\pm 1\%$.

A twin conduction calorimeter of Monk and Wadso[175], later commercialised by the LKB company (later taken over by Thermometric), eradicated some of the uncertainties produced by the calorimeter of McGlashan and Stoeckli. Recent designs of flow microcalorimeters include those of Randzio and Tomaszkiewicz,[176] Siddiqi and Lucas[177] and Christensen *et al.*.[178]

Two types of calorimeters were used in this work, the LKB 2107-101 microcalorimeter, and the Thermometric 2277 Thermal Activity flowmix microcalorimeter.

3.2.3.1 The LKB 2107 Microcalorimeter

The isothermal flow mix measuring cylinder for the LKB calorimeter used in this work is shown diagrammatically in Figure 3.7.

The mixing vessel has a separate inlet and comprises a spiral-wound 24 carat gold tube of 1 mm diameter and with a volume of 0.5 cm^3. The design is such that acceptable mixing is achieved with no vapour space. The mixing vessel is in thermal contact with a pair of matched thermocouples in the thermopiles and an aluminium heat-sink assembly, with the heat sink compound covering all the surfaces of these items. An exothermic reaction results in heat flow to the heat sink assembly, while the opposite effect is observed for the endothermic reactions. In each case the resultant temperature difference is detected by the thermopiles positioned between the vessel and the heat sink. The output from the thermopiles is amplified and fed to a digital readout system and a Perkin-Elmer 561 chart recorder. The aluminium block heat sink assembly is contained within an insulated housing. A heater and a temperature sensor are positioned within the heat sink. The entire arrangement is contained within an LKB thermostat which comprises a thermostatically controlled air bath to maintain the temperature required for this investigation. Water cooled to 287 K by a Labcon Thermostat unit is pumped through at a rate of 500 $cm^3.min^{-1}$. The LKB was used in conjunction with a LKB control unit. This

incorporates a power supply capable of providing an adjustable current to the calibration heaters within the insulated mixing vessel assembly, and a facility for heating and monitoring the temperature of the calorimeter heat sink assembly. This heating facility helps to reduce the equilibrium time of the apparatus during "startup" or when raising the operating temperature. It was always switched off when measurements with the instrument were made.

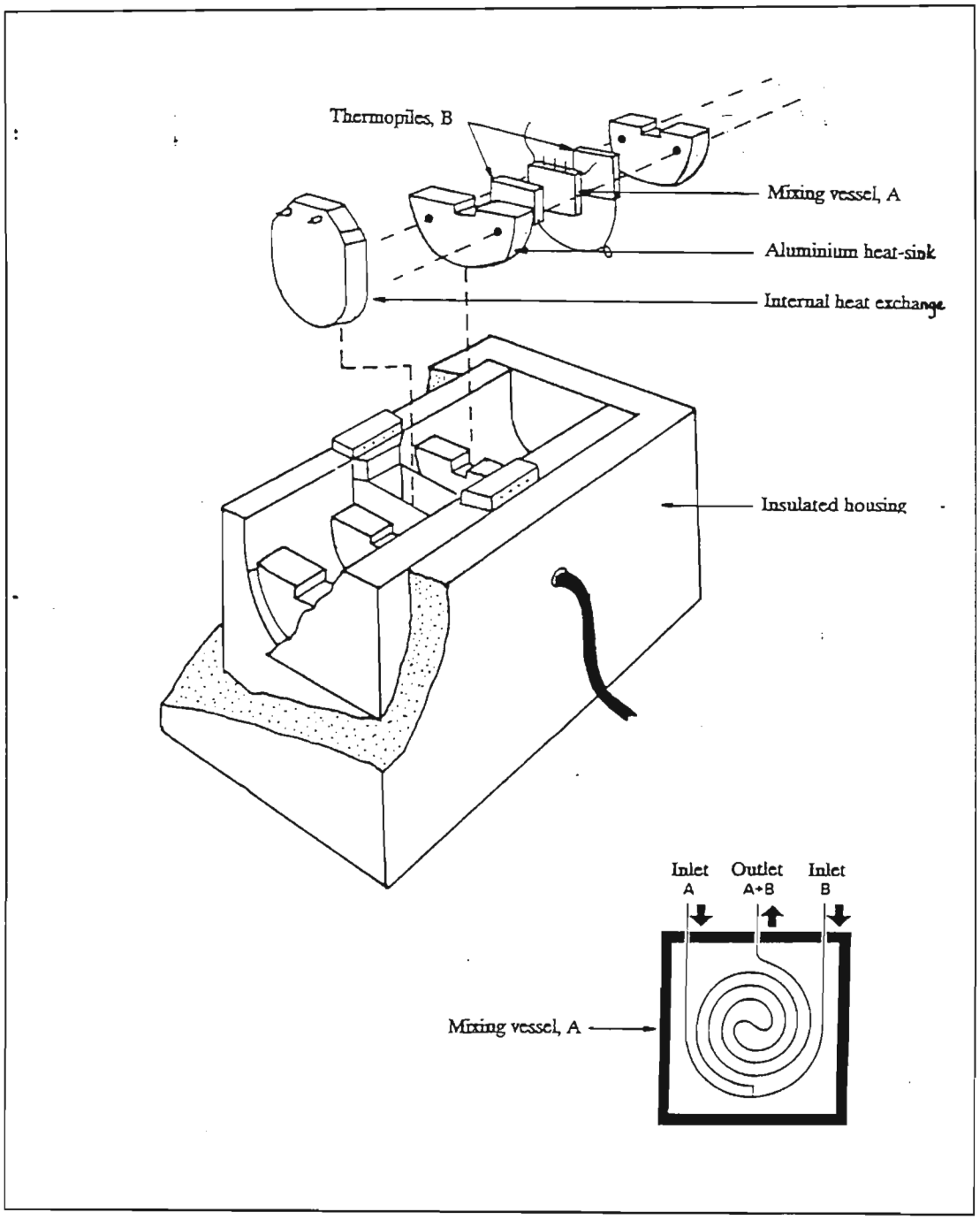

Fig. 3.7 A diagrammatic representation of the LKB flow microcalorimeter mixing cell arrangement.

Since liquids entering the microcalorimeter are required to be with 0.05 K of the experimental temperature, they were first directed through an external heat exchanger fitted into a hollow in the bottom of the air bath of the thermostat unit and then through the internal heat exchangers, situated inside the housing containing the mixing vessel assembly. Samples were introduced using two Jubilee peristaltic pumps, capable of stable flow rates ranging from 0.03 - 0.2 cm^3. min^{-1}. Viton tubing, 1.5 mm in diameter, and teflon tubing, 1.2 mm in diameter were used in the pumps and flows lines respectively.

3.2.3.2 The 2277 Thermal Activity Monitor (TAM)

The 2277 Thermal Activity Monitor is equipped with an external thermostatic water circulator (Thermometric 2219 Multitemp II) and a pair of Eldex variable speed piston pumps capable of stable flow rates from 0.05 to 3 cm^3.min^{-1}. The TAM utilizes the heat flow or heat leakage principle where heat produced in a thermally defined vessel flows away in an effort to establish thermal equilibrium with its surrounding. The calorimetric mixing device used in the TAM has a 24 carat gold flow-mix cell where two different liquids can be mixed. The flow mix cell has a small bore T-piece at the base of the measuring cup where the two incoming flows are mixed. After mixing, the reaction takes place as the mixed flow passes the spiral around the measuring cup. The measuring cup is sandwiched between a pair of Peltier thermopile heat sensors. These sensors are in contact with a heat sink. The system is designed so that the main path for the flow of heat to or from the measuring cup is

through the Peltier elements. The Peltier elements act as thermoelectric generators capable of responding to temperature gradients of less than one millionth of a degree celsius. These highly sensitive detectors convert the heat energy into a voltage signal proportional to the heat flow. Results are presented as a measure of the thermal energy produced by a sample per unit of time. Results are quantified when known power values are passed through "built in" precision resistors. Precision wire wound resistors are located within each measuring cup to represent a reaction during electric calibration. The calibration resistors are integral with the measuring cup so as to be close to the reaction. This ensures that the output from the detector will be, as near as possible, identical to the output when the power is dissipated from the resistor. During the calibration, a known current is passed through the appropriate channel heater resistor, and because the resistor value is known, a specific thermal power gives a calibration level that may then be used to determine experimental results. The entire assembly is located in a stainless steel cylinder. Each cylinder has two measuring cup assemblies just described; the Peltier elements in each measuring cup are connected in series, but in opposition, so that the resultant signal represents the difference in the heat flow from the two measuring cups. This design allows one measurement cup assembly to be used for the sample and the other to be used as the blank. This instrument is suitable for the solvents used in this investigation as outside the calorimeter unit the liquids are in contact with Teflon and glass only. Inside contacts are the gold tube of the heat exchanger and the mixing cell and the teflon tubes. Samples were introduced into the cell using two Eltron piston pumps capable of producing flow rates from 0.5 to 3.0 $cm^3.min^{-1}$.

The sensitivity and high level of precision of the TAM is largely due to the stability of the infinite heat sink which surrounds the measuring cylinders. This heat sink is formed by a closed 25 litre thermostated water bath to $\pm$ 2 x 10^{-4} K within the experimental range. Water is continuously circulated by pumping upwards into a cylindrical stainless steel tank, where it overflows into a similar but larger outer tank. The pump then re-circulates the water from the outer tank back into the inner tank. Several inactive controlling systems work together to maintain the water temperature whose signals are fed to an electronic temperature regulator unit. The 25 litre thermostat is filled with deionised water and a corrosion inhibitor containing sodium nitrate, sodium metasilicate and benzotriazole.

Figure 3.8 shows a representation of the flow principle used in the TAM.

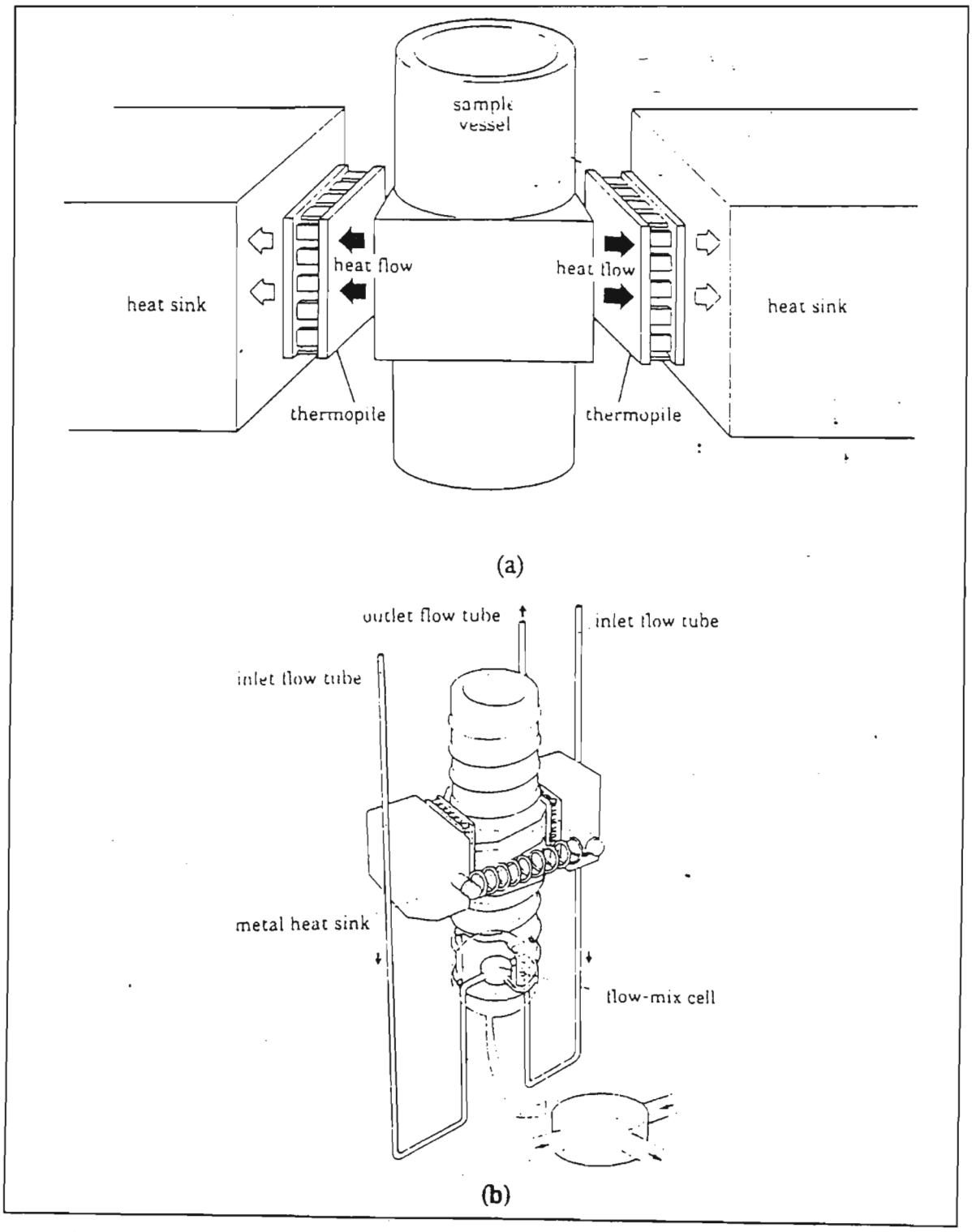

Fig. 3.8 (a) Representation of the heat flow principle used in the TAM and (b) the flow-mix measuring cup in the TAM.

3.2.3.3 Operation Procedure

For both instruments, an initial equilibrium time of at least one day was required. Power to the equipment was left on continuously for the duration of the experimental determination to ensure that thermal equilibrium was maintained in the temperature control units. The flow lines were filled with water overnight. In the morning warm methanol was pumped through each flow line at a rate of 5 $cm^3.min^{-1}$ for 15 minutes before introduction of the component liquids. For the LKB microcalorimeter the two inlets were separately flushed and primed with the two degassed sample components. A typical recorder output as a function of time for a steady state H^E measurement is represented in Figure 3.9.

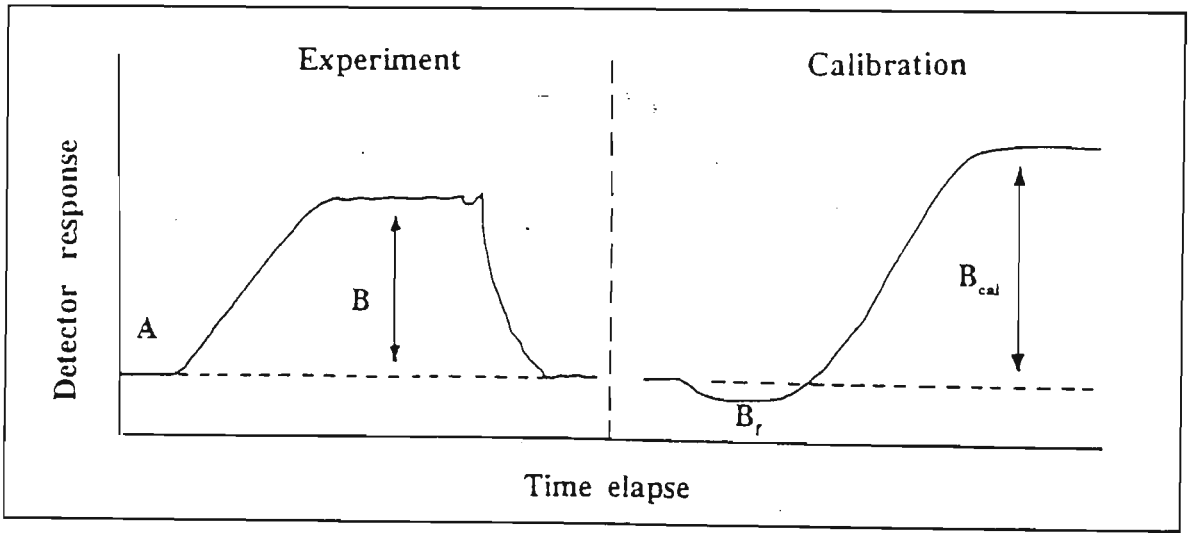

Fig. 3.9 A typical calibration and experimental detector response for the LKB microcalorimeter.

Section A represents the steady state baseline obtained without any fluid flowing through the mixing vessel. This was always recorded before commencing a set of experimental measurements. Since accurate time lapse values were required for the determination of sample flow rates, the pumps and the stopwatch were activated simultaneously. Pumping of the sample was continued until a new steady state was reached, depicted by the baseline deflection, B, in figure 3.9. Thereafter a calibration current to the calibration heater was applied in order to nullify this deflection, in the case of an endothermic reaction restoring the original baseline. In the case of an exothermic reaction, enough current was applied to reproduce this baseline, B. In practice, noise and non-uniform flow rates resulting from the peristaltic pumps operating at low speed produced regular baseline deflections on the recorder. The current was thus always adjusted to a point where the spread about the mean value on the deflected baseline was reproduced about the zero flow-baseline.

Once the regular baseline had been regained, both pumps were switched off. The molar flow rates, fl and f2 were determined by weighing the two component flasks before and after each experimental run. From these masses and the time elapsed for the experiment, the molar flow rates were determined. A Mettler AE240 electronic balance, accurate to 0.0001 mg was used for the mass determinations. For the TAM, due to sensitivity of the instrument and the absence of a control unit containing an inbuilt current supply, calibration at the individual flow rates was necessary. This involves flushing one of the component solvents through both the inlet tubings at a flow rate similar to that for the actual experimental determination. A know current, I, from an external power

source is simultaneously passed through inbuilt resistor and because R for the resistor is known, the expected thermal power, P, can be obtained from the equation

$$P = I^2R \tag{3.22}$$

and the calorimeter power reading is adjusted accordingly. Both the pumps and the external power supply were switched off, the baseline was allowed to return to zero and flow of the second sample component in one of the lines was initiated for sufficient time to coat the tubing. Experiments were carried out according to a method similar to that of the LKB microcalorimeter with the flow rates exactly like those used in the calibration.

3.2.3.4 Preparation of Mixtures and Flow Rate Determinatiom

The samples liquids were prepared in 25 cm^3 Quickfit conical flasks fitted with a modified stopper which had one 1.8 mm in diameter inlet connected by teflon tubing to the pump. This design was effective in reducing evaporation of the component samples hence reducing the problem of co-existing liquid and gaseous phases. The masses of the effluent collected after each run were compared to the amounts of pure components consumed, thus serving as a constant check against leaks in the system. For each run, a new pumping rate was set and the process carried out as described.

The friction effects due to flow of the solvent and the characteristics of the

sample components towards the teflon tubing have to be corrected for in the LKB 2107 microcalorimeter. This correction was not necessary for the TAM as the calibration takes these factors into account. For an experimental run done on the LKB microcalorimeter, the values of the baseline deflections, B, and the corresponding currents, I, required to nullify these deflections were plotted for each system (Figure 3.9). In each case the resulting graph together with the graph for the mixture from each run were employed to adjust the experimental readings for the frictional effects. These calibrations were carried out collectively at the end of a series of experimental runs for a system. Each calibration involved purging the mixing vessel with the effluent from a particular run. With the same pumping parameters as were employed for that particular run, any heating effect due to friction exhibited a deflection, Bf in Figure 3.9. The experimental detector voltage shift was thus corrected to

$$B_0 = B - B_f \tag{3.23}$$

The indicated calibration current, I_{cal}, corresponding to B_0, was then interpolated from the experimentally determined graph and was passed through the calorimeter heater, thereby producing a baseline deflection to B_{cal} in Figure 3.9. The excess molar enthalpy was thus calculated from

$$H_m^E = [\frac{B_0 (I_{cal})^2 R}{B_{cal}}]/(f_1 + f_2) \tag{3.24}$$

where R is the resistance heater. It is,however, observed that $B_0 \approx B_{cal}$

for flow rates less than 0.80 $cm^3\ min^{-1}$. Since the majority of the experimental runs were carried out at a flow rate less than this, H_E was then determined by

$$H_m^E = \frac{I_{cal}^2 R}{(f_1+f_2)} \qquad (3.25)$$

For exothermic reactions, the steady state deflections, B, was noted and a current, I, was applied to double this deflection. Heating due to frictional effects would once again produce a deflection, B_f', and hence equation 3.23 becomes

$$B_0 = B+B_f' \qquad (3.26)$$

The TAM was, however, found to give more precise results for small endothermic and exothermic reactions. In order to check the accuracy and reliability of the calorimeter, the excess enthalpies of (cyclohexane + hexane) were determined prior to the commencement of excess enthalpy determinations in this work. The IUPAC[179] commission on Thermodynamics and Thermochemistry (1970) recommended this step since results for this system obtained in five different laboratories with three different types of isothermal calorimeters shows no systematic discrepancies, and has suggested that excess molar enthalpies should be calculated according to the McGlashan Stoekli equation[174]

$$H_m^E/(Jmol^{-1}) = x_1(1-x_1)[866.1-249.4(1-2x_1)+97.0(1-2x_1)^2-31.8(1-2x_1)^3]$$

(3.27)

where x_1 is the mole fraction of cyclohexane, and for which a standard deviation of 1.1 J mol^{-1} is quoted.

The H_m^E results for the (cyclohexane + n-heptane) system determined in this work, fitted to the Redlich-Kister equation, are:

$$H_m^E/(Jmol^{-1}) = x_1(1-x_1)[878.2-210.5(1-2x_1)+81.0(1-2x_1)^2-103.1(1-2x_1)^3]$$

(3.28)

with a standard deviation of 1.6 $J.mol^{-1}$.

3.3 Experimental Considerations

3.3.1 Materials.

A tabulated synopsis of the materials, suppliers and original purities used throughout this work are given in table 3.1.

Table 3.1. Suppliers and original purities of Liquids used in this study.

Compound	Supplier	Original Purity
Propan-1-ol	Janssen Chimica.	99.1
dipropyl ether	Janssen Chimica.	99.8
dipropylamine	Janssen Chimica	98.9
tripropylamine	Janssen Chimica	99.1
dipropyl sulphide	Janssen Chimica	96.0
heptan-4-one	Janssen Chimica	98.7
propane-1-thiol	Janssen Chimica	98.7

GC-MS analysis of these materials revealed that the purity of the liquids was greater than 98.7 mass percent in all cases except dipropyl sulphide (96 mass %). Where necessary, the materials were further purified prior to use.

Propan-1-ol was dried as described by Furniss *et al.*[180] It involves refluxing the alcohol for more than 30 minutes over iodine and magnesium turnings. The dried alcohol is then recovered by distillation. Both dipropylamine and tripropylamine were distilled and subsequently dried with molecular sieve (type 4A, ±3.2 mm beads from Saarchem). Dipropylether (99.7 mass %), dipropyl sulphide and propane-1-thiol were used without further purification due to the high cost of these liquids.

Dissolved gases in liquids may be displaced upon mixing with other liquids. Spurious enthalpies and volumes of mixing, involving such liquids, may thus result. To prevent this, solvents were degassed prior to actual measurements by placing stoppered flasks containing the liquids in an ultrasonic bath for approximately twenty minutes at ambient temperature.

The hygroscopic nature of some of the solvents necessitated their water content determination. This was achieved using the Karl Fischer technique, using a 701 Karl Fischer Titrino titrometer. The method involves the calibration of an automatic titrator with water and a methanol standard. The injected sample is then compared with the standard and the water contamination recorded. In this work, the mole fraction of water in each of the liquids was determined by Karl Fischer titration to be less than 0.001.

Once the liquids were purified and dried, they were stored in a storage flask, which allowed withdrawal of the liquid by means of a syringe through a rubber septum. Air access, after removal of liquid from the flask, was through a glass

arm packed with calcium chloride and cotton wool. The flask was, in turn, stored in a double access dry glove compartment.

3.3.2 Smoothing equations

In this work, the experimentally obtained data was generally fitted to a smoothing equation. Two prevalent expansions are the Redlich-Kister equation

$$\delta H_m^E = H_m^E - x(1-x)\sum_{r=0}^{n} A_r(1-2x)^r \tag{3.28}$$

and the Padé Approximate

$$H_m^E = X_1X_2\frac{\sum_{i=0}^{n} A_i(X_1-X_2)^i}{1+\sum_{j=0}^{n} B_j(X_1-X_2)^j} \tag{3.29}$$

with the Redlich-Kister method being less intricate than that of the Padé approximate. Gilmore *et al.* [181] note, however, that the Padé approximate may produce far superior results for more complex systems.

Throughout this work, the Redlich-Kister expansion has been the adopted smoothing equation.

3.4 Partial Molar Quantities

3.4.1 Partial Molar Enthalpies

The enthalpy, H, of a solution is a function of the solution's state. Thus[152]

$$H=H(T,P,n_1,.....n_r) \tag{3.30}$$

The total differential of H in the above equation is

$$dH=\left(\frac{\partial H}{\partial T}\right)_{P,n_i} dT+\left(\frac{\partial H}{\partial P}\right)_{T,n_i} dP+\left(\frac{\partial H}{\partial n_1}\right)_{T,P,n_{i\neq j}} dn_1+...+\left(\frac{\partial H}{\partial n_r}\right)_{T,P,ni\neq r} dn_r \tag{3.31}$$

where n_i in the first two partial derivatives indicates that all mole numbers are held constant and $n_{i\neq j}$, that all mole numbers except n_1 are held constant. The **partial molar enthalpy** of substance *i* in the solution is

$$H_i \equiv \left(\frac{\partial H}{\partial n_i}\right)_{T,P,n_{j\neq i}} \tag{3.32}$$

where H is the solution enthalpy and where the partial derivative is taken with T, P and all mole numbers except n_i held constant. Equation (2) becomes

$$dH=\left(\frac{\partial H}{\partial T}\right)_{P,n_i} dT+\left(\frac{\partial H}{\partial P}\right)_{T,n_i} dP+\sum_i H_i dn_i \tag{3.33}$$

where *dH* is the infinitesimal enthalpy change that occurs when the

temperature, pressure and mole numbers of the solution are changed by dT, dP, dn_1, dn_2...

The partial molar enthalpy of substance i is the rate of change of solution enthalpy with respect to n_i at constant T and P.

3.4.2 Partial molar enthalpy at infinite dilution

Determination of the partial molar enthalpy at infinite dilution, $H^E_{i,m}(x_i=0)$, is conveniently achieved by the tangent-intercept method.[182] To eliminate the problems associated with physically drawing a tangent to the curve, an analytical method is used.

The tangent intercept method can be mathematically translated to yield a value for $H^E_{m,i}(x_i=0)$ using the following method. The Redlich-Kister expansion

$$H_m^E = x_A x_B[A+B(1-2x_A)+C(1-2x_A)^2+..] \qquad (3.34)$$

can be fitted to the H^E_m data for a particular mixture. The partial molar enthalpy at infinite dilution is then:

$$H_A^E(x_A=0)=A+B+C \qquad (3.35)$$

The above equation is proved in Appendix C.

A more common mathematical method for determining $H^E_{i,m}(x_i=0)$ is by using the reduced excess enthalpy and extrapolating the individual curves back to infinite dilution ($x_1 \rightarrow 0$)[30]. A polynomial is firstly applied to the reduced excess enthalpy as follows:

$$\frac{H_m^E}{x_1 x_2} = a + bx_1 + cx_1^2 + \ldots \qquad (3.36)$$

Extrapolation of the plot of the reduced excess enthalpy as a function of x_1, back to $x_1=0$, will give the value of $H^E_{i,m}(x_1=0)$. This value is obtained from:

$$\lim_{x_1 \rightarrow 0} \left(\frac{H_m^E}{x_1 x_2}\right) = \lim_{x_1 \rightarrow 0} (a + bx_1 + cx_1^2) = a \qquad (3.37)$$

That H^E_m/x_1x_2 at $x=0$ equals the partial molar enthalpy at infinite dilution, is proved in Appendix D.

Heats of mixing in the high dilution region have been successfully used in the interpretation of thermodynamic properties of solutions.[26-29,183,184] In the case of systems containing only one associated species, it is possible to directly evaluate the energy of bonding between the molecules of the associated component.[30] Molecules of alcohol, for example, in the pure state are bound

together by hydrogen bonds. These are broken when the alcohol is dissolved in an infinite amount of hydrocarbon. Van Ness *et al.* (1967)[28] showed that in alcohol-hydrocarbon systems, the partial molar enthalpies of mixing of alcohols at infinite dilution, $H^{E}_{i,m}(x_i=0)$ is approximately equal to the energies of hydrogen bonds in alcohols. Similarly, Stokes *et al.* (1975)[183] concluded that the limiting enthalpy of dilution of ethanol in alkanes and cycloalkanes represents essentially the enthalpy required to break all the hydrogen bonds present in the pure alcohol. The theory is presented elsewhere.[29] In this work, the above approximations have been extended to describe bond strengths in mixtures containing two associated components, where one of the components shows a relatively weak self association.

3.5 ERAS

Several molecular models are able to predict the experimentally observed behaviour of the excess enthalpy H^E, free energy G^E and heat capacity C_p^E for alcohol/alkane mixtures. Quasichemical methods such as UNIQUAC[185] and UNIFAC[186,187] or other rigid lattice models which take into account consecutive chemical association of proton donor (alcohol) molecules have been developed for predicting G^E and H^E. Even though these models are useful in describing G^E and H^E , they are unable to predict V^E because the restriction to the rigid lattice model does not allow a change of volume upon mixing to be taken into account. The volumetric behaviour at low alcohol concentrations is of special interest since most of the significant effects due to alcohol self-association through hydrogen bonding are manifest in this concentration region.[188] V^E and the apparent molar volumes, ϕ_v, of alcohols are the result of several effects. In addition to changes on the free volume upon mixing and the self-association of the alcohol molecules, there is the additional assumption of a reaction volume for hydrogen bond formation, Δv^*.[189,190] A theoretical approach has been developed in which an associated solution model is combined with a free volume contribution and, in addition, Δv^* has been taken into account. It is called the Extended Real Associated Solution (ERAS) model.

The ERAS model combines the associated solution model [191-194]with a free volume contribution using Flory's equation of state.[195] Flory's equation of state has proved to give good results for excess properties of non-polar chainlike molecules like hydrocarbons.[195-197] Originally developed to describe excess

properties of binary (alkanol + alkane) mixtures,[24] the ERAS model has been extended to describe binary mixtures composed of a strong and a weak associating component, with a relatively strong cross-association.[25]

The ERAS model has previously been applied to (alkanol + alkane) mixtures, [24,188,198] to (alkanol + amine) mixtures[25,146] and to (alkanol + alkene or alkyne) mixtures.[199]

The equations obtained for the thermodynamic excess functions are split into two additive terms which arise from the hydrogen bonding or associational effects (chemical contribution - subscript *c*) and from non-polar van der Waals interactions and from the free volume changes upon mixing between unlike molecules (physical contribution - subscript *ph*):[24,25]

$$H_m^E = H_c^E + H_{ph}^E \tag{3.38}$$

where

$$H_c^E = x_A K_A \Delta h_A^* (\phi_{A1} - \phi_{A1}^0) + x_B K_B \Delta h_B^* (\phi_{B1} - \phi_{B1}^0) + x_A K_{AB} \Delta h_{AB}^* \frac{\phi_{B1}(1 - K_A \phi_{A1})}{(V_B/V_A)(1 - K_B \phi_{B1}) + K_{AB} \phi_{B1}} - \frac{P_M^* V_c^E}{\tilde{v}_M^2} \tag{3.39}$$

and

$$H_{ph}^E = (V_A^* x_A + V_B^* x_B)\left[\frac{\phi_A P_A^*}{\tilde{v}_A} + \frac{\phi_B P_B^*}{\tilde{v}_B} - \frac{P_M^*}{\tilde{v}_M}\right] \tag{3.40}$$

and

$$V_m^E = V_c^E + V_{ph}^E \tag{3.41}$$

where

$$V_c^E = x_A K_A \Delta v_A^* (\phi_{A1} - \phi_{A1}^0) + x_B K_B \Delta v_B^* (\phi_{B1} - \phi_{B1}^0) + x_A K_{AB} \Delta v_{AB}^* \frac{\phi_{B1}(1 - K_A \phi_{A1})}{(V_B/V_A)(1 - K_B \phi_{B1}) + K_{AB} \phi_{B1}} \tag{3.42}$$

and

$$V_{ph}^E = (V_A^* x_A + V_B^* x_B)(\tilde{v}_M - \phi_A \tilde{v}_A - \phi_B \tilde{v}_B) \tag{3.43}$$

where K_A and K_B are the equilibrium constants of chain self-association of components A and of B, and Δh_A^* and Δh_B^* are the corresponding hydrogen bond enthalpies. K_{AB} and Δh_{AB}^* are the association constant and enthalpy for cross association respectively, while ϕ_{A1} and ϕ_{B1} are the hard core volume fractions of components A and of B. v_A,v_B and v_M are the reduced molar volume V_A/V_A^*, V_B/V_B^* and $V_M/(V_A^* x_A + V_B^* x_B)$ of the pure liquids and the mixture respectively. P_A^*, P_B^* and P_M^* are the corresponding reduction parameters for the pressure in the pure liquids and in the mixture respectively. P_M^* is given by[146]

$$P_M^* = \phi_A P_A^* + \phi_B P_B^* - X_{AB}\phi_A \nu_B \tag{3.44}$$

X_{AB} is an interaction parameter characterizing the difference of physical intermolecular energies. ν_B is the surface fraction of component B

$$\nu_A = 1 - \nu_B = \frac{\phi_B S_B / S_A}{\phi_A + \phi_B S_B / S_A} \tag{3.45}$$

S_A and S_B are the surface to volume ratios of the pure liquids. V_A^*, V_B^*, P_A^* and P_B^* are obtained from the thermodynamic properties of the pure substances such as the thermal expansion coefficient, $\alpha = (\partial \ln V/\partial T)_p$, the compressibility, $\kappa = -(\partial \ln V/\partial P)_T$ and the molar volumes.

$$V_i^* = V_{i,mol}\left[\frac{1 + (\alpha_i - \alpha_i^*)T}{1 + 4/3(\alpha_i - \alpha_i^*)T}\right]^3 \tag{3.46}$$

with

$$\alpha_i^* = \Delta v^* \Delta h^* \frac{(4K_i+1)^{1/2} - 2K_i(4K_i+1)^{-1/2} - 1}{2K_i V_i^* R.T^2} \tag{3.47}$$

and

$$P_i^* = (\alpha_i - \alpha_i^*) T.\tilde{V}_i^2 (\kappa_i - \alpha_i^* . T. \frac{\Delta v^*}{\Delta h^*})^{-1} \qquad (3.48)$$

The hard core volume fractions appearing in H_m^E and V_m^E of equations (1-6) have to be calculated numerically from the following coupled equations:

$$\phi_A = \frac{\phi_{A1}}{(1 - K_A \phi_{A1})^2} [1 + \frac{V_A K_{AB} \phi_{B1}}{V_B (1 - K_B \phi_{B1})}] \qquad (3.49)$$

$$\phi_B = \frac{\phi_{B1}}{(1 - K_B \phi_{A1})^2} [1 + \frac{K_{AB} \phi_{A1}}{1 - K_A \phi_{A1}}] \qquad (3.50)$$

Here ϕ_A and ϕ_B are the stoichiometric hard core volumes fractions of the pure liquids. ϕ_A and ϕ_B are defined by:

$$\phi_A = 1 - \phi_B = \frac{V_A^* x_A}{V_A^* x_A + V_B^* x_B} \qquad (3.51)$$

3.5.1 Practical execution of ERAS

The ERAS program was administered with the aid of the mathematical software package MATHCAD. The input file, created on Wordperfect and imported to DOS text, contained H_m^E, V_m^E and G_m^E experimental data over the whole concentration range. The first column of the input file contained enthalpy mole fraction and H_m^E results, followed by those of volume and Gibbs free energy. The Gibbs free energy column in the input file contained only zeros since this property was not determined in this work. The input file was then processed by the ERAS program, which required the listing of the following additional information:

T	the temperature
V_{mol}	molar volume of both component A and component B. This was calculated by dividing the molar mass of each component by its density.
K_A and K_B	self-association constants of components A and B
α_i	thermal expansion coefficient for each component
κ_i	the compressibility coefficient of each component
Δh_A^*	hydrogen bond self-association energy of component A (proton donor)
Δv_A^*	self-association volume of component A
s_i	surface to volume ratio of each component

From these parameters, the program determined both p_i^*, the reduction parameter for pressure, and V_i^*, the molar hard core volume, for each component.

A curve was then fitted to correspond to the experimental data points by simultaneously adjusting four cross term parameters characterizing mixture properties of the hydrogen bonded systems:

Δh_{AB}^*	hydrogen bond cross-association energy of component A with component B
Δv_{AB}^*	cross-association volume of A with B
X_{AB}	van der Waals interaction parameter
K_{AB}	association constant of A with B

3.6 Experimental Results

3.6.1 Experimental Excess Molar enthalpies

The H_m^E results of the determinations are shown in Tables 3.2 - 3.4. To each set of experimental values a polynomial of the type

$$\Delta/(J.mol^{-1}) = H_m^E/(J.mol^{-1}) - x_i(1-x_i)\sum_{r=0}^{n} A_r(1-2x_i)^r \qquad (3.52)$$

was fitted by the method of unweighted least squares. The coefficients A_r are given in Table 3.5 and x_i refers to the proton donor.

The H_m^Es, used in the discussion, for [x{C_3H_7OH[200] or $(C_3H_7)_2O$[196] or $(C_3H_7)_2NH$[201] or $C_3H_7COC_3H_7$[202]} + (1-x)C_7H_{16}]) and for [x$(C_3H_7)_2S$ + (1-x)C_6H_{14}][203] have been reported previously.

Table 3.2. Excess molar enthalpies of H_m^E[x{$CH_3(CH_2)_2OH$ or $(CH_3CH_2CH_2)_2NH$ or $CH_3CH_2CH_2SH$} + (1-x){$(CH_3CH_2CH_2)_2O$ or $(CH_3CH_2CH_2)_3N$ or $(CH_3CH_2CH_2)_2S$} and the deviations Δ calculated from eq. (3.53) and the parameters of Table 3.5.

x	H_m^E / J mol^{-1}	Δ / J mol^{-1}	x	H_m^E / J mol^{-1}	Δ / J mol^{-1}
	x propan-1-ol + (1-x)dipropylether				
0.00411	24.8	-1.2	0.293	768.9	-3.2
0.0153	91.1	-1.4	0.320	781.3	-0.4
0.0217	126.1	-4.0	0.376	789.7	5.1
0.0793	406.9	9.8	0.398	786.1	4.7
0.117	530.5	9.3	0.514	731.5	0.1
0.151	594.2	-11.7	0.549	711.5	-5.2
0.205	697.7	-1.1	0.580	672.1	-7.6
0.247	742.2	-1.4	0.797	378.4	-5.3
0.268	755.0	-4.0	0.856	279.0	-6.1
	x propan-1-ol + (1-x)tripropylamine				
0.0153	12.1	6.0	0.460	-256.2	-0.8
0.0390	24.8	14.5	0.561	-322.1	1.0
0.0981	-3.7	-2.8	0.656	-375.1	2.2
0.165	-42.1	-5.1	0.730	-411.5	-8.2
0.210	-75.0	-6.4	0.800	-397.8	1.6
0.270	-111.1	3.1	0.870	-340.4	5.7
0.331	-156.3	4.9	0.912	-150.2	-3.8

Table 3.2 cont.

x	H_m^E / J mol^{-1}	Δ / J mol^{-1}	x	H_m^E / J mol^{-1}	Δ / J mol^{-1}
x propan-1-ol + (1-x)dipropylsulphide					
0.0904	587.3	15.5	0.603	1077.6	-9.9
0.150	808.1	-6.8	0.759	761.1	-9.2
0.177	890.0	-9.1	0.769	757.5	14.1
0.327	1162.6	-0.4	0.810	628.5	3.3
0.400	1207.5	4.7	0.856	475.8	-4.6
0.457	1209.2	6.0			
x dipropylamine + (1-x)dipropylether					
0.00551	3.1	1.4	0.308	63.1	0.3
0.0182	8.0	2.4	0.350	68.0	0.5
0.0273	10.4	2.2	0.485	79.2	2.3
0.0832	24.2	1.2	0.598	76.2	-0.8
0.0959	26.2	0.1	0.760	60.0	-1.6
0.160	38.1	-1.6	0.870	38.8	-0.4
0.204	47.3	-0.4	0.912	30.3	2.3
0.255	54.1	-1.6			

Table 3.2 cont.

x	H_m^E / J mol^{-1}	Δ / J mol^{-1}	x	H_m^E / J mol^{-1}	Δ / J mol^{-1}
x dipropylamine + (1-x)tripropylamine					
0.0152	19.4	1.1	0.411	302.0	1.3
0.0510	58.4	0.0	0.445	305.4	-0.3
0.163	172.2	0.9	0.524	303.4	-1.8
0.171	179.4	1.2	0.554	301.1	-0.7
0.247	231.6	-3.6	0.623	288.3	0.6
0.274	250.1	-1.3	0.760	234.2	0.2
0.337	280.5	-0.1	0.905	125.1	-0.1
0.357	290.6	3.1			
x dipropylamine + dipropylsulphide					
0.0625	16.5	-4.0	0.451	121.4	-2.0
0.0963	32.2	0.7	0.537	126.8	1.4
0.153	52.2	0.0	0.681	112.0	1.5
0.195	68.6	1.6	0.719	102.7	-0.5
0.283	95.4	1.2	0.786	86.4	-0.5
0.305	102.0	2.1	0.837	73.5	2.0
0.386	112.8	-3.3	0.882	53.1	-2.4

TABLE 3.2 cont.

x	H_m^E / J mol^{-1}	Δ / J mol^{-1}	x	H_m^E / J mol^{-1}	Δ / J mol^{-1}
	x propane-1-thiol + (1-x)dipropylether				
0.0830	34.1	-2.2	0.500	132.5	-5.7
0.137	50.1	-3.0	0.633	132.2	0.2
0.170	60.8	-4.9	0.742	118.1	6.6
0.191	74.3	0.8	0.782	101.3	0.9
0.236	93.6	4.6	0.830	78.9	-5.6
0.323	117.0	3.1			
	x propane-1-thiol + (1-x)tripropylamine				
0.156	176.2	-1.4	0.570	440.2	4.0
0.246	268.9	-1.6	0.687	395.7	-4.5
0.300	326.0	6.8	0.772	340.0	4.4
0.407	388.1	-6.2	0.856	237.0	-2.1
	x propane-1-thiol + (1-x)dipropylsulphide				
0.0941	-8.2	-0.3	0.400	-14.5	-0.2
0.142	-10.3	0.0	0.506	-13.7	-0.3
0.197	-12.1	0.2	0.611	-11.7	0.1
0.243	-13.3	0.0	0.710	-8.7	0.4
0.347	-13.9	0.4	0.876	-3.8	-0.2

Table 3.3. Excess molar enthalpies H_m^E[x{$CH_3CH_2CH_2OH$ or $(CH_3CH_2CH_2)_2NH$ or $(CH_3CH_2CH_2SH$} + (1-x){$(CH_3CH_2CH_2)_2CO$ }] and the deviations Δ calculated from eq. (3.53) and the parameters of Table 3.5.

x	H_m^E / J mol^{-1}	Δ / J mol^{-1}	x	H_m^E / J mol^{-1}	Δ / J mol^{-1}
	x propan-1-ol + (1-x)heptan-4-one				
0.0481	294.3	2.1	0.499	1120.1	-2.3
0.117	608.2	-18.9	0.581	1035.0	-6.7
0.178	860.1	13.0	0.732	815.2	7.8
0.255	1041.4	8.4	0.769	740.2	6.8
0.323	1122.7	-1.2	0.878	451.4	-10.3
0.350	1140.1	-3.5			
	x dipropylamine + (1-x)heptan-4-one				
0.00783	-4.1	-3.7	0.420	124.8	-1.7
0.0484	-5.4	-6.6	0.489	143.4	-0.7
0.0727	4.3	-0.4	0.661	154.5	1.2
0.113	18.0	4.1	0.736	141.4	1.9
0.224	54.3	1.7	0.793	120.5	-0.8
0.320	91.3	0.0	0.830	104.6	-1.4
0.337	97.5	-0.4			
	x propane-1-thiol + (1-x)heptan-4-one				
0.0403	7.5	0.2	0.478	64.0	0.4
0.0862	15.1	0.6	0.613	68.2	0.2
0.177	27.1	-0.4	0.728	59.0	-0.8
0.219	33.0	-0.2	0.848	39.2	0.5
0.426	58.8	-0.1			

Table 3.4. Excess molar enthalpies $H_m^E[x\{(CH_3CH_2CH_2)N$ or $CH_3CH_2CH_2SH\} + (1-x)\{C_7H_{16}\}]$ and the deviations Δ calculated from eq. (3.53) and the parameters of Table 3.5.

x	H_m^E / J mol^{-1}	Δ / J mol^{-1}	x	H_m^E / J mol^{-1}	Δ / J mol^{-1}
		x tripropylamine + (1-x)heptane			
0.0465	5.5	-0.2	0.242	19.0	0.2
0.0586	6.0	-0.4	0.355	21.4	-0.3
0.0854	9.1	0.0	0.449	21.2	-0.1
0.132	12.7	0.2	0.555	18.6	0.0
0.166	14.9	-0.1	0.675	15.1	0.2
0.198	17.2	0.2	0.742	11.9	0.1
0.223	17.7	0.0	0.821	7.7	-0.2
		x propane-1-thiol + heptane			
0.0900	217.2	7.7	0.580	724.1	5.1
0.160	326.1	-7.6	0.601	719.3	4.0
0.191	377.0	-5.0	0.644	696.4	-0.4
0.236	444.3	-2.5	0.670	680.2	1.8
0.320	570.1	16.5	0.838	417.8	-2.0
0.491	683.8	-17.1	0.869	348.1	0.1

TABLE 3.5. Parameters A_r and standard deviations σ for representation of molar excess enthalpies at 298.15 K by eq. (3.53).

	A_0	A_1	A_2	A_3	σ/J mol^{-1}
xC_3H_7OH					
+ $(1-x)(C_3H_7)_2O$	2960	1206	1066	1187	5
+ $(1-x)(C_3H_7)_3N$	-1131	1355	-855	1127	6
+ $(1-x)(C_3H_7)_2S$	4746	1104	836	1347	10
+ $(1-x)(C_3H_7)_2CO$	4486	1491	1212	-600	10
$x(C_3H_7)_2NH$					
+ $(1-x)(C_3H_7)_2O$	309	-52	23	35	2
+ $(1-x)(C_3H_7)_3N$	1226	67	176	-315	2
+ $(1-x)(C_3H_7)_2S$	502	-31	-80	-120	2
+ $(1-x)(C_3H_7)_2CO$	585	-373	-220	-56	3
xC_3H_7SH					
+ $(1-x)(C_3H_7)_2O$	553	-64	-48	-82	4
+ $(1-x)(C_3H_7)_3N$	1721	-440	-167	29	5
+ $(1-x)(C_3H_7)_2S$	-54	-24	-11	-22	0.2
+ $(1-x)(C_3H_7)_2CO$	260	-128	-35	97	1
$x(C_3H_7)_3N$					
+ $(1-x)C_7H_{16}$	81	40	-2	2	0.3
xC_3H_7SH					
+ $(1-x)C_7H_{16}$	2820	-856	-73	885	9

3.6.2 Experimental Excess Molar Volumes

The V_m^E results are given in Table 3.6 together with the deviations Δ, calculated from the smoothing Redlich-Kister equation:

$$\Delta/(J.mol^{-1}) = V_m^E/(J.mol^{-1}) - x(1-x)\sum_{r=0}^{n} A_r(1-2x)^r \qquad (3.53)$$

The coefficients A_r, determined by the method of least squares, are given in Table 3.7.

Table 3.6. Excess molar volumes $V_m^E[x\{C_3H_7OH$ or $(C_3H_7)_2NH$ or $C_3H_7SH\}$ + $(1-x)\{(C_3H_7)_2O$ or $(C_3H_7)_3N$ or $(C_3H_7)_2S$ or $(C_3H_7)_2CO\}]$ and the deviations Δ calculated from equation (3.52) and the parameters of Table 3.7.

x	V_m^E / $cm^3\ mol^{-1}$	$\Delta.10^3$ / $cm^3\ mol^{-1}$	x	V_m^E / $cm^3\ mol^{-1}$	$\Delta.10^3$ / $cm^3\ mol^{-1}$
$xCH_3CH_2CH_2OH + (1-x)(CH_3CH_2CH_2)_2O$					
0.0894	-0.1505	7.2	0.656	-0.3519	0.2
0.120	-0.2080	-9.1	0.692	-0.3311	4.0
0.240	-0.3014	-9.2	0.711	-0.3214	3.1
0.290	-0.3485	8.7	0.770	-0.2883	-3.4
0.337	-0.3581	1.7	0.806	-0.2600	4.7
0.413	-0.3792	0.3	0.836	-0.2333	-2.3
0.452	-0.3869	-2.5	0.900	-0.1368	0.3
0.492	-0.3846	1.1	0.925	-0.1197	3.2
0.556	-0.3764	3.8	0.957	-0.0751	4.1
0.578	-0.3798	-3.5	0.979	-0.0361	2.4
$xCH_3CH_2CH_2OH + (1-x)(CH_3CH_2CH_2)_3N$					
0.103	-0.3806	-5.9	0.652	-0.8275	-2.1
0.222	-0.6249	10.9	0.707	-0.7407	2.0
0.307	-0.7604	14.8	0.788	-0.6393	11.1
0.398	-0.8044	9.9	0.822	-0.5767	7.7
0.471	-0.8308	10.6	0.912	-0.3747	-2.6
0.521	-0.8459	1.0	0.939	-0.2461	7.6
0.574	-0.8568	16.2			

Table 3.6 cont.

x	V_m^E / $cm^3\ mol^{-1}$	$\Delta.10^3$ / $cm^3\ mol^{-1}$	x	V_m^E / $cm^3\ mol^{-1}$	$\Delta.10^3$ / $cm^3\ mol^{-1}$
	$xCH_3CH_2CH_2OH + (1\text{-}x)(CH_3CH_2CH_2)_2S$				
0.111	0.0772	-0.8	0.601	0.0936	1.1
0.215	0.1098	0.5	0.652	0.0849	-0.5
0.271	0.1162	0.7	0.667	0.0830	-0.2
0.356	0.1164	0.1	0.813	0.0577	0.7
0.430	0.1119	0.2	0.836	0.0511	-0.7
0.439	0.1090	-1.9	0.902	0.0344	0.0
0.515	0.1036	0.4	0.926	0.0269	-0.1
	$xCH_3CH_2CH_2OH + (1\text{-}x)(CH_3CH_2CH_2)_2CO$				
0.127	0.0124	1.0	0.662	-0.0063	-1.2
0.185	0.0157	-0.1	0.732	-0.0081	-0.4
0.265	0.0176	-1.1	0.887	-0.0047	0.1
0.407	0.0141	-0.7	0.939	-0.0016	0.8
0.510	0.0090	2.4			
	$x(CH_3CH_2CH_2)_2NH + (1\text{-}x)(CH_3CH_2CH_2)_2O$				
0.055	-0.0011	2.6	0.531	0.0198	-0.7
0.155	-0.0023	-2.2	0.624	0.0174	-0.8
0.236	0.0045	-2.4	0.663	0.0168	0.0
0.286	0.0149	3.5	0.718	0.0148	2.5
0.381	0.0187	0.8	0.783	0.0126	9.4
0.394	0.0182	-0.2	0.801	0.0119	9.3
0.465	0.0201	-0.3	0.882	0.0059	-1.4

Table 3.6 cont.

x	V_m^E / $cm^3\ mol^{-1}$	$\Delta.10^3$ / $cm^3\ mol^{-1}$	x	V_m^E / $cm^3\ mol^{-1}$	$\Delta.10^3$ / $cm^3\ mol^{-1}$
	$x(CH_3CH_2CH_2)_2NH + (1-x)(CH_3CH_2CH_2)_3N$				
0.038	0.0191	3.6	0.482	0.1422	1.9
0.075	0.0286	-3.6	0.564	0.1184	-0.9
0.130	0.0602	1.6	0.593	0.1081	0.3
0.187	0.0811	-4.2	0.668	0.0818	8.0
0.237	0.1097	3.3	0.755	0.0290	-2.0
0.301	0.1333	5.4	0.802	0.0002	5.7
0.378	0.1377	-5.2	0.913	-0.0252	3.7
0.426	0.1419	-3.2	0.964	-0.0082	1.8
	$x(CH_3CH_2CH_2)_2NH + (1-x)(CH_3CH_2CH_2)_2S$				
0.069	-0.0056	-1.9	0.454	-0.0626	-2.7
0.085	-0.0057	-1.1	0.522	-0.0683	-2.0
0.118	-0.0070	-0.4	0.610	-0.0609	2.7
0.139	-0.0095	-1.3	0.807	-0.0139	-1.0
0.195	-0.0120	2.2	0.835	0.0030	0.6
0.296	-0.0276	3.3	0.877	0.0067	-0.7
0.349	-0.0374	4.0	0.900	0.0054	-6.3
0.400	-0.0561	-4.8			

Table 3.6 cont.

x	V_m^E / $cm^3\ mol^{-1}$	$\Delta.10^3$ / $cm^3\ mol^{-1}$	x	V_m^E / $cm^3\ mol^{-1}$	$\Delta.10^3$ / $cm^3\ mol^{-1}$
	$x(CH_3CH_2CH_2)_2NH + (1-x)(CH_3CH_2CH_2)_2CO$				
0.038	-0.0234	-5.5	0.379	-0.0235	0.6
0.065	-0.0266	0.0	0.488	-0.0151	0.9
0.106	-0.0332	1.4	0.592	-0.0123	0.7
0.181	-0.0356	2.7	0.794	-0.0097	-0.7
0.291	-0.0321	-1.1	0.928	-0.0023	0.3
0.373	-0.0247	-1.3			
	$xCH_3CH_2CH_2SH + (1-x)(CH_3CH_2CH_2)_2O$				
0.085	-0.0103	2.0	0.559	0.0214	-0.2
0.118	-0.0144	-1.6	0.657	0.0211	1.2
0.171	-0.0119	-1.6	0.723	0.0162	-0.6
0.261	0.0013	2.3	0.839	0.0094	-0.1
0.431	0.0154	-1.2	0.915	0.0048	0.1
	$xCH_3CH_2CH_2SH + (1-x)(CH_3CH_2CH_2)_3N$				
0.127	0.1593	-2.3	0.827	0.2180	-3.0
0.236	0.2908	4.9	0.891	0.1512	3.1
0.368	0.3860	-4.0	0.935	0.0861	-4.2
0.538	0.4210	-7.5	0.949	0.0800	8.7
0.618	0.4060	7.0			

Table 3.6 cont.

x	V_m^E / $cm^3\ mol^{-1}$	$\Delta.10^3$ / $cm^3\ mol^{-1}$	x	V_m^E / $cm^3\ mol^{-1}$	$\Delta.10^3$ / $cm^3\ mol^{-1}$
		$xCH_3CH_2CH_2SH + (1-x)(CH_3CH_2CH_2)_2S$			
0.116	0.0037	-0.1	0.688	0.0153	-0.1
0.385	0.0127	0.5	0.770	0.0141	0.4
0.501	0.0143	-0.5	0.868	0.0099	0.3
0.601	0.0158	0.0	0.933	0.0047	-0.7
		$xCH_3CH_2CH_2SH + (1-x)(CH_3CH_2CH_2)_2CO$			
0.054	0.0204	-0.3	0.587	0.1285	1.8
0.131	0.0477	0.4	0.687	0.1180	-2.0
0.228	0.0760	0.1	0.874	0.0722	2.0
0.343	0.1019	-0.6	0.902	0.0560	-1.5
0.489	0.1230	-0.1			

Table 3.7. Parameters A_r and standard deviations σ for representation of molar excess volumes at 298.15 K by equation (3.53)

	A_0	A_1	A_2	A_3	$\sigma.10^3$ / $cm^3\ mol^{-1}$
xC_3H_7OH					
+ $(1-x)(C_3H_7)_2O$	-1.542	-0.569	-0.413	-0.127	7
+ $(1-x)(C_3H_7)_3N$	-3.384	0.186	-1.246	-0.050	15
+ $(1-x)(C_3H_7)_2S$	0.419	0.219	0.279	0.066	1
+ $(1-x)(C_3H_7)_2CO$	0.030	0.173	-0.007	-0.128	1
$x(C_3H_7)_2NH$					
+ $(1-x)(C_3H_7)_2O$	0.083	0.001	-0.102	-0.107	2
+ $(1-x)(C_3H_7)_3N$	0.549	0.400	-0.676	0.102	5
+ $(1-x)(C_3H_7)_2S$	-0.260	0.157	0.461	-0.431	4
+ $(1-x)(C_3H_7)_2CO$	-0.062	-0.079	-0.232	-0.199	2
xC_3H_7SH					
+ $(1-x)(C_3H_7)_2O$	0.081	-0.071	-0.188	-0.088	2
+ $(1-x)(C_3H_7)_3N$	1.707	-0.011	-0.374	-0.079	6
+ $(1-x)(C_3H_7)_2S$	0.059	-0.034	0.003	0.005	0
+ $(1-x)(C_3H_7)_2S$	0.496	-0.145	0.054	-0.006	1

3.6.3 Partial Molar Enthalpies and Excess Enthalpies at $x = 0.5$

Heats of mixing in the high dilution region have been successfully used in the interpretation of thermodynamic properties of solutions.[26-30,204] The interpretation is simpler than that of concentrated solutions since the molecules of interest are effectively isolated, and therefore exert little influence, on one another. In the case of systems containing only one associated species, it is possible to directly evaluate the energy of bonding between the molecules of the associated component.[30] Molecules of alcohol, for example, in the pure state are bound together by hydrogen bonds. These are broken when the alcohol is dissolved in an infinite amount of hydrocarbon. It has been demonstrated that in alcohol-hydrocarbon systems, assuming that the contributions of non-specific interactions in the examined systems is small, the partial molar enthalpies of mixing of alcohols at infinite dilution, $H^{E}_{i,m}(x_i = 0)$ is approximately equal to the energies of hydrogen bonds in alcohols. In this work, the above approximations have been extended to describe bond strengths in mixtures containing two associated components, where one of the components shows a relatively weak self association.

Table 3.8 presents the partial molar enthalpies at infinite dilution for each liquid and for each mixture used in this study. H_m^E data not recorded in this work for [x{C_3H_7OH[200] or $(C_3H_7)_2O$[196] or $(C_3H_7)_2NH$[201] or $C_3H_7COC_3H_7$[202]} + (1-x)C_7H_{16}] and for [x$(C_3H_7)_2S$ + (1-x)C_6H_{14}][203] have been reported previously.

Table 3.8. Excess partial molar enthalpies at infinite dilution, $H_{i,m}^E(x_i=0)$, evaluated from the coefficient **a** of eq. (3.35) for all mixtures with standard errors in parentheses.

Mixture		$H_{i,m}^E(x_i=0)$ / J mol^{-1}
xC_3H_7OH	+ (1-x)C_7H_{16}	25330 (246)
$x(C_3H_7)_2NH$	+ (1-x)C_7H_{16}	2470 (35)
xC_3H_7SH	+ (1-x)C_7H_{16}	2720 (144)
$x(C_3H_7)_2O$	+ (1-x)C_7H_{16}	845 (2)
$x(C_3H_7)_3N$	+ (1-x)C_7H_{16}	120 (4)
$x(C_3H_7)_2S$	+ (1-x)C_6H_{14}	1890 (96)
$x(C_3H_7)C_2O$	+ (1-x)C_7H_{16}	4780 (19)
xC_3H_7OH	+ (1-x)$(C_3H_7)_2O$	6230 (50)
	+ (1-x)$(C_3H_7)_3N$	810 (116)
	+ (1-x)$(C_3H_7)_2S$	7870 (202)
	+ (1-x)$(C_3H_7)_2CO$	6600 (129)
$x(C_3H_7)_2NH$	+ (1-x)$(C_3H_7)_2O$	470 (32)

Table 3.8

cont.

	+ $(1-x)(C_3H_7)_3N$	1260 (23)
	+ $(1-x)(C_3H_7)_2S$	250 (26)
	+ $(1-x)(C_3H_7)_2CO$	-340 (93)
xC_3H_7SH	+ $(1-x)(C_3H_7)_2O$	360 (53)
	+ $(1-x)(C_3H_7)_3N$	1130 (95)
	+ $(1-x)(C_3H_7)_2S$	-115 (3)
	+ $(1-x)(C_3H_7)_2CO$	200 (3)

Table 3.9. The hydrogen bond interaction energy, $\Delta H_{H\text{-}bond}$, from eq. (3.55), using $H^{E}_{i,m}(x_i = 0)$s.

System	$\Delta H_{H\text{-}bond}$ / kJ mol^{-1}
-OH...N	-24.7 ± 0.3
-OH...O	-20.0 ± 0.3
-OH...S	-19.4 ± 0.3
-OH...O=C	-23.5 ± 0.3
-NH...N	- 1.3 ± 0.1
-NH...O	- 2.8 ± 0.1
-NH...S	- 4.1 ± 0.1
-NH...O=C	- 7.6 ± 0.1
-SH...N	- 1.7 ± 0.1
-SH...O	- 3.2 ± 0.1
-SH...S	- 4.7 ± 0.1
-SH...O=C	- 7.3 ± 0.1

-OH = propan-1-ol N = tripropylamine S = dipropylsulphide
-NH = dipropylamine O = dipropylether
-SH = propane-1-thiol O=C = heptan-4-one

Table 3.10 records H_m^Es at $x = 0.5$ for all the individual liquids and mixtures. All $H_m^E(x = 0.5)$ values for individual liquids were recorded for these liquids mixed together with a polar solvent (hexane or heptane).

Table 3.10. $H_m^E(x=0.5)$ for all systems

Mixture		$H^E(x=0.5)/J\ mol^{-1}$
xC_3H_7OH	+ C7H16	610
$x(C_3H_7)_2NH$	+ C7H16	452
xC_3H_7SH	+ C7H16	680
$(C_3H_7)_2O$	+ C7H16	205
$(C_3H_7)_3N$	+ C7H16	19
$(C_3H_7)_2S$	+ C7H16	389
$(C_3H_7)C_2O$	+ C7H16	812
xC_3H_7OH	+ $(1-x)(C_3H_7)_2O$	750
	+ $(1-x)(C_3H_7)_3N$	-250
	+ $(1-x)(C_3H_7)_2S$	1219
	+ $(1-x)(C_3H_7)_2CO$	1100
$x(C_3H_7)_2NH$	+ $(1-x)(C_3H_7)_2O$	125
	+ $(1-x)(C_3H_7)_3N$	305
	+ $(1-x)(C_3H_7)_2S$	79
	+ $(1-x)(C_3H_7)_2CO$	144
xC_3H_7SH	+ $(1-x)(C_3H_7)_2O$	133
	+ $(1-x)(C_3H_7)_3N$	425
	+ $(1-x)(C_3H_7)_2S$	-14
	+ $(1-x)(C_3H_7)_2CO$	65

Table 3.11. $\Delta h_{H\text{-bond}}$ evaluated using from eq. (3.56) using $H_m^E(x=0.5)$ from Table 3.10.

System	$\Delta h_{H\text{-bond}}$ / J mol^{-1}
-OH...N	-879
-OH...O	- 65
-OH...S	220
-OH...O=C	-322
-NH...N	-166
-NH...O	-532
-NH...S	-762
-NH...O=C	-1120
-SH...N	-274
-SH...O	-752
-SH...S	-1083
-SH...O=C	-1471

-OH = propan-1-ol N = tripropylamine S = dipropylsulphide
-NH = dipropylamine O = dipropylether
-SH = propane-1-thiol O=C = heptan-4-one

3.6.4 ERAS

Table 3. Thermodynamic properties of the pure substances at 298 K.

	K	p^*	V_{mol}	V^*	α	κ	s	Δh^*	Δv^*
		$J.cm^{-3}$	$cm^3.mol^{-1}$	$cm^3.mol^{-1}$	$10^{-4}\ K^{-1}$	$10^4\ MPa^{-1}$	nm^{-1}	$kJ.mol^{-1}$	$cm^3.mol^{-1}$
C_3H_7OH	197	414	75.2	61.1	10.2	10.1	14.9	-25.1	-5.6
$(C_3H_7)_2NH$	0.55	516	138.1	106.5	13.1	12.2	13.9	-7.5	-4.2
xC_3H_7SH	0.60	514	90.6	69.0	14.2	13.5	14.2	-6.8	-3.9
$(C_3H_7)_2O$	0	440	137.7	106.0	12.6	14.4	14.2	0	0
$(C_3H_7)_3N$	0	488	190.3	146.5	12.6	13.0	13.8	0	0
$(C_3H_7)_2S$	0	567	140.7	103.3	16.2	15.8	14.2	0	0
$(C_3H_7)_2CO$	0	491	139.8	112.4	9.8	9.2	14.1	0	0

Table 3.13. ERAS model parameters characterizing mixture properties of some hydrogen bonded systems.

Mixture	X_{AB}[a]	$-\Delta h^*_{AB}$[b]	$-\Delta v^*_{AB}$[c]	K_{AB}
C_3H_7OH				
+ $(C_3H_7)_2O$	6.0	18.6	7.0	60
+ $(C_3H_7)_3N$	15.0	26.6	9.5	140
+ $(C_3H_7)_2S$	6.7	14.8	6.4	45
+ $(C_3H_7)_2CO$	17.0	18.0	6.1	75
$(C_3H_7)_2NH$				
+ $(C_3H_7)_2O$	2.8	6.4	3.9	0.50
+ $(C_3H_7)_3N$	4.7	5.5	4.1	0.52
+ $(C_3H_7)_2S$	5.1	7.0	5.6	0.50
+ $(C_3H_7)_2CO$	6.8	7.6	5.3	0.45
xC_3H_7SH				
+ $(C_3H_7)_2O$	2.4	6.5	5.1	0.55
+ $(C_3H_7)_3N$	5.5	4.5	2.7	0.37
+ $(C_3H_7)_2S$	4.2	8.6	5.0	0.65
+ $(C_3H_7)_2CO$	6.8	8.7	3.6	0.50

[a]Units: $J.cm^{-3}$

[b]Units: $kJ.mol^{-1}$

[c]Units: $cm^3.mol^{-1}$

Captions to the figures:

Fig. 3.10. Excess enthalpy and excess volumes of (propan-1-ol + di-n-propylether) at 298 K.
* experimental data, —— ERAS model, ····· chemical contribution to ERAS, ------ physical contribution to ERAS.

Fig. 3.11. Excess enthalpy and excess volumes of (propan-1-ol + tri-n-propylamine) at 298 K.
* experimental data, —— ERAS model, ····· chemical contribution to ERAS, ------ physical contribution to ERAS.

Fig. 3.12. Excess enthalpy and excess volumes of (propan-1-ol + di-n-propylsulphide) at 298 K.
* experimental data, —— ERAS model, ····· chemical contribution to ERAS, ------ physical contribution to ERAS.

Fig. 3.13. Excess enthalpy and excess volumes of (propan-1-ol + heptan-4-one) at 298 K.
* experimental data, —— ERAS model, ····· chemical contribution to ERAS, ------ physical contribution to ERAS.

Fig. 3.14 Excess enthalpy and excess volumes of (di-n-propylamine + di-n-propylether) at 298 K.
* experimental data, —— ERAS model, ····· chemical contribution to ERAS, ------ physical contribution to ERAS.

Fig. 3.15. Excess enthalpy and excess volumes of (di-n-propylamine + tri-n-propylamine) at 298 K.
* experimental data, —— ERAS model, ····· chemical contribution to ERAS, ------ physical contribution to ERAS.

Fig. 3.16. Excess enthalpy and excess volumes of (di-n-propylamine + di-n-propylsulphide) at 298 K.
* experimental data, —— ERAS model, ····· chemical contribution to ERAS, ------ physical contribution to ERAS.

Fig. 3.17. Excess enthalpy and excess volumes of (di-n-propylamine + heptan-4-one) at 298 K.
* experimental data, —— ERAS model, ····· chemical contribution to ERAS, ------ physical contribution to ERAS.

Fig. 3.18. Excess enthalpy and excess volumes of (propane-1-thiol + di-n-propylether) at 298 K.
* experimental data, —— ERAS model, ····· chemical contribution to ERAS, ------ physical contribution to ERAS.

Fig. 3.19. Excess enthalpy and excess volumes of (propane-1-thiol + tri-n-propylamine) at 298 K.
* experimental data, —— ERAS model, ····· chemical contribution to ERAS, ------ physical contribution to ERAS.

Fig. 3.20. Excess enthalpy and excess volumes of (propane-1-thiol + di-n-propylsulphide) at 298 K.
* experimental data, —— ERAS model, ····· chemical contribution to ERAS, ------ physical contribution to ERAS.

Fig. 3.21. Excess enthalpy and excess volumes of (propane-1-thiol + heptan-4-one) at 298 K.
* experimental data, —— ERAS model, ····· chemical contribution to ERAS, ------ physical contribution to ERAS.

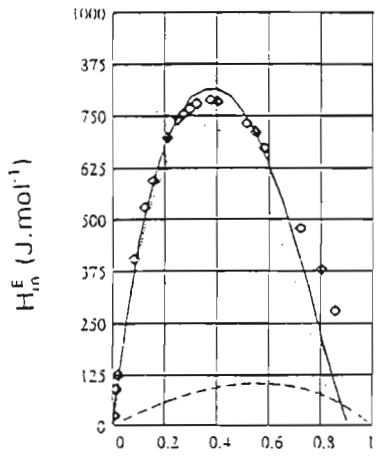

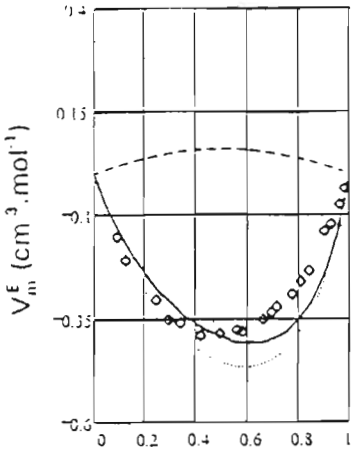

Fig. 3.10 x(propan-1-ol)

x(propan-1-ol)

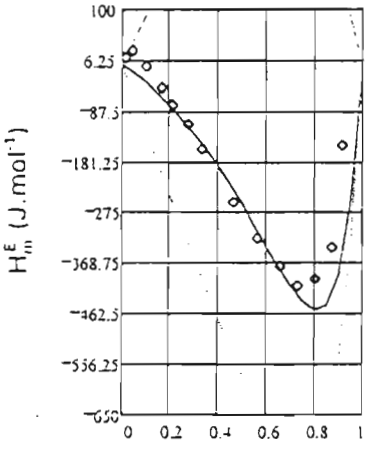

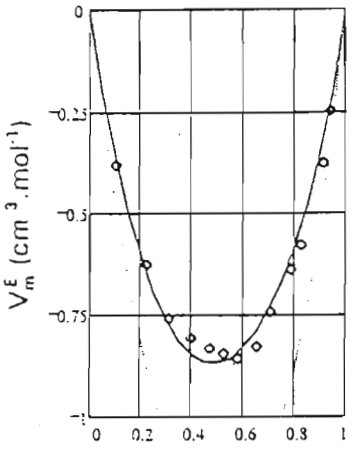

Fig. 3.11 x(propan-1-ol)

x(propan-1-ol)

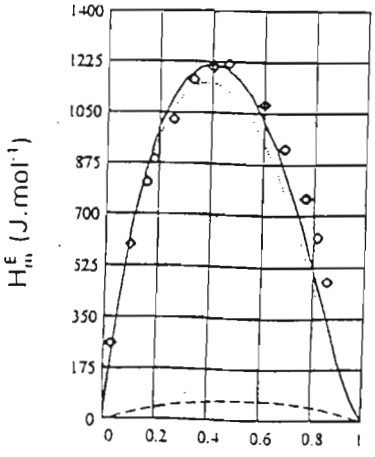

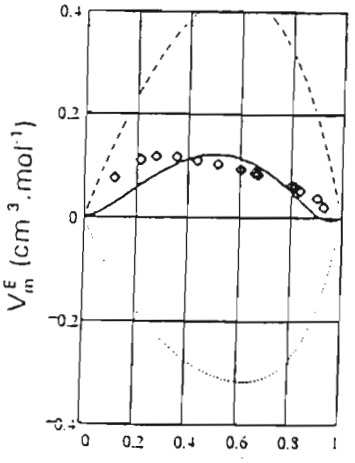

Fig. 3.12 x(propan-1-ol)

x(propan-1-ol)

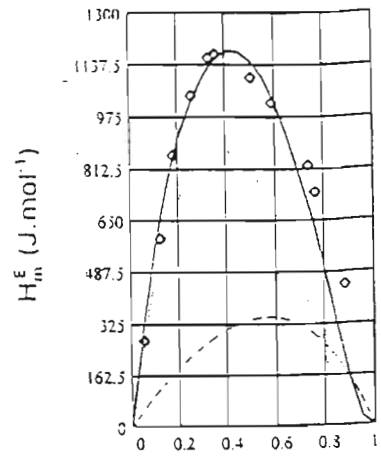

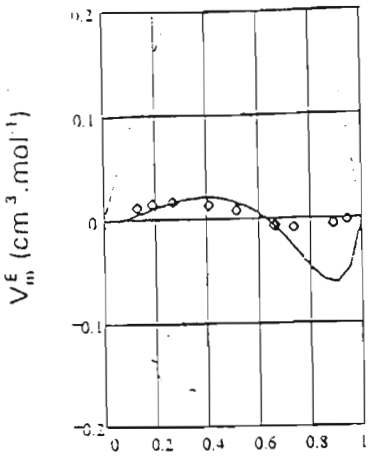

Fig. 3.13 : x(propan-1-ol) x(propan-1-ol)

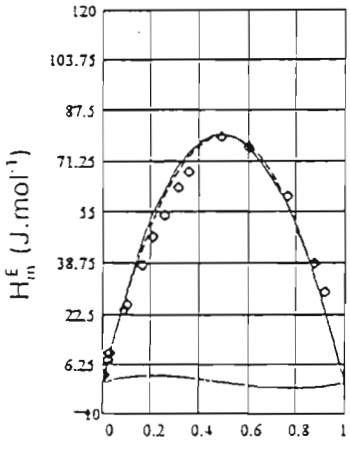

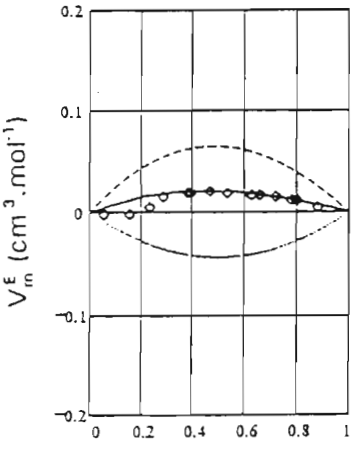

Fig. 3.14 x(dipropylamine) x(dipropylamine)

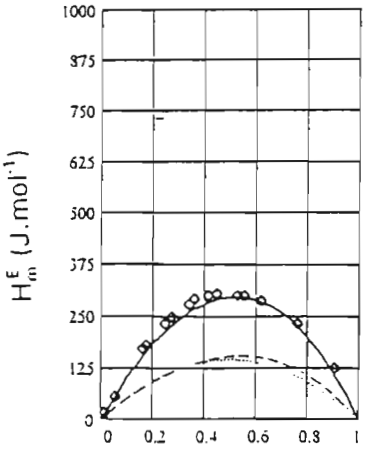

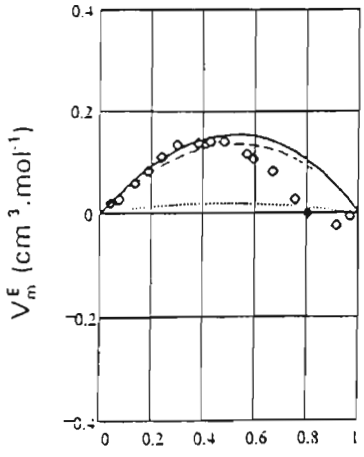

Fig. 3.15 x(dipropylamine) x(dipropylamine)

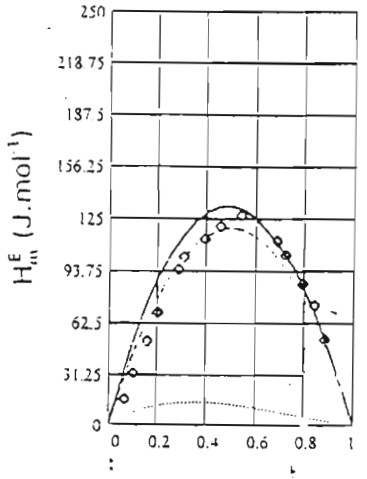

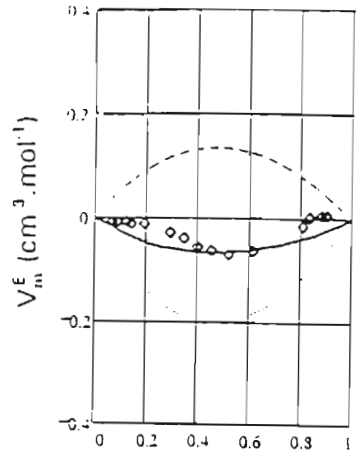

Fig. 3.16

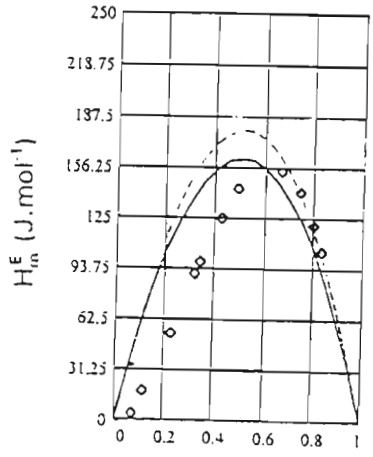

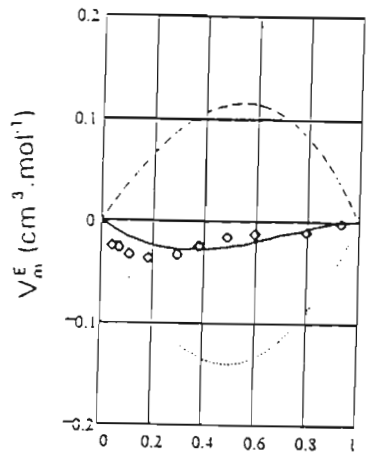

Fig. 3.17

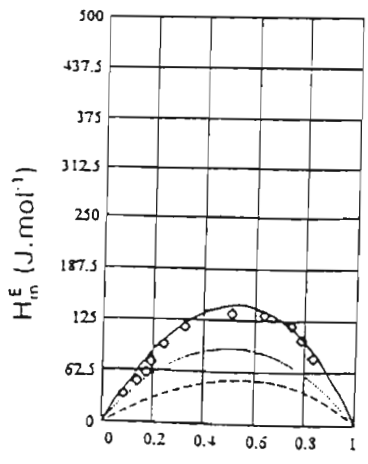

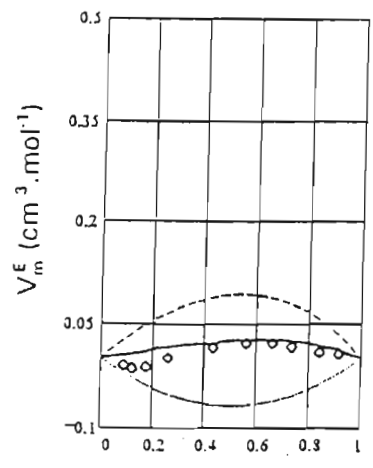

Fig. 3.18

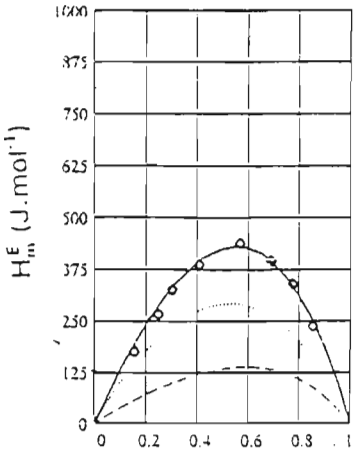

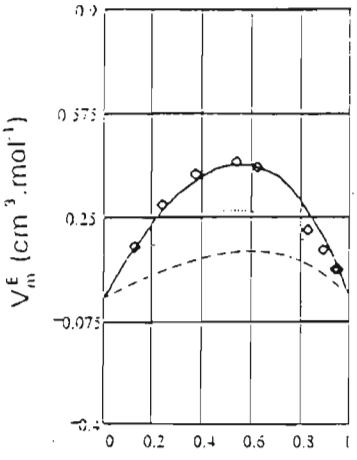

Fig. 3.19 x(propane-1-thiol) : x(propane-1-thiol)

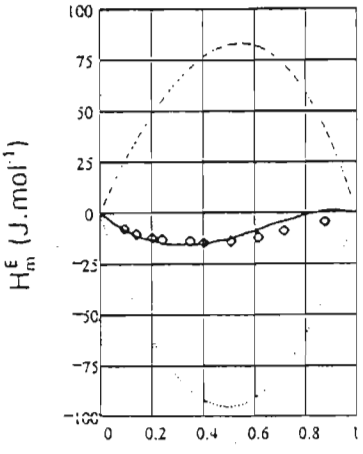

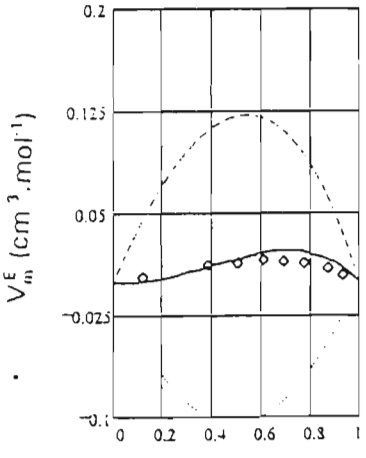

Fig. 3.20 x(propane-1-thiol) x(propane-1-thiol)

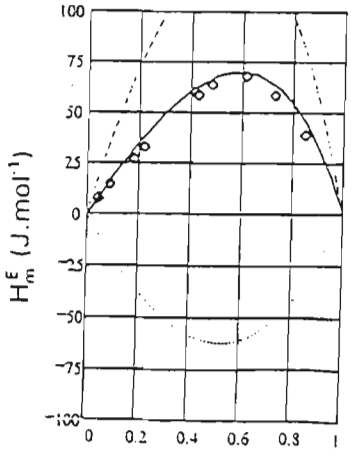

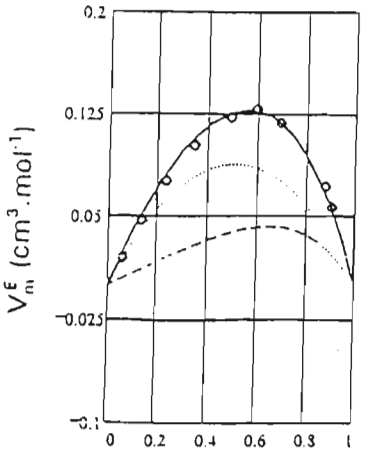

Fig. 3.21 x(propane-1-thiol) x(propane-1-thiol)

3.7 Discussion

3.7.1 H_m^E data

No previous work on the systems considered in this project were found in the literature.

a) Related Systems

A comparison of some related systems revealed the consistency of our data. For example, experimental H_m^E data by Villamanan *et al.*[205] on a binary liquid mixture of propan-1-ol and diethyl ether, exhibited a H_{max}^E value of about 720 J mol^{-1}, at a mole fraction of 0.39 of propanol while that for (propan-1-ol + dibutyl ether) was approximately 870 J mol^{-1} at a mole fraction of 0.38 of propanol. The H_{max}^E for (propan-1-ol + dipropyl ether) determined in this work was found to be 790 J mol^{-1} at a propanol mole fraction of 0.38 (see Table 3.2). In 1926, Hirobe[206] determined the H_{max}^E of the (propan-1-ol + diethyl ether) system to be 732 J mol^{-1} at a mole fraction of 0.42 of propanol.

Funke *et al.*[25] produced experimental H_m^E data on binary liquid mixtures of alcohols and tertiary amines and obtained the following H_{max}^E data:

{x butanol + (1-x)triethylamine}	-1500 J.mol^{-1} at x = 0.65
{x propanol + (1-x)triethylamine}	-1420 J.mol^{-1} at x = 0.65
{x ethanol + (1-x)triethylamine}	-1300 J.mol^{-1} at x = 0.65

The H_{max}^E for the {x(propan-1-ol) + (1-x)tripropylamine} system determined

in this work was found to be -415 J mol^{-1} at a mole fraction of 0.71 of propanol (see Table 3.2). These results illustrate the effect that different alkyl chain lengths have on the enthalpy of mixing results. The results of Funke *et al.* show a more negative H^E_{max} value as the alkyl side chain of the alcohol increases in length, while their results coupled with those in this work show a more negative H^E_{max} value as the alkyl side chain of the tertiary amine (proton acceptor) decreases in length. The latter finding might result from increased steric hinderance as the proton acceptor side chains increase in bulk which contribute to inhibiting the access that a lone pair of electrons of the proton acceptor has to the hydrogen atom of the proton donor.

Work on (propan-1-ol + butan-2-one)[207] displayed a H^E_{max} of about 1310 J mol^{-1} at a mole fraction of 0.5 while the (propan-1-ol + propan-2-one) mixture of Tsimerimg[208] yielded a H^E_{max} of 1383 J mol^{-1} at a propanol mole fraction of 0.49. Earlier work by Paz-Andrade [209] the (propan-1-ol + propan-2-one) system recorded a H^E_{max} of 1251 J mol^{-1} at a propanol mole fraction of 0.41.

The H^E_{max} for the {x(propan-1-ol) + (1-x)heptan-4-one} system determined in this work was found to be 1130 J mol^{-1} at a mole fraction of 0.45 of propanol (see Table 3.3).

Kauer *et al.* [210] did some work, at different temperatures, on the (diethylamine + triethylamine) system. They recorded a H^E_m value, at a mole fraction of 0.5 and a temperature of 298.15 K, of 339 J mol^{-1}. For the same system and at the same temperature, Bittrich *et al.*[211] recorded a H^E_{max} of

360 J mol^{-1} at a mole fraction of 0.5. The H^E_{max} value for the (dipropylamine + tripropylamine) mixture in this work was 306 J mol^{-1} at x = 0.45 of dipropylamine.

No previous excess enthalpy data was available on any systems involving thiols.

b) This Work

The experimental values for H^E_m are positive over the whole concentration range for all mixtures except for $\{xC_3H_7OH + (1-x)(C_3H_7)_3N\}$ and $\{xC_3H_7SH + (1-x)(C_3H_7)_3N\}$ (Table 3.2).

The enthalpy change as a result of hydrogen bonding between dissimilar species is masked in most of these mixtures by positive enthalpic effects resulting from dissociation. An interpretation of all the results presented here is possible if one assumes that the overall H^E_m for these mixtures is due to three separate terms.[184]

$$H_m^E = \Delta H_{AH} + \Delta H_B + \Delta H_{H\text{-}bond} \qquad (3.54)$$

where H^E_m is the heat of mixing for hydrogen donor (AH) with hydrogen acceptor (B), ΔH_{AH} accounts for a positive contribution due to the breakdown of bonds between hydrogen donor molecules; ΔH_B corresponds to a positive contribution due to the breakdown of bonds between hydrogen acceptor molecules and $\Delta H_{H\text{-}bond}$ involves a negative contribution due to the

association of AH and B molecules. The small enthalpic contribution (positive or negative) due to B...B reorganization, caused by the entry of AH, is neglected in this model.

Partial molar enthalpies at infinite dilution, $H^E_{i,m}(x_i=0)$, have previously been employed in the direct evaluation of the energy of hydrogen bonding between self-associated alcohol molecules [26,27,30](see chapter 3.4). Stokes *et al.*[184] later concluded that the limiting enthalpy of dilution of ethanol in alkanes and cycloalkanes represents essentially the enthalpy required to break all the hydrogen bonds present in the pure alkanol. Thus the $H^E_{i,m}(x_i=0)$ of the alcohol in a nonself-associated liquid like an alkane, is approximately equal to the hydrogen bond energy in the alcohol.

In an attempt to quantify the strengths of the hydrogen bond energies of the systems considered in this work, we have extended this relatively simple technique of the use of $H^E_{i,m}(x_i=0)$ to describe hydrogen bond strengths in mixtures containing only one associated component, to describe bond strengths in mixtures containing two associated components, where one of the components shows a relatively weak self-association.

A measure of the self association between molecules of AH and a measure of the self association between molecules of B can be obtained from $H^E_{AH,m}(x_{AH}=0)$[AH + hydrocarbon] and $H^E_{B,m}(x_B=0)$[B + hydrocarbon] respectively. Similarly, a measure of the AH...B interaction is obtained by a comparison of the sum of $H^E_{AH,m}(x_{AH}=0)$[AH + hydrocarbon] and $H^E_{B,m}(x_B=0)$[B + hydrocarbon] with $H^E_{AH,m}(x_{AH}=0)$[AH + B]. Thus, from equation 3.55 the hydrogen bond interaction energy ($\Delta H_{H\text{-bond}}$) can be calculated from

$$\Delta H_{H-bond} = H^{E}_{AH,m}(x_{AH}=0)[AH...B] - H^{E}_{AH,m}(x_{AH}=0)[AH+hydrocarbon] - H^{E}_{B,m}(x_{B}=0)[B+hydrocarbon] \quad (3.55)$$

The results are reported in Table 3.9. The precision of $H^{E}_{i,m}(x_i=0)$ is dependent on the precision of H^{E}_{m} data at high dilutions, and is estimated to be no better than 300 J mol^{-1}.

Table 3.8 shows that the hydrogen bonding enthalpy for propan-1-ol self association, obtained from $H^{E}_{C3H7OH}(x_{C3H7OH}=0)[xC_3H_7OH + (1\text{-}x)C_7H_{16}]$, was calculated to be -25.3 kJ mol^{-1}. This result compares well with the hydrogen bond enthalpies for alcohols obtained by Funke *et al.*[25] using the Extended Real Associated Solution (ERAS) model (-25.1 kJ mol^{-1}). Using partial molar enthalpies at infinite dilution, Van Ness *et al.*[28] and Wóycicka *et al.*[30] estimate the alcohol self association to be -24.2 ± 0.4 kJ mol^{-1} and -23.4 kJ mol^{-1} respectively. The strong alcohol self association is reflected in the H^{E}_{m} curves, which are skewed towards small mole fractions of alcohol. This nonsymmetry with respect to alcohol concentration also suggests that appreciable fractions of the hydrogen bonds are broken only when the alcohol component is dilute. The dipropylamine self association enthalpy was evaluated to be -2.5 kJ mol^{-1}. This was far lower than the diethylamine self association energy estimated by both Funke *et al.*[25] (-8.5 kJ mol^{-1}) using ERAS and Cibulka *et al.*[212](-10.3 kJ mol^{-1}) who based his estimate on regression on vapour pressures and liquid molar volumes. The propane-1-thiol self association enthalpy was calculated at -2.7 kJ mol^{-1}.

If the results of the other workers is correct, the above comparison of the hydrogen bond self-association energy results of the non-alcohol systems with those of other workers seems to indicate that the use of $H^{E}_{i,m}(x_i = 0)$ to quantify hydrogen bond strengths is only truly appropriate in strongly self-associated liquids. Assuming this to be true, we therefore predict that the interaction energies for the self association of the two amines, the ether, the sulphide and the thiol as well as the cross association of the N-H...N, N-H...O, NH...S, SH...N, SH...O and SH...S hydrogen bonded systems will be underestimated. The results will none-the-less still be informative in discussing the *relative* propensities and strengths of the hydrogen bonded interactions we predict might be underestimated.

The hydrogen bond energies for the O-H...N, O-H...O, OH...S hydrogen bonded systems were calculated to be (-24.7 ± 0.3) $kJ.mol^{-1}$, (-20.0 ± 0.3) $kJ.mol^{-1}$ and (-19.4 ± 0.3) $kJ.mol^{-1}$ respectively (see Table 3.9). The cross association energies for the NH...N, NH...O, NH...S, SH...N, SH...O and SH...S systems were found to be (-1.3 ± 0.1), (-2.8 ± 0.1), (-4.1 ± 0.1), (-1.7 ± 0.1), (-3.2 ± 0.1) and (-4.7 ± 0.1) $kJ.mol^{-1}$ respectively. Some interesting trends are immediately observable. The order of thermodynamic hydrogen bond strengths for systems involving OH as the proton donor, as defined in terms of enthalpies of interaction ($\Delta H_{H\text{-}bond}$), is OH..N > OH...O > OH...S. Therefore, when OH is the proton donating moiety, the proton accepting ability of the atoms under consideration is in the order N > O > S. This is the same tendency exhibited by all the methylated hydrogen bonded systems in the *ab initio* molecular orbital study (see chapter 2.5). An examination of the gas phase basicities of dimethyl ether, trimethylamine and dimethyl sulphide as well as dipropyl ether, tripropylamine and dipropyl

sulphide as well as the electronegativities of the proton accepting atoms involved may provide a clue as to the trends established above.

Table 3.14. Gas phase basicities[213] for the molecules studied in this work.

Molecules	Gas Phase Basicity /kJ mol^{-1}
$(CH_3)_3N$	909
$(CH_3)_2O$	771
$(CH_3)_2S$	807
$(C_3H_7)_3N$	946
$(C_3H_7)_2O$	814
$(C_3H_7)_2S$	833

From Table 3.14 it is evident that if the hydrogen bonded interaction were solely a function of gas phase basicities of the proton acceptors, the proton accepting ability would decrease in the order N > S > O. The electronegativities of the relevant proton acceptor atoms decrease in the order O > N > S (3.5, 3.0 and 2.5, respectively). A combination of these two factors, basicity and electronegativity, might acknowledge a proton accepting ability in the order N > O > S, consistent with the experimentally observable trend. It is proposed, in these cases, that the hydrogen bond strength is a function of a combination of the basicities and electronegativities of the proton acceptors. Reimann and Heintz[146] explained

that this could be understood qualitatively by the fact that the free electron pair located at the N atom has a higher polarizability, and therefore acts as a more efficient proton acceptor than either O or S (see chapter 2.5).

However, for the liquid phase systems involving dipropylamine and propane-1-thiol as proton donors, the proton accepting ability of atoms under consideration is in the opposite order i.e. S > O > N. In order to support the validity of this finding and to test that it was not simply due to the limitations of the technique employed, a semi-quantitative evaluation of all the same systems was undertaken. The technique utilizes the excess enthalpy at the mid-point of the curve, $H_m^E(x=0.5)$, and has been used previously in the literature for comparative purposes.[205] Semi-quantitatively the excess enthalpy may be expressed for each mixture by an adaptation of eq. 3.56 thus:

$$\begin{aligned}\Delta h_{H\text{-}bond} = {} & H_m^E(x=0.5)[AH...B] \\ & -H_m^E(x=0.5)[AH+hydrocarbon] \\ & -H_m^E(x=0.5)[B+hydrocarbon]\end{aligned} \qquad (3.56)$$

where $\Delta h_{H\text{-}bond}$ refers to the semi-quantitative interaction energy.

Table 3.10 lists $H_m^E(x=0.5)$ for each monomer and complex, while Table 3.11 records $\Delta h_{H\text{-}bond}$. It confirms that this semi-quantitative technique reveals the same propensities of all the examined groups as does the $H_{i,m}^E(x_i=0)$ technique. The order of the proton accepting ability of the atoms in systems involving OH as the proton donor is N > O > S while that of the atoms in systems involving NH or SH as proton donors is S > O > N. This

result supports that found previously using partial molar enthalpies at infinite dilution and indicates that they are indeed authentic.

The anomaly established in the systems involving NH or SH as proton donors, may be due to the fact that the formation of a hydrogen bond in the liquid phase is "greatly affected by the interference of neighbouring (propyl) groups, which reduce the available surface area that one atom (proton acceptor) is offering to the other (proton donor)".[214] Thus steric hinderance, due to the condensed nature of liquids, may inhibit the access that the hydrogen atom of the proton donor has to a lone pair of electrons of the proton acceptor. This assertion is tested using "recommended" intermolecular van der Waals values assembled by Bondi.[215] We list the relevant data in Table 3.15.

Table 3.15. Functional group contributions to the van der Waals volumes and surface area.

Group	Surface Area	Volume
	$cm^2\ mol^{-1} \times 10^9$	$cm^3\ mol^{-1}$
-O-[a]	0.6	3.7
>N-	0.23	4.33
-S-	-	10.8
>C=O	1.6	11.70

[a] alkyl ethers

Although no surface area data is available for -S-, it is larger than that for -O- and >N- (considering the van der Waals radii of 1.85, 1.4 and 1.5 Å, respectively)[126], and intuitively similar to >C=O (see van der Waals volumes in Table 3.15). The data reveals that the functional group contributions to the van der Waals surface area for compounds such as used in this work are, in decreasing order : S > O > N. This is identical to the results obtained for the calculation of $\Delta H_{H\text{-}bond}$ and $\Delta h_{H\text{-}bond}$ (see chapter 3.6.3) when -NH or -SH is used as the proton donor, and may be an important factor in explaining the order of the hydrogen bond strengths when a relatively weak hydrogen donor (NH or SH) is involved in hydrogen bonding. In such systems, it seems that the available surface area of the proton acceptor is the dominant factor in determining the relative strengths of hydrogen bonding.

This hypothesis was tested using heptan-4-one as a proton acceptor, for which the oxygen atom is more exposed than in the ether molecule, and where the C=O group has roughly the same van der Waals volume and an assumed similar surface area as does the -S- group.[215] Results using the oxygen in heptan-4-one as the proton acceptor show that the order of bond strength of the interactions are NH...O=C or SH...O=C > NH...S or SH...S (see Table 3.9). This is opposite to the result for hydrogen bonding using the oxygen in dipropyl ether and supports the concept that the available surface area of the proton acceptor plays an important role in determining the relative strengths of hydrogen bonding. This result (that O is a better proton acceptor than S) mirrors the results found using *ab initio* values and also the results obtained for the mixtures when OH was used as the proton donor in the liquid phase (see Table 3.9). Therefore, it appears that in weakly

hydrogen bonded systems where basicity and electronegativity effects seem to be small, available surface area of the proton acceptor becomes the dominant factor, otherwise the converse is true.

It is also possible that the difference in order of bond strength of interactions between hydrogen bonds formed with ketones and ethers as proton acceptors is due to the unlike character of the O atoms. Inarrea *et al.*,[216] however, concluded from their results that the different behaviour of alkanols in each non-alkanol component is mainly due to the dipole-dipole interactions and that the unlike character of the O atoms in ketone and ether seemingly play a less important role.

Thus in systems involving a relatively weak hydrogen donor,ie. a secondary amine and a thiol, the hydrogen bond strength is a function of available surface area of the hydrogen acceptor molecules. The results of Villamanan *et al.*,[205] in an investigation of the interactions between oxygen and hydroxyl groups of (alcohol + ether), support this hypothesis. Their synopsis of their results "indicate that interactions between alcohol and ether which are a consequence of the interactions between the hydroxyl and oxygen groups increase almost linearly with the surface fraction of the oxygen in the ether molecule".

3.7.2 Excess Volumes of Mixing

No literature results were found for the systems studied in this work. V_m^Es of (dipropyl ether + ethanol) and (dipropyl ether + butan-1-ol) have been

measured by Inarrea *et al.*[216] at 298.15 K, where $V^E(x=0.5)$ was found to be -0.29 and -0.51 $cm^3\ mol^{-1}$ respectively. Our $V^E(x=0.5)$ for (dipropylether + propan-1-ol) lies between these two values at -0.38 $cm^3\ mol^{-1}$ (see Table 3.6). $V^E(x=0.5)$ for (diethylamine + triethylamine) was found to be 0.100 $cm^3\ mol^{-1}$ by Letcher and Bayles[217] while the $V^E(x=0.5)$ for (dipropylamine + tripropylamine) in this work was found to be 0.140 $cm^3\ mol^{-1}$. No volumes of mixing data was available for any thiols.

V_m^E values for (propan-1-ol + tripropylamine), (propan-1-ol + dipropyl ether) and (diproylamine + heptan-4-one) are negative over the entire concentration range (see Table 3.6) while those for (propan-1-ol + heptan-4-one), (dipropylamine + dipropyl ether), (dipropylamine + dipropyl sulphide) and (propane thiol + dipropyl ether) are only negative at certain concentration regions. V_m^E data for other (alcohol + amine) mixtures also exhibit strongly negative values.[25]

Volumes of mixing data have limited usage in the interpretation of the strength of an interaction. Besides the strength of the interaction, other factors which have a bearing on the excess volume of mixing include the size and shape of the interacting molecules and their "packing" effects. The more similar their size and shape, the less their volume change on mixing. Hence, dipropyl ether, with only two propyl side chains, should pack better with dipropylamine than the tertiary amine with three propyl side chains. In isolation, the excess volume results are thus of limited value in a comparative analysis of hydrogen bond strengths between proton donors and proton acceptors of varying size and shape. However, taken in tandem with enthalpy changes due to mixing, they are of quantitative value. The

ERAS model is a theoretical approach which uses both excess enthalpy and excess volume data and calculates, amongst other things, the hydrogen bond interaction energy.

3.7.3 ERAS

The results and hypotheses postulated in section 3.7.1, that in systems involving a relatively weak hydrogen donor the hydrogen bond strength is in the order XH...S > XH...O > XH...S (where X = N o r S) and that this strength is a function of available surface area of the hydrogen acceptor atoms, is further tested in a third hydrogen bond strength analysis involving the ERAS model (see section 3.5). The ERAS model is a theoretical approach in which an associated solution model is combined with a free volume contribution and, in addition, the reaction volume, Δv^*, has been taken into account. Originally developed to describe excess properties of binary (alkanol + alkane) mixtures,[24] the ERAS model has been extended to describe binary mixtures composed of a strong and a weak associating component, with a relatively strong cross-association.[25]

The ERAS model is able to give relatively good predictions of V^E throughout the concentration range. The ERAS model parameters used in this work relating to the pure substances are listed in Table 3.12.[24,25,218] The unknown cross term parameters K_{AB}, Δh^*_{AB}, Δv^*_{AB} and X_{AB} have been adjusted simultaneously to the experimental data of H^E_m and V^E_m and are listed in Table 3.13.

In this work, cross complex hydrogen bonding is assumed. In the ERAS

model, Δh^*_{AB} is the hydrogen bonding energy, Δv_{AB} represents the molar volume effect due to hydrogen bond formation and X_{AB} refers to intermolecular interactions characterizing physical van der Waals forces.[198] The strong negative experimentally observed V^E_m values, together with the previously reported negative H^E_m values for the (propan-1-ol + tripropylamine) mixture require values for Δh^*_{AB} and Δv^*_{AB} which are more negative than those obtained for propan-1-ol self-association. These two parameters are assumed to be constants independent of the alcohol molecule considered and their values are -25.1 kJ mol^{-1} and -5.6 cm^3 mol^{-1} respectively).[190,24] A Δh^*_{AB} value of -26.5 kJ mol^{-1} and a Δv^*_{AB} value of -10.2 cm^3 mol^{-1} is obtained from the ERAS model (see Table 3.13).

Δh^*_{AB} is compared in Table 3.16 with hydrogen bond interaction energies reported previously using partial molar enthalpies at infinite dilution.

In this work for hydrogen bonded interactions, the ERAS model generally predicts enthalpies of hydrogen bonding that are higher than that obtained for $\Delta H_{H\text{-bond}}$, which is consistent with the predictions that the non-alcoholic mixtures would deliver hydrogen bond strengths which would be underestimated. The most significant result, though, from the perspective of this investigation is that the order of the hydrogen bond strengths is the same using both techniques (OH...N > O > S, NH or SH...S > O > N). It further cements our assertion that in liquid mixtures where the proton donor shows a relatively weak self-association, the available surface area of the proton acceptor is the dominant factor in determining the relative strengths of hydrogen bonding.

Table 3.16. Δh^*_{AB}, the ERAS evaluated hydrogen bonding energy and the hydrogen bond interaction energy, $\Delta H_{H\text{-}bond}$, calculated from partial molar enthalpies at infinite dilution.

System	$\Delta H_{H\text{-}bond}$	Δh^*_{AB}
	kJ mol^{-1}	kJ mol^{-1}
-OH...N	-24.7	-26.6
-OH...O	-20.0	-18.6
-OH...S	-19.4	-14.8
-OH...O=C	-23.5	-18.0
-NH...N	- 1.3	- 5.5
-NH...O	- 2.8	- 6.4
-NH...S	- 4.1	- 7.0
-NH...O=C	- 7.6	- 7.6
-SH...N	- 1.7	- 4.5
-SH...O	- 3.2	- 6.5
-SH...S	- 4.7	- 8.6
-SH...O=C	- 7.3	- 8.7

-OH = propan-1-ol
-NH = dipropylamine
-SH = propane-1-thiol
N = tripropylamine
O = dipropyl ether
S = dipropyl sulphide
O=C = heptan-4-one

Literature enthalpy changes for related systems compare favourably with those determined in this work. The vapour phase determinations of ΔH^0 for the methanol-diethyl ether and for the methanol-trimethylamine complexes have been determined to be 19.6 ± 2.9 kJ mol^{-1} and 24.6 ± 2.9 kJ mol^{-1} respectively.[219,220]

West *et al.*[221] evaluated the OH...S hydrogen bond involving phenol and n-butyl sulphide in CCl_4 to be 17.5 ± 1.2 kJ mol^{-1} while Mathur *et al.*[222] estimated the SH...N bond involving benzenethiol and pyridine in CCl_4 to be 10.0 kJ mol^{-1}. Vinogradov and Linnell[35] postulated from their results that increasing the electronegativity of the donor atom A in the hydrogen bonded system A-H...B increases the strength of the hydrogen bond. Thus the hydrogen bond strength increase in the order SH < NH < OH. Our results appear to show the following order: SH ≈ NH < OH. They conclude by declaring that many factors, including steric effect, formation of complexes possessing stoichiometries other than 1:1, formation of cyclic structures, etc. also influence the thermodynamic parameters of hydrogen bonding interactions. Hence the imperative necessity for consistency in this comparative analysis of the hydrogen bond strengths of various systems. We have tried to maintain this by ensuring that all liquids have the same side chain component and by looking at results in the infinite dilute proton donor region, which eliminates proton donor self-association, and limits the complexes to 1:1 stoichiometries.

CHAPTER 4

PART C - EXPERIMENTAL INFRARED LIQUID STUDY OF MOLECULAR INTERACTIONS

4.1 Introduction

4.1.1 The Vibrations of Molecules

Chemical bonding between two atoms can be viewed as a balancing of forces. On the one hand there is repulsion between the positively charged nuclei and between the negatively charged electron clouds of both atoms, while on the other there is attraction between the nucleus of one atom and the electrons of the other, and vice versa. The two atoms settle at a mean internuclear distance such that these forces are just balanced and the energy of the whole system is at a minimum. At the minimum the internuclear distance is referred to as the equilibrium distance, r_{eq}, or as the bond length. Compression and extension of the bond in a diatomic molecule is assumed to behave like a spring and obey Hooke's law. Thus[223]

$$f = -k(r - r_{eq}) \qquad (4.1)$$

where f is the restoring force, k the force constant and r the internuclear distance. In this case the energy curve is parabolic and has the form

$$E=\frac{1}{2}k(r-r_{eq})^2 \qquad (4.2)$$

This simple harmonic oscillator model, while only an approximation, forms an excellent basis for the discussion of vibrational spectra.

An elastic bond has a certain frequency dependent upon the reduced mass of the system and the force constant, but independent of the amplitude of displacement. The oscillation frequency is:[56]

$$\omega_{osc}=\frac{1}{2\pi}\sqrt{\frac{k}{\mu}}Hz \qquad (4.3)$$

where μ is the reduced mass of the system. Conversion of this frequency to a wavenumber is achieved by dividing by the speed of light, c :

$$\bar{\omega}=\frac{1}{2\pi c}\sqrt{\frac{k}{\mu}}cm^{-1} \qquad (4.4)$$

The vibrational energies (in joules) for any given system may be calculated from the Schrodinger equation (for the simple harmonic oscillator):

$$E_v=(v+\frac{1}{2})hc\bar{\omega}_{osc} \quad (v=0,1,2,...) \qquad (4.5)$$

where v is called the *vibrational quantum number*. Converting to the spectroscopic units, cm^{-1}, we obtain:

$$\varepsilon_v = \frac{E_v}{hc} = (v + \frac{1}{2})\bar{\omega}_{osc} \qquad (4.6)$$

The lowest vibrational energy, when $v = 0$, is called the zero-point energy. Its value:

$$\varepsilon_0 = \frac{1}{2}\bar{\omega}_{osc} (in\ cm^{-1}) \qquad (4.7)$$

implies that no molecule can ever have zero vibrational energy.

The *selection rule* for the simple harmonic oscillator undergoing vibrational changes is

$$\Delta v = \pm 1 \qquad (4.8)$$

Vibrational energy changes will only give rise to an observable spectrum if the vibration can interact with radiation, i.e. if the vibration involves a change in the dipole moment of the molecule. Applying the simple selection rule we get

$$\begin{aligned} \varepsilon_{v+1 \to v} &= (v + 1 + \frac{1}{2})\bar{\omega}_{osc} - (v + \frac{1}{2})\bar{\omega}_{osc} \\ &= \bar{\omega}_{osc}\ cm^{-1} \end{aligned} \qquad (4.9)$$

for emission and

$$\varepsilon_{v \to v+1} = \bar{\omega}_{osc}\ cm^{-1} \qquad (4.10)$$

for absorption. Since the difference between energy levels expressed in cm^{-1} gives directly the wavenumber of the spectral line absorbed or emitted,

$$\bar{\nu}_{spectosocpic} = \varepsilon = \bar{\omega}_{osc} \ cm^{-1} \tag{4.11}$$

Real bonds, however, do not obey simple harmonic motion. For small compressions and extensions the bond may be considered to be perfectly elastic but for greater amplitudes a more complicated behaviour must be assumed.[223]

A mathematical expression which fits the anharmonic energy curve was derived by P. M. Morse and is called the Morse function.[223] When this function is used in the Schrödinger equation, the pattern of the allowed vibrational energy levels is found to be:

$$\varepsilon_v = (v+\frac{1}{2})\bar{\omega}_e - (v+\frac{1}{2})^2\bar{\omega}_e x_e \ cm^{-1} \tag{4.12}$$

where ϖ_e is the harmonic vibrational wavenumber and x_e is the corresponding anharmonicity constant. The selection rules for the anharmonic oscillator are found to be

$$\Delta v = \pm 1, \pm 2, \pm 3, \ldots \tag{4.13}$$

In a polyatomic molecule containing N atoms, the total number of coordinates is 3N, indicating that the molecule has 3N degrees of freedom, since each coordinate may be specified independently of the others. In general, for a non-linear molecule, the translational and rotational movement account for three degrees of freedom each, leaving the molecule with a total

of 3N-6 vibrational degrees of freedom. If the molecule is linear, there is no rotation about the bond axis; hence only 2 degrees of rotational freedom exist, leaving 3N-5 degrees of vibrational freedom.[223]

4.1.2 The Aim of this Investigation

When hydrogen bonding occurs between a proton donor group A-H and an acceptor group B, and a hydrogen bonded complex is formed, one of the most important vibrational effects observed in the infrared region is the shift of the absorption band due to the A-H stretching vibration to lower frequencies. This is due to the weakening of the force constant for the A-H stretching mode caused by the formation of the hydrogen bond.[3]

The aim of this particular section is specifically to look at the shift in the A-H stretching vibration, as a result of hydrogen bonding, in an attempt to confirm and verify the thermodynamic liquid phase findings in this work. Many efforts have been made to correlate thermodynamic hydrogen bonding parameters with various physico-chemical properties such as infrared frequency shifts.[35] The shift in the A-H stretching frequency has assumed a quantitative importance with respect to the hydrogen bond energy[3] in that it has been used as a comparative measure of the interaction strengths of various hydrogen bonded systems. A direct relationship between the shift in the infrared stretching wavenumber, $\Delta\nu$(AH), caused by hydrogen bonding, and the magnitude of $-\Delta H$, the change in enthalpy, was first suggested by Badger and Bauer in 1937.[130] Some theoretical justification was later given by Purcell and Drago.[224]

In the *ab initio* investigation detailed earlier (see chapter 2), correlations were found to exist between $\Delta\nu$(AH), as a result of hydrogen bonding, and the theoretically determined ΔH of interaction (see section 2.4.5). Since $\Delta\nu$(AH) was found to be a good indicator of the comparative strengths of the various hydrogen bonds determined theoretically, consistency calls for a similar correlation to exist in the experimental liquid phase results.

In Chapter 3, some interesting characteristics of the hydrogen bonded complexes studied thermodynamically were established. The order of hydrogen bond strengths for systems involving OH as the proton donor, as defined in terms of the enthalpies of interaction ($\Delta H_{H\text{-}bond}$), was found to be OH..N > OH...O > OH...S. Therefore, when OH is the proton donor, the proton accepting ability of the atoms under consideration is in the order N > O > S. This is the same tendency exhibited by all the methylated hydrogen bonded systems in the *ab initio* molecular orbital study (see section 2.4). However, for the liquid phase systems involving dipropylamine and propane thiol as proton donors, the proton accepting ability of the atoms under consideration is in the opposite order, i.e. S > O > N.

Verification of these thermodynamic findings is the principal purpose of this liquid phase infrared study. This was achieved by determining the shift in the A-H stretching wavenumber for the liquid mixtures under consideration; the larger the shift, the greater the interaction energy. In an effort to explain this phenomenon, we have postulated that in the liquid phase systems involving a relatively weak hydrogen donor, i.e. a secondary amine or a thiol, the hydrogen bond strength appears to be related to the available surface area of the hydrogen bond acceptor atom. Verification of this hypothesis will also

be sought in this study.

This liquid infrared examination was undertaken with the aid of a Fourier transform spectrometer.

4.1.3 Fourier Transform Infrared Spectroscopy (FTS)

Because conventional sources were weak and detectors insensitive, good signal-to-noise ratios were difficult to obtain in the far infrared region, from about 400 cm^{-1} to about 10 cm^{-1}. FTS was developed to look at this region.[223] FTS, which relies on interferometric measurements, is found to have considerable advantages over conventional dispersive spectroscopy. They include :

i) Speed. Each observation point of the spectrum must be examined for a given time in order to achieve a given resolution. In the conventional method, each point is examined consecutively, whereas in a Fourier transform infrared (FT-IR) instrument, all the points are scanned simultaneously.

ii) In a conventional instrument, the radiation is brought to a focus on a slit. A very fine slit gives good resolving power since only a narrow spread of frequencies falls on the detector at any one moment, but the total amount of energy passing through the instrument is low, necessitating "noisy" amplifiers. In FT-IR parallel beams are used throughout, and there is no need to bring the radiation to a focus except for convenience at the sample and at the detector. All the source energy passes through the instrument and the

resolving power is governed solely by the mirror traverse and computer capacity.

iii) The resolving power of a FT-IR instrument is constant over the entire spectrum while in a prism or grating instrument the resolving power depends on the angle which the monochromator makes with the radiation beam. It therefore varies with frequency and leads to poor results at the ends of the spectrum.

iv) The presence of a computer for FT-IR work means that other tasks like the improvement of the signal-to-noise ratio, removal of solvent peaks, correction of baseline drift, expansion of parts of the spectrum, offsetting window absorption, etc. can be carried out automatically.

The principle of operation involves a parallel beam of radiation, directed from the source to the interferometer, consisting of a beam splitter, B, and two mirrors, M_1 and M_2 (Fig. 4.1).

The beam splitter is a plate of suitably transparent material (e.g. potassium bromide) coated so as to reflect just 50 % of the radiation falling on it. Therefore half the radiation goes to M_1, and half to M_2, and returns from both these mirrors along the same path. It is then recombined to a single beam at the beam splitter. If monochromatic radiation is emitted by the source, the recombined beam leaving B shows constructive or destructive interference, depending on the relative path lengths B to M_1 and B to M_2.

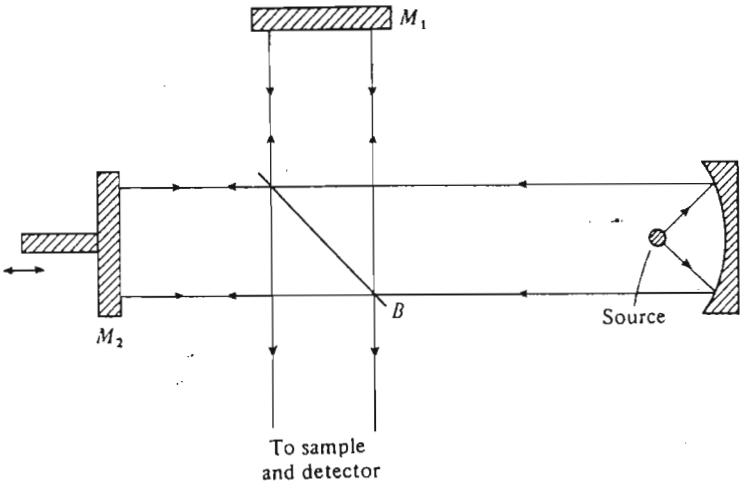

Fig. 4.1. The interferometer unit of a Fourier tranform spectrometer[223].

If the path lengths differ by an integral number of wavelengths, constructive interference gives an intense beam leaving B, whereas if the difference is a half-integral number of wavelengths, the beams cancel at B. Therefore, as the mirror M_2 is moved towards or away from B, the detector sees radiation alternating in intensity. If the source emitted two separate monochromatic frequencies, the interference patterns of the two frequencies would be overlaid, resulting in the detector seeing a more complicated fluctuation as M_2 is moved. However, by a mathematical process known as Fourier transformation, it is possible to calculate the original frequencies and intensities of both components of the source from the observed fluctuations. Therefore, if the recombined beam from such a source is directed through a sample before reaching the detector, sample absorptions will show up as gaps in the frequency distribution, which after transformation, yields a normal absorption spectrum.

4.2 Experimental Section

The infrared spectra were run on a BRUKER IFS 88 Fourier transform spectrometer, which was operated by OPUS:[225] a menu oriented Fourier transform infrared (FT-IR) software package for PC based data systems. OS/2 was the operating system chosen by BRUKER[225] because it offers favourable prerequisites with regard to price and performance. OPUS is controlled by a mouse pointer which facilitates easy, accurate manipulation of both the infrared spectra and the spectrometer.

The computer utilized to take charge of the operation of OPUS contained a 80386-DX processor. The working memory of the PC had a RAM size of 16 MB. The computer was equipped with a standard VGA graphics card for displaying the graphical user interface of the software package. Two serial interfaces (COM1 and COM2) and a parallel interface (LPT1) were provided in addition to an interface card for connecting a bus mouse.

The design of the BRUKER FT-IR spectrometer has an Acquisition Processor inserted between the optics and the data systems. This performs the data collection and Fourier transformation of the data with phase correction before further routing to the computer.

4.2.1 Operation of OPUS

The measurement module of OPUS/IR offers complete control of the FT-IR spectrometer including definition of measured conditions, input of sample specific text, data collection and spectral calculation.

Each measurement method is assigned a special "experiment". This consists of a complete set of measurement parameters which gives the correct combination of source, filter, beamsplitter, measurement channel and detector. The setting up of suitable measurement conditions takes place by selecting one of the pre-defined experiments. The FT- and acquisition parameters had been preset to meaningful values.

Input of text into the "sample name", "sample form" and "operator name" fields were stored with the measured data files. The text appears in the information field of the file status bar when displaying the spectra. Input of the text is optional.

Since elimination of the frequency characteristics of the source and spectrometer from the sample spectrum was desired, a reference or background spectrum (without sample substance) was measured which displays the results of these effects. The elimination was done directly after the sample measurement by division by the background. Sample measurement was then effected with the aid of the "start sample measurement" button. A variety of manipulative options of the resulting spectrum was then available for maximum accuracy including the improvement of the signal-to-noise ratio, correcting baseline drift, expanding

parts of the spectrum, etc.

4.2.2 Materials

Propan-1-ol, dipropyl ether, dipropylamine, dipropyl sulphide, heptan-4-one and propane-1-thiol were of the same purities and received the same treatments as described in the thermodynamic analysis in section 3.3.1. The tertiary amine used in this particular study was tributylamine. It was obtained from BDH , had a purity in excess of 98.6 % and was distilled at a temperature of 207-215 °C.

In the infrared spectrum of the proton donor molecules, propan-1-ol, dipropylamine and propane-1-thiol, considered in this investigation, it was important to isolate and identify the free A-H stretching band, and distinguish it from the bonded A-H stretching peak. In the case of propan-1-ol, it was necessary to determine a concentration, in CCl_4, that would eliminate the strong bonded O-H stretching peak, leaving only the band due to free O-H stretching of the molecule. This dilution process was necessary so as to avoid overlap with the bonded O-H stretching peak which results from hydrogen bonding, when propan-1-ol is mixed with other liquids consisting of hydrogen bond acceptor molecules. The most favourable concentration for this purpose, for the propan-1-ol:CCl_4 mixture, was found to be 0.090 M. Similarly, that for dipropylamine: CCl_4 was determined to be 0.61 M. Since the S-H stretching peak in propane thiol is very weak, the pure liquid was used in the mixtures, although it was necessary to dilute it in CCl_4 to obtain the free S-H stretching peak as a reference for the

calculations of the shifts in this peak as a result of hydrogen bonding. In these cases, the background spectrum of these systems was that of pure of CCl_4.

For the liquid mixtures involving the mixed hydrogen bonded interactions, the concentrations were as follows:

Table 4.1. Concentrations of the hydrogen bonded liquid mixtures, diluted in CCl_4.

Hydrogen Bond	Proton Donor concentration/ mol dm^{-3}	Proton Acceptor concentration/ mol dm^{-3}
$C_3H_7OH.O(C_3H_7)_2$	0.083	0.53
$C_3H_7OH.N(C_4H_9)_3$	0.083	0.39
$C_3H_7OH.S(C_3H_7)_2$	0.083	0.53
$C_3H_7OH.OC(C_3H_7)_2$	0.083	0.52
$(C_3H_7)_2NH.O(C_3H_7)_2$	0.46	1.80
$(C_3H_7)_2NH.N(C_4H_9)_3$	0.46	1.32
$(C_3H_7)_2NH.S(C_3H_7)_2$	0.46	1.78
$(C_3H_7)_2NH.OC(C_3H_7)_2$	0.46	1.75

The following mixtures, propane-1-thiol:dipropyl ether, propane-1-thiol:tributylamine, propane-1-thiol:dipropyl sulphide, and propane-1-thiol:heptan-4-one were not diluted in CCl_4, and were mixed according to a

one-to-one molar relationship.

Higher concentrations of the proton acceptors were used in each mixture, relative to those of the proton donors, to ensure that all available proton donating molecules in the mixture were involved in heteroassociation.

4.3 Results

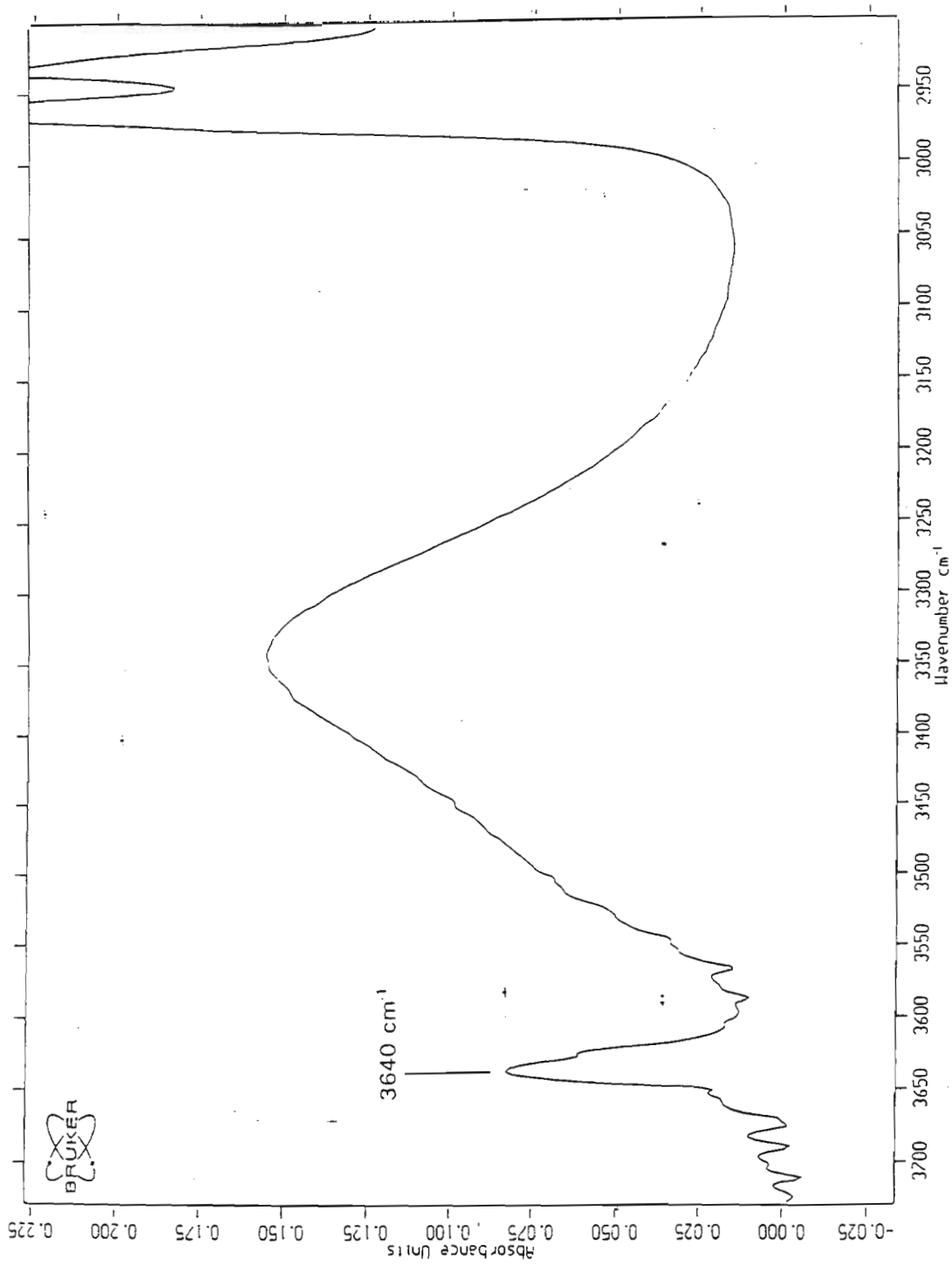

Fig. 4.2. Infrared spectrum of the OH stretching band of propan-1-ol (0.35 M).

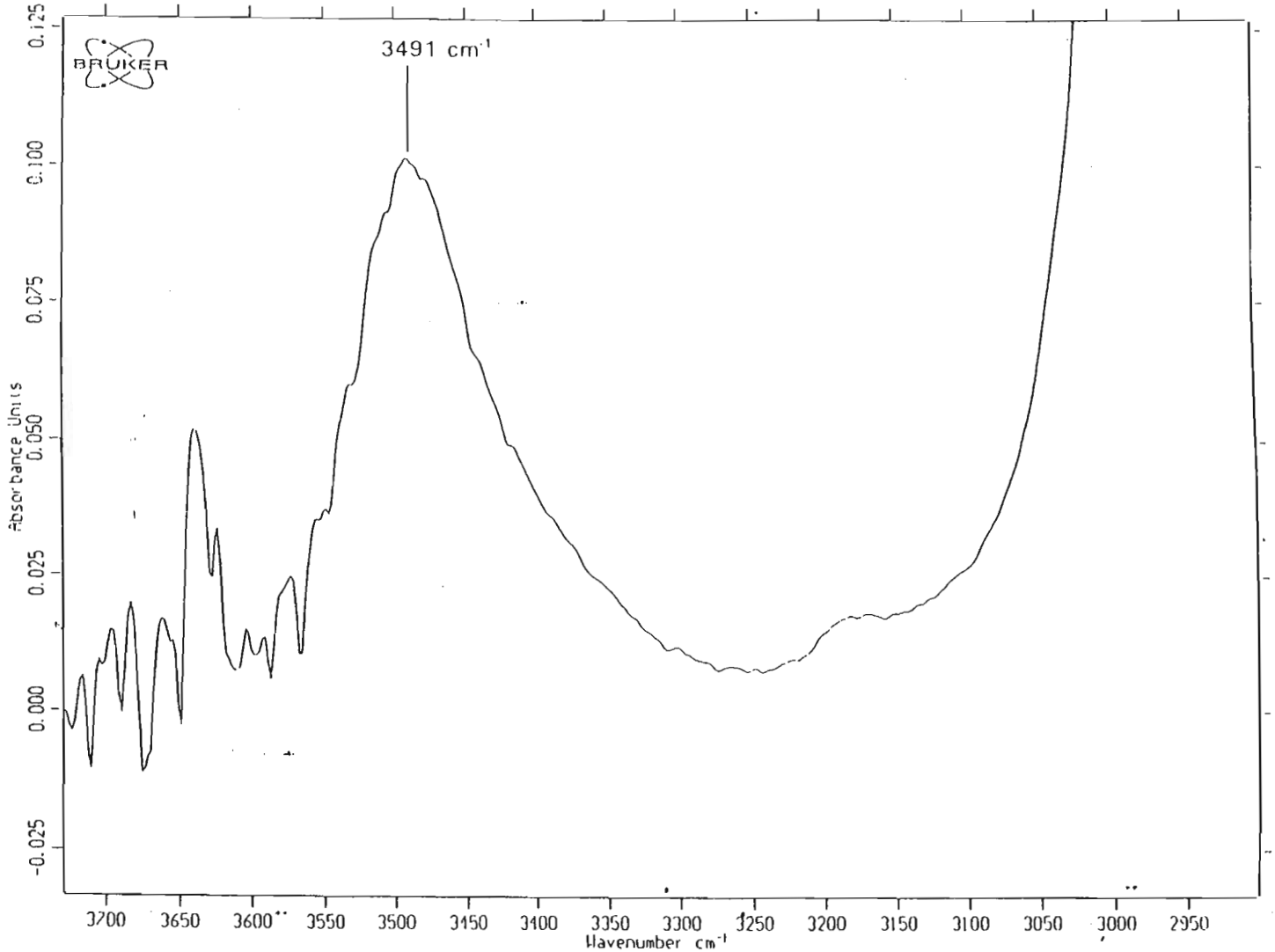

Fig. 4.3. Infrared spectrum of the OH stretching region of a mixture of propan-1-ol (0.083 M) and dipropyl ether (0.53 M).

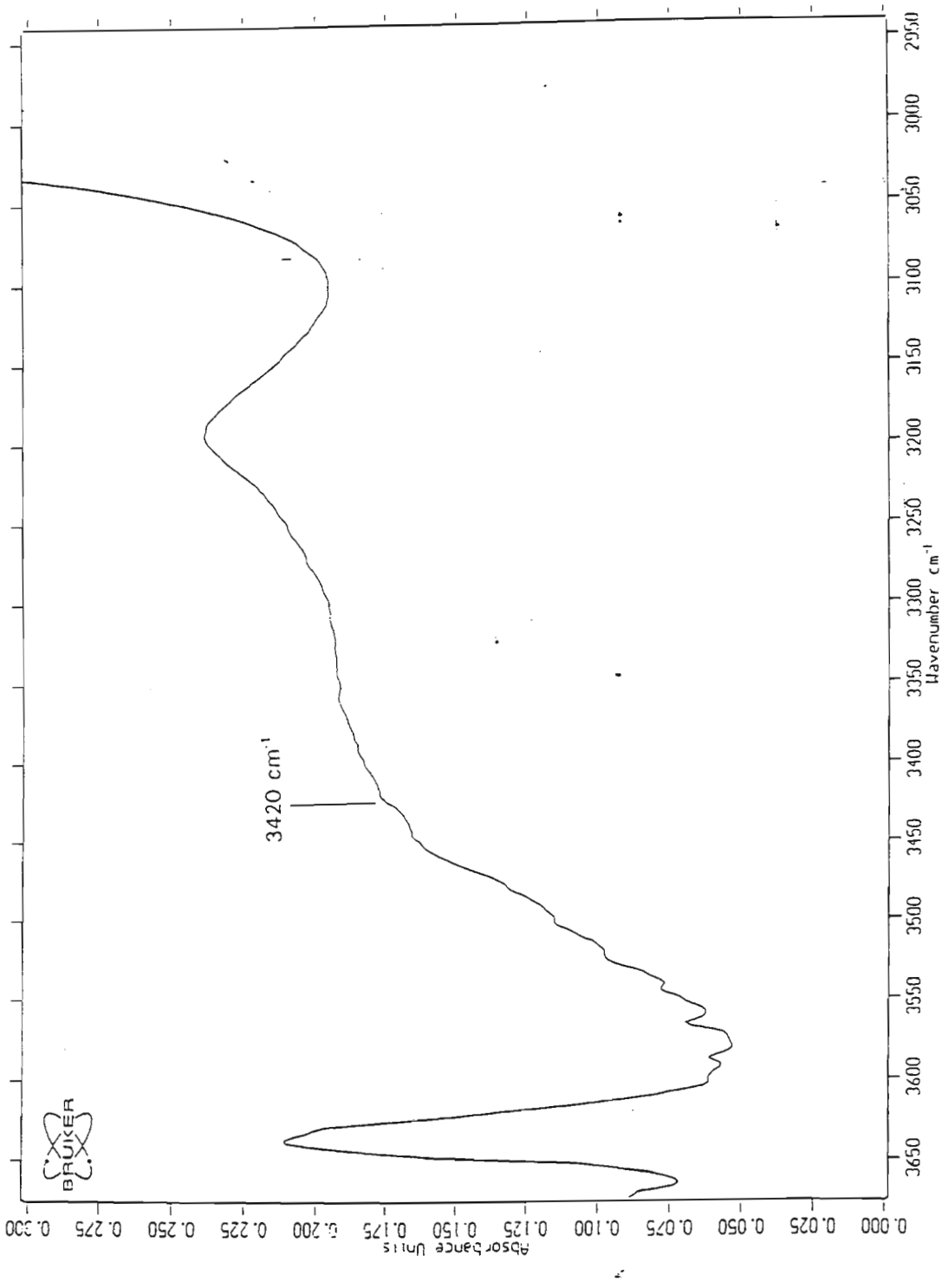

Fig. 4.4. Infrared spectrum of the OH stretching region of a mixture of propan-1-ol (0.083 M) and tributylamine (0.39 M).

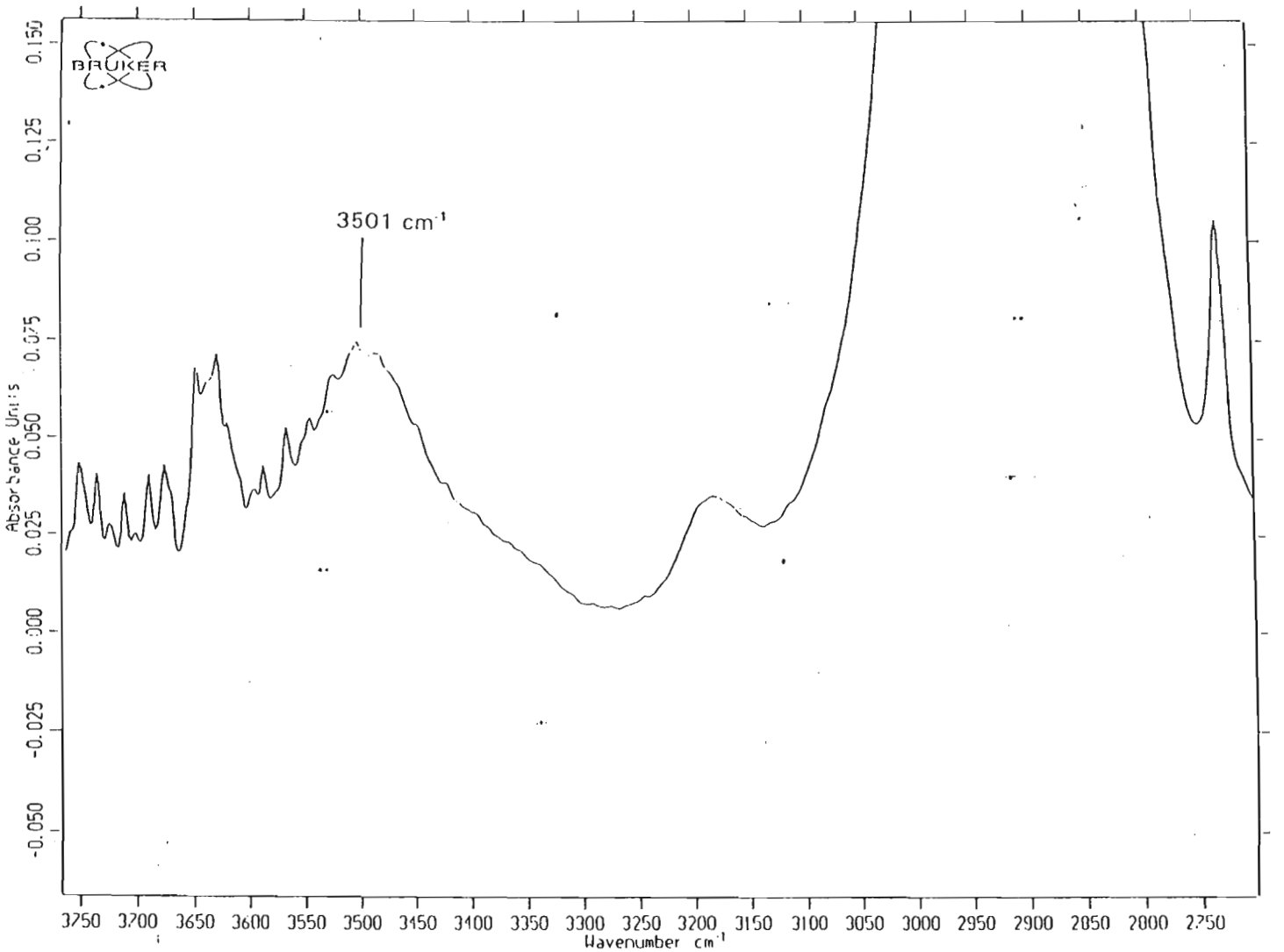

Fig. 4.5. Infrared spectrum of the OH stretching region of a mixture of propan-1-ol (0.083 M) and dipropyl sulphide (0.53 M).

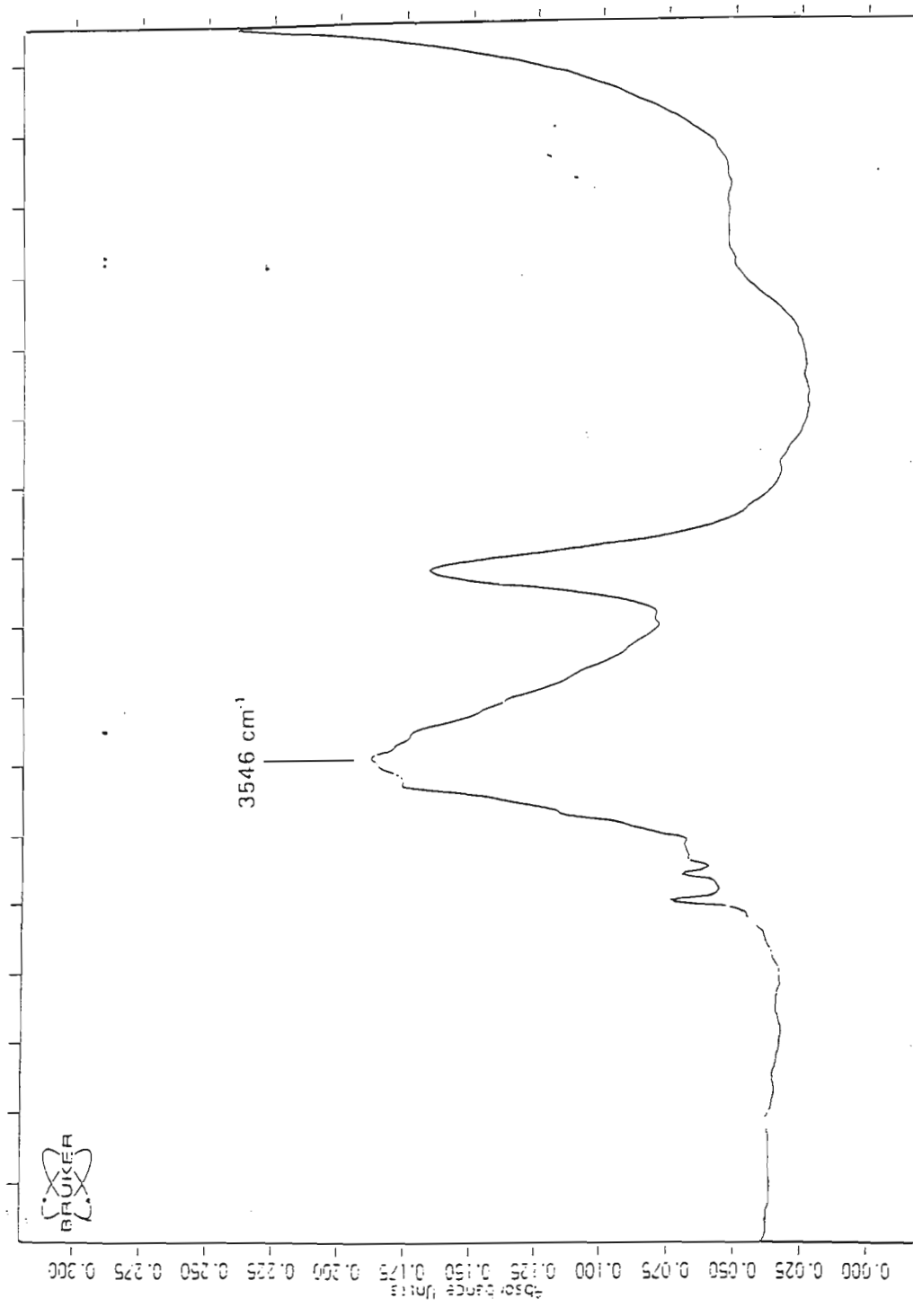

Fig. 4.6. Infrared spectrum of the OH stretching region of a mixture of propan-1-ol (0.083 M) and heptan-4-one (0.52 M).

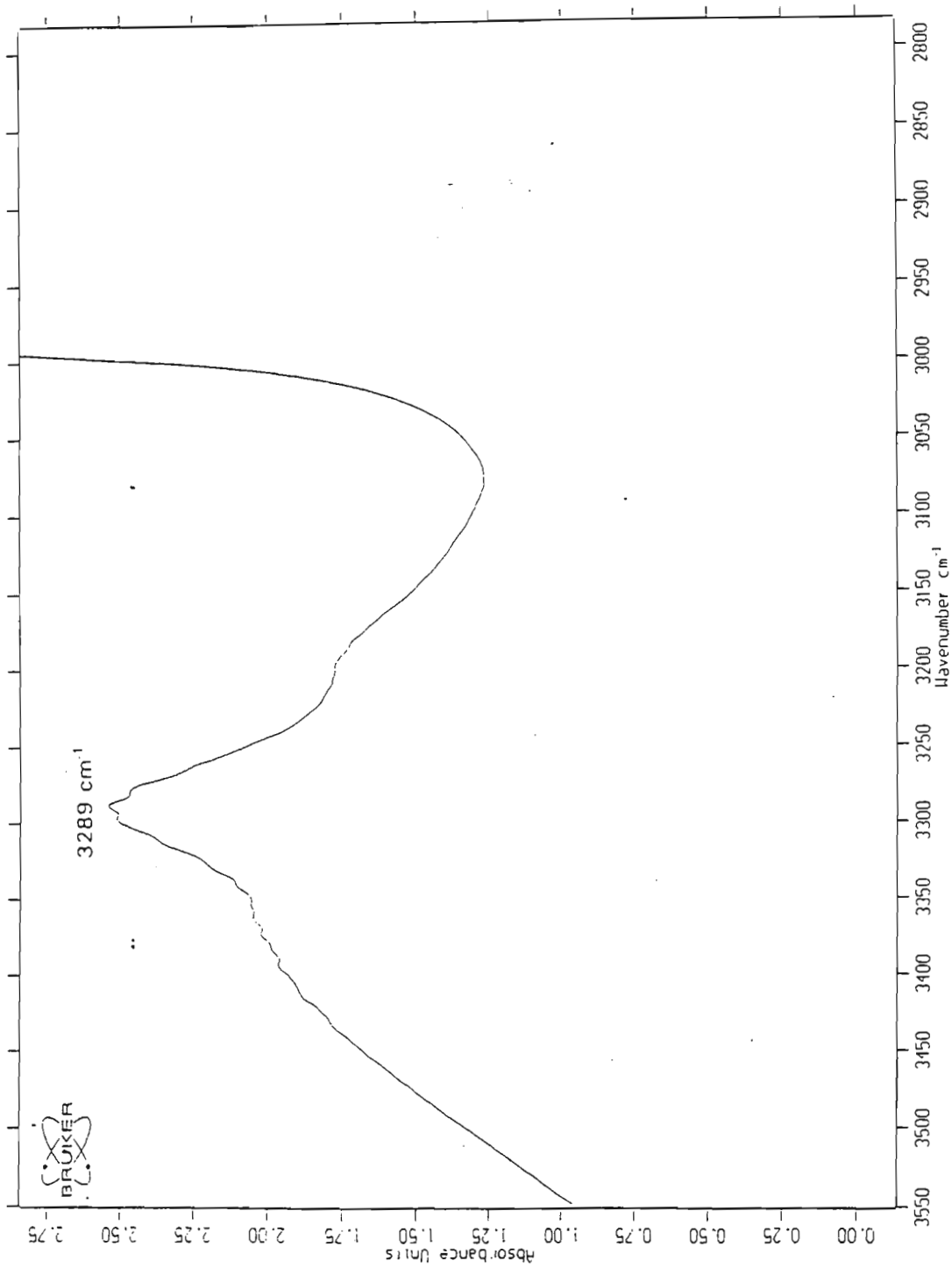

Fig. 4.7. Infrared spectrum of the NH stretching region of undiluted dipropylamine.

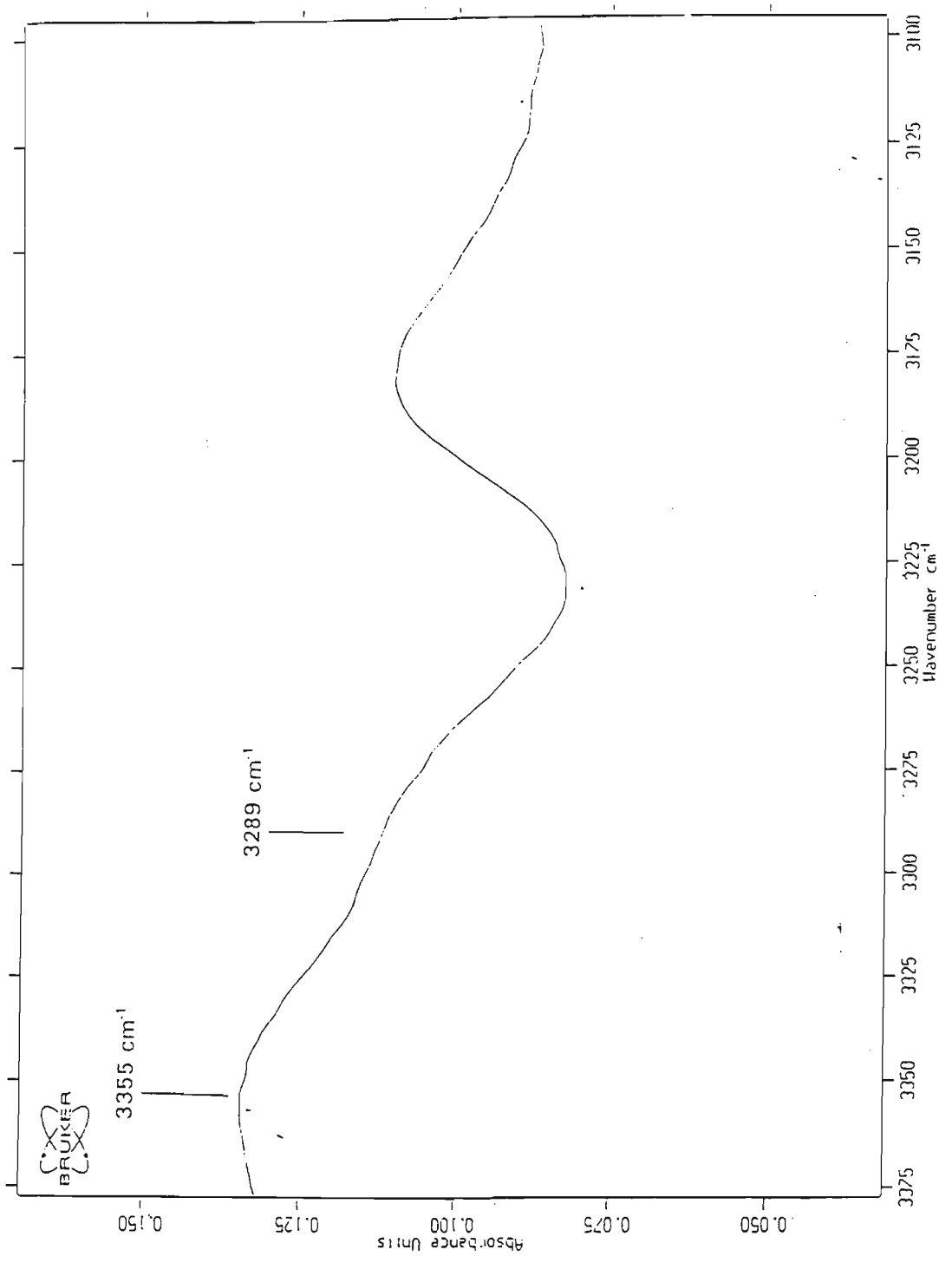

Fig. 4.8. Infrared spectrum of the free NH stretching band of dipropylamine (0.61 M).

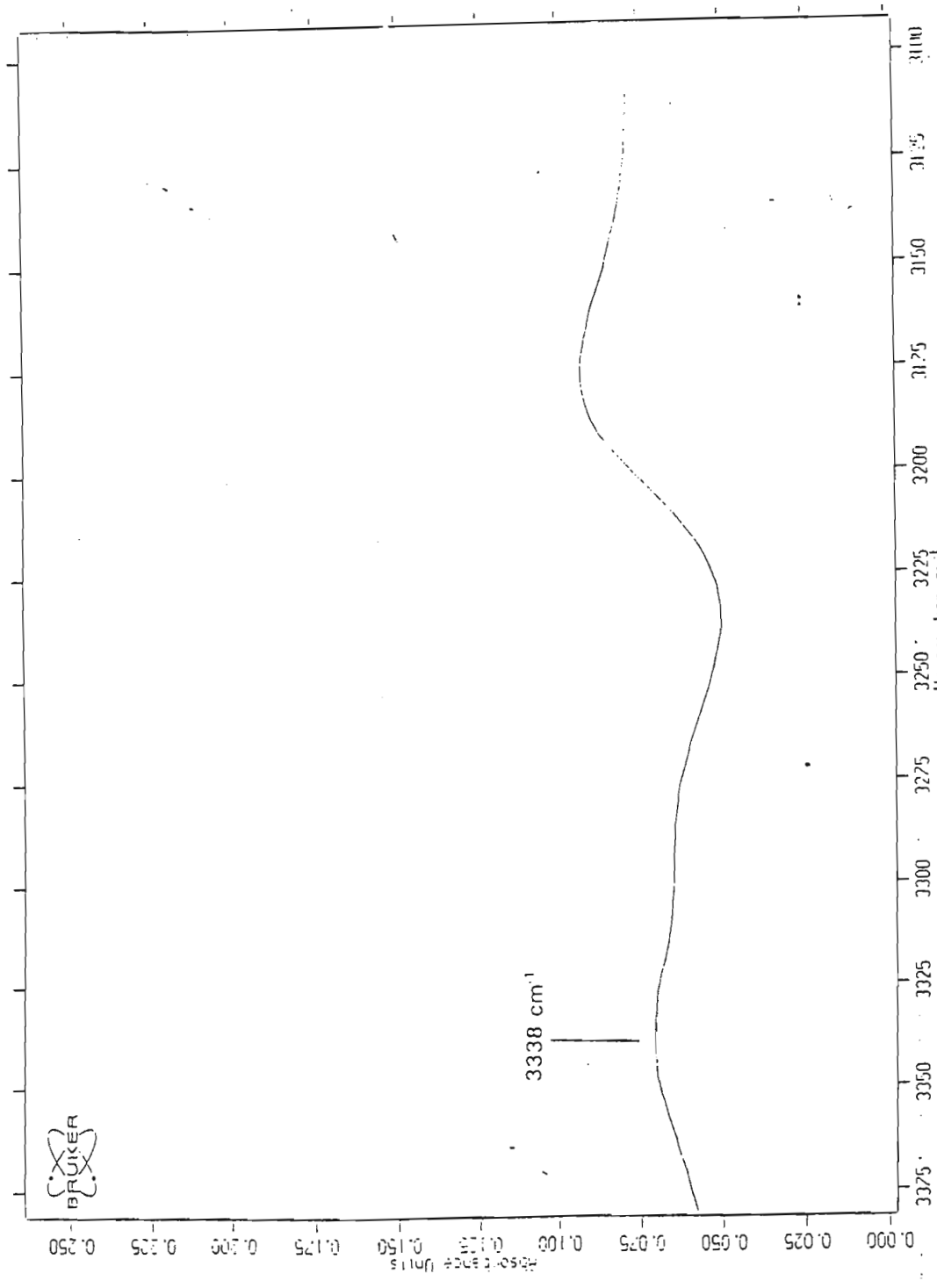

Fig. 4.9. Infrared spectrum of the NH stretching region of a mixture of dipropylamine (0.46 M) and dipropyl ether (1.80 M).

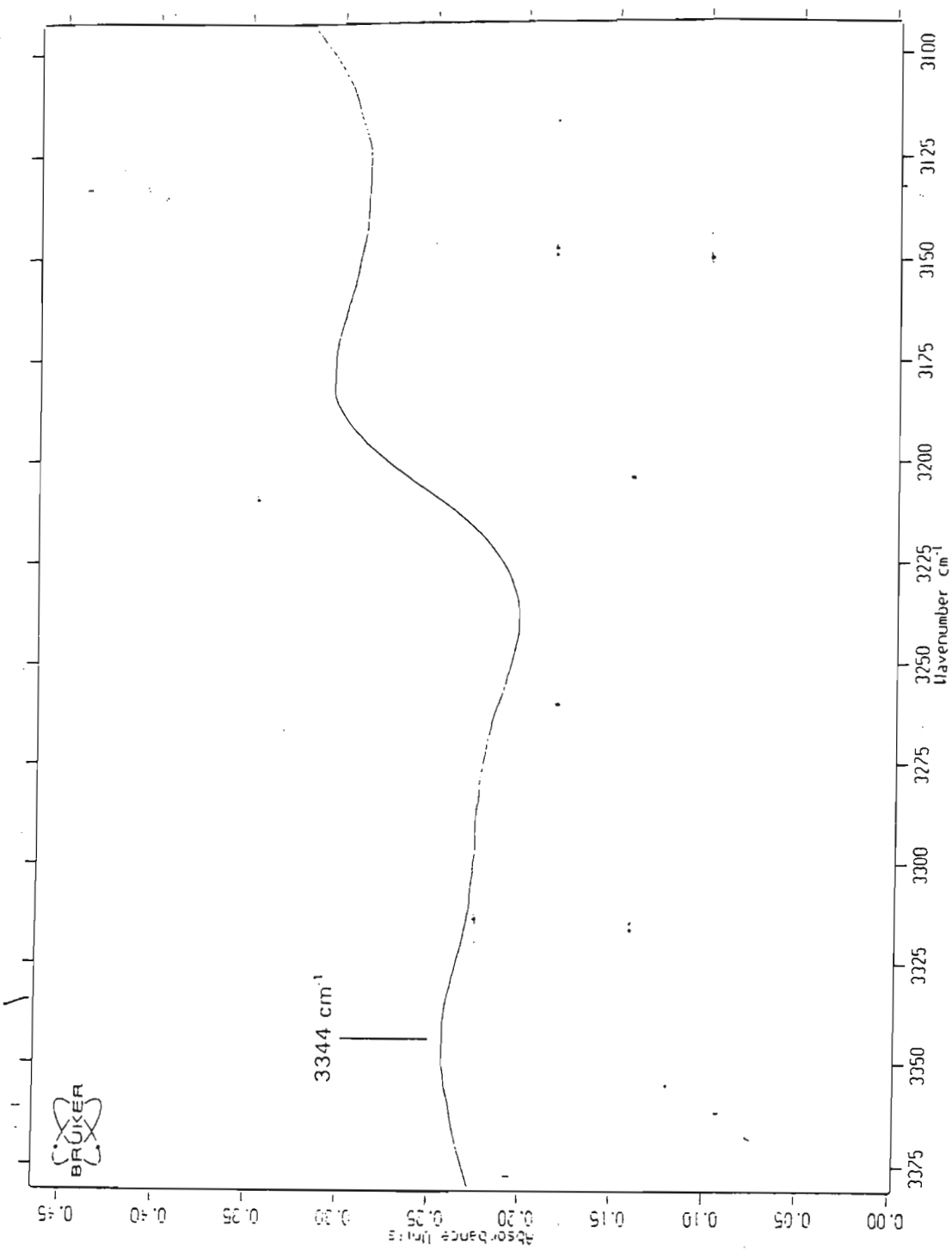

Fig. 4.10. Infrared spectrum of the NH stretching region of a mixture of dipropylamine (0.46 M) and tributylamine (1.32 M).

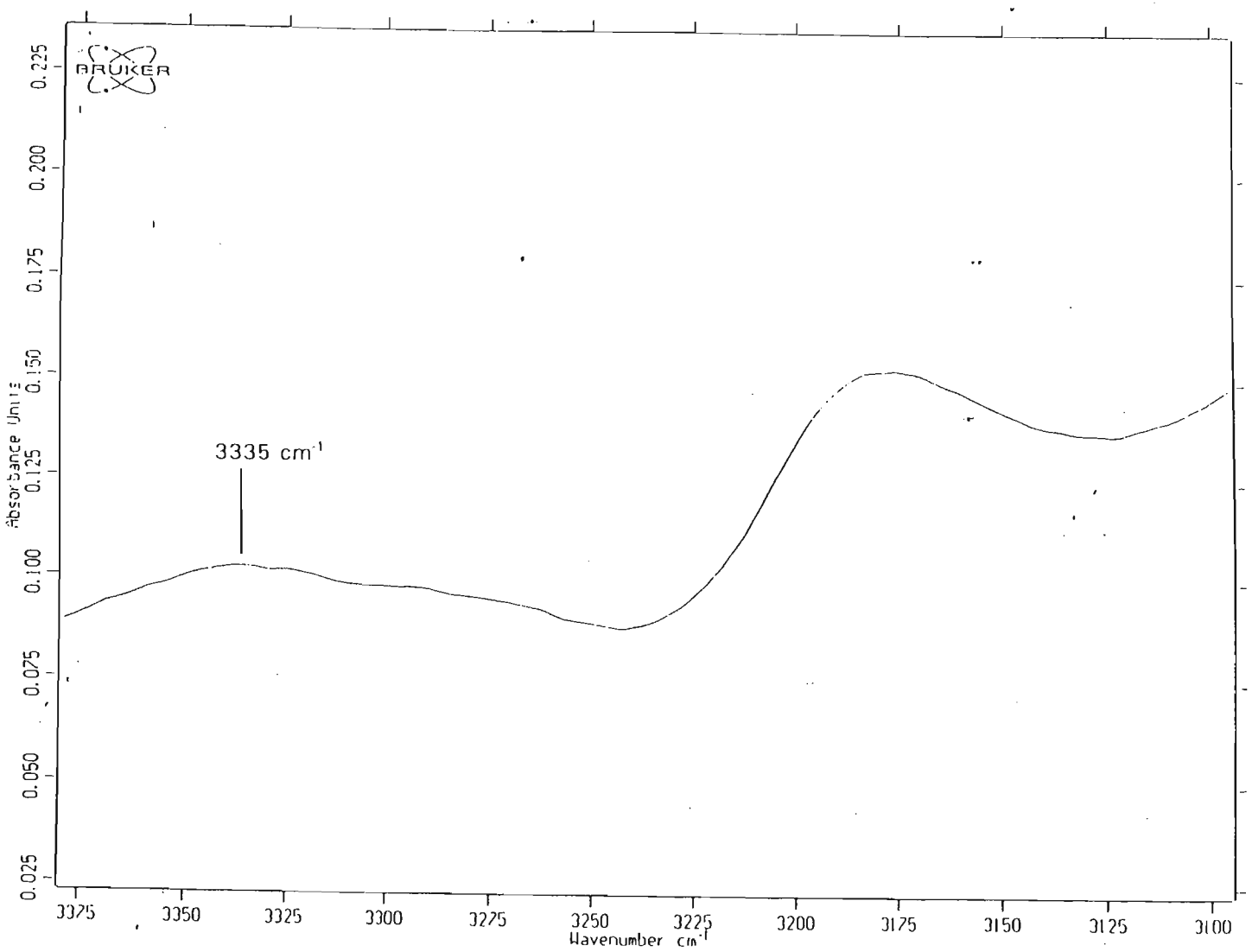

Fig. 4.11. Infrared spectrum of the NH stretching region of a mixture of dipropylamine (0.46 M) and dipropyl sulphide (1.78 M).

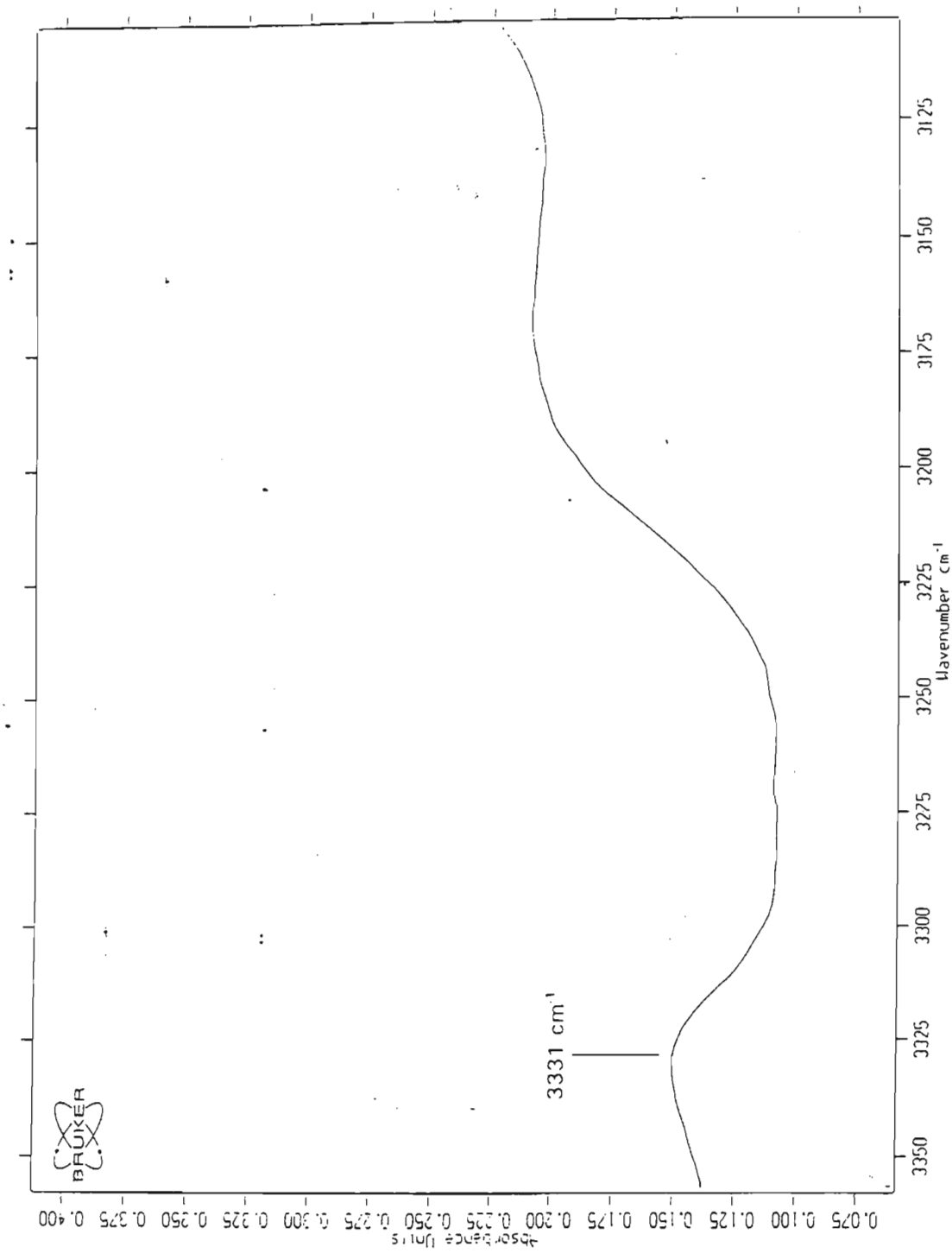

Fig. 4.12. Infrared spectrum of the NH stretching region of a mixture of dipropylamine (0.46 M) and heptan-4-one (1.75 M).

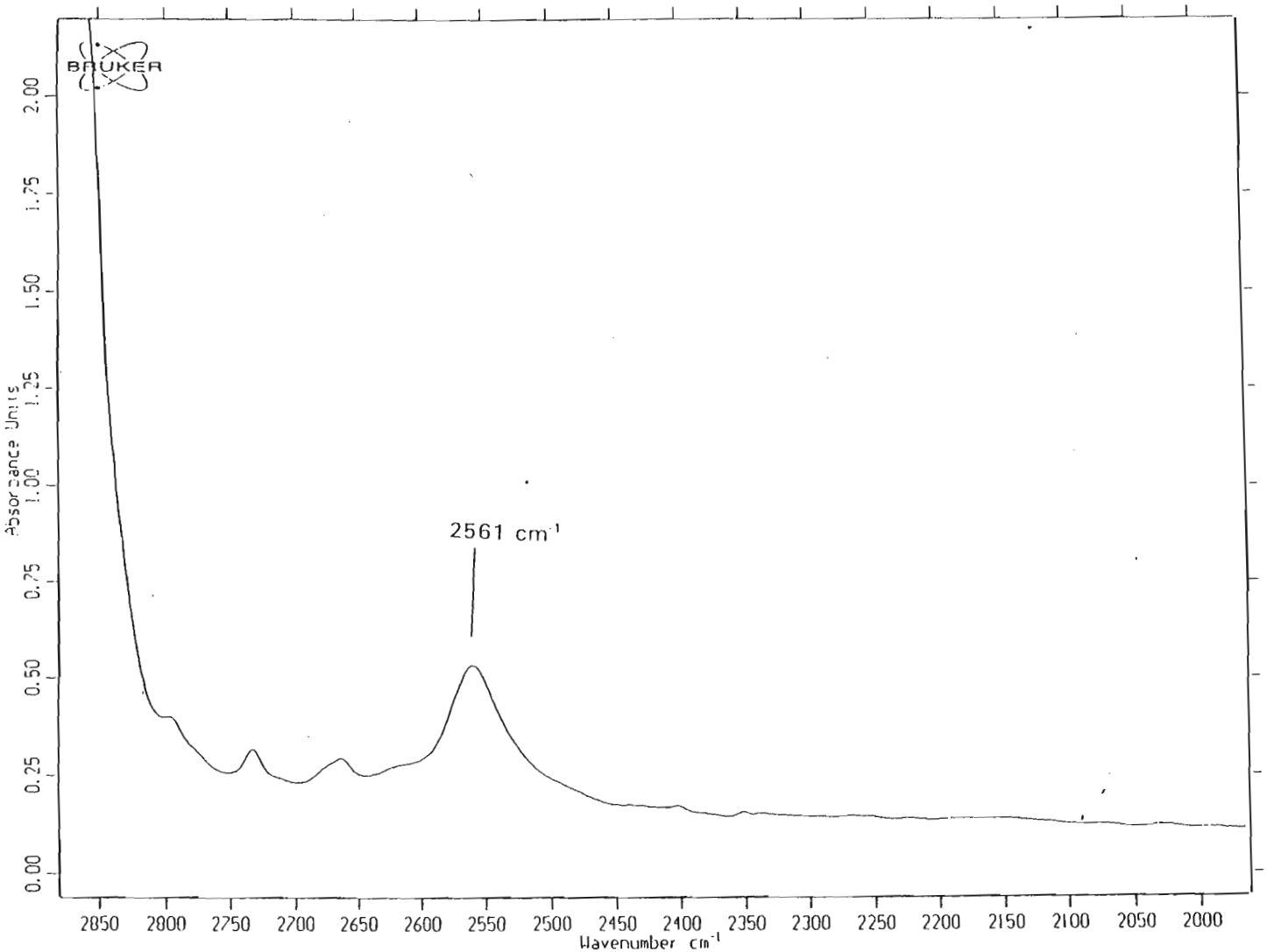

Fig. 4.13. Infrared spectrum of the SH stretching region of undiluted propane-1-thiol.

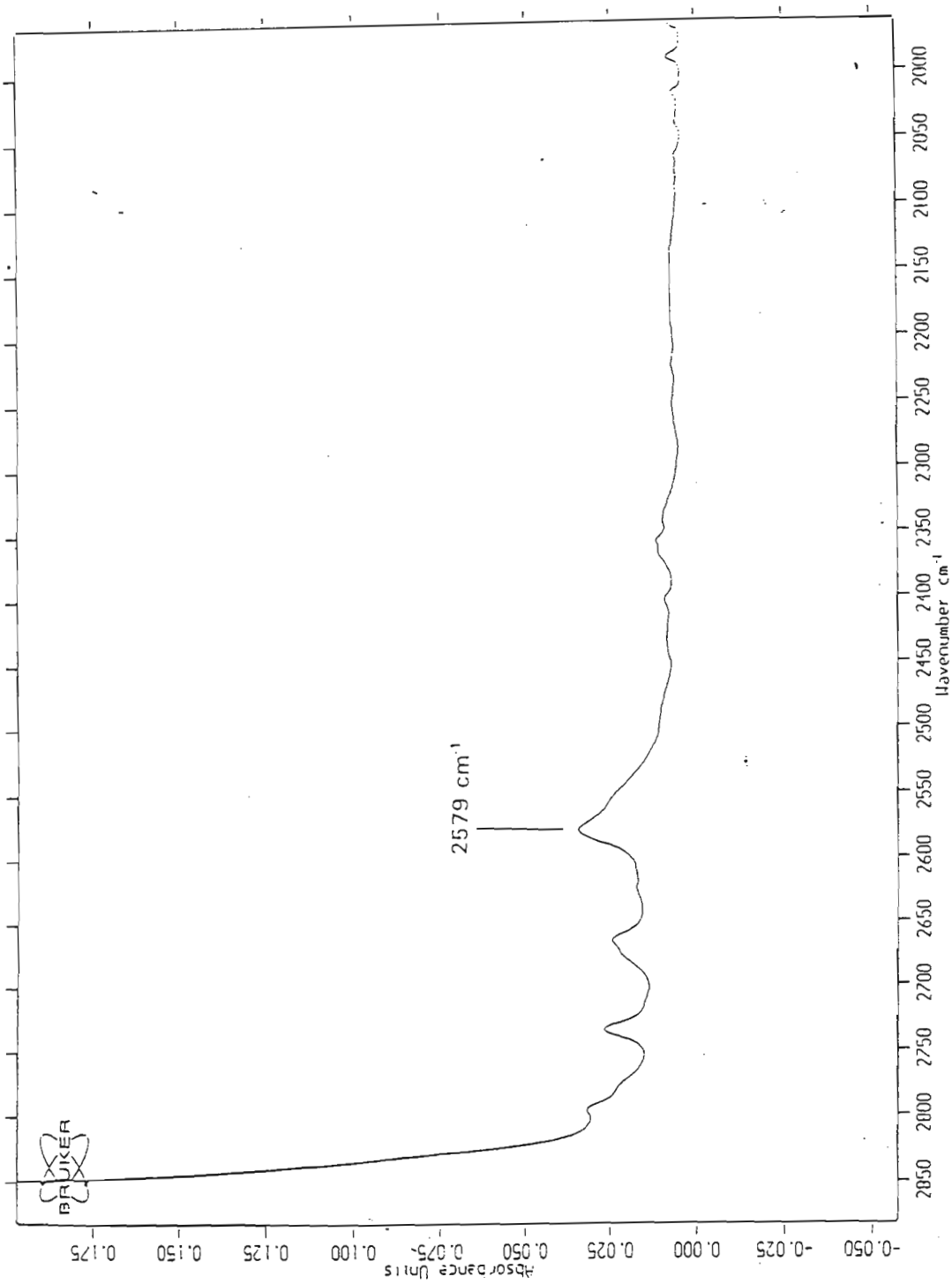

Fig. 4.14. Infrared spectrum of the free SH stretching band of propane-1-thiol (1.84 M) in CCl_4.

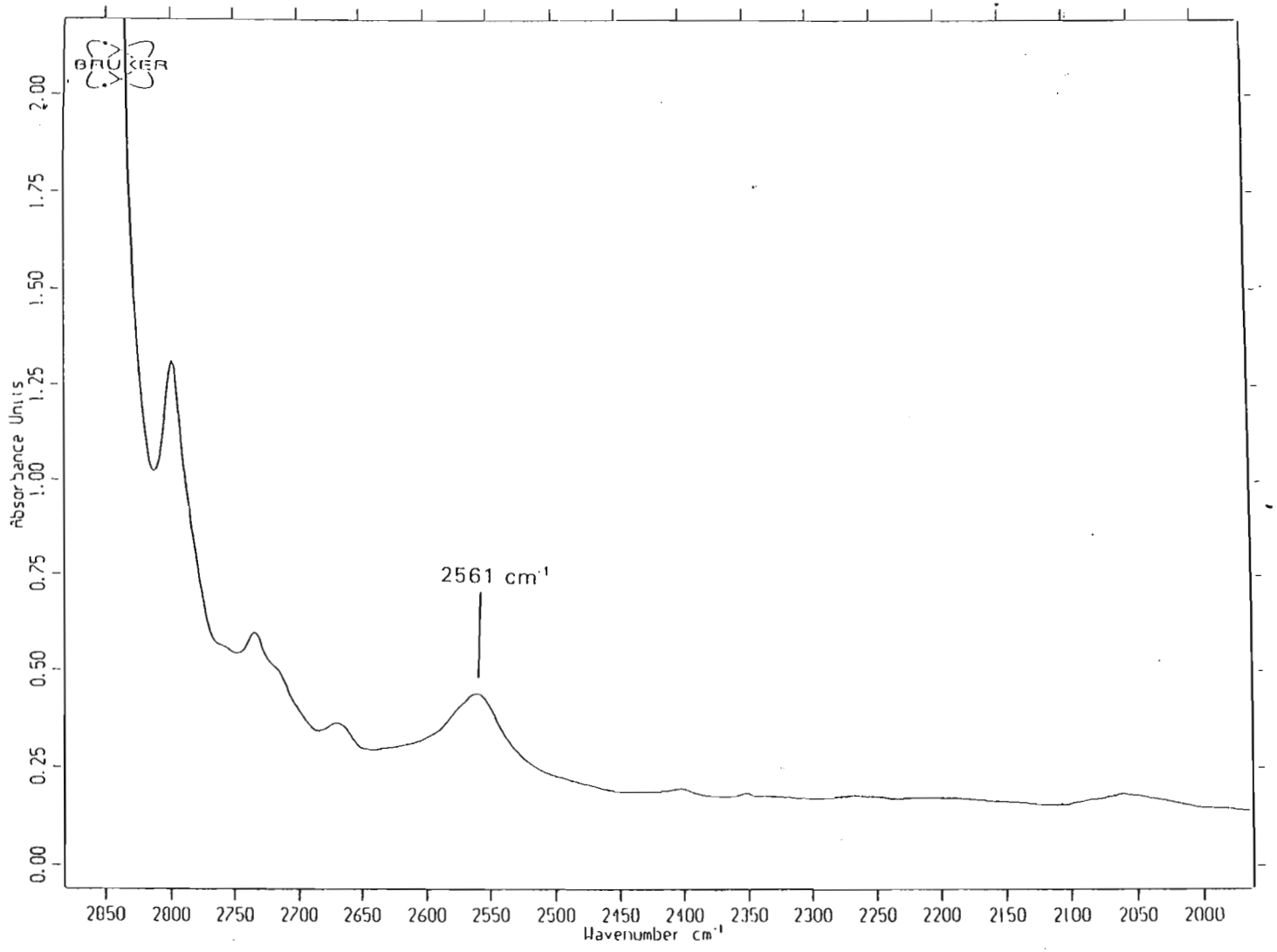

Fig. 4.15. Infrared spectrum of the SH stretching region of a mixture of propane-1-thiol (3.13 M) and dipropyl ether (4.91 M).

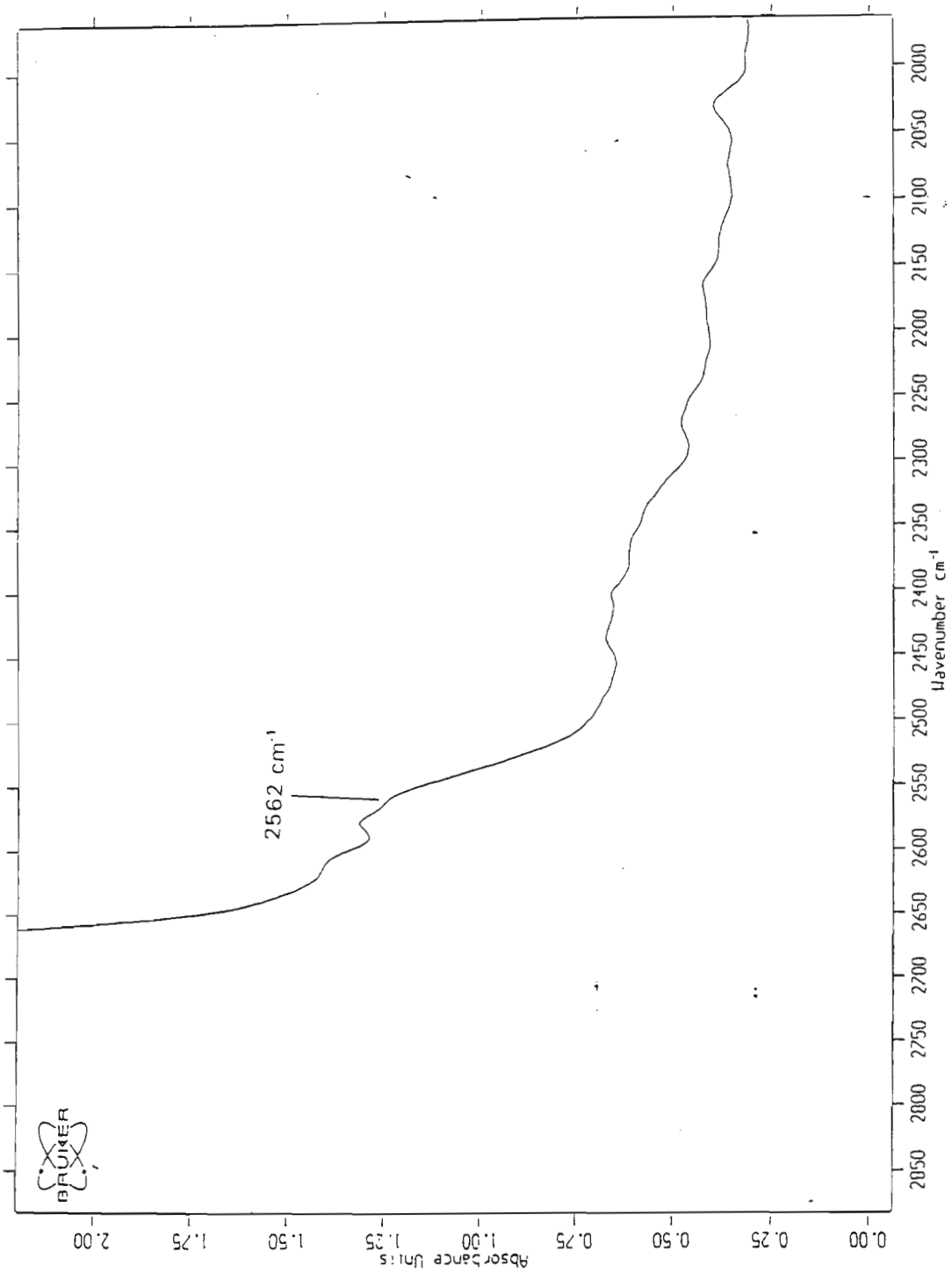

Fig. 4.16. Infrared spectrum of the SH stretching region of a mixture of propane-1-thiol (3.13 M) and tributylamine (2.95 M).

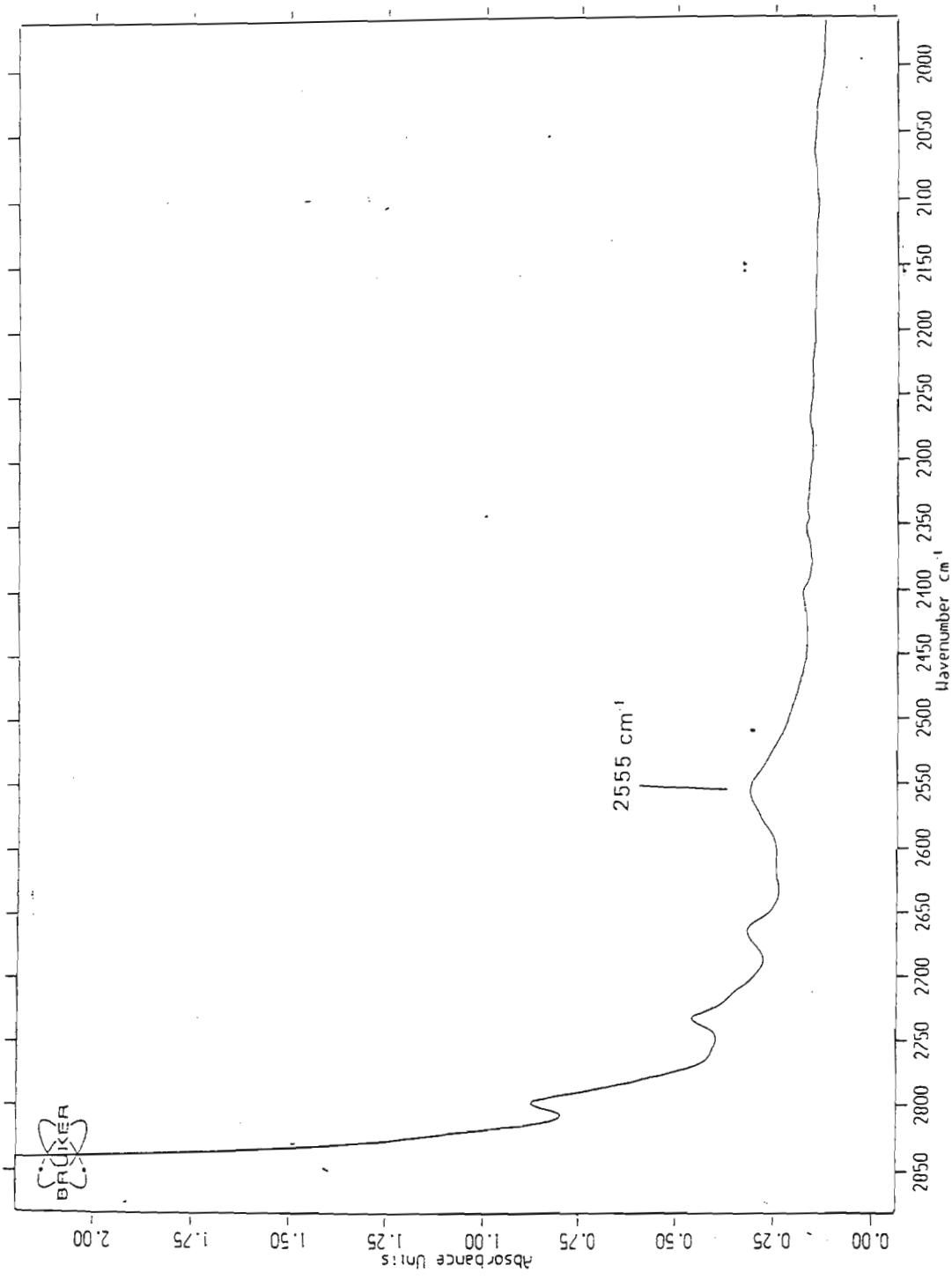

Fig. 4.17. Infrared spectrum of the SH stretching region of a mixture of propane-1-thiol (3.13 M) and dipropyl sulphide (4.57 M).

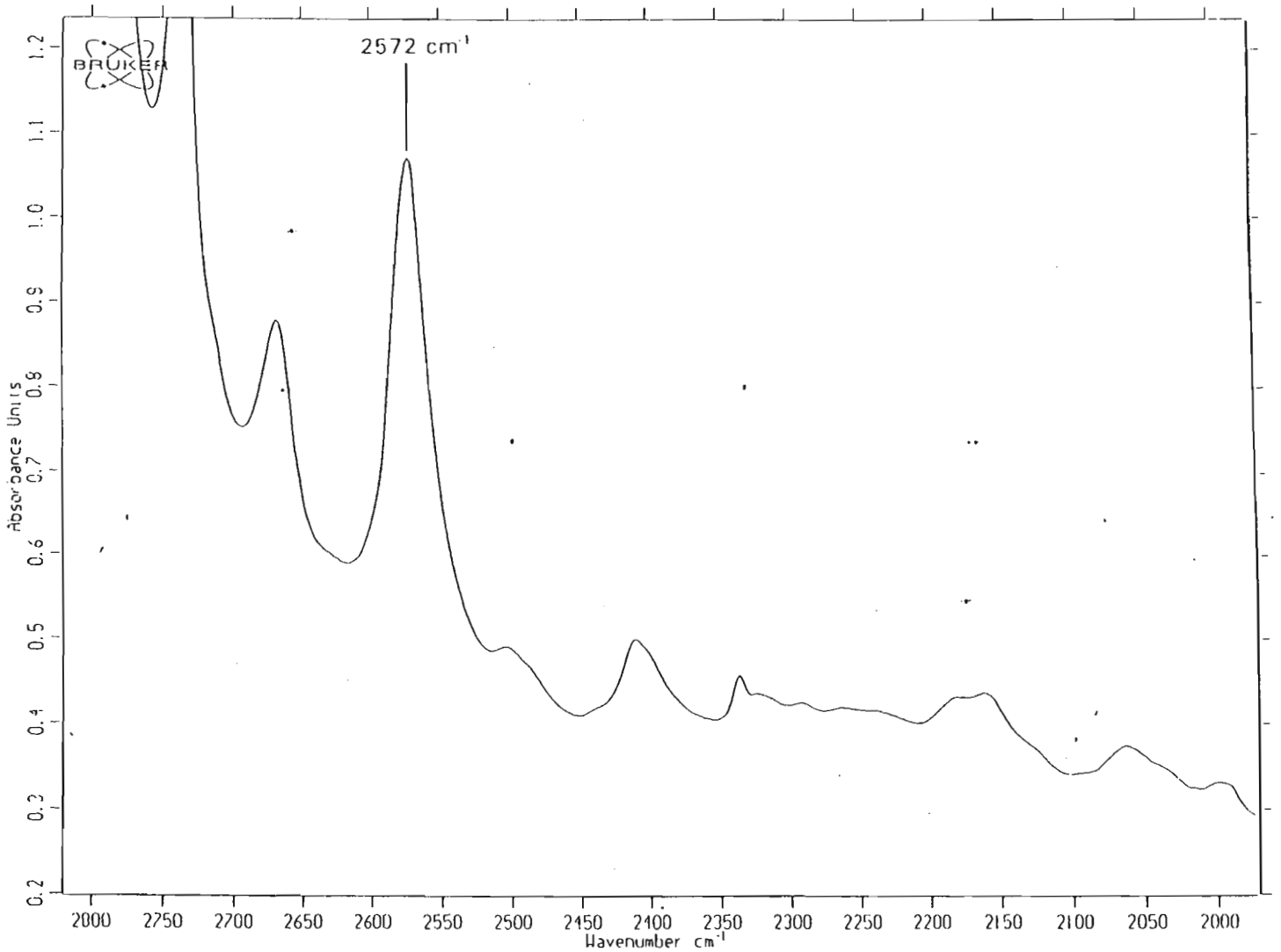

Fig. 4.18. Infrared spectrum of the SH stretching region of a mixture of propane-1-thiol (3.13 M) and heptan-4-one (4.38 M).

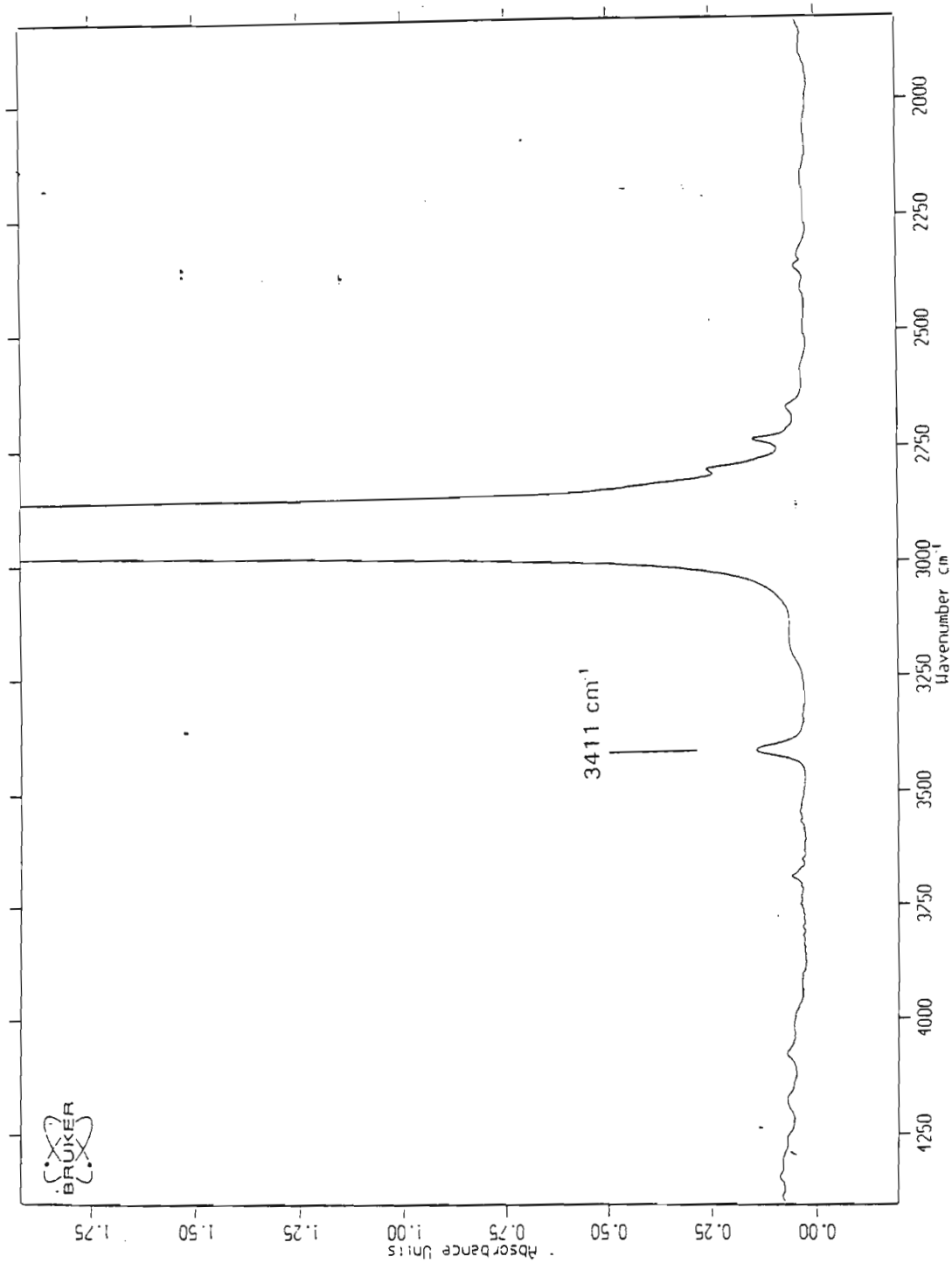

Fig. 4.19. Infrared spectrum of heptan-4-one (0.63 M) in CCl_4.

Table 4.2. The free A-H stretching wavenumbers, ν(AH), for the three proton donors in this study.

Substance	ν(AH)/cm^{-1}
propan-1-ol	3640
dipropylamine	3355
propane-1-thiol	2579

Table 4.3. The A-H stretching wavenumbers, ν(AH), and their shifts, $\Delta\nu$(AH), for the hydrogen bonded liquid mixtures

System	ν(AH)/cm^{-1}	$\Delta\nu$(AH)[a]/cm^{-1}
OH...O	3491	-149
OH...N	3420	-220
OH...S	3501	-139
OH...O=C	3546	-94
NH...O	3338	-17
NH...N	3344	-11
NH...S	3335	-20
NH...O=C	3331	-24
SH...O	2561	-18
SH...N	2562	-17
SH...S	2555	-24
SH...O=C	2572	-7

[a] $\Delta\nu(AH) = \nu(AH)_{MIXTURE} - \nu(AH)_{FREE}$

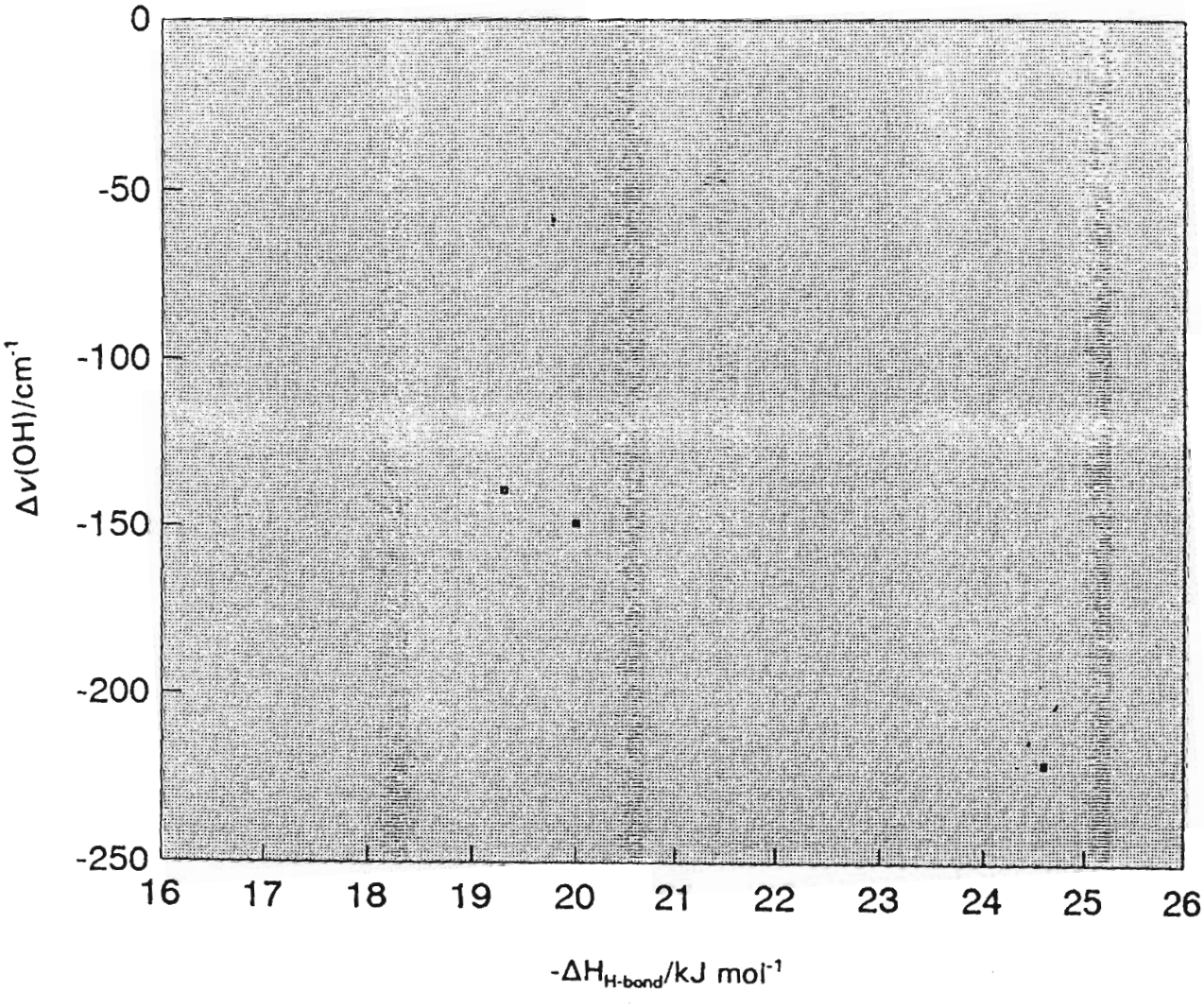

Fig. 4.20. A plot of the shift in the OH stretching band versus the experimentally determined enthalpy of interaction.

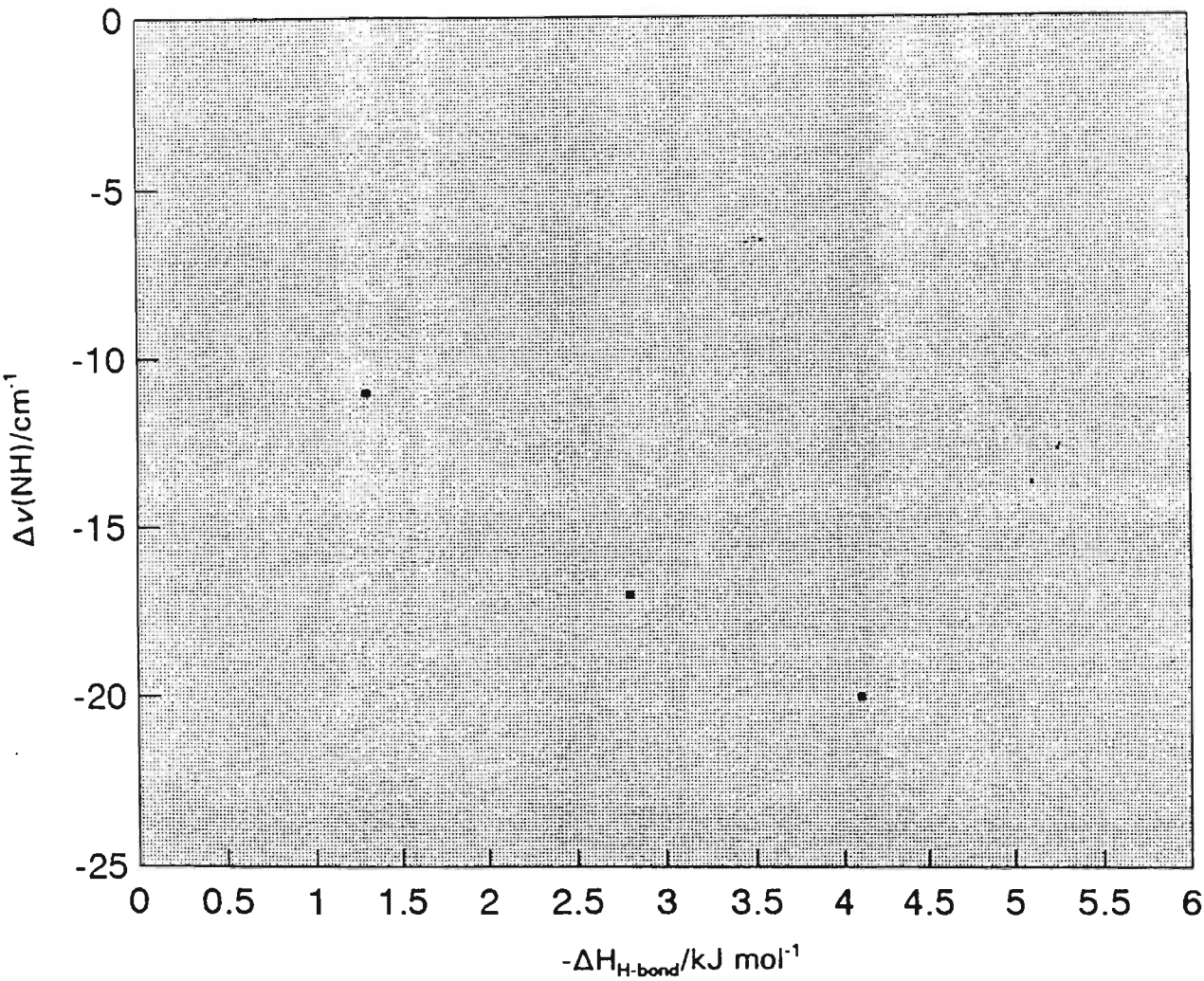

Fig. 4.21. A plot of the shift in the NH stretching band versus the experimentally determined enthalpy of interaction.

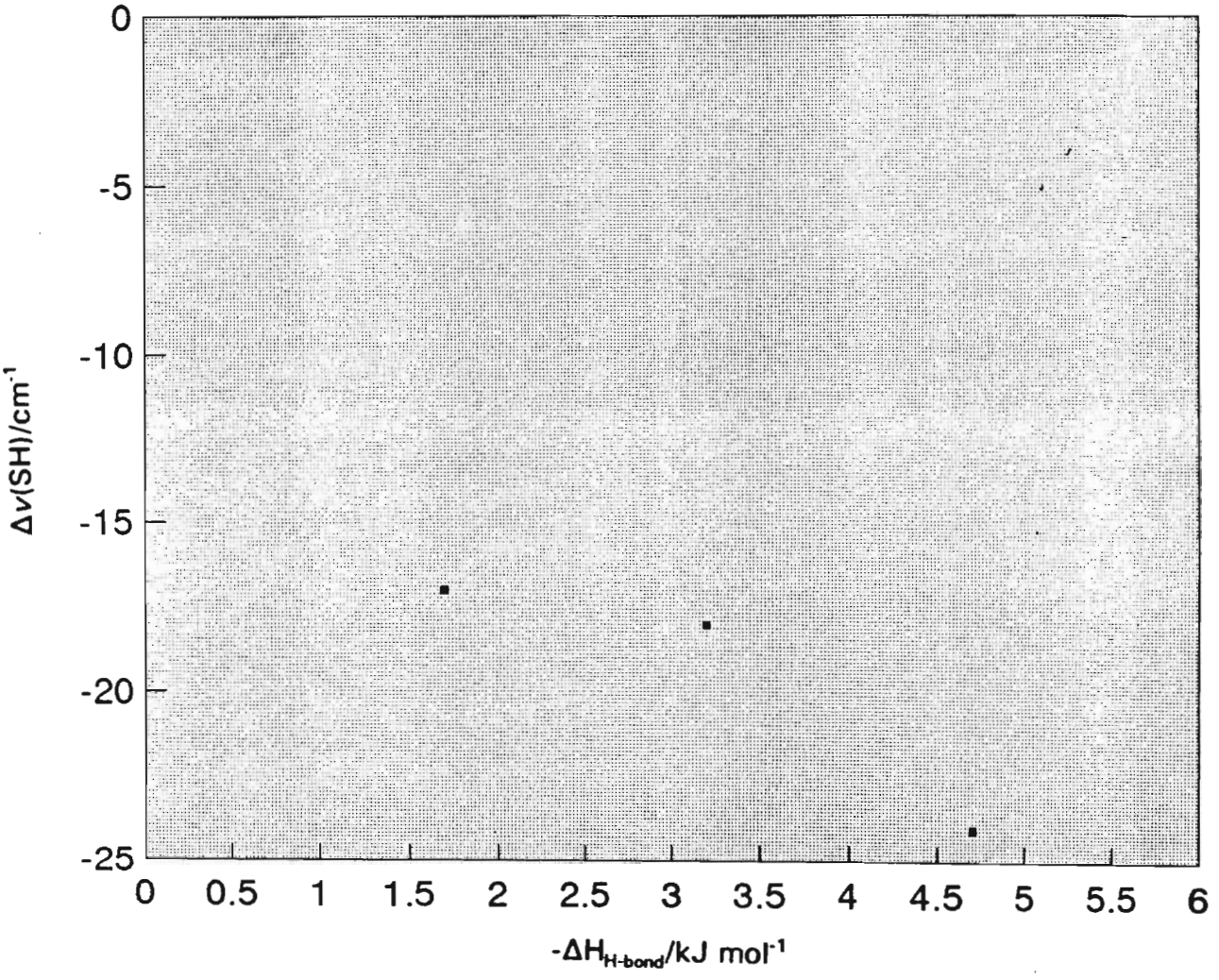

Fig. 4.22 *A plot of the shift in the SH stretching band versus the experimentally determined enthalpy of interaction.*

4.4 Discussion

As discussed previously, the aim of this particular section was to look specifically at the shift in the A-H stretching band, as a result of hydrogen bonding, in an attempt to confirm and verify the thermodynamic liquid phase findings in this work. The first task was to determine the position of the absorption band due to the free A-H stretching vibration in the pure proton donating liquid. Fig. 4.2 is the spectrum for propan-1-ol in CCl_4 at a concentration of 0.35 M, in the spectral region 3750-2900 cm^{-1}. The peak at 3640 cm^{-1} is the absorption due to the free O-H stretching vibration, while that at 3346 cm^{-1} is due to the bonded O-H stretching vibration resulting from self-association. As hydrogen bonding causes ν(AH) to shift to lower frequencies, we would expect that the mixtures involving heteroassociated hydrogen bonding would manifest a wavenumber value for ν(AH) somewhere between 3640 and about 3300 cm^{-1}. This band would clearly be impossible to observe because of the above explained band at 3346 cm^{-1}. In order to eliminate this band, higher dilutions of propan-1-ol in CCl_4 were necessary in order to isolate the propan-1-ol molecules from one another and so diminish the chances of self-association. It was found that a propan-1-ol concentration of 0.090 M in CCl_4 eliminates the band due to the bonded O-H stretching vibration as a result of self-association. This was thus the propan-1-ol:CCl_4 dilution settled on for each of the mixture ν(AH) determinations. Figs. 4.3 - 4.6 show the spectra of the propan-1-ol mixtures in the A-H stretching vibration region, which each display the emergence of a bonded O-H stretching vibration peak as a result of hydrogen bonding. Even when the concentration of proton acceptor was increased significantly, the peak at 3640 cm^{-1}, as a result of the free O-H stretching vibration,

remained. A summary of the shifts in ν(AH) for the alcohol systems is contained in Table 4.3, and clearly shows that $\Delta\nu$(AH) increases in the sequence OH...N > OH...O > OH...S. In Chapter 3, it was established that the order of hydrogen bond strengths for systems involving OH as the proton donor, as defined in terms of enthalpies of interaction ($\Delta H_{H\text{-}bond}$), was also found to be OH..N > OH...O > OH...S thus revealing a correlation in the liquid phase between $\Delta\nu$(AH) and $\Delta H_{H\text{-}bond}$. This is further confirmed in Fig. 4.20 where $\Delta\nu$(OH) is plotted as a function of $\Delta H_{H\text{-}bond}$. The emergence of a linear relationship means that, in so far as the alcohol systems involving the proton acceptor atoms N, O and S are concerned, the order of hydrogen bond strengths as determined thermodynamically, is supported.

The spectrum of undiluted dipropylamine in the region 3400-3100 cm^{-1} is shown in Fig. 4.7. Of the three peaks present, one is due to the free N-H stretching vibration and one due to the bonded N-H stretching vibration as a result of dipropylamine self-association. Clearly the latter would diminish in intensity as the dipropylamine is diluted with CCl_4. Fig. 4.8 illustrates the spectrum of dipropylamine in CCl_4, at a molarity of 0.61 M, and indicates that the band at 3295 cm^{-1} is the one that diminishes as a result of dilution, signifying that this band is due to the bonded N-H stretching vibration. The band due to the free NH stretching vibration must be located at a higher wavenumber, which is the one observed at 3355 cm^{-1}. Figs. 4.9 -4.12 show the spectra of the dipropylamine mixtures in the N-H stretching vibration region. An outline of the shifts in ν(AH) for the secondary amine heteroassociated hydrogen bonded systems is contained in Table 4.3, and demonstrates that $\Delta\nu$(AH) increases in the sequence NH...S > NH...O > NH...N. The smaller shifts in ν(AH) compared with the alcohol systems

illustrate the energetic superiority of the hydrogen bonds involving the OH moiety. The sequence above is the same as that for the thermodynamically determined enthalpy of interaction in the liquid phase systems involving dipropylamine as the proton donor.

A similar inspection of the trends displayed in the propane-1-thiol mixtures, as illustrated in Figs. 4.13 - 4.18, and summarized in Table 4.3, reveals that $\Delta\nu$(AH) increases in the sequence SH...S > SH...O > SH...N, again the same as that for the thermodynamically determined enthalpy of interaction in the liquid phase systems involving propane-1-thiol as the proton donor. The shifts are comparable in magnitude with those observed in the secondary amine systems. Figs. 4.21 and 4.22, which show both $\Delta\nu$(NH) and $\Delta\nu$(SH) as functions of $\Delta H_{H\text{-}bond}$, clearly demonstrate a monotonic relationship and confirm again, as in the case of the alcohol systems, the authenticity of the thermodynamically determined results involving the atoms N, O and S as proton acceptors.

The anomaly established in the systems involving NH or SH as proton donors, where the proton accepting ability of the relevant atoms is the reverse of that in the alcohol systems, and decreases in the order S > O > N, may be due to steric hindrance where the condensed nature of liquids inhibits the access that a hydrogen atom of the proton donor has to a lone pair of electrons of the proton acceptor. This hypothesis, tested using heptan-4-one as a proton acceptor, for which the oxygen atom is more exposed than in the ether molecule, and where the C=O group has roughly the same van der Waals volume and a similar surface area as does the -S- group[215] (see section 3.7.1), seemed a feasible one from the results

determined in the thermodynamic study, where the order of bond strength of the interactions are NH...O=C or SH...O=C > NH...S or SH...S (see section 3.7). The above thermodynamic finding is mirrored in this infrared study for systems involving -NH as the proton donor, but not in systems involving -SH, where the SH...O=C interaction records the lowest $\Delta\nu$(SH) value. Fig. 4.19 is the spectrum of heptan-4-one in CCl_4, and shows a band at 3411 cm^{-1} which also appears in the spectra of the mixture of propan-1-ol and heptan-4-one. It is the CO stretch overtone and was not confused with the OH stretching vibration.

5.0 Conclusion

The properties and characteristics of binary systems involving single AH...B hydrogen bonds have been considered in this work. On the basis of the *ab initio* MO results recorded in Chapter 2, the following conclusions can be made:

(i) A direct correlation exists between the strength of the hydrogen bond and the intramolecular A-H bond length. The higher the interaction energy, the longer the A-H bond.

(ii) An inverse relationship exists between the strength of the hydrogen bond and the distance of separation of the A and B atoms, relative to the sum of their van der Waals radii. This latter property, obtained by subtracting the sum of the van der Waals radii for the two electronegative atoms (A and B) involved in each hydrogen bond from the heavy atom bond distance gives the interposed "space" between the two heavy atoms that the bridging hydrogen atom occupies in the hydrogen bonded interaction, and is effectively a measure of the covalency of the hydrogen bond. This available "space" decreases with increasing strength of the hydrogen bond.

(iii) An inverse relationship exists between the strength of the hydrogen bond and the deviations from linearity of that bond. The less stable the hydrogen bond, the greater the deviation of the $A\hat{H}...B$ bond angle from 180°. The linearity of the hydrogen bond

is less sensitive to the particular type of hydrogen bond when B is nitrogen than when it is oxygen or sulphur.

(iv) The electronic energies, the deviations from linearity of the AH...B hydrogen bond, the lengthening of the covalent A-H bond, the Mulliken charge shifts, the shifts in position and intensity of the A-H stretching band and the shifts in the A-H deformation modes clearly illustrate that the proton accepting competence of the three atoms considered in this work decreases in the order N > O > S.

(v) Similarly, the proton donating ability of the three hydrogen donor moieties studied in this work decreases in the order O-H > N-H ≈ S-H.

(vi) The Mulliken charge shifts, partitioned among the A, H and B atoms that participate in the hydrogen bond, demonstrate that the bridging hydrogen atom donates a sizeable fraction of electron density, the relative amount being dependent on the particular interaction. Also, the electron density decreases around the hydrogen atom as the hydrogen bond strength increases.

(vii) The direction of charge transfer, on complexation, is from $(CH_3)_2O$, $(CH_3)_3N$ and $(CH_3)_2S$ to CH_3OH, $(CH_3)_2NH$ and CH_3SH, as appropriate, as indicated by the positive overall Mulliken charge values for the electron donors and negative values for the electron acceptors. When the proton acceptor atom, B, is nitrogen, the amount of charge redistributed by B is larger than when B is

oxygen, which in turn, is larger than when B is sulphur.

(viii) Whereas the other complexes display an increase in the length of the A-H bond, a red shift of ν(AH), and an increase in the intensity of the A-H stretching band, consistent with the formation of a hydrogen bond, the $CH_3SH...S(CH_3)_2$ complex exhibits a decrease in the length of the A-H bond, a blue shift of ν(AH) and a decrease in the intensity of the A-H stretching band. Although the electronic energy change for this complex is negative, it is clear that this interaction is extremely weak since the absolute values of all these properties are close to zero.

(ix) The hydrogen bond interaction is mainly electrostatic in nature, but also involves some covalent character. This covalent contribution to the hydrogen bond energy is in the form of the charge transfer.

(x) The correlative plots serve to illustrate that, in most cases, there is no single relationship that connects all nine types of hydrogen bond, and that each type of hydrogen bond, involving a different proton donor, has a different dependence on the properties considered, such as ΔH, than do the others.

(xi) No significant structural changes occur in the interacting monomers upon hydrogen bonded complexation.

From the thermodynamic results recorded in Chapter 3, the following conclusions can be made:

(i) The technique of using the partial molar enthalpy at infinite dilution, $H^{E}_{i,m}(x_i=0)$, to determine hydrogen bond interactive strengths only gives good quantitative results for systems involving alcohols. The ERAS model and results from other sources show that the change in enthalpy for non-alcoholic systems is generally underestimated.

(ii) Based on the results from all three thermodynamic procedures applied to the experimental data, the order of hydrogen bond strengths for the liquid phase systems involving the O-H bond as the proton donor, is OH..N > OH...O > OH...S. Therefore, when OH is the proton donating moiety, the proton accepting ability of the atoms under consideration is in the order N > O > S.

(iii) For the liquid phase systems involving dipropylamine and propane-1-thiol as proton donors, the proton accepting ability of atoms under consideration is in the opposite order i.e. S > O > N.

(iv) This result established in the liquid systems involving NH or SH as proton donors was considered to be related to the available surface area of the proton acceptor. This was based on the assumption that the only difference between the interaction involving a proton donor and either dipropyl ether or heptan-4-one was the difference in the available surface area of the respective proton acceptor functional groups. The hypothesis was tested using heptan-4-one as a proton acceptor, for which the oxygen atom is more exposed than in the corresponding ether, and where the C=O group has roughly the same van der Waals volume and a similar surface area

as does the -S- group (see section 3.7). Results show that the order of thermodynamic stability of the interactions are NH...O=C or SH...O=C > NH...S or SH...S (see Table 3.15). Therefore, once the difference between the available surface areas of the two proton accepting moieties involved is compensated for, the proton accepting ability of the O and S atoms assumes the same order as that when OH is the proton donating moiety.

In the infrared spectroscopic study, detailed in Chapter 4, the following conclusions have been reached:

(i) As in the thermodynamic analysis, the order of hydrogen bond stabilities for the liquid state systems involving OH as the proton donor, is also OH..N > OH...O > OH...S. The proton accepting ability thus decreases in the order N > O > S.

(ii) The proton accepting ability of atoms under consideration for the liquid phase systems involving dipropylamine and propane-1-thiol as proton donors is in the opposite order, i.e. S > O > N which is similar to the result obtained thermodynamically for the same systems.

(iii) The results on the binary systems involving a proton donor and heptan-4-one are not totally consistent with those established in the thermodynamic study. The above thermodynamic finding is mirrored in this infrared study for systems involving -NH as the proton donor, but not in systems involving -SH, where the SH...O=C interaction records the lowest $\Delta\nu$(SH) value.

An analysis of the liquid phase results, determined in both the thermodynamic and infrared studies, reveals the consistency of most of the findings in these investigations. The most important correlative result is the relationship which exists in the liquid phase between $\Delta\nu$(AH), the shift in the A-H stretching wavenumber, and $\Delta H_{H\text{-}bond}$, the hydrogen bond interaction energy. This is illustrated in section 4.4 in Figs. 4.20 - 4.22 where $\Delta\nu$(AH) is plotted as a function of $\Delta H_{H\text{-}bond}$ for all three systems involving a different proton donor. A direct relationship between these two properties, in all three cases, gives added support to the findings of the thermodynamic study in respect of the order of hydrogen bond stabilities, and appear to obey the Badger-Bauer rule, which predicts a direct relationship between the shift in the infrared AH stretching frequency, caused by hydrogen bonding, and the magnitude of -ΔH, the calorimetric enthalpy of dimerization. ΔH values for phenol - base systems have also been found to obey this same relationship.

In Chapter 3, it was proposed that the available surface area of the proton acceptor atom was the dominant strength determining factor in liquid mixtures involving weakly self-associated proton donors. In these mixtures, the proton accepting ability of atoms under consideration is in the order S > O > N, which is opposite to that for liquid mixtures in which the proton donor is strongly self-associated (alcohols). It was proposed that, in weakly hydrogen bonded liquid systems, steric hindrance, due to the condensed nature of liquids, may inhibit the access that a proton donor has to the lone pair of electrons of the proton acceptor. This hypothesis, tested using heptan-4-one as a proton acceptor, for which the oxygen atom is more exposed than in the analogous ether molecule, and where the C=O group has roughly the same van der Waals volume and a similar surface area as

does the -S- group, appeared correct, based on the results determined in the thermodynamic study, where the order of bond strength of the interactions are NH...O=C or SH...O=C > NH...S or SH...S (see section 3.7).Therefore, as stated earlier, once the difference between the available surface areas of the two proton accepting moieties involved, is corrected for, the proton accepting ability of the O and S atoms assumes the same order as that when OH is the proton donor. This also implies that if a suitably similar molecule, with N (proton acceptor) having an available surface area similar to that of S and C=O, were found and subjected to the same analysis, the order of proton accepting strengths would be N > O > S, mirroring that found in the case of hydrogen bonds involving OH as the proton donor.

The above thermodynamic finding (NH...O=C or SH...O=C > NH...S or SH...S) is mirrored in the infrared study (chapter 4) for systems involving NH as the proton donor, but not in systems involving -SH, where the SH...O=C interaction records the lowest $\Delta\nu$(SH) value. This implies that either the proposal that the available surface area of the proton acceptor atom is the dominant strength determining factor in liquid mixtures involving weakly self-associated proton donors is flawed, or the assumption on which it is based, namely that the only difference between the interaction involving a proton donor and either dipropyl ether or heptan-4-one, is the difference in the available surface area of the respective proton acceptor functional groups, is incorrect.

Vinogradov and Linnell[35] have expressed the concern that there are no extensive systematic comparisons of thermodynamic parameters obtained by different experimental methods. This study has hopefully addressed that concern in some small way.

References

1. L. Pauling, *The Nature of the Chemical Bond*, Cornell University Press, New York, 1939.

2. L. Stryer, *Biochemistry*, 3rd ed., Freeman, New York, 1988.

3. G. C. Pimentel and A. L. McClellan, *The Hydrogen Bond*, Freeman, San Francisco, 1960.

4. E. I. Nagy-Felsobuki and K. Kimura, *J. Phys. Chem.*, **94**, 8041 (1990).

5. J. O. Williams, J. N. Scarsdale and L. Schafer, *J. Mol. Structure*, **76**, 11 (1981).

6. S. Wolfe, B. M. Pinto, V. Varma and R. Y. N. Leung, *Can. J. Chem.*, **68**, 1051 (1990).

7. M. C. L. Gerry and R. M. Lees, *J. Mol. Structure*, **61**, 231 (1976)

8. K. Raghavachari, *J. Chem. Phys.*, **81**, 2717 (1984).

9. A. Rank, R. Dutler and D. Yang, *Can. J. Chem.*, **68**, 258 (1990).

10. A. J. Barnes, H. E. Hallam and G. F. Scrimshaw, *Trans. Faraday Soc.*, **65**, 3150 (1969).

11. N. Sheppard, *J. Chem. Phys.*, **17**, 79 (1949).

12. A.Tsuboyama, K.Takeshita, S.Konaka and M.Kimura, *Bull. Chem. Soc. Japan,* **57**, 3589 (1984).

13. U. Blukis, P. H. Kasai and R. J. Myers, *J. Chem. Phys.*, **38**, 2753 (1963).

14. S.Ilieva, B. Galabov and J.R. Durig, *J. Mol. Structure (Theochem)*, **200**, 543 (1989).

15. J. Ellwood, D. Steele and D. Gerrard, *Spectrochim. Acta*, **50A**, 3 (1994).

16. G.Maes, *Spectrochim. Acta*, **24A**, 1055 (1968)

17. L. Pierce and M. Hayashi, *J. Chem. Phys.*, **35**, 479 (1961).

18. J. E. Wollrab and V. W. Laurie, *J. Chem. Phys.*, **48**, 5058 (1968)

19. D. C. McKean, *J. Chem. Phys.*, **79**, 2095 (1983)

20. G. Gamer and H. Wolff, *Spectrochim. Acta,* **29A**, 129 (1973)

21. M. J. Buttler and D. C. McKean, *Spectrochim. Acta*, **21**, 485 (1965).

22. J. E. Wollrab and V. W. Laurie, *J. Chem. Phys.*, **51**, 1580

(1969).

23. W. F. Murphy, F. Zerbetto, J. L. Duncan and D. C. McKean, *J. Phys. Chem.*, **97**, 581 (1993).

24. A. Heintz, *Ber. Bunsenges. Phys. Chem.* **89**, 172 (1985).

25. H. Funke, M. Wetzel and A. Heintz, *Pure Appl. Chem.* **61**, 1429 (1989).

26. S. Murakami, K. Amaya and R. Fujishiro, *Bull. Chem. Soc. Japan*, **37**, 1776 (1964).

27. C. G. Savini, D. R. Winterhalter and H. C. van Ness, *J. Chem. Eng. Data*, **10**, 168 (1965).

28. H. C. van Ness, J. Van Winkle, H. H. Richtol and H. B. Hollinger, *J. Phys. Chem.*, **71**, 1483 (1967).

29. R. H. Stokes and H. T. French, *J. Chem. Soc., Faraday Trans. I*, **76**, 537 (1980).

30. M. K. Woycicka and W. M. Recko, *Bull. Acad. Pol. Sci., Ser. Sci. Chem.* **20**, 783 (1972).

31. W. Kauzmann, *Quantum Chemistry*, Academic Press Inc., New York, 1957.

32. M. Rigby, E. B. Smith, W. A. Wakeham and G. C. Maitland, *The Forces Between Molecules,* Clarendon Press, Oxford, 1986.

33. I. G. Kaplan, *Theory of Molecular Interactions,* Elsevier, Amsterdam, 1986.

34. M. D. Joesten and L. D. Schaad, *Hydrogen Bonding*, Marcel Dekker, Inc., New York, 1974.

35. S. N. Vinogradov and R. H. Linnell, *Hydrogen Bonding*, Van Nostrand Reinhold Company, New York, 1971.

36. A. G. Williamson, *An Introduction to Non-Electrolyte Solutions*, Oliver and Boyd, London, 1967.

37. C. J. Paral and P. Hobza, *Int. J. Quantum Chem.* **42**, 581 (1992).

38. R. S. Mulliken and W. B. Person, *Ann. Rev. Phys. Chem.*, **13**, 107 (1962).

39. G. A. Yeo and T. A. Ford, *Struct. Chem.*, **3**, 75 (1992).

40. L. Pauling, *Proc. Nat. Acad. Sci. U.S.,* **14**, 359 (1928).

41. C. A. Coulson, *Research (London),* **10**, 149 (1957).

42. S. A. Francis, *J. Chem. Phys.*, **19**, 505 (1951).

43. C. M. Huggins and G. C. Pimentel, *J. Phys. Chem.*, **60**, 1615 (1956).

44. M. Van Thiel, E. D.Becker and G. C. Pimentel, *J. Chem. Phys.*, **27**, 486 (1957).

45. W. Gordy and S. C. Stanford, *J. Chem. Phys.*, **9**, 204 (1941).

46. H. Tsubomura, *Bull. Chem. Soc. Japan*, **27**, 445 (1954).

47. C. A. Coulson and U. Danielson, *Arkiv. Fysik,* **8**, 239 (1954).

48. G. C. Pimentel, *J. Chem. Phys.*, **19**, 446 (1951).

49. E. Clementi, *J. Chem. Phys.*, **34**, 1468 (1961).

50. K. Kitaura and K. Morokuma, *Int. J. Quantum Chem.*, **10**, 325 (1976).

51. E. J. Rosenbaum, *Physical Chemistry,* Meredith Corporation, New York, 1970.

52. J. C. Davis Jnr., *Advanced Physical Chemistry*, The Ronald Press Co., New York, 1965.

53. N. Bohr, *Phil. Mag.*, **26**, 1 (1913).

54. I. N. Levine, *Quantum Chemistry,* 2nd Ed., Allyn & Bacon, Inc.,

Boston, 1974.

55. E. Schrödinger, *Ann. Physik*, **79**, 361 (1926).

56. E. Schrödinger, *Ann. Physik,* **80**, 437 (1926).

57. E. Schrödinger, *Ann. Physik*, **81**, 109 (1926).

58. E. Cartmell and G. W. A. Fowles, *Valency and Molecular Structure*, 2nd ed., Butterworths, London, 1961.

59. K. B. Lipkowitz and D. B. Boyd, *Reviews in Computational Chemistry*, Academic Press, New York, 1990.

60. T. Clark, *A Handbook of Computational Chemistry*, John Wiley & Sons, New York, 1985.

61. W. J. Hehre, L. Radom, P. von R. Schleyer and J. A. Pople, *Ab initio Molecular Orbital Theory*, Wiley, New York, 1986.

62. J. P. Lowe, *Quantum Chemistry*, Academic Press, New York, 1978.

63. S. Wilson, *Chemistry by Computer*, Plenum Press, New York and London, 1986.

64. P. W. Atkins, *Molecular Quantum Mechanics*, Clarendon Press, Oxford, 1970.

65. D. W. Rogers, *Computational Chemistry using the PC*, VCH Publishers Inc., New York, 1990.

66. R. Grahn, *Arkiv. Fysik.*, **15**, 257 (1959).

67. H. Umeyama and K. Morokuma, *J. Am. Chem. Soc.*, **99**, 1316 (1977).

68. K. Morokuma, *J. Chem. Phys.*, **55**, 1236 (1971).

69. S. Yamabe and K. Morokuma, *J. Am. Chem. Soc.*, **97**, 4458 (1975).

70. W. A. Lathan and K. Morokuma, *J. Am. Chem. Soc.*, **97**, 3615 (1975).

71. W.A.Lathan, G.R.Pack and K. Morokuma, *J. Am. Chem. Soc.*, **97**, 6624 (1975).

72. H. Umeyama and K. Morokuma, *J. Am. Chem. Soc.*, **98**, 7208 (1976).

73. Gaussian-92, Revision C.4, M. J. Frisch, G. W. Trucks, M. Head-Gordon, P. M. Gill, M. W. Wong, J. B. Foresman, B. G. Johnson, H.B. Schlegel, M. A. Robb, E. S. Replogle, R. Gomperts, R. L. Andreas, K. Raghavachari, J. S. Binkley, C. Gonzalez, R. L. Martin, D. J. Fox, D. J. DeFrees, J. Baker, J. J. P. Stewart and J. A. Pople, Gaussian, Inc., Pittsburgh, PA, 1992.

74. C. Møller and M. S. Plesset, *Mol. Phys.*, **46**, 618 (1934).

75. M. M. Francl, W. J. Pietro, W. J. Hehre, J. S. Binkley, M. S. Gordon, D.J. DeFrees and J.A.Pople, *J. Chem. Phys.*, **77**, 3654 (1982).

76. W. J. Hehre, W. A. Lathan, R. Ditchfield, M. D. Newton and J. A. Pople, Gaussian 70, Program 236, QPCE, Indiana University, Indiana.

77. J. S. Binkley, R. A. Whiteside, P. C. Harihan, R. Seegar, D. J. DeFrees, H. B. Schlegel, S. Topiol, L. Kahn and J. A. Pople, Gaussian 76, QPCE, Indiana University, Indiana.

78. J. S. Binkley, R. A. Whiteside,, R. Krishnan, R. Seegar, D. J. DeFrees, H. B. Schlegel, S. Topiol, L. Kahn and J. A. Pople, Gaussian 80, Carnegie-Mellon University, Pittsburgh.

79. J. S. Binkley, M. J. Frisch, D. J. DeFrees, K. Raghavachari, R. A. Whiteside, H. B. Schegel, E. M. Fleuder and J. A. Pople, Gaussian 82, Carnegie-Mellon University, Pittsburgh.

80. M. J. Frisch, J. S. Binkley, H. B. Schlegel, K. Raghavachari, C. F. Melius, R. L. Martin, J. J. P. Stewart, F. W. Bobrowicz, C. M. Rohlfing, L. R. Kahn, D. J. DeFrees, R. Seeger, R. A. Whiteside, D. J. Fox, E. M. Fleuder and J. A. Pople, Gaussian 86, Carnegie-Mellon Quantum Chemistry Publishing Unit, Pittsburgh.

81. M. J. Frisch, M. Head-Gordon, , H. B. Schlegel, K. Raghavachari, J. S. Binkley, C. Gonzalez, D. J. DeFrees, D. J. Fox, R. A. Whiteside, R. Seeger, C. F. Melius, J. Baker, R. L. Martin, L. R. Kahn, J. J. P. Stewart, E. M. Fleuder, S. Topiol and J. A. Pople, Gaussian 86, Gaussian, Inc., Pittsburgh.

82. M. J. Frisch, M. Head-Gordon,J. B. Foresman, G. W. Trucks, K. Raghavachari, H. B. Schlegel, M. Robb, J. S. Binkley, C. Gonzalez, D. J. DeFrees, D. J. Fox, R. A. Whiteside, R. Seeger, C. F. Melius, J. Baker,L. R. Kahn, J. J. P. Stewart, E. M. Fleuder, S. Topiol and J. A. Pople, Gaussian 90, Gaussian, Inc., Pittsburgh.

83. H. B. Schlegel, *J. Comp. Chem.*, **3**, 214 (1982).

84. B. A. Murtaugh and R. W. H. Sargent, *Comput. J.*, **13**, 185 (1970).

85. R. Fletcher and M. J. D. Powell, *Comput. J.*, **6**, 163 (1963).

86. SCHAKAL-92, E. Keller, Kritallographisches Institut der Universitat, Hebelstr. 25, Freiburg i. Br., Germany, 1992.

87. I. J. Kurnig, M. M. Szczesniak, and S. Scheiner, *J. Chem. Phys.*, **87**, 2214 (1987).

88. G. A. Yeo and T. A. Ford, *J. Mol. Structure*, **226**, 183 (1992).

89. E. Knözinger and O. Schrems, *Vibrational Spectra and Structure*,

Volume 16, J.R.Durig (ed), Elsevier, Amsterdam, 1987.

90. N. R. Kestner, *J. Phys. Chem.*, **48**, 252 (1968).

91. S.F. Boys and F. Bernardi, *Mol. Phys.*, **19**, 553 (1970).

92. G. A. Yeo and T. A. Ford, *J. Mol. Structure,* **200**, 507 (1989).

93. Y. Dimitrova and S. D. Peyerimhoff, *J. Phys. Chem.*, **97**, 12731 (1993).

94. G. A. Yeo and T. A. Ford, *J. Chem. Soc., Faraday Trans.*, **86**, 3067 (1990).

95. S. Skaarup, L. L. Griffin and J. E. Boggs, *J. Am. Chem. Soc.*, **98**, 3140 (1976).

96. J. E. Wollrab and V. W. Laurie, *J. Chem. Phys.*, **48**, 5058 (1968).

97. T. Kojima, *J. Phys. Soc. Japan*, **15**, 1284 (1960).

98. H. Dreizler and H.D.Rudolph, *Z. Naturforsch.*, **17A**, 712 (1962).

99. W. L. Jorgensen and L. Salem, *The Organic Chemists Book of Orbitals,* Academic Press, New York, 1973.

100. B. M. Gimarc, *Molecular Structure and Bonding. The qualitative molecular approach*, Academic Press, New York, 1979.

101. M. J. S. Dewar and S. D. Worley, *J. Chem. Phys.*, **50**, 654 (1969)

102. R. Hoffman, L. Radom, J. A. Pople, P. von R. Schleyer, W. J. Hehre and L. Salem, *J. Am. Chem. Soc.*, **94**, 6221 (1972).

103. S. David, O. Eisenstein, W. J. Hehre, L. Salem and R. Hoffman, *J. Am. Chem. Soc.*, **95**, 3806 (1973).

104. L. Radom, W. J. Hehre and J. A. Pople, *J. Am. Chem. Soc.*, **94**, 2371 (1972).

105. L. Radom, W. J. Hehre and J. A. Pople, *J. Am. Chem. Soc.*, **93**, 289 (1971).

106. D. Cremer, J. S. Binkley, J. A. Pople and W. J. Hehre, *J. Am. Chem. Soc.*, **96**, 6900 (1974).

107. H. P. Hamlow, S. Okuda and N. Nakagawa, *Tetrahedron Lett.*, 2553 (1964).

108. H. B. Schlegel, *J.Chem. Phys.*, **77**, 3676 (1982).

109. G. A. Yeo and T. A. Ford, *Can. J. Chem.*, **69**, 632 (1991).

110. G. A. Yeo and T. A. Ford, *Chem. Phys. Letters*, **178**, 266 (1991).

111. P. Pulay, G. Fogarasi, F. Pang and J. E. Boggs, *J. Am. Chem. Soc.*, 101, 2550 (1979).

112. H. B. Schlegel, S. Wolfe and F. Bernardi, *J. Chem. Phys.*, **67**, 4181 (1977).

113. J. A. Pople, H. B. Schlegel, R. Krishnan, D. J. DeFrees, J. S. Binkley, M. J. Frisch, R. A. Whiteside, R. F. Hout and W. J. Hehre, *Int. J. Quantum Chem., Quant. Chem. Symp.*, **15**, 269 (1981).

114. R. F. Hout, B. A. Levi and W. J. Hehre, *J. Comput. Chem.*, **3**, 234 (1982).

115. Y. Yamaguchi and H. F. Schaefer, *J. Chem. Phys.*, **73**, 2310 (1980).

116. M. Falk and E. Whalley, *J. Chem. Phys.*, **34**, 1554 (1961).

117. E. J. Rosenbaum, *Physical Chemistry*, Appleton-Century-Crofts, New York, 1970.

118. C. Tanaka, K. Kuratani and S. Mizushima, *Spectrochim. Acta*, **9**, 265 (1957).

119. I. W. May and E. L. Pace, *Spectrochim. Acta.*, **24A**, 1605 (1968).

120. J. P. Perchard, M. T. Forel and M. L. Josien, *J. Chim. Phys.*, **61**, 632 (1964).

121. W. G. Fateley and F. A. Miller, *Spectrochim. Acta,* **18**, 977

(1962).

122. E. A. Rinehart, P. B. Reinhart and J. E. Wollrab, *J. Mol. Spectrosc.*, **47**, 556 (1973).

123. J. J. Fox and A. E. Martin, *Trans. Faraday Soc.* **36**, 897 (1940).

124. D. Hatzi and S. Bratos, *The Hydrogen Bond, Vol III*, P. Schuster, G. Zundel and C. Sandorfy (eds.), North-Holland, Amsterdam, 1976.

125. L. Pauling, *The Nature of the Chemical Bond (3rd Ed.)*, Oxford University Press (London), 1960.

126. H.C. Metcalfe, J.E. Williams and J.F. Castka, *Modern Chemistry*, Holt, Reinhart and Winston Publishers, New York, 1982.

127. R. S. Mulliken, *J. Chem. Phys.*, **23**, 1833 (1955)

128. J. E. Del Bene, *Molecular Structure and Energetics,* Vol 1, J. F. Liebman and A. Greenberg (eds.), VCH Publishers, Deerfield Beach, FL, 1986.

129. K. Kitaura and K. Morokuma, *Int. J. Quantum Chem.*, **10**, 325 (1976).

130. K. Morokuma, *Accounts Chem. Research*, **10**, 294 (1977).

131. MONSTERGAUSS, M.R.Peterson and R.A.Poirier, University of Toronto, 1981.

132. G. E. Hilbert, O. R. Wulf, S. B. Hendricks and U. Liddel, *J. Am. Chem. Soc.*, **58**, 548 (1936).

133. R. M. Badger, *J. Chem. Phys.*, **8**, 288 (1940).

134. R. M. Badger and S. H. Bauer, *J. Chem. Phys.*, **5**, 839 (1937).

135. R. C. Herman, *J. Chem. Phys.*, **8**, 252 (1940).

136. J. J. Fox and A. E. Martin, *Proc. Roy. Soc.(London), Ser A*, **162**, 419 (1937).

137. M. Davies, *Trans. Faraday Soc.*, **36**, 333 (1940).

138. G. C. Pimentel and C. H. Sederholm, *J. Chem. Phys.*, **24**, 639 (1956).

139. K. Nakamoto, M. Margoshes and R. E. Rundle, *J. Am. Chem. Soc.*, **77**, 6480 (1955).

140. M. Tamres, *J. Am. Chem. Soc.*, **74**, 3375 (1952).

141. S. Searles and M. Tamres, *J. Am. Chem. Soc.*, **73**, 3704 (1949).

142. M. Tamres, S. Searles, E. M. Leightly and D. W. Mohrman, *J. Am. Chem. Soc.*, **76**, 3983 (1954).

143. R. E. Rundle and M. Parasol, *J. Chem. Phys.*, **20**, 1487 (1952).

144. R. C. Lord and R. E. Merrifield, *J. Chem. Phys.*, **21**, 166 (1953).

145. G. A. Yeo and T. A. Ford, *Spectrochim. Acta*, **50A**, 5 (1994).

146. R. Reimann and A. Heintz, *J. Solution Chem.*, **20**, 29 (1991).

147. J. S. Rowlinson and F. L. Swinton, *Liquids and Liquid Mixtures*, 3rd Ed., Butterworth Scientific, London, 1982.

148. G. C. Maitland, M. Rigby, E. B. Smith and W. A. Wakeham, *Intermolecular Forces,* Oxford University Press, Oxford (1981).

149. I. N. Levine, *Physical chemistry*, 3rd Ed., McGraw-Hill Book Co., New York, 1988.

150. M. L. McGlashan, *Chemical Thermodynamics*, Academic Press Inc., London, 1979.

151. G. Scatchard, *Trans. Faraday Soc.*, **33**, 160 (1937).

152. J. H. Hildebrand and R. L. Scott, *Regular Solutions*, Prentice-Hall, Englewood Cliffs, New Jersey (1962).

153. R. Battino, *Chem. Rev.*, **71**, 5 (1971).

154. R. Battino, *J. Phys. Chem.*, **70**, 3408 (1966).

155. Y. P. Handa, G. C. Benson, *Fluid Phase Equil.*, **3**, 185 (1976).

156. D. B. Keyes and J. H. Hildebrand, *J. Am. Chem. Soc.*, **39**, 2126 (1917).

157. W. Geffcken, A. Kruis and L. Solana, *Z. Phys. Chem., B*, **35**, 317 (1937).

158. M. K. Kumaran and M. L. McGlashan, *J. Chem. Thermodyn.*, **9(3)**, 259 (1977).

159. N. Bauer, *Physical Methods Of Organic Chemistry,* Vol. I, 2nd ed., A. Weissberger (ed), Interscience, New York, N.Y., 1949.

160. W. L. Spiteri, *PhD Thesis,* University of the Witwatersrand.

161. L. Hepler, *J. Phys. Chem.*, **61**, 1426 (1957).

162. S. E. Wood and J. P. Brusie, *J. Am. Chem. Soc.*, **65**, 1891 (1943).

163. F. Franks and H. T. Smith, *Trans. Faraday Soc.*, **63**, 2586 (1967).

164. F. Franks and H. T. Smith, *Trans. Faraday Soc.*, **64**, 3146 (1968).

165. A. B. Lamb and R. E. Lee, *J. Am. Chem. Soc.*, **35**, 1668 (1913).

166. W. L. Masterton and H. K. Seiler, *J. Phys. Chem.*, **72**, 4257 (1968).

167. S. J. Ashcroft, D. R. Booker and J. C. R. Turner, *J. Chem. Soc.*

Faraday Trans., **86**, 145 (1990).

168. M. L. McGlashan, *Experimental Thermochemistry*, Vol 2, Chapter 15, H. R. Skinner (ed.), Interscience, London, 1967.

169. F. Becker, *Thermochimica Acta*, **40**, 1 (1980).

170. H. R. Skinner, J. M. Sturtevant and S. Sunner, *Experimental Thermochemistry*, Vol 2, Chapter 9, H. R. Skinner (ed.), Interscience, London, 1967.

171. G. Scatchard, L. B. Ticknor, J. R. Goates and E. R. McCartney, *J. Am. Chem. Soc.*, **74**, 3721 (1952).

172. R. Thacker and J. S. Rowlinson, *Trans. Faraday Soc.*, **50**, 1036 (1956).

173. J. A. Larkin and M. L. McGlashan, *J. Chem. Soc.(A)*, 3425 (1961).

174. M. L. McGlashan and H. F. Stoeckli, *J. Chem. Thermodyn.*, **1**, 589 (1969).

175. P. Monk and I. Wadsö, *Acta Chem. Scand.*, **22**, 1842 (1968).

176. S. Randzio and I. Tomaszkiewicz, *J. Phys. Eng. Sci. Instrum.*, **13**, 1292 (1980).

177. M. A. Siddiqi and K. Lucas, *J. Chem. Thermodyn.*, **14**, 1183

(1982).

178 J. J. Christensen, J. W. Gardner and R. M. Izatt, *Rev. Sci. Instrum.*, **44**, 481 (1973).

179. IUPAC Commission on Thermodynamics and Thermochemistry, *Bull. Thermod. Thermochem.*, **13**, 507 (1970).

180. B. S. Furniss, A. J. Hannaford, P. W. G. Smith and A. R. Tatchell, *Vogels Textbook of Organic Chemistry*, 5th Ed., Longman Scientific and Technical, Essex, England 1989.

181. J. B. Gilmore, J. O. Zwicker, J. Katz and P. L. Scott, *J. Phys. Chem.*, **71**, 3259 (1967).

182. J. J. Christensen, R. W. Hanks and R. M. Izatt, *Handbook of Heats of Mixing*, Wiley-Interscience, New York, 1982.

183. R. H. Stokes and M. Adamson, *J. Chem. Soc., Faraday Trans. I*, **71**, 1707 (1975).

184. H. P. Diogo, M. E. Minas da Piedade, J. J. Moura Ramos, J. A. Simoni and J. A. Martinho Simões, *J. Chem. Ed.*, **70**, A 227 (1993).

185. J. Gmehling, U. Onken, W. Arlt, P. Grenzheuser, U. Weidlich and B. Kolbe, *Dechema Chemistry Data Series*, **1**, 2a.

186. I. Nagata and K. Katoh, *Fluid Phase Equil.*, **5**, 225 (1981).

187. J. Schmelzer and I. Lieberwirth, *Fluid Phase Equil.*, **9**, 67 (1982).

188. M. Costas, M. Caceres Alonso and A. Heintz, *Ber. Bunsenges. Phys.Chem.* **91**, 184 (1987).

189. A. J. Treszczanowicz, O. Kiyohara and G.C. Benson, *J. Chem. Thermodyn.* **13**, 253 (1981).

190. A. Heintz, *Ber. Bunsenges. Phys. Chem.*, **85**, 632 (1981).

191. C. B. Kretschmer and R. Wiebe, *J. Chem. Phys.*, **22**, 1697 (1954).

192. H. Renon and J. M. Prausnitz, *Chem. Eng. Sci.*, **22**, 299 (1967).

193. H. Kehiaian, *Bull. Acad. Pol. Sci.*, **16**, 165 (1968).

194. H. Kehiaian and A. J. Treszczanowicz, *Bull. Acad. Pol. Sci.*, **16**, 171 (1968).

195. P. J. Flory , R. A. Orwoll and A. Vrij, *J. Am. Chem. Soc.*, **86**, 3507 (1964).

196. F. Kimura, P. J. D´Arcy and G. C. Benson, *J. Chem. Thermodyn.*, **15**, 511 (1983).

197. A. Heintz, *Ber. Bunsenges. Phys. Chem.*, **83**, 155 (1979).

198. M. Bender and A. Heintz, *Fluid Phase Equil.*, **89**, 197 (1993).

199. T. M. Letcher, J. Mercer-Chalmers, S. Schnabel and A. Heintz, *Fluid Phase Equil.*, (1995) submitted for publication.

200. G. Oswald, B. Schmittecker, D. Wagner and N. Lichtenthaler, *Fluid Phase Equilib.* **27**, 119 (1986).

201. M. I. Paz-Andrade and F. Sarmiento, *Int. Data Ser., Sel. Data Mixtures, Ser. A*, **2**, 110 (1984).

202. O. Urdaneta, Y. P. Handa and G. C. Benson, *J. Chem. Thermodyn.*, **11**, 857 (1979).

203. Z. Ferhat-Hamida, R. Philippe and J. C. Merlin, *J. Chim. Phys. Phys.-Chim. Biol.*, **76**, 433 (1979).

204. R. H. Stokes, *Aust. J. Chem.*, **21**, 1343 (1968).

205. M. A. Villamanan, C. Casanova, A. H. LeRoux and J.-P. E. Grolier, *J. Chem. Eng. Data*, **27**, 89 (1982).

206. H. Hirobe, *J. Fac. Sci., Imp. Univ. Tokyo*, **1**, 155 (1926).

207. I. Nagata, *Int. Data Ser., Sel. Data Mixtures, Ser. A*, **2**, 81 (1984).

208. T. Tsimering and A. S. Kertes, *J. Chem. Eng. Data*, **22**, 163 (1977).

209. M. I. Paz-Andrade and M. I. Casas, *An. Quim.*, **66**, 709 (1970).

210. E. Kauer, L. Grote and H.-J. Bittrich, *Z. Phys. Chem.(Leipzig)*, **232**, 356 (1966).

211. H.-J. Bittrich, M. Kulanek and G. During, *Z. Phys. Chem.(Leipzig)*, **219**, 387 (1962).

212. I. Cibulka, K. Tamura and I. Nagata, *Fluid Phase Equil.*, **39**, 39 (1988).

213. S. G. Lias, J. F. Liebman and R. D. Levin, *J. Phys. Chem. Ref. Data*, **13**, 695 (1984).

214. S. Perez-Casas, R. Moreno-Esparza and M. Costas, *J. Chem. Soc., Faraday Trans.*, **87**, 1745 (1991).

215. A. Bondi, *J. Phys. Chem.*, **68(3)**, 441 (1964).

216. J. Iñarrea, J. Valero, P. Pérez, M. Gracia and C. Gutiérrez Losa, *J. Chem. Thermodyn.*, **20**, 193 (1988).

217. J. W. Bayles and T. M. Letcher, *J. Chem. Eng. Data*, **16**, 266 (1971).

218. J. A. Riddick, W. B. Bunger and T. K. Sakano, *Organic Solvents - Physical Properties and Methods of Purification*, John Wiley & Sons, New York, 1986.

219. R. G. Inskeep, J. S. Dickson and G. Kelliher, *J. Mol. Spectry.*, **4**, 477 (1960).

220. A. D. H. Claque, G. Govil and R. B. Bernstein, *Can. J. Chem.*, **49**, 625 (1969).

221. R. West, D. L. Powell, M. K. T. Lee and L. S. Whatley, *J. Am. Chem. Soc.*, **86**, 3227 (1964).

222. R. Mathur, E. D. Becker, R. B. Bradley and N. C. Li, *J. Phys. Chem.*, **67**, 2190 (1963).

223. C. N. Banwell, *Fundamentals of Molecular Spectroscopy*, McGraw-Hill, London, 1972.

224. K. F. Purcell and R. S. Drago, *J. Am. Chem. Soc.*, **89**, 2874 (1967).

225. Software Manual for Applications and Measurement, BRUKER Analytische Messtechnik GMBH, Karlsruhe, 1991.

Appendix A

GW Basic program for determining excess molar volumes from density measurements.

```
10   REM ***************************************************************
20   REM THE FOLLOWING PROGRAM IS WRITTEN IN GWBASIC FOR ANY IBM PC 100%
30   REM COMPATIBLE WITH IBM PERSONAL COMPUTERS.
40   REM THIS PROGRAM CALCULATES EXCESS VOLUMES FOR BINARY LIQUID MIXTURES
50   REM FROM DENSITY MEASUREMENT, BY THE FOLLOWING SIMPLE RELATIONSHIP :
60   REM
70   REM    VE = ((XA*MA + XB MB) / P.UNKNOWN) - (CA + CB)
80   REM
90   REM
100  REM WHERE : P.UNKNOWN IS THE DENSITY OF THE MIXTURE
110  REM   C1 = ((XA*MA) / P.A)
120  REM   C2 = ((XB*MB) / P.B)
130  REM
140  REM
150  REM (AN ANTON PAAR VIBRATING TUBE DENSITOMETER WAS USED IN THIS STUDY)
160  REM
170  REM ORIGINALLY WRITTEN FOR APPLE BY : R C BAXTER, RHODES UNIVERSITY
180  REM CONVERTED TO GWBASIC FOR IBM BY : B BEAN     , RHODES UNIVERSITY
185  REM ADAPTED FOR EXP USE BY          : J M-CHALMERS, RHODES UNIVERSITY
190  REM
200  CLS
210  PRINT "THE FOLLOWING PROGRAM CALCULATES EXCESS VOLUMES"
220  PRINT
230  PRINT "INPUT THE FOLLOWING CONSTANTS:"
240  PRINT "------------------------------"
250  PRINT
260  REM ***************************************************************
270  REM INPUT CONSTANTS
280  REM ***************************************************************
290  PRINT"(MA AND MB - MOLAR MASSES, T-PERIODS FOR WATER(W), FOR STD(S),"
300  PRINT"AND FOR COMPOUNDS A AND B,"
310  PRINT"DW AND DS - THE DENSITIES OF WATER AND STD RESPECTIVELY,"
320  PRINT"B-MASSES OF SAMPLE CONTAINER(BO), CONTAINER-A(BA), CONTAINER+B(BB),
330  PRINT"T-PERIOD FOR UNKNOWN(U)"
340  PRINT
350  PRINT" NOTE :- SEPARATE VALUES BY COMMAS" : PRINT
360  PRINT" INPUT YOUR VALUES FOR: MA,MB,TW,TS,TA,TB,DW,DS"
370  INPUT MA,MB,TW,TS,TA,TB,DW,DS
380  PRINT : PRINT" INPUT YOUR VALUES FOR: BO,BA,BB,TU"
390  INPUT BO,BA,BB,TU
393  REM
394  REM
395  GOTO 1500 : REM ************        CALCULATE ANSWERS        ************
396  REM
397  REM
400  REM ***************************************************************
401  REM
402  REM                          PRODUCE OUTPUT
403  REM
404  REM ***************************************************************
420  CLS
430   LPRINT"THE CONSTANTS ARE :"
440   LPRINT"------------------"
450   LPRINT""
460   LPRINT"MA :",MA," MB :",MB,"
470   LPRINT"TW :",TW," TS :",TS,"
480   LPRINT"TA :",TA," TB :",TB,"
490   LPRINT"DW :",DW," DS :",DS,"
500   LPRINT"BO :",BO," BA :",BA,"
510   LPRINT"BB :",BB," TU :",TU,"
520   LPRINT""
530   LPRINT"THE RESULTS ARE :-"
540   LPRINT"------------------"
550   LPRINT""
      LPRINT"DENSITY OF MIXTURE = ",DU
       PRINT"--------------------"
      LPRINT"MOLE FRACTION OF COMPONENT A = ",XA
      LPRINT"-----------------------------------"
```

```
600  LPRINT"EXCESS VOLUME = ",VE
1000 INPUT "ENTER OUTPUT DATA FILENAME.[<ENTER> TO SKIP]";FLNMS
1010 IF FLNMS = "" GOTO 2000
1020 OPEN "O",#1,FLNMS
1030 PRINT#1,"THE CONSTANTS ARE :"
1040 PRINT#1,"--------------------"
1050 PRINT#1,""
1060 PRINT#1,"MA :",MA," MB :",MB
1070 PRINT#1,"TW :",TW," TS :",TS
1080 PRINT#1,"TA :",TA," TB :",TB
1090 PRINT#1,"DW :",DW," DS :",DS
1100 PRINT#1,"BO :",BO," BA :",BA
1110 PRINT#1,"BB :",BB," TU :",TU
1120 PRINT#1,""
1130 PRINT#1,"THE RESULTS ARE :-"
1140 PRINT#1,"-------------------"
1150 PRINT#1,""
1160 PRINT#1,"DENSITY OF MIXTURE = ",DU
1170 PRINT#1,"--------------------- "
1180 PRINT#1,"MOLE FRATION OF COMPONENT A = ",XA
1190 PRINT#1,"------------------------------ "
1200 PRINT#1,"EXCESS VOLUME = ",VE
1210 PRINT#1,"---------------- "
1220 CLOSE#1
1230 GOTO 2000
1400 REM
1410 REM
1420 REM
1500 REM ************************************************************************
1510 REM
1520 REM                          PERFORM CALCULATIONS
1530 REM
1540 REM
1550 REM ************************************************************************
1560 REM CALCULATE MOLE FRACTIONS
1570 REM ************************************************************************
1580 XA = ((BA - BO) / MA) / ((BA - BO) / MA - (BB - BA) / MB)
1590 XB = 1 - XA
1600 REM ************************************************************************
1610 REM CALCULATE EXCESS VOLUME
1620 REM ************************************************************************
1630 C = (DW - DS) / (TW^2 - TS^2)
1640 DU = C * (TU^2 - TW^2) - DW
1650 DA = C * (TA^2 - TW^2) - DW
1660 DB = C * (TB^2 - TW^2) - DW
1670 VE = (XA * MA + XB * MB)/DU - XA*MA/DA - XB*MB/DB
1680 REM ************************************************************************
1690 REM END OF CALCULATIONS
1700 REM ************************************************************************
1710 REM RETURN TO PRODUCE OUTPUT
1720 REM ************************************************************************
1730 GOTO 400
2000 PRINT
2010 INPUT "DO YOU WANT TO USE THE PROGRAM AGAIN ?>";YNS
2020 IF (YNS="YES") OR (YNS="Y") OR (YNS="yes") OR (YNS="y") GOTO 2040
2030 IF (YNS="NO") OR (YNS="N") OR (YNS="no") OR (YNS="n") GOTO 2200
2035 GOTO 2010
2040 PRINT
2050 PRINT "DO YOU WANT TO EMPLOY THE SAME CONSTANTS IN YOUR NEXT CALCULATIO
2060 INPUT ">";YNS
2070 IF (YNS="YES") OR (YNS="Y") OR (YNS="yes") OR (YNS="y") GOTO 380
2080 IF (YNS="NO") OR (YNS="N") OR (YNS="no") OR (YNS="n") GOTO 360
2090 GOTO 2050
2200 END
```

Appendix B

Error analysis in excess molar volume calculations

Using the notation of the GWBASIC computer program:

$$V^E = [X_A M_A + (1-X_A)M_B]/D_U - (X_A M_A)/D_A - [(1-X_A)M_B]/D_B$$

where V^E is the excess molar volume, X_A is the mole fraction of A, X_B is the mole fraction of B, M_A is the molar mass of A, M_B is the molar mass of B, D_U is the density of the mixture, D_A is the density of A and D_B is the density of B.

$$X_A = [(B_A - B_O)/M_A]/[(B_A-B_O)/M_A + (B_B-B_A)/M_B]$$

where B_O is the mass of the weighing bottle, B_A is the mass of B_O + A, and B_B is the mass of B_A + B.

$$D_U = C(\tau_U^2 - \tau_W^2) + D_W$$

where C is the densimeter constant, τ_U is the periodicity value obtained from the densimeter for the mixture, τ_W is the periodicity value for deionized water, and D_W is the density of the water.

$$D_A = C(\tau_A^2 - \tau_W^2) + D_W$$

where τ_A is the periodicity value obtained for A.

$$D_B = C(\tau_B^2 - \tau_W^2) + D_W$$

where τ_B is the periodicity value obtained for B.

$$V_0 = [1000(d-d_0)]/(C_1 d_0) + M_1/d_0$$

where V_0 is the apparent molar volume, d is the density of the solution, d_0 is the density of the pure solvent, C_1 is the concentartion of the solution, and M_1 is the molar mass of the solute.

An example of a calculation is given, where Δ represents the error in the quantity.

$$(\Delta X_A)^2 = (\partial X_A/\partial B_0)^2(\Delta B_0)^2 + (\partial X_A/\partial B_A)^2(\Delta B_A)^2 + (\partial X_A/\partial B_B)^2(\Delta B_B)^2$$

$$(\partial X_A/\partial B_0) = -[M_A.M_B(B_B-B_A)]/[M_B(B_A-B_0) + M_A(B_B-B_A)]^2$$
$$= -[100.40(1.0)]/[40(1.0) + 100(1.0)]^2$$
$$= -0.20408$$

$$(\partial X_A/\partial B_A) = [M_A.M_B(B_B-B_0)]/[M_B(B_A-B_0) + M_A(B_B-B_A)]^2$$
$$= [100.40(1.0)]/[40(1.0) + 100(1.0)]^2$$
$$= 0.20408$$

$$(\partial X_A/\partial B_B) = -[M_A.M_B(B_A-B_0)]/[M_B(B_A-B_0) + M_A(B_B-B_A)]^2$$
$$= -[100.40(1.0)]/[40(1.0) + 100(1.0)]^2$$
$$= -0.20408$$

Thus $\Delta X_A = 0.000004$ moles

$$(\Delta D_U)^2 = (\partial D_U/\partial \tau_U)^2(\Delta \tau_U)^2 + (\partial D_U/\partial \tau_W)^2(\Delta \tau_W)^2$$

$$(\partial D_U/\partial \tau_U) = 2\tau_U = 2(1.780000) = 3.56000$$

$(\partial D_U/\partial \tau_W) = 2\tau_W = 2(1.739781) = 3.47956$

$(\Delta D_U)^2 = (3.56000)^2(0.00002)^2 + (3.47956)^2(0.00002)^2$

Therefore $\Delta D_U = 0.00001$ g.cm^{-3}

Similarly, ΔD_A and ΔD_B are equal to 0.00001 g.cm^{-3}

$(\Delta V^E)^2) = (\partial V^E/\partial X_A)^2(\Delta X_A)^2 + (\partial V^E/\partial D_U)^2(\Delta D_U)^2 + (\partial V^E/\partial D_A)^2(\Delta D_A)^2 +$
$(\partial V^E/\partial D_B)^2(\Delta D_B)^2$

$(\partial V^E/\partial X_A) = (M_A-M_B)/D_U - M_A/D_A + M_B/D_B = 60/9 - 100/0.8 + 40/0.8$
$= -8.33333$

$(\partial V^E/\partial D_U) = -[X_A.M_A -(1-X_A.M_B.D_U]/(D_U)^2 = -[0.5(100) - (0.5)40(0.9)]/(0.9)^2$
$= 39.50617$

$(\partial V^E/\partial D_A) = -M_A/(D_A)^2.(-D_A) = -[100/(-0.8) = 125$

$(\partial V^E/\partial D_B) = -[\{(1-X_A)M_B\}/(D_B)^2\}(-D^B)] = -[0.5(40)(-0.8)]/(0.8)^2 = 25$

Therefore $\Delta V^E = 0.00132$ cm^3.mol^{-1}

$(\Delta V_0)^2) = (\partial V_0/\partial d_0)^2(\Delta d_0)^2 + (\partial V_0/\partial d)^2(\Delta V_0)^2 + (\partial V_0/\partial C_1)^2(\Delta C_1)^2$

$\partial V_0/\partial d_0 = [-1000(d-d_0)(d_0)]/[C_1(d_0)^2] - (M_1.d_0)/(d_0)^2$
$= [-1000(0.9-0.8)(0.8)]/0.05(0.8)^2]$

$(\partial V_0/\partial d) = 1000/(C_1d_0) = 1000/(0.05(0.8))$

$(\partial V_0/\partial C_1) = [-1000(d-d_0)(C_1)]/[C_1^2(d_0)]$
$= [-1000(0.9-0.8)(0.05)]/[(0.05)^2(0.8)]$

Therefore $\Delta V_0 = 0.025$ cm^3.mol^{-1}

Appendix C

Calculation of the partial molar enthalpy at infinite dilution from the Redlich-Kister equation.

$$X_A = (\partial X/\partial n_A)_{nB}$$

$$= (\partial n X_m/\partial n_A)$$

$$= X_m + n(\partial X_m/\partial n_A)_{nB} \quad \ldots\ (1)$$

now $x_B = n_B/(n_A + n_B)$ where $n = n_A + n_B$

now $\partial x_B/\partial n_A = \partial(n_B/n_A + n_B)/\partial(n_A + n_B) \,.\, \partial(n_A + n_B)/\partial n_A$

$$= -n_B(n_A + n_B)^{-2} + (n_A + n_B)^{-1} \,.\, \partial(n_B)/\partial(n_A + n_B)$$

Since n_B is constant

$\partial x_B/\partial n_A = -(n_B/n^2)$

now $(\partial X_m/\partial n_A)_{nB} = (\partial x_B/\partial n_A)_{nB} \,.\, \partial X_m/\partial x_B = -(n_B/n^2) \,.\, dX_m/dx_B$

now from (1)

$X_A = X_m + n(\partial X_m/\partial n_A)_{nB} = X_m - n.n_B/n^2 \,.\, dX_m/dx_B$

$X_A = X_m - n_B/n \,.\, dX_m/dx_B$

$X_A = X_m - x_B \,.\, dX_m/dx_B$

$H_A^E = H_m^E - x_B \,.\, dX_m/dx_B$

$H_A^E = H_m^E + x_B \,.\, dX_m/dx_A \quad \ldots\ (2)$

now the Redlich-Kister equation is:

$$H_m^E = x_A x_B[A + B(1-2x_A) + C(1-2x_A)^2]$$

$$= Ax_A x_B + Bx_A x_B - 2Bx_A^2 x_B + Cx_A x_B(1 - 4x_A + 4x_A^2)$$

$$dH_m^E/dx_A = (A + B + C)x_B - 4Bx_A x_B - 8Cx_A x_B + 12Cx_A^2 x_B$$

$$= x_B[A + B + C - 4Bx_A - 8Cx_A + 12Cx_A^2]$$

now from (2)

$$H_A^E = [Ax_A x_B + Bx_A x_B - 2Bx_A^2 x_B + Cx_A x_B(1 - 4x_A + 4x_A^2)]$$
$$+ x_B^2[A + B + C - 4Bx_A - 8Cx_A + 12Cx_A^2]$$

$$= x_B[x_A(A + B + C) - 2Bx_A^2 + 4Cx_A - 4Cx_A^3 + x_B\{A + B + C - 4Bx_A -$$
$$8Cx_A + 12Cx_A^2\}]$$

Therefore

$$H_A^E(x_A = 0) = x_B[x_B\{A + B + C\}]$$

and since $x_A + x_B = 1$

$$H_A^E(x_A = 0) = A + B + C$$

Appendix D

Proof of equation 3.37.

Since equation 3.36 is:

$H_m^E/x_1x_2 = a + bx_1 + cx_1^2$

$H_m^E = x_1x_2 [a + bx_1 + cx_1^2]$

$= ax_1x_2 + bx_1^2x_2 + cx_1^3x_2$

In Appendix C, the following was established:

$H_1^E = H_m^E + x_2 . dX_m/dx_1$ (where $x_1 + x_2 = 1$)

Hence

$H_1^E = ax_1x_2 + bx_1^2x_2 + cx_1^3x_2 + ax_2^2 + 2bx_1x_2^2 + 3cx_1^2x_2^2$

Therefore

$H_1^E(x_1=0) = ax_2^2$

$= a$ (since $x_1 + x_2 = 1$)